Cardiff University

School of Chemistry

Novel Multi-Metallic Luminescent Complexes Towards Dual-Functional Cellular and Therapeutic Applications

A thesis submitted for the degree of Doctor of Philosophy by:

Rebeca Glory Balasingham

November 2012

Abstract

School of Chemistry
Doctor of Philosophy
Novel Multi-Metallic Luminescent Complexes Towards Dual-Functional Cellular and Therapeutic Applications by Rebeca Balasingham.

A series of novel multi-metallic luminescent Au(I) and Re(I) complexes have been synthesised targeting functionality as cellular imaging and/or therapeutic agents. Both the ligands and their complexes have been characterised by a variety of spectroscopic and spectrometric techniques. Several complexes were also characterised by X-ray crystal diffraction and/or elemental analysis.

In both chapters two and three the modulation of the luminescent properties of a series of mono- and di-metallic $[Re(CO)_3(N\text{^}N)L]^+$ type complexes bearing functionalised alkyl chains by hydrophobically driven, intra- and intermolecular conformational changes is reported. Additionally, the first application of di-metallic Re(I) complexes in cellular imaging is reported with specific localisation in the nucleoli or ER and Golgi apparatus.

In both chapters four and five the synthesis of novel mono- and di-metallic Au(I) complexes is reported. Several complexes demonstrated cytotoxicity as well as compartemental localisation in cellular imaging demonstrating their potential as dual-functional cellular imaging and/or therapeutic agents.

As an extension to the work discussed in Chapters two to five, the synthesis of novel multi-metallic luminescent complexes is reported in Chapter six. For the tri-hetero-metallic complex incorporating Au(I) and Re(I) units, cytotoxicity towards four cancer cell lines and non-specific localization throughout the entire cell is described.

Acknowledgements

To the following people I owe thanks, without your guidance and support this thesis could not have been completed. Thank you!

To my supervisors, Dr. Mike Coogan and Dr. Simon Pope, to you I owe my deepest thanks. Without your belief in me I would not have had the belief in myself to complete this research. I am thankful that I was lucky enough to have not one, but two of you to look to for guidance, motivation, encouragement, support and friendship. I will be forever grateful for all that you have done.

Huge thanks goes to all the technical support staff, Dr. Rob Jenkins, Robin Hicks, Dave Walker and Benson Kariuki. None of this would have been possible without you.

Thank you to Catrin for your time and guidance through the confocal sessions.

A special thanks to Natalie, Flo, Charlie, Kate, Woody and Ollie. Thanks for all your help, your infectious passion for chemistry and most of all your friendship. Natalie, the last three years would not have been the same without you, thanks for always being there.

Thank you also to all the other members of the department for who have helped me; Andy, Breandan, Elena, Jay, Jenn, Kate, Lucy, Menna, Shaun. Stacey, Steve, Tim, Tracey, Vikki and Wei.

Throughout my three years I have been fortunate to not only make new friendships but to also strengthen my existing ones. A special thanks to Dave and Paula. Dave for letting me share your soon to be wife, and Paula, for everything. Thank you for your continued friendship and honesty and for always putting things in perspective.

To my older friends; Abby, Alex, Becca, Cat, Emily, Kel, Mel, Mercedes, Morg and Soph thank-you for always being there, for the welcomed distractions and for being you!

Eternal thanks goes to my mum, my sister Rachael and my brothers Luke and Jamie. Thanks for your love, guidance and friendship. My academic accomplishments could not have been achieved without your understanding and it is to you I dedicate this thesis.

Contents

Chapter 1. Introduction: Metal Complexes in Luminescence Imaging and Therapeutics.

Chapter 2. The Modulation of Luminescent Properties Of Mono-Metallic Re(I) Complexes Bearing Axial Functionalised Alkyl Chains by Hydrophobically Driven, Intra- And Intermolecular Conformational Changes.

Chapter 3. Hydrophobic Modulation of Emission Lifetimes For Both Mono- and Di-Metallic Re(I) Complexes Linked Through Functionalized Alkyl Chains Towards Cellular Imaging Applications.

Chapter 4. Luminescent Di-metallic Au(I) Complexes Bearing Functionalised Alkyl Chains Towards Therapeutic Applications.

Chapter 5. Luminescent Mono- and Di-Metallic Au(I) Complexes Incorporating Anthraquinone-Based Ligands Towards Dual-Functional Therapeutic And Cellular Imaging Applications.

Chapter 6. Luminescent Multi-Metallic Complexes Incorporating an Au(I) Alkyne Unit Towards Dual-Functional In Therapeutic And Cellular Imaging Applications.

Abbreviations

Spectroscopy and Techniques	
NMR	Nuclear magnetic resonance
UV-Vis	Ultraviolet-Visible
IR	Infra-red
MS	Mass spectrometry
ES	Electrospray
HR	High resolution
FLIM	Fluorescence lifetime imaging mapping
m/z	Mass/charge ratio
δ	Chemical shift
Ppm	Parts per million
S	Singlet
D	Doublet
T	Triplet
M	Multiplet
MHZ	Megahertz
{H}	Proton decoupled
Λ	Wavelength
υ	Frequency
Å	Angstroms

Photophysical	
IC	Internal conversion
ISC	Intersystem crossing
MC	Metal centred
IL	Intra-ligand
ILCT	Intra-ligand charge transfer
MLCT	Metal-ligand charge transfer
MMLCT	Metal-metal-ligand charge transfer
LMMCT	Ligand-metal-metal charge transfer
HOMO	Highest occupied molecular orbital
LUMO	Lowest unoccupied molecular orbital
Nm	Nanometre
^{1}IL/MLCT	Singlet excited state
T	Lifetime
ESIPT	Excited state intramolecular proton transfer

Solvents, compounds and chemical

DCM	Dichloromethane
DMF	Dimethyl formamide
TEA	Triethylamine
PBS	Phosphate buffer solution
Fac	*Facial*
TMS	Trimethylsilyleacetyline
^{t}Bu	*Tert*-butyl
TM	Transition metal
Bipy	2-2’ bipyridine
Phen	1, 10-phenanthroline
Neoc	2,9-dimethyl-1,10-phenanthroline
Me	Methyl
Me-4-Phen	3,4,7,8 tetramethyl-1,10-phen
Me_2-Ph_2-Phen	2,9-dimethyl-4,7-diphenyl-1,10-phen
Ph	Phenyl
PPh_3	Triphenylphosphine
$Pd(PPh_3)_4$	[tetrakis(triphenylphosphine)palladium(0)]
$Pd_2(dba)_3$	tris-[(dibenzylideneacetone)dipalladium(0)].
PTA	1,3,5-triaza-7-phosphaadamantane
DPPE	1,2-Bis(diphenylphosphino)ethane
DPPM	1,2-Bis(diphenylphosphino)methane
DPQ	Dipyrido-[3,2-f:2',3'-h]-quinoxaline
DPPZ	Dipyrido-[3,2-a:2',3'-c]-phenazine
DO3-A	1,4,7,10-tetraazacyclododecane-1,4,7-triacetic acid
AQ	Anthraquinone
DHAQ	Di-hydroxy anthraquinone
NHC	Nitrogen heterocyclic carbine
HABA	2-(4’hydroxobenzene)-benzoic acid

Chapter 1. Introduction: Metal Complexes in Luminescence Imaging and Therapeutics.

Chapter 1.

1. Introduction

In recent years there has been increasing interest in the enhancement of the luminescence properties of transition metal (TM) complexes.[1,2] The ability to engineer the electronic and so photophysical properties of these complexes through ligand sensitisation can help to develop research in several areas, including: employment as photocatalysts, luminescent probes or sensors, sensitizers or as luminophores in biological cell imaging.[3,4,5]TMs such as Re(I) and Au(I) are among the variety of metals favoured as a result of their phosphorescent emission at room temperature. Additionally, heavy TM complexes for applications as therapeutic agents are being increasingly investigated.

1.1. Luminescence spectroscopy

1.1.1. The Jablonski Diagram

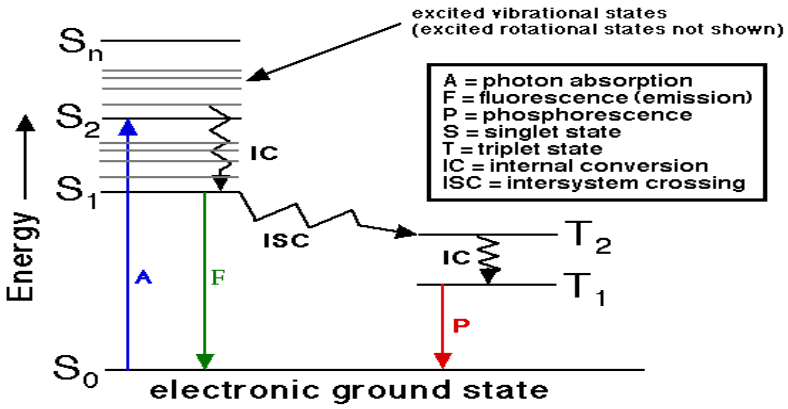

Figure 1.1 The Jablonski diagram. Reproduced from ref. 6.

Luminescence is the emission of light in the absence of heat. The luminescent behaviour of a molecule is determined by its photophysical properties and the photophysics of a complex can be explained using the Jablonski diagram. First the absorption of a photon occurs resulting in an electron being promoted from a ground state singlet (S_0) to an excited state singlet (S_1). When in the excited state there are two dominant pathways an excited species could follow, (i) photophysical change, this path includes luminescence (radiative) and quenching (non-radiative), or, (ii) chemical change (the complex is altered chemically forming an entirely new complex), this path includes isomerisation and direct reaction. It is the photophysical change of a complex that is the primary focus of the work described herein.

Following the excitation by absorption of a photon, the excited state formed is of high energy and generally unstable so it must undergo some form of deactivation. The excited state singlet initially loses some of its excess energy through internal relaxation to the lowest vibrational level of the excited state, this is a non-radiative process and is represented by the zig-zag line labelled internal conversion (IC) on Figure 1.1. The molecule is still in the excited state so will inevitably lose its remaining excess energy. This excess energy is lost *via* a number of different ways, including, molecular rotations, vibration, heat and light. The energy lost as emitted light is referred to as luminescence, and as very little heat is given off in this process, it can often be referred to as 'cold light'. This light can be emitted through one of two pathways, fluorescence or phosphorescence, both of which display initial intramolecular energy transfer processes where the initial excess energy is lost *via* a non-radiative process. As previously mentioned there is a second non-radiative pathway in photophysics that could compete with luminescence denoted 'quenching' and this involves interaction with another molecule or atom, otherwise referred to as a quencher species.

1.1.1.1.Fluorescence

Fluorescence involves an immediate emission of light shortly after it is absorbed resulting in the electron residing once again in the electronic ground state. This process is fast as it is spin- allowed. It has lifetime (the average time a molecule spends in the excited state) which ranges from 10^{-9} to 10^{-6} seconds.[7] As a result of IC the energy emitted differs from that which is absorbed, it is generally of lower energy and longer wavelength (red-shifted). This difference in the absorbed and emitted wavelength is referred to as the Stokes shift. [4]

1.1.1.2.Phosphorescence

In this process the energy is absorbed in the same way as fluorescence however, emission of the absorbed light does not occur immediately. Phosphorescence involves the storage of energy being lost slowly over a long period of time 10^{-6} to 10^{-1} hours[11] resulting in a long lifetime. Once in the excited singlet state intersystem crossing (ISC) occurs, this involves the forbidden transition from the excited singlet state (S_1) to the excited triplet state (T_1). ISC is a non- radiative transition brought about by spin-orbit coupling (a process facilitated by the heavy atom effect, more common in 2^{nd} and 3^{rd} row TMs). Internal relaxation to the lowest level of excited triplet state follows which enables phosphorescence to occur. The phosphorescence process is slow (a spin forbidden process); it involves the conversion of a

excited triplet (T_1) state back to a ground singlet state (S_o) and light can be detected from the sample for some time after the photon irradiation source is removed.

1.1.2. Autofluorescence and Stokes Shift

The application of heavy TM complexes as luminophores (fluorophores) in biochemistry is an area receiving considerable attention in the research field however, the presence of autofluorescence can be problematic. Autofluorescence is the fluorescence of any substance other than the fluorophore of interest[8] and is typically from the natural species in the cell. It tends to have a small Stokes shift, < 50 nm, and a small emission lifetime, < 10 ns. Molecules possessing a large Stokes shift and/or a large emission lifetime can allow a clearer distinction between the emitted light from the fluorophore and the background emission from autofluorescence. For a complex displaying a large Stokes shift an optical filter (a device which can selectively transmit light of different wavelength) can be used to filter out the autofluorescence.[9,10]

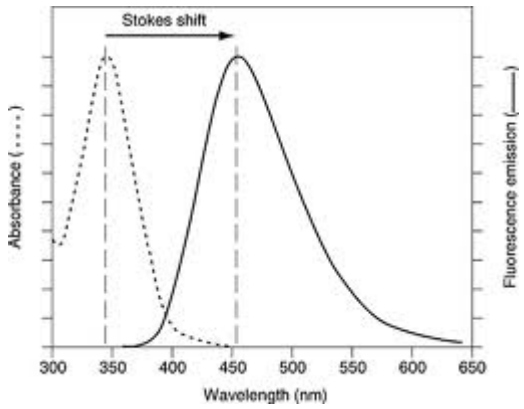

Figure 1.2 Spectra illustrating a Stokes Shift. Reproduced from ref. 11.

A complex possessing a long emission lifetime allows for a technique called time-gating to be used to reduce the effect of autofluorescence. Time-gating is a method which allows for a snap-shot of the luminescene of the fluorophore to be seen and usually requires phosphorescent emitting species.

1.1.3. Charge transfer processes

A charge transfer process involves the transfer of an electron within a molecule upon absorption of a photon. The possible excited states for heavy metal complexes include, metal to ligand charge transfer (MLCT), ligand to metal charge transfer (LMCT), ligand to ligand

charge transfer (LLCT) and intra ligand charge transfer (ILCT). The process is determined by: metal centres, chemical structures, triplet state energy levels of ligand, intra- and intermolecular interactions and local environments. Although it has proven impossible to negate any transfer process completely, it is possible from data accumulated over the years on the appearance of emission spectra, energies and lifetimes to predict where each of these processes are occurring.[13, 14]

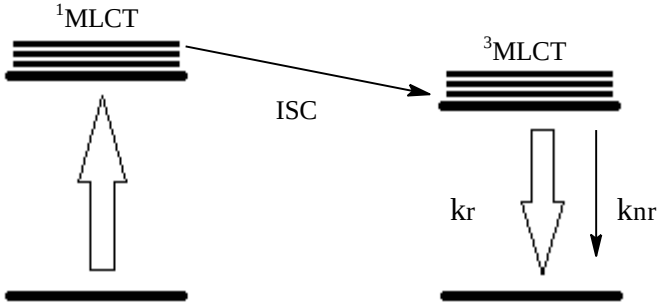

Figure 1.3 Generation and deactivation of a ^{3}MLCT state.

MLCT is a process which can result in luminescence. For the purpose of this thesis when discussing MLCT we refer to a redox process that requires a low oxidation state metal and a reducible ligand. Once the electron is transferred to the excited singlet state (S_1) it is able to undergo ISC, this is a non-radiative process which converts the excited singlet state (S_1) to a triplet excited state (T_1). Once the electron resides in T_1, the lowest spin forbidden level, emission occurs. The ^{3}MLCT in a complex is a phosphorescent process.[14]

1.1.4. FRET- Förster resonance energy transfer

FRET consists of a non-radiative transfer of energy between an initially excited donor molecule and an acceptor molecule. FRET efficiency is dependant on: the degree of spectral overlap of donor emission and acceptor absorption, the orientation of chromophores and the distance between the chromophores.[15] In bichromophoric molecules additional consideration of the choice of ligands can efficiently tune the emission towards different parts of the UV-vis region. The photophysical properties of fluorophores such as quantum dots, lanthanide and TM complexes are being increasingly investigated for applications using FRET as they overcome some of the problems associated with the more common organic chromophores used (small Stokes shift/short lifetimes).

1.2. Ligands

A ligand is an ion or molecule that bonds to a metal centre to form a co-ordination complex. Ligands, in a simple crystal-field model, can be thought of as negative charges that perturb the energy levels of the metal ion when co-ordinated. This is referred to as d-d splitting. The magnitude and order of the d-orbitals in the splitting are dependent on: the number of d electrons on the metal, the metal oxidation state, the arrangement of ligands and the nature of the ligand (*i.e.* geometry and symmetry).

1.2.1. Spectrochemical series

The spectrochemical series of ligands is an ordering of ligands based on their co-ordination strength, it is somewhat independent of the metal ion but the ordering is not absolute. The general trend is:

$Br^- < Cl^- < F^- < OH^- < H_2O < CH_3CN < Py < NH_3 < Bipy < Phen < PPh_3 < CN^- = CO$

Weak-field ligands — Strong-field ligands

π donors — π acceptors

Δ_o Δ_o Δ_o

Figure 1.4 A Spectrochemical series and the ligands effects on Δ_o.

The π-acceptor ligands / π-acids are ligands which accept electron density from the metal through π-bonding. π-acceptors can be found on the right hand side of the series; these ligands result in much larger splitting. The π-donor ligands / π-bases can be found on the left hand side of the series and result in much smaller splitting. Pyridine is found in an intermediate position of the spectrochemical series, and it is one of the most versatile ligands in photochemistry.

1.2.2. Dewar-Chatt Duncanson Model:

This is potentially one of the more useful bonding models for explaining metal-ligand interactions in TM complexes. It describes the bonding between an unsaturated ligand (carbonyls or alkenes) and a metal ion. There are two types of bonding, σ-donation from the ligand to the metal, and π bonding from the filled d-orbital on the metal to an empty π* orbital on the ligand. The latter form of bonding is referred to as back bonding. As both types of

bonding leads to a strengthening of the bond, the bonding can be defined as synergic.

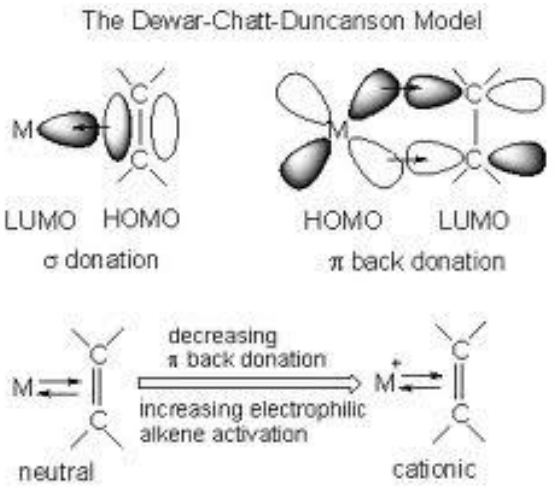

Figure 1.5 Dewar-Chatt-Duncanson Model. Reproduced from ref. 16.

1.3. Biological imaging

Biological imaging techniques are used primarily in diagnostics and treatment. X-rays, magnetic resonance imaging (MRI), ultrasound and tomography[17] are the more commonly used imaging techniques, each specialising in the imaging of a certain area in the body (bones, heart and blood flow). None of the techniques mentioned have the ability to provide high resolution images[17] and so, despite lacking the ability to view large objects in great detail, confocal fluorescence microscopy has found its niche in biological imaging. Confocal fluorescence microscopy can produce high quality images of minute sample sizes with relative ease and is thus able to produce individual images of cells and smaller cellular components.[18]

1.3.1. Confocal fluorescence microscopy

Luminescence is the light which is emitted by a substance; emission of light is necessary if a sample is to be viewed using confocal fluorescence microscopy. If light is not emitted by a cell, a fluorescent dye can be used as a 'stain'. There are a vast number of commercially available dyes, including dyes specific in the targeting of organelles. If required, more than one dye can be used at any one time to allow for a more detailed analysis.

Confocal microscopy produces increased optical resolution in comparison to other wide-field microscopes. The pin hole situated beneath the light source produces a narrow beam of light, eliminating reflected or out of focus light,[19] this increases the sensitivity and the resolution of the image. The narrow light beam then passes through the beam splitter and one small, thin region of the cell. The fluorescent light emitted from sample is then reflected by the beam splitter toward the detector to produce an accurate well-defined image of that region. A three-dimensional image is constructed through combining each small thin segment imaged.

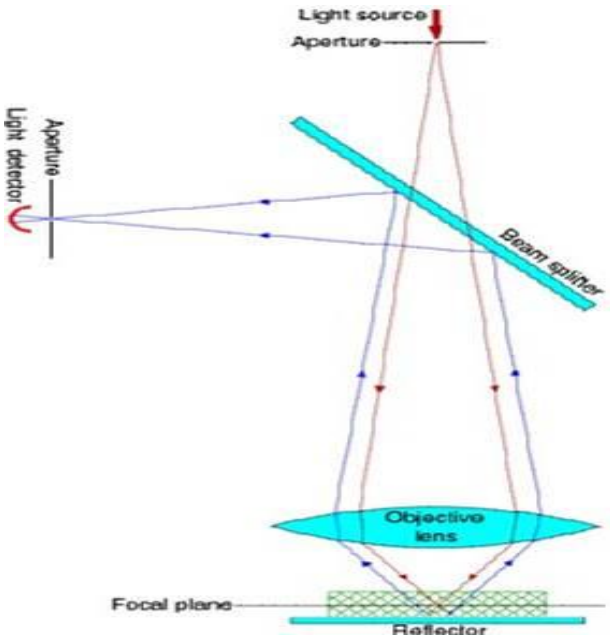

Figure 1.6 Confocal Microscope with the key features highlighted. Reproduced from ref. 20.

1.3.2. Ideal properties of cellular imaging agents

In order for a compound to be useful for bioimaging there are several characteristics that it must possess including the previously discussed photophysical attributes (large Stokes shift and long lifetime). [23] These are:

(i) Photostability. Photobleaching is the permanent loss of fluorescence. Compounds that are easily photobleached, for example many organic flurophores, are not ideal luminescent probes for bioimaging.

(ii) Toxicity. Compounds must be non-toxic. Cytotoxicity of phosphorescent heavy metal compounds is dependent on structure. The lipophilicity of a compound can sometimes be correlated with their cytotoxicity, generally the more lipophilic a compound is, the more cytotoxic it is.[21]

(iii) Uptake. To be a successful bioimaging agent it is necessary for the compound to pass, without the aid of a chemical agent, through the cell membrane into the cell. The cell membrane consists of a phospholipid bilayer and numerous protein channels so although water soluble complexes are ideal, a balance between the hydrophobic and hydrophilic characteristics of a molecule need to be maintained. The negative surface on the cell indicates that positively charged molecules are preferred.[21,22]

There are two different routes a molecule can take to enter the cell, energy-dependent or energy-independent. An energy-dependent process, for example endocytosis (being encapsulated in an endosome) or active transport, occurs at temperatures around 37 ˚C (for mammalian cells at least) and so using low incubation temperatures (such as 4 ˚C) it is possible to reduce this uptake mechanism. Energy independent processes include passive diffusion through channel proteins or directly through lipid bilayer.[21]

1.4. Metals in cellular imaging

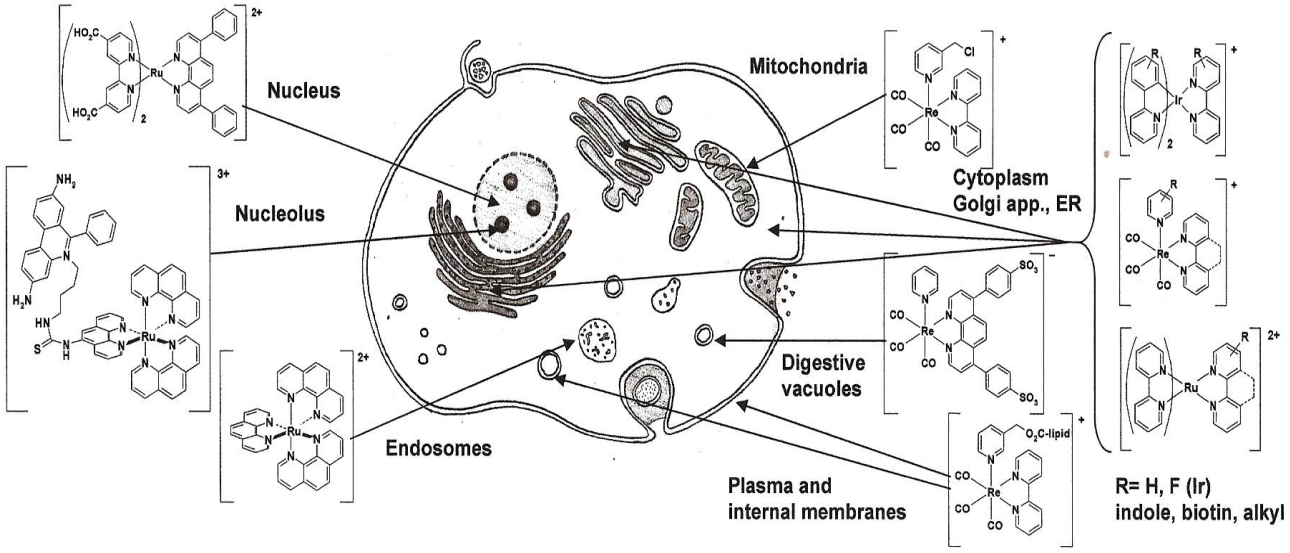

Figure 1.7 A detailed structure of a cell highlighting the localisation patterns of varying d^6 metals. Reproduced from ref. 23.

A cell consists of several organelles, each with their own function. With the number of complexes reported for cellular imaging agents increasing, a preference for localisation in a specific organelle is ideal. A brief summary of the different localisation patterns of different d^6 metal complexes can be seen in figure 1.7.[23] Further examples of metals in imaging are discussed in the following sections.

1.4.1. Lanthanides in imaging

Lanthanide complexes display characteristics that would enable them to be efficient luminophores for cell imaging; they have Stokes shifts greater than 200 nm and emission lifetimes in the range of 0.2-1.5 m.[24] The sharp emission intervals exhibited by complexes of this type enable all other signals to be removed, allowing optimum sensitivity to be achieved. However, despite lanthanide complexes exhibiting the ideal properties for use as a lumophore, there are certain drawbacks to using them in research areas such as biological cell imaging and these drawbacks result from their electronic configuration. Exciting an electron from the ground state is extremely difficult in lanthanide complexes due to excitation involving a f→f transition which is Laporte forbidden. To overcome this obstacle a sensitizing chromophore or 'antenna' for indirect excitation is required.[25] The requirement for an antenna makes this process for lanthanides more complicated (Figure 1.8).

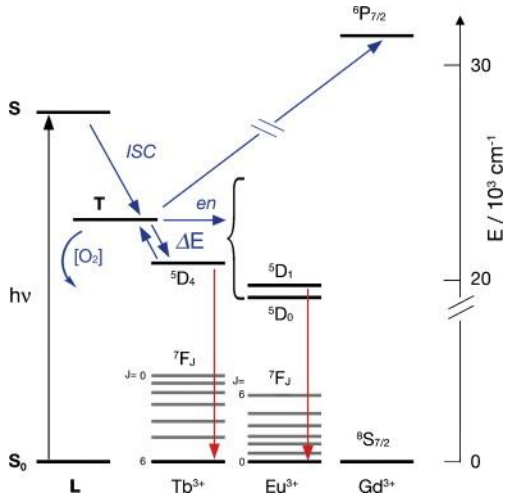

Figure 1.8 The antenna effect for sensitization of the luminescence in some lanthanide cations. Reproduced from ref. 25.

Despite the drawbacks associated with using lanthanides in imaging, a DO3A-type Eu^{III} complex has been shown to target exposed Ca^{2+} ions, binding to scratched/damaged bone surface.[25b]

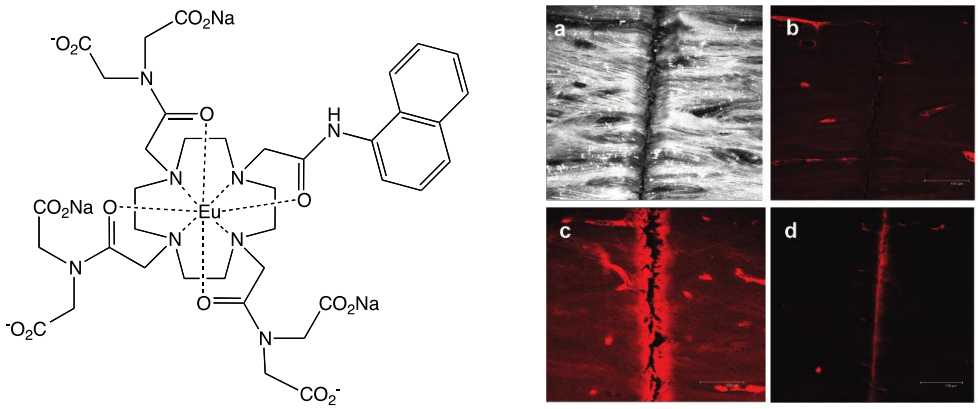

Figure 1.9 A polycarboxylate terminated Eu^{III} complex (LHS) and microscopy images of bone sample immersed in 10^{-3} M solution of the complex. (a) reflected light image: 0 h; (b) control; (c) 4 h; (d) 24 h. Reproduced from ref. 25b.

1.4.2. TM complexes in imaging

The useful photophysical properties of some TMs have resulted in them being heavily investigated for applications as cell imaging agents.[21,22] TM residing in the 2nd and 3rd row of the periodic table, with d^6, d^8, and d^{10} electronic configurations, result in more effective ISC than 1st row complexes leading to highly intense phosphorescent emission. Heavy TMs with a d^6 configuration such as Ru(II), Re(I), Ir(III) and Os(II), when bonded to one or more aromatic bidentate ligands show the ideal photophysical and redox properties required to be useful luminophores. Additionally, the cationic charges associated with metals of this nature increase the likelihood of them being able to interact with the negative surface of the cell[26] and therefore enter the cells.

The photophysical properties of a TM complex are reliant on the ligands attached, in the case of MLCT systems, the ligand attached acting as an electron acceptor.[27]Having both a high degree of stability and tunability, diimine ligands (specifically polypyridines) are generally employed for this role. The diimines, 1,10'-phenanthroline and 2,2'-bipyridine have attracted the greatest attention due to the suitable energy of their lowest occupied molecular orbital (π^*). If the level of the π^* orbital is too low it can result in an increase in the rate of non-radiative decay. If the level of the π^* orbital is too high the rate of both the ^{3}MLCT and non-radiative decay decrease. Both extremes can render a complex a poor luminophore.[4,23,28] It is possible to have more than one diimine ligand attached to the TM and to also have variation in the diimine ligand structure. Variation of the diimine ligand structure can allow for the electronic properties of the complex to be finely tuned.[23] The reducible properties of the diimine ligand make them fitting candidates for allowing the $d\pi \rightarrow \pi^*$ MLCT to occur. The synthetic versatility of both the TM and diimine ligands in a complex allow for research into the expansion of lifetimes, the deactivation processes and the alteration in energy.[14]

1.4.2.1.Iridium in imaging

There have been several investigations into the cellular distribution of highly lipophilic Ir(III) biscyclometallated complexes of the type $[Ir(C\hat{}N)_2(N\hat{}N)]^+$ (where C^N is a monoanionic ligand).[23,29,30] Complexes of this type can have tunable luminescence (red→blue) with lifetimes in the order of μs and quantum yields that reach values of up to 70 % in organic solvents.[23,29] The majority of biscyclometallated Ir(III) complexes reported have demonstrated non-specific localisation in the cytoplasm of Hela cells.[23,29,30]

The first example of a cell imaging application of a complex of this type was reported by Li *et al.*[29] in 2008 with complexes 1 and 2.

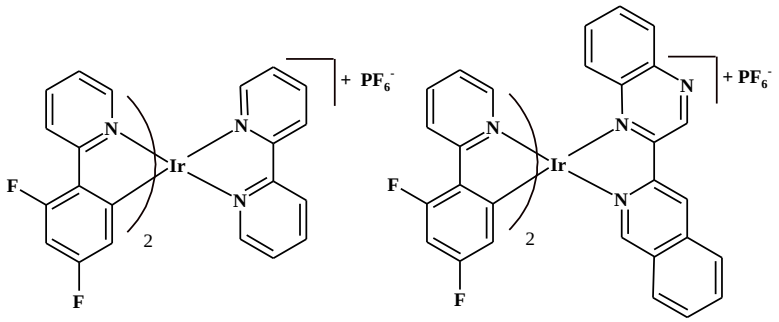

1 **2**

Figure 1.10 Iridium complexes 1 and 2 (varying in the diimine unit) were the first iridium complexes reported with cellular imaging properties.[29]

Complex 1 and 2 both displayed low toxicity with staining of the cytoplasm (Figure 1.10). Shortly after reporting complexes 1 and 2, Lo *et al.*[31] reported a second series of Ir(III) biscyclometallated complexes which demonstrated the structure-function relationship for complexes of this type. The nine complexes in the series varied in the cyclometallated unit and/or the alkyl chain length, thus varying the lipophilicity of the complexes (Figure 1.11). For compounds a-c the lipophilic nature of the complex was shown to increase with the chain length, C_{18}>C_{10}>C_2, however the cellular uptake properties did not follow the same linear fashion, but followed the trend C_{10}>C_2>C_{18} (Figure 1.11). The increased lipophilicity but minimal cellular uptake efficiency of the complex with chain length C_{18} is suggestive of the formation of aggregates; the lipophilic compound arranged in a conformation to minimise any contact with the aqueous media hindering cellular uptake.

The cytotoxic properties of the compounds displayed dependency on the cyclometallated unit and followed the trend 5>4>3.[31] The increased lipophilic nature of compound 5c (C_{18}), when compared to complexes 3-4, resulted in nuclear as well as cytoplasm staining being observed in the Hela cells but the accumulation of this complex was only observed at temperatures > 4 ˚C which indicate that uptake occurred *via* energy dependent processes.

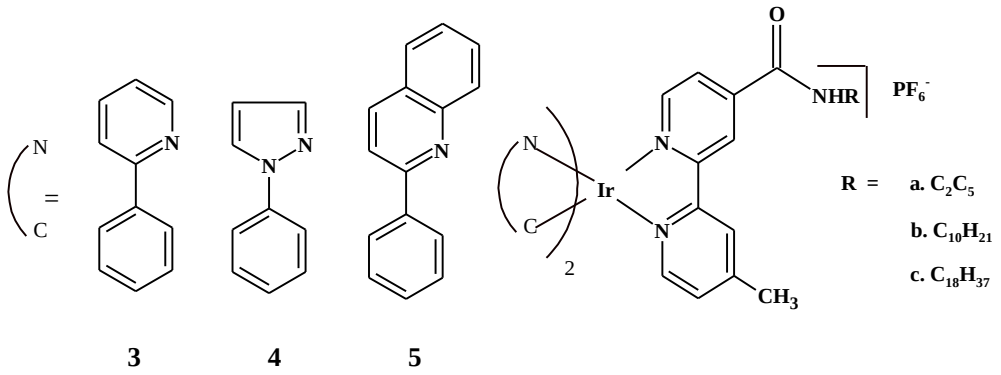

3 **4** **5**

Figure 1.11 Iridium complexes 3-5(a-c) were the second series of iridium complexes reported by Lo *et al*. exhibiting cellular imaging properties.[31]

The variation of the different properties within this series of complexes demonstrates the need of a balance in the lipophilic nature of a compound. If a compound is too lipophilic it is unlikely to be taken up into the cell; an aqueous media is used to 'transport' the compound into the cell, if the compound is too lipophilic it will aggregate and will have limited uptake. If the compound is not lipophilic enough, the compound will not sufficiently cross the outer/inner cell membranes and so specific localisation will not be achieved.

Following Lo's report, collaborative work between Lo and Lam *et al*. in 2010[32] led to a series of Ir(III) dipyridoquinoxaline complexes, varying again *via* the cyclometallated substituents and the alkyl spacers (Figure 1.12). These dipyridoquinoxaline complexes were shown to stain the nucleoli of MCDK cells (Figure 1.13). Localisation in the nucleoli was only visible after long incubation times > 90 mins and was attributed to the complexes residing in hydrophobic pockets of proteins (intercalated into the base-pairs of double stranded DNA).

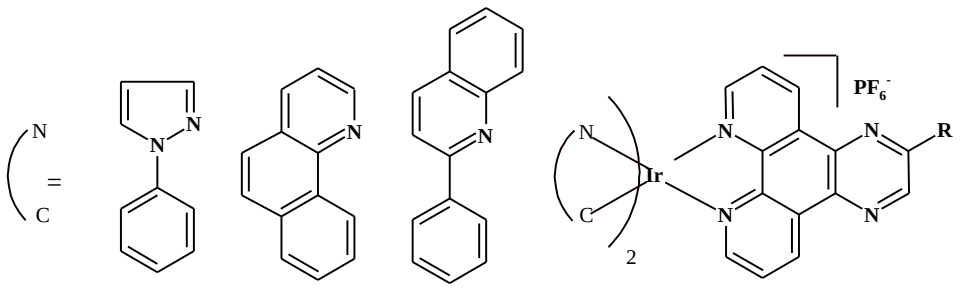

ppy **pzq** **pq** **R = H**

R = CONH(CH2)3CH3

Figure 1.12 Iridium complexes 6-12 reported by Lo and Lam *et al*. each exhibited specific organelle staining with nucleoli localisation.[32]

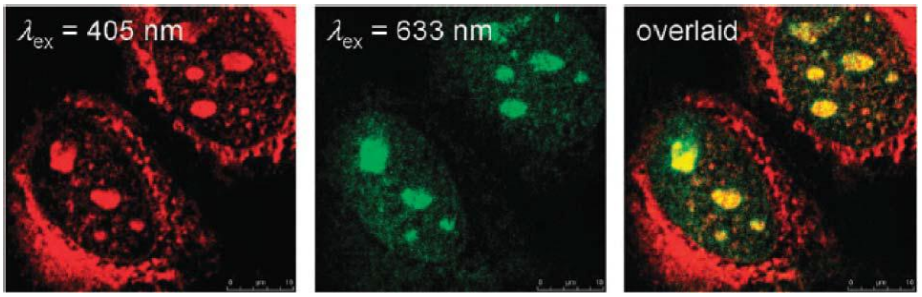

Figure 1.13 Fluorescence laser-scanning confocal microscopy images of fixed MDCK cells treated successfully with fibrillarin antibody (20 µL mL^{-1}, 1 h), Alexa 633 antirabbit IgG antibody (20 µL mL^{-1}, 30 min), and [Ir(ppy)$_2$(R=H)]$^+$. Reproduced from ref. 32.

Both the Li and Lo groups have reported more than twenty iridium complexes exhibiting cytoplasmic staining. Some of the complexes reported are inclusive of bioconjugated complexes; there are several complexes conjugated with a specific molecule for receptor targeting bioimaging applications, for example, indoles or estradiol.[23,31,32] Complexes of this type have shown suitability for applications as bioimaging agents,[29] OLEDS,[33] sensors[34,35] and switches.[36] An interesting report by Velders *et al.*[30] described the suitability of an Ir(III) tris diimine complex as a biomarker in diagnostics. The successful incorporation of 1/2/3 peptides onto the phen unit in the [Ir(phen)$_3$]$^{3+}$ complex resulted in the increased uptake of the compound into the cell. Once inside the cell, the successful visualisation of the chemokine receptor 4 (CXCR4) using FLIM and confocal microscopy was observed. CXCR4 is over expressed in twenty three types of cancer cells.

There have been a huge number of examples of Ir(III) luminophores where good cell uptake and low cytotoxicity with cytoplasmic staining was observed. Occasionally, nuclear staining has been reported which seems dependent on hydrophobic interactions with the cell. However, despite a large number of examples existing, it is still difficult to predict how changes in structure will relate to cell localisation and so further research is required.

1.4.2.2.Ruthenium in cell imaging

The most studied luminescent Ru(II) system is based around a tris-diimine complex, for example a [Ru(N^N)$_2$(N^N)]$^{2+}$. With the tris-diimine system, variation in the nature of substituents on the diimines can 'tune' the luminescence of the compound. Ruthenium polypyridyls tend to have lifetimes in the order of µs and quantum yields that reach the values of 60 % in organic solvents.[1,23] Despite the favourable photophysical properties of complexes of this type, when compared to the number of Ru-based complexes investigated for applications as O_2 sensors or DNA intercalators, there are few examples of Ru-based

complexes reported as suitable cellular imaging agents.[37-41]

A report by Musatkina *et al.*[42] demonstrated how the uptake of Ru(II)-polypyridyl type complexes is dependent on the nature of the diimines with compounds 13-16 (Figure 1.14). The bipy analogues show poor cell uptake, whereas the extended hydrocarbon system of bathophenanthroline shows nuclear staining.

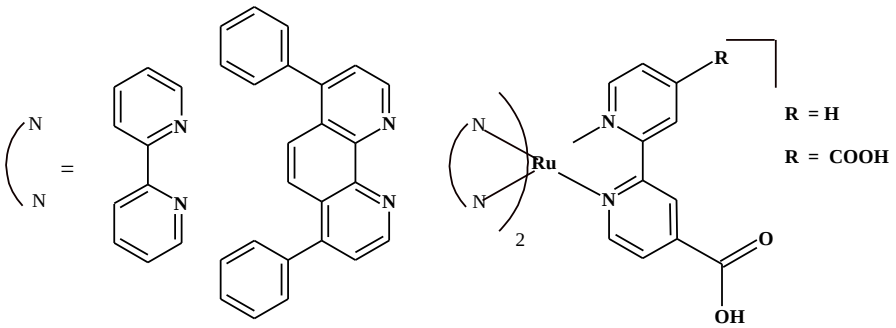

Figure 1.14 Ruthenium complexes 13-16 reported by Musatkina *et al.*[42] highlight the effect of diimines on cell uptake.

Uptake of a complex of the type $[Ru(N\hat{}N)_2(N\hat{}N)]^{2+}$ can be problematic, but there have been several reports where-by the formation of a bioconjugate molecule *via* the addition of estradiol/biotin/peptide to the diimine, has resulted in an increase in uptake and has shown cell department localisation.[43-46] Puckett *et al.*[44] demonstrated how the inclusion of a peptide can improve the uptake efficiency of a Ru(II) tris-diimine complex; $[Ru(bipy)_2(dppz)]^{2+}$ showed poor cellular uptake, however, when conjugated with octarginine, staining of the endosomes was observed and when conjugated with fluorescein, nuclear staining was observed. The difference in localisation of the two complexes was attributed to the differences in their lipophilicity. The difference in their lipophilicity was later confirmed with the synthesis of two $[Ru(Phen)(bipy)(dppz)]^{2+}$ type complexes inclusive of octarginine. The first of the two complexes was inclusive of octarginine only and displayed cytoplasmic staining; the second complex was inclusive of octarginine, but also incorporated a fluorescein conjugate and staining of the cystol, nuclei and nucleoli of HeLa cells was observed (Figure 1.15).[47]

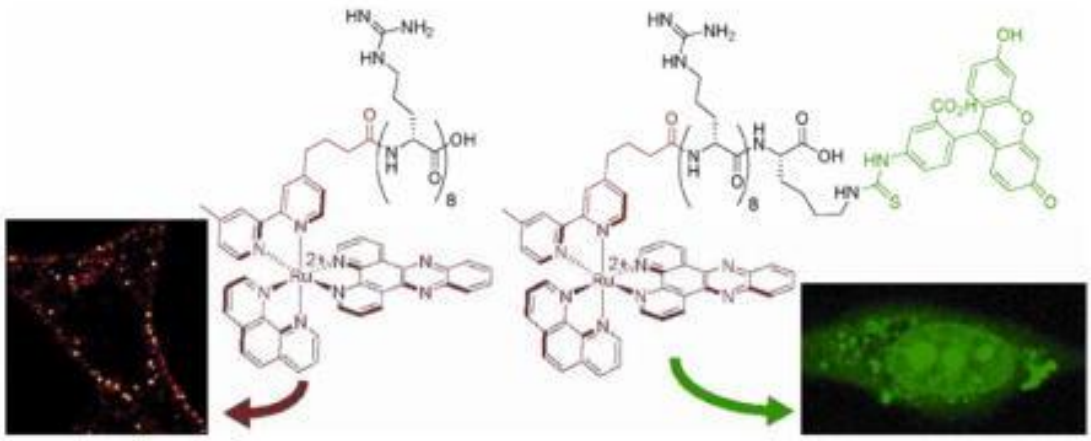

Figure 1.15 [Ru(Phen)(bipy)(dppz)]$^{2+}$ type complexes 17 and 18 inclusive of octarginine (LHS) and octarginine and fluorescein (RHS). Reproduced from reference 47.

An interesting report by Zhang *et al.*[48]demonstrated a Ru(II) complex as a sensor of NO. In absence of NO, the diaminophenyl-substituted Ru(II) compound, compound 19, was non-emissive. In the presence of NO, compound 19 reacts forming compound 19b, an emissive complex (Figure 1.16). Incubation of compound 19 with Gardenia cells resulted in staining of the nucleus and membranes only (Figure 1.17). However, similarly to the Ir complexes discussed, there are unexplored areas of research into this type of compounds with regards to cellular imaging.

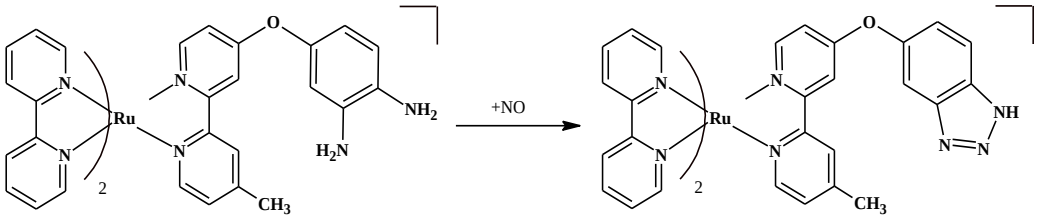

19 **19b**

Fig

Figure 1.16 Rutheium complexes19 and 19b.[48]

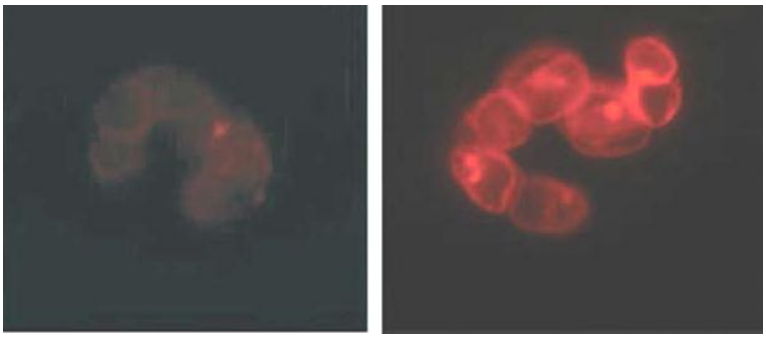

Figure 1.17 Luminescence images of Gardenia cells incubated with complex 19 at different incubation times, 1 h (LHS) and 5 h (RHS). Reproduced from ref. 48.

1.4.2.3. Rhenium in cell imaging

Fac-$[Re(CO)_3(N\hat{}N)L]^+$ type complexes permit a simpler system for exploring modifications in structure and charge on the lipophilicity and toxicity of a complex in comparison to the Ir(III) and Ru(II) complexes discussed above. Many studies involving Re(I) have focused on the *fac*-$[Re(CO)_3(N\hat{}N)L]^+$ type complexes due to the advancement in their photophysical and photochemical properties as well as their inter- and intramolecular processes.[4,20,21] Neutral complexes of this type (*e.g.* L=Cl, Br) tend to have lifetimes in the order of ns and quantum yields that reach the values of 0.1 % in organic solvents. Cationic complexes of this type tend to have lifetimes in the order of μs and quantum yields that can reach exceptional values of 80 % in organic solvents.[23]

The majority of complexes of this type use a halide or an acetonitrile complex as a precursor for introducing the desired axial ligand.[23] The axial ligand will determine the stability of the complex towards substitution. The axial ligand also affects the energy difference between the highest occupied molecular orbital and the lowest unoccupied molecular orbital which has an impact on the predominant charge transfer process that can occur. The main effect of this is seen in the emission and adsorption energies. The stabilisation of the metal dπ using a π accepting ligand results in a blue-shift in excitation and emission wavelengths due to the increased excited state lifetime and decreased rate of non-radiative decay.[25] Numerous investigations have been carried out where the axial ligands or their substituents are π-acceptors, π-neutral or weak π-donors and the same conclusions were drawn; little change in the electronic nature of a complex is seen when altering the axial ligand in comparison to the changes seen with varying the diimine ligand,[23] these changes however, are essential in developing the photophysics of a molecule.

The first example of Re(I) in cell imaging was reported by Zubieta *et al.* in 2004[28] with the bisquinoline based complex, complex 20 (Figure 1.18). Complex 20 was observed to accumulate in the periphery of the leukocytes. Since this report, our group has taken the leading role in the research of complexes of the type *fac*-$[Re(CO)_3(N\hat{}N)L]^+$ reporting the first example of a *fac*-$[Re(CO)_3(N\hat{}N)L]^+$ species in cell imaging in 2007 with complexes 21-27 (Figure 1.19).[20]

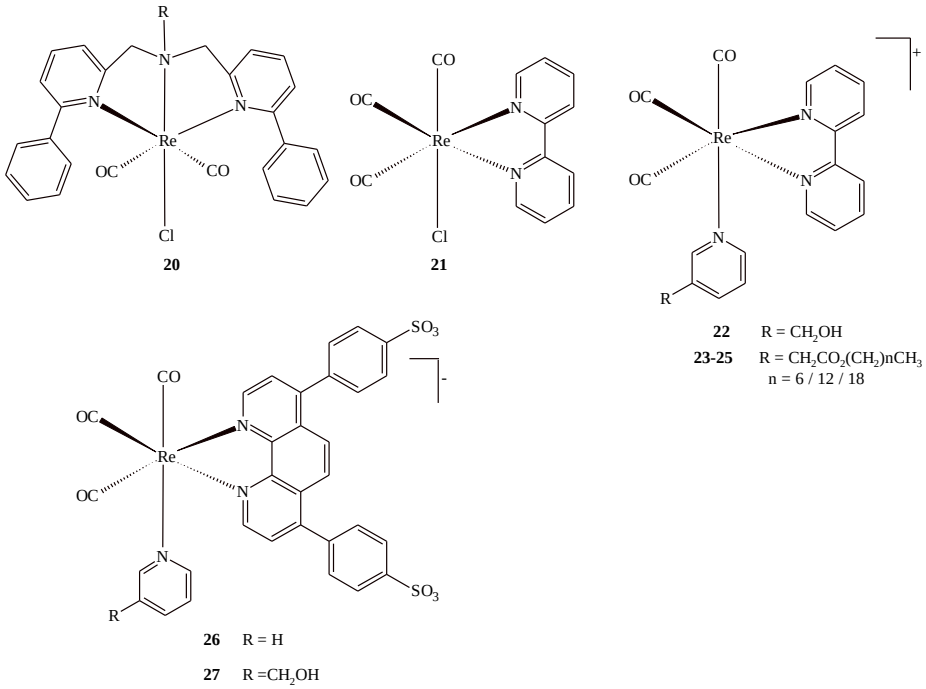

Figure 1.18 Compounds 20-27.[28,57]

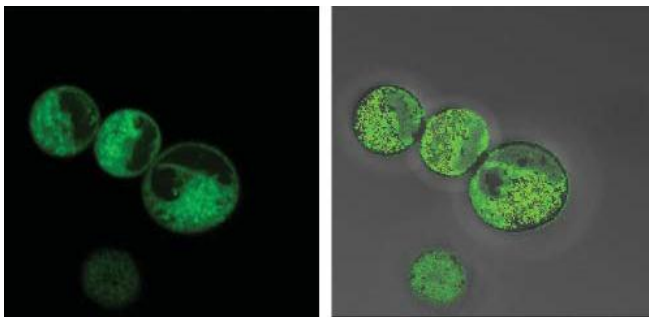

Figure 1.19 Rhenium complex 24 in MCF7 showing cytoplasmic and perinuclear staining. Reproduced from ref. 57.

Similarly to the Ir(III) complexes discussed previously (complexes 1-5[31]), complexes 21-27 demonstrated the structure-function relationship for complexes of this type. Again, the complexes varied in the cyclometallated unit and/or the alkyl chain length or functional group, thus varying the lipophilicity of the complexes (Figure 1.18). The toxicity of the complex was shown to increase with the lipophilicity of the complex; cell lysis was observed with complex 25 (C_{18} alkyl chain length) only. The shorter chained complexes showed good uptake and low toxicity with accumulation in the membrane and membrane structures of the cytoplasm.[49] Small changes in a complex was shown to lead to variation in the localisation pattern observed. For complex 22, the hydroxyl derivative, accumulation in the membrane was observed; following chlorination of the hydroxyl group, specific-staining was observed *via* staining of the mitochondria (Figure 1.20).[50]

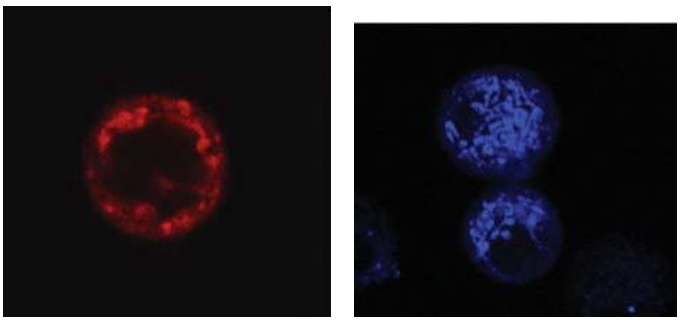

Figure 1.20 Rhenium complexes 22 (LHS) and 23 (RHS) in MCF7 showing different staining. Reproduced for ref. 49 and 50.

1.4.2.4.Gold in imaging

Gold chemistry is of increasing interest due to gold's ability to form luminescent materials.[51,52] The favourable photophysical properties of gold complexes can be attributed to a number of factors including: the nature of the ligands; M-M interactions; and the geometry around the metal centre. The M-M interactions (also referred to as aurophilic interactions) are proposed as key in governing the unique photophysical properties of Au(I) complexes.[51,53] Unlike the aforementioned d^6 heavy TMs, research into luminescent gold complexes for applications as cellular imaging agents is relatively new and thus understudied compared to the Re(I), Ru(II), Ir(III). There are few examples of gold complexes as imaging agents. One of the more interesting examples to date is a gold alkynyl species which was reported by Dyson *et al.*[53] which combined imaging capability with therapeutic activity. The incorporation of a water soluble phosphine ligand, PTA, resulted in a luminescent Au(I) complex which was shown to permeate throughout the entire cell (Figure 1.21).[53]

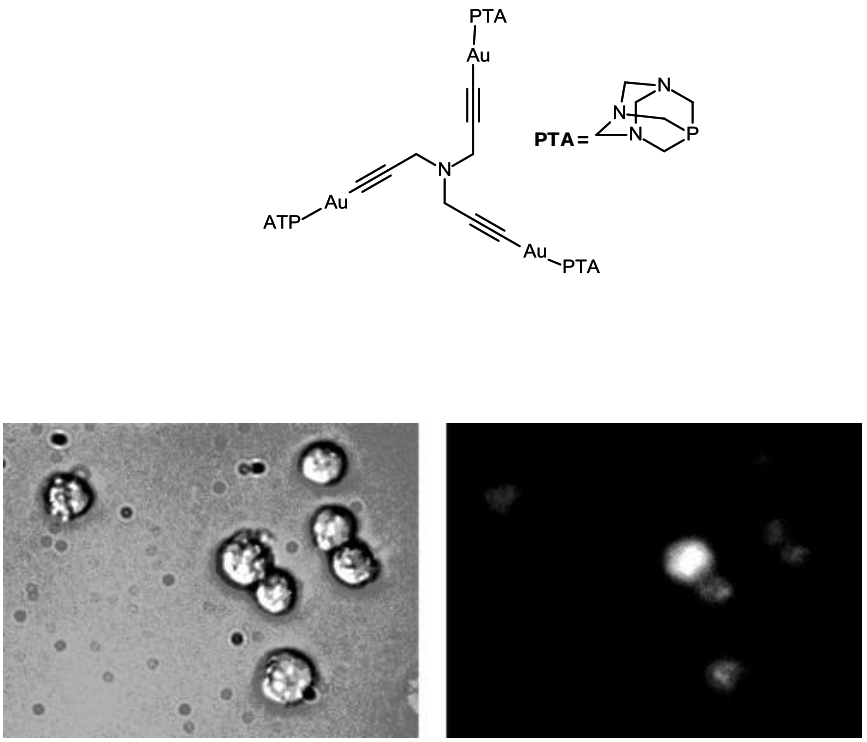

Figure 1.21 An Au(I)-alkyl complex incorporating a water soluble PTA ligand shows non specific cell localisation throughout an entire cell. Cell images reproduced from ref. 53.

Gold is highly researched for its therapeutic potential with applications of both Au(I) and Au(III) based complexes having been studied for many years. Despite the number of studies into gold as a therapeutic agent, its mechanistic details are poorly understood. Gold has a higher affinity for thiolates when compared to nitrogen or oxygen and so binds to DNA weakly, this suggests DNA-based cytotoxic-mechanism is unlikely and promotes as a target.[51] Further discussion of Au(I) based complexes in therapeutics and cellular imaging can be found in Chapter 5.

1.5. TM complexes in therapeutics

The cytotoxicity of a complex can be efficiently tuned through modification of its composition. This was previously discussed with Ir(II) and Re(I) complexes where-by increasing the lipophilic nature of the complex resulted in an increased cytotoxic effect. The ease of modifying the structure and so properties of a TM complex has led to their cytotoxic effects being heavily investigated for applications in therapeutics. To be a successful therapeutic agent, a compound must be able to cross the cell membranes, this is critical for useful cytotoxic properties. Once inside the cell, cytotoxicity can arise from the inhibition of cellular function/activity and or the distribution of structures. To date there are a wide range of metals used in therapeutics, some of which are discussed in detail below.

1.5.1. Platinum in therapeutics

Platinum is now one of the more widely used metals in therapeutics for the treatment of cancer, with several complexes already in clinical use (Figure 1.22).[51] The most common platinum-based compound is cisplatin. Cisplatin is a neutral complex that passes with ease into the cell. Once inside the cell the neutral compound undergoes intracellular hydrolysis to the more reactive complex $[Pt(NH_3)_2(H_2O)_2]^{2+}$. The interaction of cisplatin with both DNA and RNA has been extensively studied and cisplatin-DNA interaction is now known to be responsible for cell death.[51,52] A number of cisplatin-DNA compounds have been formed and their crystal structures have shown irreversible binding of the platinum compound to two adjacent N donors on the same DNA strand. This interaction is thought to inhibit replication, transcription and repair functions of the DNA, resulting in apoptosis (programmed cell death). This interaction with DNA can also account for the limited activity of the trans complex when compared to the cis.[51,52] Despite there being ample evidence suggesting a cisplatin-DNA interaction there have been reports questioning the exact mechanism of interaction.[51]

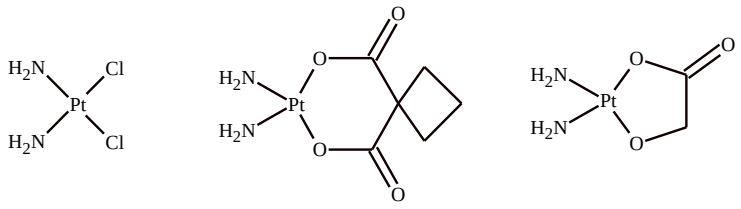

Figure 1.22 Cisplatin (LHS), carboplatin (centre) and 254-*S* (RHS).[51]

1.5.2. Ruthenium in therapeutics

Similarly to Pt, Ru based complexes have been extensively studied for applications as therapeutic agents. When compared to the previously discussed Pt-based complexes, Ru-type complexes have more synthetic versatility; a higher number of ligands can be situated around the octahedral ruthenium atom when compared to the square planar Pt(II) complex. Additionally, a higher number of different bonds can be formed using a Ru unit when compared to Pt, therefore mechanistically, Ru-based complexes are not restricted to DNA-binding. The suggested route for uptake into cells for Ru-based complexes is *via* uptake with iron using transferrin apoprotein.[54]

The first ruthenium compounds to enter clinical trials were KP1010 and NAMI-A (Figure 1.23). For the two structurally similar Ru(III) complexes, different anticancer activity was observed. KP1019 displayed higher activity towards primary cancers (main tumour mass) whereas activity towards secondary cancers was observed with NAMI-A. RAPTA compounds displayed similar characteristics as the structurally dissimilar NAMI-A compound with activity against secondary cancers being observed (Figure 1.23); RAPTA has since been considered as the most successful Ru-based anticancer complex. Again, despite the high level of research that has been conducted with Ru-based complexes for application in therapeutics there is still a requirement for understanding the mechanism of action.[54]

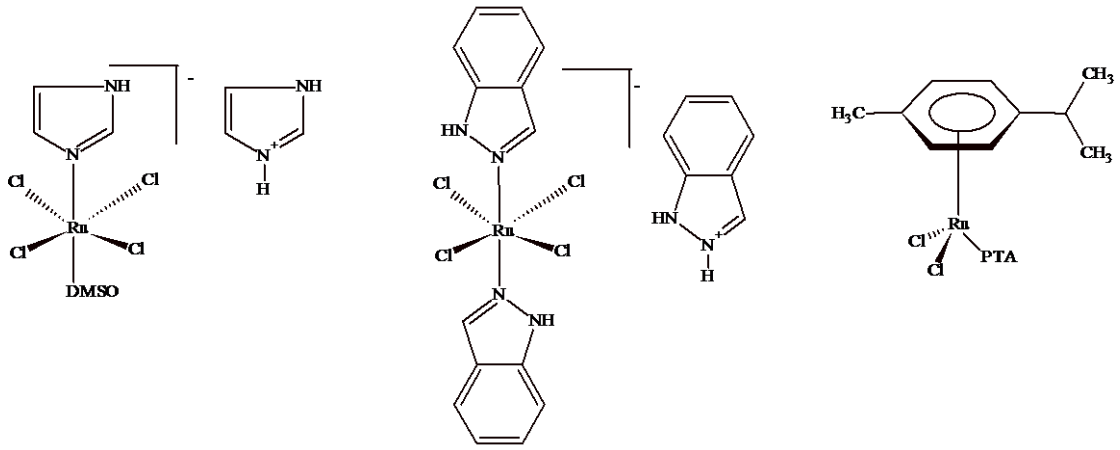

Figure 1.23 NAMI-A (LHS), KP1019 (centre) and RAPTA (RHS)[51]

1.6. Aims

The work within this thesis aims to: further understand the solvent dependent photophysical properties of Re(I)-based complexes; explore the photophysical and cytotoxic properties of Au(I)-based complexes with a view to biological imaging and/or therapeutic potentials; and finally, explore the potential applications of hetero-metallic complexes based on Re(I)/Ru(II)/Ir(III) with Au(I) as dual-functioning cellular and therapeutic agents.

1.7. General measurements

1.7.1. Photophysical data

All starting materials, reagents and solvents were purchased from commercial suppliers and used as supplied unless otherwise stated. ^{1}H-NMR and ^{13}C-NMR spectra were recorded at 400 and 100 MHz respectively on a Bruker Avance DPX, or 250 MHz and 62 MHz respectively on a Bruker Avance DPX 250. ^{31}P-NMR were recorded on a Jeol Eclipse 300MHz at 121 MHz. All NMR spectra were referenced to residual solvent peaks unless otherwise reported. IR spectra were recorded on a Perkin Elmer 1600 FT IR as thin films or nujol mulls and are reported in wavenumbers (cm^{-1}). UV-vis data were recorded as solutions on a Jasco 570 spectrophotometer. Mass spectra were recorded on a VG Fisons Platform II or at the EPSRC national mass spectrometry service, Swansea (HRMS). Elemental analyses were performed by Warwick Analytical Services (University of Warwick). All photophysical data were obtained on a JobinYvon-Horiba Fluorolog spectrometer fitted with a JY TBX picosecond photodetection module. Luminescence lifetimes were obtained using either 295 nm or 372 nm nanoLEDs operating at 1 MHz. All lifetime data were collected using the JY-Horiba FluoroHub single photon counting module in multi-channel scaler mode. Lifetimes were obtained using the provided software, DAS6. Estimated errors are τ_{em} ± 10% and excitation and emission maxima are limited in accuracy to the monochromator slit width of 5 nm.

1.7.2. Method for cytotoxicity analysis

Anti-tumour evaluation in MCF7, LoVo, A549 and PC3 cell lines was performed by MTT assay. Compounds were prepared as 0.1–100 mM stock solutions dissolved in DMSO and stored at -20 °C. Cells were seeded into 96-well microtitre plates at a density of 5×10^3 cells per well and allowed 24 h to adhere. Decimal compound dilutions were prepared in medium immediately prior to each assay (final concentration 0.1–100 μM). Experimental medium was DMEM +10% FCS (PC3 and Lovo) or RPMI +10% heat inactivated FCS (A549 and MCF7). Following 96 h compound exposure at 37 °C, 5% CO_2, MTT reagent (Sigma Aldrich) was added to each well (final concentration 0.5 mg/ml). Incubation at 37 °C for 4 h allowed reduction of MTT by viable cells to an insoluble formazan product. MTT was removed and formazan solubilised by addition of 10% Triton X-100 in PBS. Absorbance was read on a Tecan Sunrise spectrophotometer at 540 nm as a measure of cell viability; thus

inhibition relative to control was determined (IC_{50}).

1.7.2. Method for cellular imaging

Human adenocarcinoma cells (MCF-7), obtained from the European Collection of Cell Cultures, Porton Down, Wiltshire, U.K., were maintained in Hepes modified minimum essential medium (HMEM) supplemented with 10% fetal bovine serum, penicillin, and streptomycin. Cells were detached from the plastic flask using trypsin−EDTA solution, and suspended in an excess volume of growth medium. The homogeneous cell suspension was then distributed into 1 mL aliquots with each aliquot being subject to incubation with the complexes final concentration 50 μg mL−1, at 4 °C for 30 min. Cells were finally washed three times in phosphate buffer saline (PBS, pH 7.2), harvested by centrifugation (5 min, 800 g), and mounted on a slide for imaging. Preparations were viewed using a Leica TCS SP2 AOBS confocal laser microscope using X63 objective, with excitation at 405 nm and detection at 510−580 nm. Z-plane slices were used to record multiple single-plane views cell populations to estimate percentage uptake of lumophores.

1.8. References

1. J. Wilkinson, H. Puschmann, J. A. K. Howard, C. E. Foster and J. A. G. Williams, *Inorg. Chem.*, 2006, **45**, 8685.
2. L. Prodi, F. Bolletta, M. Montalti and N. Zaccheroni, *Science.Direct.*, 2000, **205**, 59.
3. A. J. Amoroso, R. J. Arthur, M. P. Coogan, J. B. Court,V. Fernández-Moreira, A. J. Hayes, D. Lloyd, C. Millet and S. J. A. Pope, *New J. Chem.*, 2008, **32**, 1097.
4. M. P. Coogan, V. Fernández-Moreira, J. B. Hess, S. J.A. Pope and C. Williams, *New J. Chem.*, 2009, **33**, 1094.
5. A. Juris, V. Balzoni, F. Barigelletti, S. Campagna, P. Belser and A. Von Zelewsky, *Coord. Chem. Rev.*, 1988, **84**, 85.
6. www.shsu.edu accessed 10/8/2012
7. J. R. Lacowicz. *Principles of Fluorescence spectroscopy,* 3rd ed., Springer. 2006.
8. F. W. D. Rost. *Quantitative Fluorescence Microscopy*, Cambridge University Press. 1991.
9. N. Billington, and A. W. Knight, *Anal Biochem*., 2001, **291**, 175.
10. M. Neumann, and D. Gabel, *J. Histoche. Cytochem*., 2002, **50**, 437.
11. www.Current.Protocols.com. Accessed 15/7/2012.
12. V. Yam and K. Lo, *Coord. Chem. Rev.*, 1998, **184,** 157.
13. L. Sacksteder, A. P. Zipp, E. A. Brown, J. Streich, J. N. Demas and B. A. Degraff, *Inorg. Chem.*, 1990, **29**, 4335.
14. L. Karki and J. T. Hupp, *Inorg. Chem.*, 1997, **36,** 3318.
15. (a) M. J. Li, W. M. Kwok, W. H. Lam. C. H. Tao, V. Wing-Wah and D. L. Phillips, *Organometallics*., 2009, **28**, 1620; (b) J. A. Braun, C. L. Caluwe, P. Szwarc, *Chem. Phys.Lett*., 1978, **54,** 469; (c) B. Messier, P. Gauthier, S. Gravel and D. Durocher, *J. Photochem. Photobiol. Chem*., 1990, **52**, 165. (d). S. Speiser, *Chem. Rev*., 1996, **96**, 1953.
16. **www.cas.utpb.edu.co.uk.** Accessed 02/5/2012.
17. F. L. Thorp-Greenwood and M. P. Coogan, *Dalton. Trans*., 2011, **40**, 6129.
18. J. B. Pawlet, *Handbook of Biological Confocal Microscopy*, Springer, New York, 2006.
19. N. Billington and A. W. Knight, *Anal. Biochem*., 2001, **291**, 175.
20. A. Juris, V. Balzani, F. Barigellatti, S. Campagna, P. Belser and A. Von Zelewsky, *Coord. Chem. Rev*., 1998, **84**, 85.
21. T. J. Henly, *Coord. Chem. Rev.*, 1989, **93**, 269.
22. V. Fernández-Moreira, F. L. Thorp-Greenwood, and M. P. Coogan, *Chem. Commun*., 2010, **46**, 186.
23. J. C. G. Bunzil, S. Comby, and A. S. Chauvin, *J. Rare Earths*., 2007, **25**, 257.
24. (a) H. L. Handl and R. J. Giles, *Life. Sciences.*, 2005, **77**, 361; (b) C. A. Tolman, *Chem. Rev.*, 1977, **77**, 313.
25. L. Jin, P. A. Mclean, B. G. Neel and H. H. Wortis, *J. Exp. Medicine*., 2002, **195**, 1999. (b) B. McMahon, P. Mauer, C.P. McCoy, T.C. Lee, T. Gunnlaugsson, *J. Am. Chem. Soc.*, 2009, **131**, 17542.
26. J. N. Demas, and B. A. Degraff, *Coord. Chem. Rev.*, 2000, **211**, 317.
27. K. A. Stephenson, S. R. Banerjee, T. Besenger, O. O. Sogbein, M. K. Levadala, N. McFarlane, J. A. Lemon, D. R. Boreham, K. P. Maresca, J. D. Brennan, J. W. Babich, J. Zubieta and J. F. Valliant, *J. Am. Chem. Soc*., 2004, **126**, 8598.
28. M. Yu, Q. Zhao, L. Shi, F. Li, Z. Zhou, H. Yang, T. Yia and C. Huang, *Chem. Commun*., 2008, 2115.
29. J. Kuil, D. Steununberg, P. T. K. Chin, J. Oldenburg, K. Jalink, A. H. Velders and F. W. Leewen, *Chem. BioChem*., 2011, **12**, 1897.

30. K. K. Lo, P. K. Lee and J. S. Y. Lau, *Organometallics*., 2008, **27**, 2998.
31. K. Y. Zhang, S. P. Y. Li, M. Y. Zu, I. W. S. Or, M. S. H. Cheung, Y. W. Lam and K. K. W. Lo, *Inorg. Chem*., 2010, **49**, 2530.
32. J. O. Huh, M. H. Lee, H. Jang, K. Y. Hwang, J. S. Lee, S. H. Kim, and Y. Do, *Inorg. Chem*., 2008, **47**, 6566.
33. K. K. Lo, D. C. Ng and C.-K. Chung, *Organometallics*., 2001, **20**, 4999.
34. A. Habibagahi, Y. Mebarki, Y. Sultan, G. P. Yap and R. J. Crutchley, *ACS, Appl. Mater. Interfaces*., 2009, **1**, 1785.
35. F. Zapata, A. Caballero, A. Espinosa, A. Tárraga and P. Molina, *Dalton. Trans*., 2009, 3900.
36. C. A. Puckett and J. K. Barton, *J. Am. Chem. Soc*., 2007, **129**, 46.
37. B. Onfelt, L. Gostring, P. Lincoln, B. Norden and A. Onfelt, *Mutagenesis*, 2002, **17**, 317.
38. M. J. P. Leiner, *Anal. Chim. Acta*., 1991, **255**, 209.
39. C. A. Puckett and J. K. Barton, *J. Am. Chem. Soc*., 2009, **131**, 8739.
40. K. K-W. Lo, T. K.-M. Lee, J. S.-Y. Lau, W.-L. Poon and S.-H. Cheng, *Inorg. Chem*., 2008, **47**, 200.
41. E. Musatkina, H. Amouri, M. Lamoureux, T. Chepurnykh and C.Cordier, *J. Inorg. Biochem*., 2007, **101**, 1086.
42. U. Neugebauer, Y. Pellegrin, M. Devocelle, R. J. Forster, W. Signac, N. Morand and T. E. Keyes, *Chem. Commun*., 2008, 5307.
43. C. A. Puckett and J. K. Barton, *J. Am. Chem. Soc*., 2008, 5307.
44. K. K.-W. Lo and T. K.-M. Lee, *Inorg. Chem*., 2004, **43**, 5275.
45. K. K.-W. Lo and T. K.-M. Lee, *Inorg. Chem. Acta*., 2007, **360**, 293.
46. C. A. Puckett and J. K. Barton, *J. Am. Chem. Soc*., 2009, **25**, 8738.
47. R. Zhang, Z. Q. Ye, G. L. Wang, W. Z. Zhang and J. L. Yuan, *Chem. –Euro.J*., 2010, **16**, 6884.
48. A. J. Amoroso, M. P. Coogan, J. E. Dunne, V. Fernández-Moreira, J. B. Hess, A. J. Hayes, D. Lloyd, C. Millet, S. J. A. Pope and C. Williams, *Chem. Commun*.,2007, 3007.
49. A. J. Amoroso, R. J. Arthur, M. P. Coogan, J. B. Court, V. Fernández-Moreira, A. J. Hayes, D. Lloyd, and S. J. A. Pope, *New. J. Chem*,,2008, **32**, 1097.
50. P. J. Sadler and Z. Guo, *Pure & Appl. Chem*., 1998, **70**, 863.
51. P. Pil and S. J. Lippard, *Encyclopedia of Cancer. Ac. Press*., 1997, **1**, 392.
52. M. A. Fuertes, J. Castillo, C. Alonso and J. M. Prez, *Current. Med. Chem*., 2003, **10**, 257.
53. E. Vergara, E. Cerrada, A. Casini, O. Zava, M. Laguna and P. J. Dyson, *Organometallics*., 2010, **39**, 2596.
54. S. Page, *Edu. In. Chem*., 2012, 26.

Chapter 2 The Modulation of Luminescent Properties Of Mono-Metallic Re(I) Complexes Bearing Axial Functionalised Alkyl Chains by Hydrophobically Driven, Intra- And Intermolecular Conformational Changes.

2.1. Introduction

The first half of this chapter reports the synthesis of a series of novel long-chained ligands bearing a terminal chromophore moiety or methyl group coordinated to a *fac*-$[Re(CO)_3(N\text{^}N)]^+$ core for investigations into solvent-dependent luminescent properties. The second half of the chapter reports the synthesis of novel $[Re(CO)_3(bipy)]^+$ complexes and coumarin-based ligands appended with a biotin moiety to investigate their avidin-biotin binding properties and to further understand the solvent-dependent luminescent properties of all the complexes reported herein.

2.1.1. *fac*-[Re(CO)$_3$(N^N)L]

Many studies involving d^6, low spin Re(I) have focused on *fac*-$[Re(CO)_3(N\text{^}N)L]$ type complexes due to their stability, redox properties and luminescent characteristics, with bipy and phen diimines being the more commonly investigated. Useful properties of complexes of this type include: the ability to add ligands step-wise, the presence of only one diimine ligand (which allows for the charge transfer process to be controlled) and the ability to synthesise a huge range of diimine and axial pyridines or derivatives. The latter property allows for the electronic and photophysical properties of the complex to be 'tuned'. This best achieved through the variation of the diimine unit, however, variation of the axial ligand has proven vital for investigations into cell imaging, lipophilicity etc. [1,2,3]

With excitation around 340-420 nm and their well-known ^{3}MLCT emission around 530-600 nm (allowing visible detection) *fac*-$[Re(CO)_3(N\text{^}N)L]$ complexes display the desirable large Stokes shifts required to be effective luminophores. Additionally, cationic derivatives of this type of complex typically show an extension in the emission lifetime from 100's of ns to μs. [4-8]

2.1.2. Solvent-dependant photophysical properties

The photophysical and photochemical properties of a *fac*-$[Re(CO)_3(N\text{^}N)L]$ type complexes can be tuned through variation in the co-ordinating ligands and the solvent properties. The latter has been less exploited in the investigation into the enhancement of luminescence properties of TM complexes, despite solvatochromic studies being routinely used to identify the charge transfer nature of excited state.

The first investigation into the effect that water solvent has on the emission properties of *fac*-$[Re(CO)_3(N\text{^}N)L]^+$ type complexes was reported by our group in 2009[9] as an extension of the report discussing the first application of a *fac*-$[Re(CO)_3(N\text{^}N)L]^+$ complex in cellular

imaging.[2] In the investigation, a series of ligands equipped with varying lengths of aliphatic chain, C_2, C_6 and C_{12} were synthesised and co-ordinated to a $[Re(CO)_3(bipy)]^+$ unit. The luminescent properties of all three complexes were then measured in both acetonitrile and water. The biggest effect of the change of solvent was seen with the C_{12} aliphatic chain (Figure 2.1).

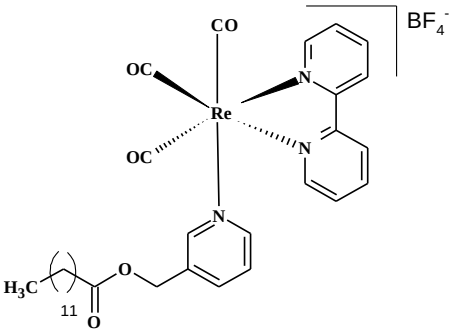

Figure 2.1 The photophysical properties of *fac*-$[Re(CO)_3(bipy)L(C_{12})]^+$ was greatest effected when the solvent was changed from acetonitrile to water.[9]

When measured in acetonitrile the expected emission properties were observed, λ_{em} = 555 nm and τ = 176 nm. However, in water the emission was blue-shifted, λ_{em} = 523 nm, and the lifetime dramatically extended, τ = 688 ns. These results are contrary to what are predicted in the simple solvation model (in which very polar solvent can stabilise dipolar excited state), which therefore suggests a partial shielding of the central $[Re(CO)_3(bipy)]^+$ unit from the solvent.[9]

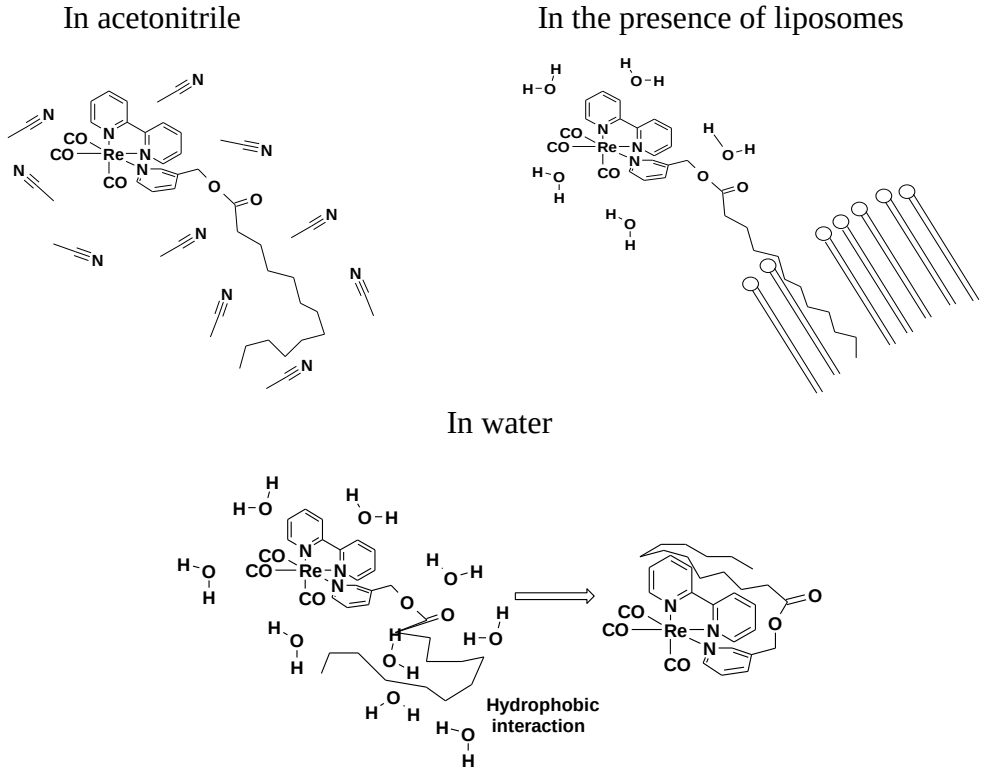

Figure 2.2 Cartoon diagram depicting the orientation of the alkyl chaing in different solvents.

When the complex equipped with a C_{12} chain was introduced to an aqueous media, in the presence of lipid membranes, the same photophysical data for MeCN was observed (Figure 2.2). This observation, along with the observed emission and lifetime of complex in H_2O being similar to that in hexane (Figure 2.3), led to the proposed hypothesis that intramolecular hydrophobically driven interactions were occurring.

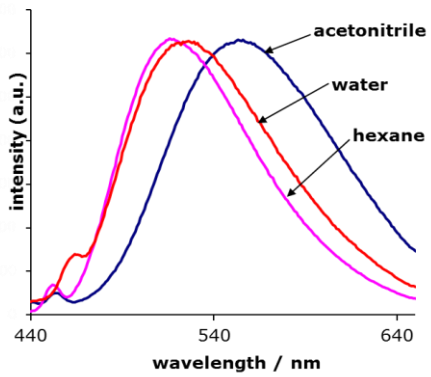

Figure 2.3 Reproduced steady state emission spectra for $[Re(CO)_3(bipy)L(C_{12})]^+$ recorded in different media (λ_{exc} 345 nm).[9]

2.1.3. Hydrophobic interactions

A hydrophobic molecule is one that does not have a favourable interaction with polar environments such as water and so will tend to arrange itself into a conformation that minimises its contact with that solvent. There are several conformations known, some more energy favourable than others. If a complex contains a hydrophilic region (head) attached to a hydrophobic region (tail) when in a polar solution, it simultaneously forms aggregates. These aggregates tend to be either a micelle or a bilayered structure and are formed as a result of a process referred to as the hydrophobic effect (Figure 2.4).

Figure 2.4 The arrangements of both the micelle and bilayered structure. [15]

The aggregate structure is dependent on both the length of the hydrophobic region (hydrocarbon chain), and size of the hydrophilic region. In complexes where a sufficiently sized aliphatic chain is attached to a polar group it may be energetically unfavourable for one of the two aggregates discussed above to form, but more favourable for chain wrapping or fold-back to occur.[16]

2.1.4. Resonance Energy Transfer (RET)

Resonance energy transfer (RET) was discussed briefly in Chapter 1. It describes the process where the energy that is absorbed by one molecule (donor) is transferred non-radiatively to a second molecule (acceptor) (Figure 2.5). RET can occur between intra- and intermolecular chromophores but is dependent on the orientation and distance between the chromophores. When investigating intramolecular hydrophobic interactions, in particular the mechanisms by which they occur (*e.g.* chain wrapping/ fold back) RET can be a useful technique to probe conformation.

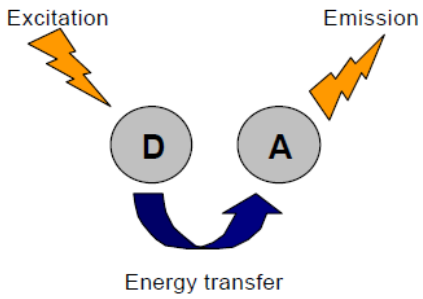

Figure 2.5 Acceptor emitting energy transferred from the donor.[10]

There are two mechanisms by which non-radiative energy transfer can occur; Förster and Dexter energy transfer. The main difference between these two transfer processes is the distance over which they can occur. Förster energy transfer results from Coulombic interactions (dipole-dipole interactions) between the donor and acceptor, it can occur over a large distance 10-100 Å, and is strongly dependent on spectral overlap. This process is most efficient for singlet-singlet transitions as multiplicity-conserving transitions have large transition dipoles (Figure 2.6). The rate of energy transfer is shown in Figure 2.7.[11,12]

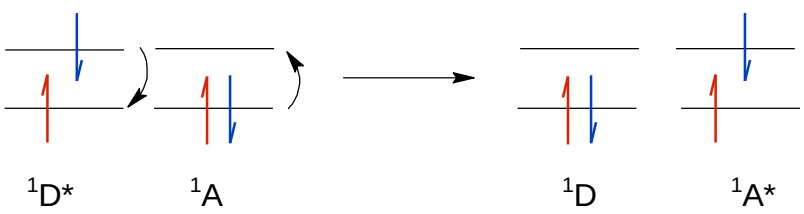

Figure 2.6 Förster energy transfer, singlet-singlet

$$K = 1/\tau_D (R_0/r)^6$$

Figure 2.7 Förster energy transfer. (K= rate of energy transfer, τ_D = decay time of donor excited state, R_0 = Förster distance (distance where energy transfer is 50 %, around 20-60 Å) and r = donor-acceptor distance.

Dexter energy transfer is a shorter range process and can only occur for distances less than 10 Å. It is dependant on temperature and orbital overlap and its efficiency decreases exponentially with distance. The donor and acceptor exchange an electron, the exchanged electron occupies the vacant orbital of the acceptor, thus Dexter energy transfer can be applied to produce the triplet state of the molecule of interest (acceptor).[11-14]

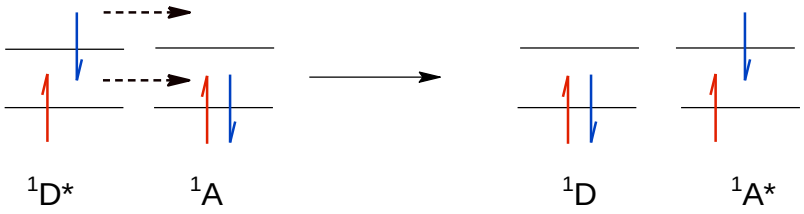

Figure 2.8 Dexter energy transfer, singlet-singlet

Whenever the R_0 (Förster distance) is smaller than the molecular contact distances, electron exchange (Dexter) is dominant. The rate of electron transfer is dependent on the following equation.

$$k_{ET} = \exp(-2r/L)\, J$$

Figure 2.9 Dexter energy transfer. Rate of Dexter electron transfer (r = donor to acceptor distcance, L = constant related to orbital radii of donor and acceptor, J= extent of spectral overlap).

2.1.5. Biotinylation in exploring RET

To understand any RET processes which may be occurring between two chromophores on the same molecule (thus exploring any intramolecular hydrophobic interactions) the effects of intermolecular interactions between the two chromophores should also be known. The binding of up to four biotins to avidin can result in fluorophores being brought within their Förster distances. For many organic fluorophores, where Stokes shifts are small, this can result in self quenching through RET. Biotin-avidin binding is an area of research that can allow the exploration into RET between two chromophores on separate molecules.

Avidin is a tetrameric glycoprotein found in chicken egg whites with a molecular weight of *ca.* 4 × 15000.[17,18] It has four substrate binding sites each with a depth of *ca.* 15 Å specific for the binding of a small molecule of biotin, otherwise known as vitamin H (Figure 2.10),[19] (Biotin is a water soluble molecule often found in the biochemical pathway of fat metabolism). The affinity between avidin and biotin is the strongest known non-covalent bond between a protein and a ligand with a dissociation constant / K_d = 10^{-15} M. The numerous hydrogen bonds and VDW interactions which are formed when biotin binds to the hydrophobic avidin pocket result in avidin: biotin binding being irreversible (high eq constant) and thus the biotinylation of molecules is widely used in diagnostics which require the use of irreversible bonds with specific linkages between biological macromolecules.[17-19]

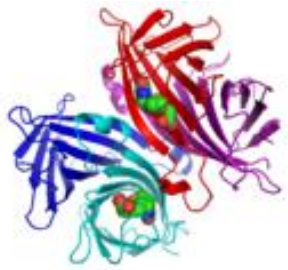

Figure 2.10 Tetrameric structure of streptavidin (homologous protein of avidin) with two bound biotins.[18]

2.1.6. Biotinylation of TM

The biotinylation of fluorophores can aid in cellular uptake as biotinylated species can be actively transported into cells by some of the existing mechanisms for biotin uptake.[17,19-21] The conjugation of TM complexes to biotin seems a promising route for delivery of TM complexes into cells. The Lo group have taken the leading role inr research into biotinylated complexes reporting both Ir(III) and Re(I) biotinylated complexes. Both types of biotinylated

complexes have reported show photophysical properties identical to that of the parent complexes. Several examples of both TM complexes (Ir(III)/Re(I)) exist where biotin is appended to pendant chains of varying length and incorporating different linking units (ester/amide).[22-29]

2.1.6.1. Biotinylated Ir(III) complexes

The binding pockets of avidin are small and hydrophobic in nature and so when biotinylated complexes are bound to avidin an increase in emission intensity can sometimes be seen. Lo *et al.*[26] highlighted the effect of different chain lengths on the emission intensity of biotinylated Ir(III) complexes when bound to avidin (Figure 2.11).[26]

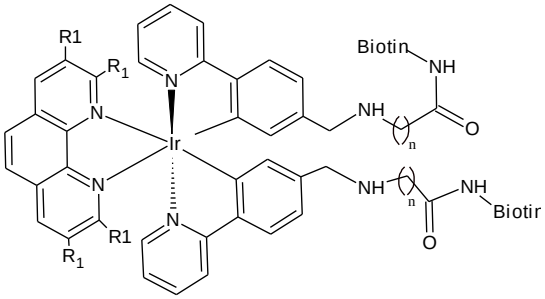

1a. R1 = Me; n = 2

1b R1 = Me; n = 6

1c R1 = Ph; n = 2

1d R1 = Ph; n = 6

Figure 2.11 Ir(III)-biotin complexes reported by Lo *et al*.[26]

For the smaller chain lengths (C_2 chain, **1a** and **1c**) a two-fold increase in emission intensity was observed. This increase in emission was attributed to the increased rigidity of the complex and the shielding nature of the hydrophobic pocket, however, the presence of the shorter chain led to higher K_d values (less efficient binding). K_d values are a lot smaller with **1a** (C_2 chain with methyl substituent) when compared to **1c** (C_2 chain with phen substituent) which suggests the substituent (as well as chain length) has some effect on binding properties of the complex. Further research by this group reported the length of the spacer had the greater effect on the binding efficiency of biotinylated complexes to avidin.[26]

The reports by the Lo *et al* group can be summarised with the need for a compromise; too short a chain will lead to a poor binding efficiency where as too long a chain leads to diminished emission enhancement;'C_6 appears to be a reasonable compromise'.[1]

2.1.6.2.Biotinylated Re(I) complexes

Lo *et al.*[27-29] have also dominated research in this area having reported several successful variations in the biotinylation of Re(I) complexes in addition to reporting the first class of luminescent biotinylation reagents derived from $[Re(CO)_3(N\text{^}N)]^+$ type complexes. In 2005 analogous results to those of the iridium complex were reported. Through the employment of different spacer arms (ethyl and hexyl), different linking groups between the Re(I) luminophore and biotin group (Figure 2.12), and the variation of diimines (phen, Me4-phen, Me2-Ph2-phen, and dpq), a catalogue of twelve Re(I)-biotin complexes were synthesised. The luminescence data reported an increase in both the emission intensity and the lifetimes when Re(I)-biotin complexes were bound to avidin. As the spacer arms were increased, a smaller increase in emission enhancement was observed, this was attributed to the increased exposure of the complex to the solvent. Variations in the substituent position of pyridine to which the biotin was bound found that the *meta*-substituted variant had a longer emission lifetime than the *para*-substituted.[27] Further examples by the group showed an increased emission enhancement factor of *ca*. 3.05-8.05 for the C_6 and C_2 spacer arms.[28]

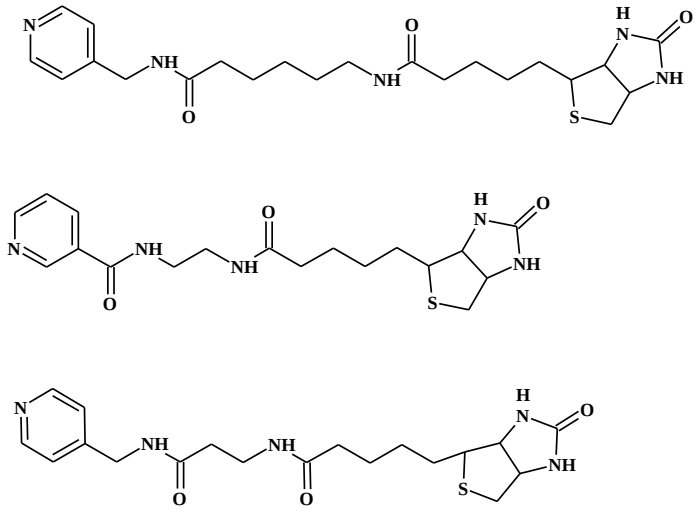

Figure 2.12 The different biotin ligands which were attached to Re(I). Each complex showed enhanced emission intensity when bound to avidin[27]

There is only one example of cellular imaging with Re(I)-biotin to date and this again was reported by the Lo *et al.*[29] group (Figure 2.13). The following Re(I)-biotin isothiocynate complex showed intense cytoplasmic staining of the cell with partial organelle staining and also presented cytotoxicity values similar to the anticancer drug cisplatin.[29]

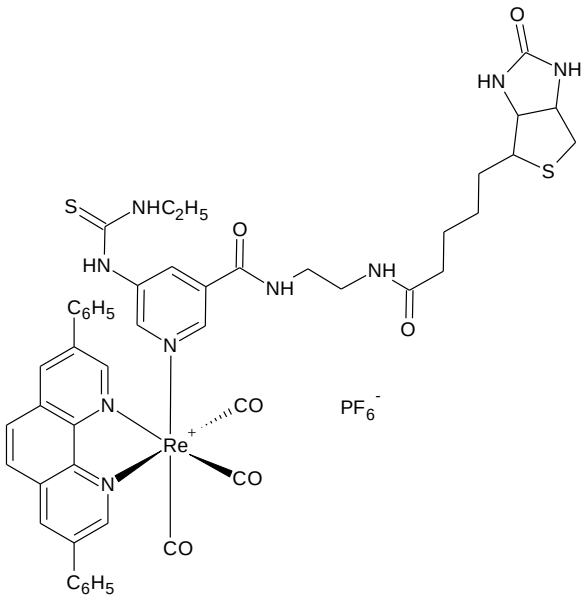

Figure 2.13 Re(I)-biotin isothiocyanate complex found to localise in cytoplasm.[29]

2.2 Overview

It is possible that different ligands can impose a greater influence on both the structural and photophysical properties of a complex. In light of the unusual photophysical observations for varying aliphatic chained complexes seen for the C_{12} aliphatic chain length, the aims of the work described in this chapter was to further analyse the solvent effect on hydrophobically driven inter- or intramolecular interactions. Two different series of novel luminescent complexes were synthesised. The first series of Re(I) complexes was synthesised to investigate the effect of variations in aliphatic chain lengths, linker units and diimine groups on the hydrophobic interactions. The second series of Re(I) complexes was synthesised to investigate the effect of a fluorescent chromophore moiety on these interactions when appended to the terminal position of varying lengths of aliphatic chain. Avidin: biotin binding was also investigated to evaluate the effect of intermolecular energy transfer processes between the chromophores. This latter scenario affords the possibility of photophysical studies on the distance dependent (and therefore indicative of molecular conformation) energy transfer processes that are possible between donor and acceptor components in luminescent systems.

2.3. Results and discussion (part 1)

2.3.1. Synthesis of long aliphatic chained complexes

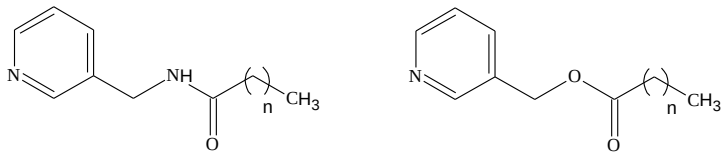

L1-3

L1 n = 6

L2 n = 12

L3 n = 18

L4-6

L4 n = 6

L5 n = 12

L6 n = 18

Figure 2.14 Structure of ligands with varying aliphatic chain length, L^1-L^6.

L^1-L^3 were isolated following a reaction of 3-amino methyl pyridine with the appropriate long chain acid chloride. The analogous ligands, **L^4-L^6**, were isolated using hydroxyl methyl pyridine as a substitute for 3-amino methyl pyridine, n = C_6, C_{12}, C_{18} respectively. ^{1}H NMR spectra were obtained in $CDCl_3$ where the synthesis of each ligand was confirmed by the appearance of new CH_2 linker environments between +3.97 and +4.85 ppm (Figure 2.14).

The synthesis of the cationic complexes $[Re(CO)_3(bipy)L^{1-6}]^+$, $[Re(CO)_3(phen)L^{1-6}]^+$ and $[Re(CO)_3(neoc)L^{1-6}]^+$, was achieved following literature precedent.[30] Each complex was reacted with **L^{1-6}** in a 1:1.1 ratio in chloroform over 12 hours. Column chromatography was used to isolate the pure complexes as their tetrafluoroborate salts in modest yields of 13 % to 58 % (Figure 2.15). ^{1}H NMR spectra were obtained for each complex in $CDCl_3$ confirming the presence of the ligand and were consistent with what was expected for the desired product. MS (ES) and HRMS analysis for each of the complexes was carried out which gave good mass ions in all cases; peaks associated with the parent cation $[M\text{-}BF_4]^+$ with the correct isotope distribution was observed in all cases. Solid state IR studies were also carried out for all complexes which showed subtle changes in the ν(CO) in comparison to the ligands and the $[Re(CO)_3(N\text{^}N)]^+$ precursors. All the complexes studied showed two carbonyl stretching frequencies at around 2030 and 1921 cm^{-1} with very slight variation in wavenumbers directly relating to the electron density available at the Re(I) centre.

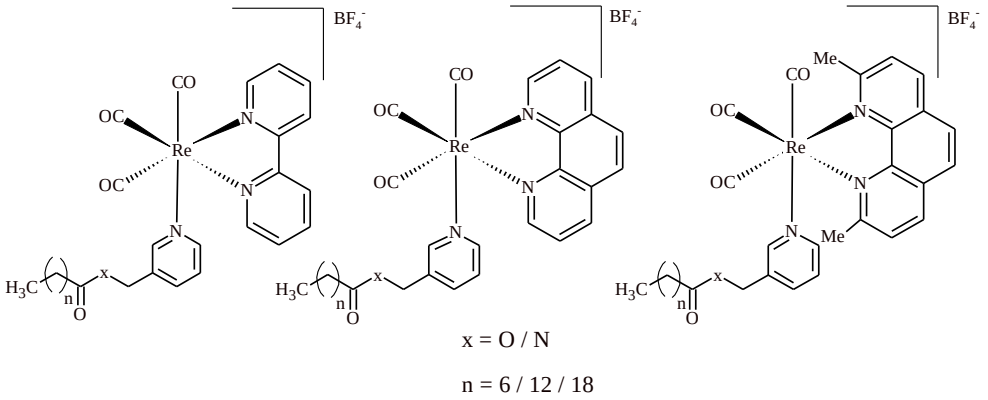

Figure 2.15 Structures of complexes discussed herein.

2.3.2. UV-Vis absorption spectroscopy

The electronic absorption spectra for the complexes $[Re(CO)_3(N\text{^}N)L^{1\text{-}6}]^+$ were obtained in acetonitrile solution at room temperature. For each of the complexes an intense absorption band in the high energy region of the spectrum (< 330 nm) was typically assigned to spin-allowed intra ligand (^{1}IL)($\pi \rightarrow \pi^*$) transitions. A structureless shoulder peak is expected in the region of 340-400 nm for the spin-allowed metal to ligand charge transfer transition (^{1}MLCT) (Re(I) d$\pi \rightarrow \pi^*$ NN), but this peak was not apparent in any of the complexes. The absence of the ^{1}MLCT peak is assumed to be the result of the broad IL peak (Table 2.1).

2.3.3. Luminescence spectroscopy

Luminescence spectra were obtained in acetonitrile solution at room temperature. Following excitation at 345 nm, $[Re(CO)_3(N\text{^}N)L^{1\text{-}6}]^+$ displayed the expected broad structureless emission band around 550 nm, corresponding to the ^{3}MLCT transition. With excitation of 345 nm and detection at 550 nm respectively, time-resolved lifetime measurements in acetonitrile detected single exponential lifetimes over 132-292 ns corresponding to the expected values for the varying diimines (Table 1 and 2). When the solvent was changed from acetonitrile to water a slight blue-shift in emission wavelength was occassionally seen, accompanied with an increase in emission lifetime for some complexes. The C_{12} chain length demonstrated, in all three sets of analogous complexes, to have the more consistent, predictable luminescent properties when the solvent was changed.

Table 2.1 The absorption and emission data for rhenium based complexes of L1-6 in both acetonitrile and water. λ_{exc} = 345 nm.

Compounds	Abs (nm)	Em(MeCN) (nm)	Lifetime MeCN (ns)	Em (H_2O) (nm)	Lifetime H_2O (ns)
Re-bipy-L^1	273	553	132	551	136
Re-phen-L^1	276	547	257	542	486
Re-neoc-L^1	277	529	292	532	357
Re-bipy-L^2	274	556	128	554	137
Re-phen-L^2	270	547	216	541	489
Re-neoc-L^2	280	528	226	532	307
Re-bipy-L^3	275	554	125	552	141
Re-phen-L^3	273	544	247	546	437
Re-neoc-L^3	275	532	271	532	301
Re-phen-L^4	273	541	248	539	486
Re-neoc-L^4	221	530	292	530	325
Re-phen-L^5	274	546	257	536	312
Re-neoc-L^5	280	542	153	539	270
Re-phen-L^6	273	544	247	546	437
Re-neoc-L^6	275	532	271	532	301

2.3.3.1. Luminescent properties of $[Re(CO)_3(bipy)(L^1\text{-}L^3)]^+$

For the ester complexes of $[Re(CO)_3(bipy)(L^1\text{-}L^3)]^+$ (discussed in the introduction) a blue shift in emission maxima and an increase in emission lifetime was observed however, for the amide comples, when the solvent was changed from acetonitrile to water, this was not the case. The amide complexes of bipy $\mathbf{L^1\text{-}L^3}$ showed no dramatic increase in either emission wavelength or lifetime when the solvent was changed suggesting the nature of the linker (amide/ester) governs the degree of any intramolecular hydrophobic chain wrapping. This conclusion, although apparent for the bipyridine complexes was not consistently observed for the other diimine complexes in this study.

2.3.3.2. Luminescent properties of $[Re(CO)_3(neoc)(L^1\text{-}L^6)]^+$

The $[Re(CO)_3(neoc)(L^1\text{-}L^6)]^+$ complexes each displayed an increase in the emission

lifetime upon changing from acetonitrile to water. For the complex of $\mathbf{L^5}$ (C_{12} chain, ester linker), this increase in lifetime was accompanied by a small blue shift in emission maxima of 3 nm, from 542 nm in MeCN to 539 nm in H_2O. This was the only complex to exhibit a shift in emission maxima, however, the shift was too small to be considered relevant.

2.3.3.3. Luminescent properties of $[Re(CO)_3(phen)(L^1\text{-}L^6)]^+$

Similarly to the neoc complexes, the $[Re(CO)_3(phen)(\mathbf{L^{3,6}})]^+$ (C_{18} ester and amide) complexes showed a dramatic increase in emission lifetime with no significant change in emission maxima. For $[Re(CO)_3(phen)(\mathbf{L^{1,2,4,5}})]^+$ (the C_2 and C_{12} ester and amide) both a blue shift in emission maxima and a dramatic change in emission lifetime was observed. The biggest shift in emission maxima was seen with $\mathbf{L^5}$ (C_{12}) with a shift 10 nm, from 546 nm in MeCN to 536 nm in H_2O, this result however was accompanied by the smallest increase in emission lifetime, 55 ns. The analogous complex, $\mathbf{L^2}$, showed the second biggest blue shift in emission maxima of 6 nm and was accompanied by a lifetime increase of 273 ns.

2.3.3.4.Variable temperature measurements

To further probe the extent of chain wrapping, variable temperature luminescence measurements were carried out for the $[Re(CO)_3(phen)(\mathbf{L^2}$and $\mathbf{L^5})]^+$ in water (Figure 2.16). An increase in the intensity of the emission maxima was seen as the temperature decreased. This increase was attributed to an enhancement in the shielding of the excited state. As the temperature is lowered the conformation of the chain is more rigid (less freedom to move). The increase in emission intensity suggests the average conformation for the chain resides around the $[Re(CO)_3(N\text{^}N)]^+$ centre resulting in the enhancement of luminescence. As the temperature is elevated there is more degrees of freedom within the chain thus a decrease in emission intensity is viewed.

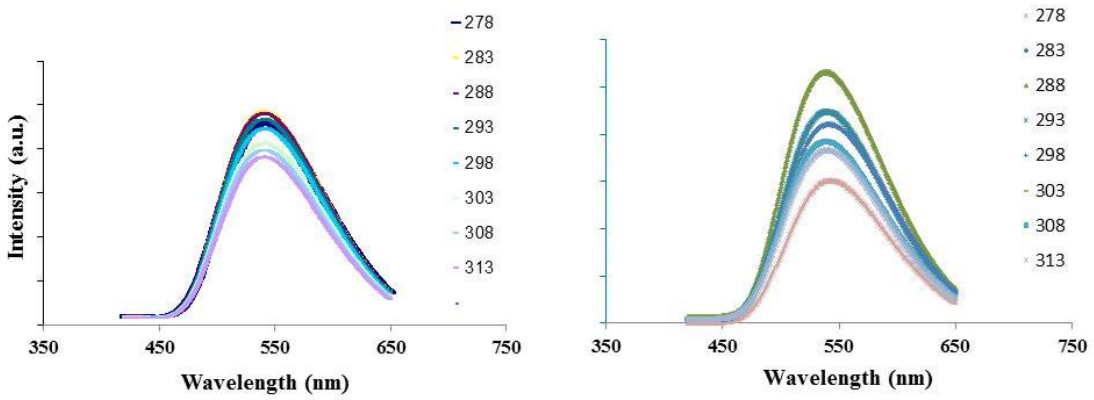

Figure 2.16 Variable temperature measurements of $[Re(CO)_3(phen)(L^2)]^+$ (LHS) and $[Re(CO)_3(phen)(L^5)]^+$ (RHS) (λ_{exc} 345 nm).

2.4. Conclusion

From the photophysical data reported, no universal model describing the behaviour of all of the complexes can be derived. The results show that for bipyridine complexes the nature of the linker group governs the degree of chain-wrapping; ester linkers appear to facilitate better chain-wrapping than amides. When looking at the alternative diimines, phen/neoc, not **all** data was complimenting of the bipy findings, however, both sets of complexes provide evidence to suggest the C_{12} chain is the optimum chain length for chain-wrapping to occur with the ester linkers displaying, for C_{12} chains, the greatest blue-shift for emission maxima.

2.5. The incorporation of a fluorescent chromophore to investigate hydrophobic interactions

To further probe the effect of hydrophobic interactions on the C_{12} alkyl chain with an ester linker, the syntheses of ligands incorporating a sensitizer (coumarin) or quencher (anthracene) moiety were attempted. The addition of a photoactive component onto the terminus of the aliphatic chain should potentially allow for a better understanding of the orientation of the chain when coordinated to a $[Re(CO)_3(N\hat{}N)]^+$ unit, and help to deduce whether intramolecular hydrophobic interactions are occurring. Anthracence and coumarin units can have very different effects on the photophysics of a complex.[31]

Anthracene (Figure 2.17) is highly luminescent in nature. It is able to participate in photo-induced energy transfer processes as either an electron donor or acceptor depending on its photophysical 'partners'.[32-35]When partnered with a $[Re(CO)_3(N\hat{}N)]^+$ type species, the excited triplet energy of anthracence is typically lower than the ^{3}MLCT energetic state. The anthracence moiety can therefore efficiently quench the luminescence of the ^{3}MLCT state. The low oxidation potential of the anthracence also results in a higher quenching rate constant.[36]

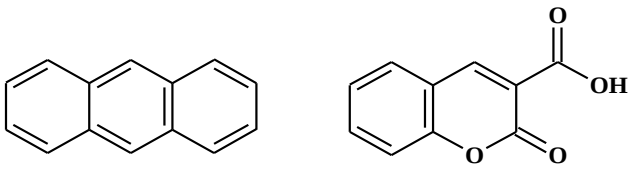

Figure 2.17 Anthracene (LHS), coumarin (RHS)

In contrast, coumarin (Figure 2.17) is a highly fluorescent chromophore whose excited singlet and triplet energy is typically higher than Re(I) based ^{3}MLCT potentially leading to energy transfer and sensitization of MLCT. In this manner, the fluorescence intensity of the coumarin fluorophore should therefore be quenched. Through the analysis of the intra molecular energy transfer efficiency, information on the orientation of the coumarin (and hence aliphatic chain) with respect to the excited states situated on the diimine ligand and/or the metal centre can be obtained.[35]The quantum yield of coumarin is in the range of 35-71 %.[35b]

2.6. Results and discussion (part 2)

2.6.1. Synthesis of dual functionalised ligand precursors

The most convenient pathway for synthesising a bi-functional alkyl chain was to proceed *via* the formation of amide and ester linking units and the most convenient way to form these functionalities was *via* the use of acid chlorides. An acid chloride enables 'activation' of a carbon promoting more facile nucleophillic substitution. The position of the ^{1}H NMR peak for the CH_2 adjacent to OH/COOH/NH_2 in the precursor can be used in most cases to distinguish products from their SM.

The ligand chosen for synthesising the precursor ligand had to be adaptable for the addition of different functional groups. A number of attempts were made to synthesise a bifunctional C_{12} chain using 1,12-dodecandiol and a *tert*-butyloxycarbonyl (BOC) / t-butyl carbamate protecting group, however low yields of the desired product were obtained (Figure 2.18). Different ratios of the BOC group were trialled as well as a mono de-protection of the di-phthalimide structure. Both proved unsuccessful and an alternative route was sought.

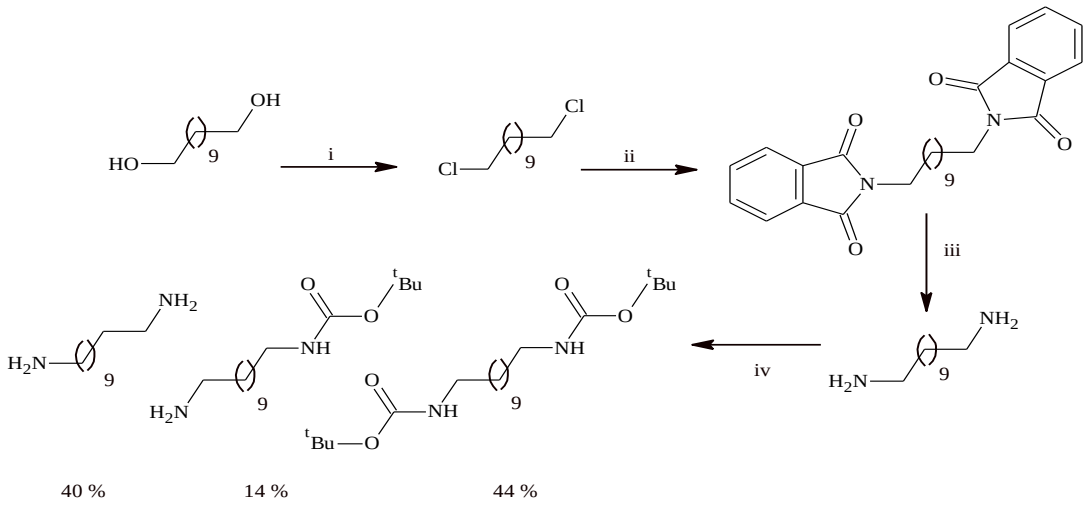

Figure 2.18 Attempted ligand synthesis. Reagents: i) $SOCl_2$; ii) potassium pthalimide, DMF, Δ; iii) hydrazine, methoxyethanol; iv) BOC, $CHCl_3$.

An alternative precursor, 1,12-dibromodecane was used in an attempt to increase the yield of a dual functionalised ligand. 1,12-dibromodecane and 1 equivalent of potassium phthalimide were reacted to form the mono protected product. The ^{1}H NMR spectra initially suggested formation of the product due to the presence of signals corresponding to both a bromo-subsituted and a phthalimide-substituted chain. However, on further analysis it was discovered that these signals had resulted from the presence of both the unreacted 1,12-dibromodecane and the bis-substituted product in a 1:1 ratio. The reaction was repeated using

different ratios of SM with and without the presence of a KI catalysts and varying the solvents, but unfortunately the same results were observed.

A pleasing result was eventually found with a reaction of 1,12-dodecandiol and nicotinoyl chloride (Figure 2.19). To a dilute solution of the diol (5 eq) in chloroform, was added nicotinoyl chloride (1 eq) and TEA. Following an aqueous work-up a new ligand, $\mathbf{L^7}$, was produced with a 50 % yield. It was also possible to recover the majority of 1,12-dodecandiol that was used in an 80 % excess. The formation of the mono-substituted, $\mathbf{L^7}$ from the symmetrical 1,12 dodecandiol was a welcomed breakthrough in this area of work.

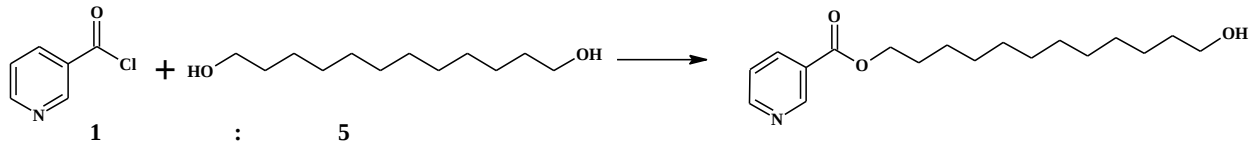

Figure 2.19 Reaction scheme for ligand precursor A.

2.6.2. Addition of a chromophoric moiety

$\mathbf{L^7}$ can be utilised as a ligand precursor allowing the addition of a chromophore moiety *via* the unreacted terminal hydroxyl group. Initially, anthracene-9-acid chloride was chosen as the chromophore moiety but when reacted with $\mathbf{L^7}$ the ^{1}H NMR spectrum gave evidence to suggest hydrolysis of the anthracene-reactant. The reaction was repeated under anhydrous conditions and pure product was obatained in a low yield. As a result of the low yielding nature of this reaction a second chromophore moiety, coumarin, was reacted with $\mathbf{L^7}$ which gave the desired product, $\mathbf{L^{10}}$ in a 48 % yield (Figure 2.20). $\mathbf{L^{8/9}}$ with varying chain lengths of C_2 and C_6 respectively, were synthesised following the same procedure as $\mathbf{L^7}$ and $\mathbf{L^{10}}$; $\mathbf{L^{8\text{-}10}}$, n = C_2, C_6, C_{12} respectively.

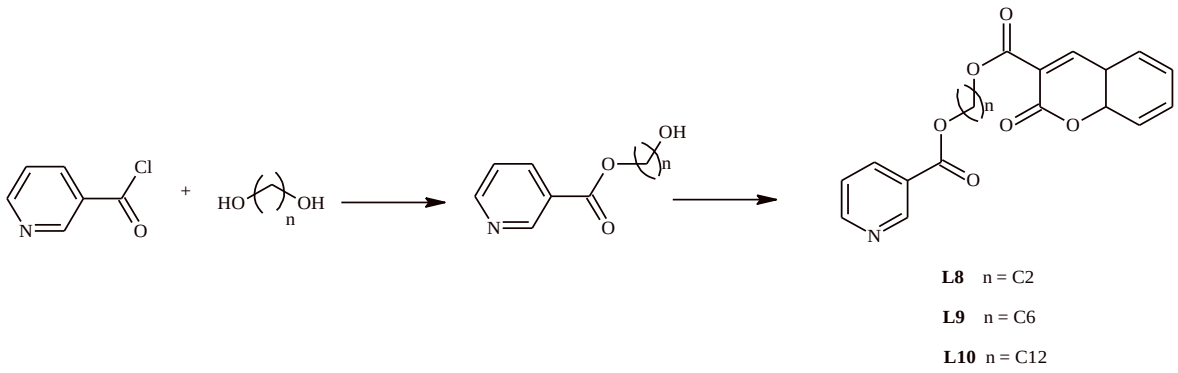

Figure 2.20 Ligand syntheses.

2.6.3. Synthesis of complexes

L$^{8\text{-}10}$ were coordinated to $[Re(CO)_3(bipy)]^+$ and $[Re(CO)_3(phen)]^+$ following literatre precedent. The six complexes were formed in yields ranging from 18-43% (Figure 2.21).

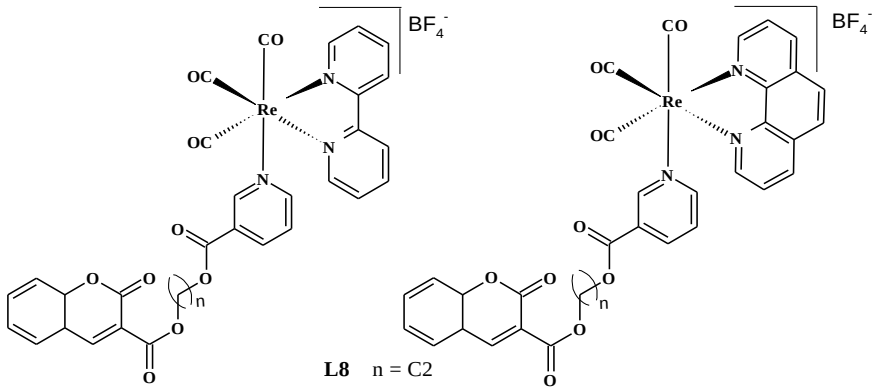

L8 n = C2

L9 n = C6

L10 n = C12

Figure 2.21 $[Re(CO)_3(bipy)L^{8\text{-}10}]^+$and $[Re(CO)_3(phen)L^{8\text{-}10}]^+$.

2.6.3.1. UV-Vis absorption and luminescence spectroscopy

The photophysical properties of $[Re(CO)_3(bipy)(\mathbf{L}^{8\text{-}10})]^+$ and $[Re(CO)_3(phen)(\mathbf{L}^{8\text{-}10})]^+$ were studied and are summarised in Table 2. The emission spectra of complexes of **L**$^{8\text{-}10}$ in acetonitrile and water are shown in Figures 2.22-2.24. The electronic absorption spectra obtained for the complexes generally show absorption < 330 nm. The intense absorption bands around 222-290 nm was assigned to the spin allowed ^{1}IL ($\pi\rightarrow\pi^*$) (coumarin/NN) transitions and the broad shoulder displayed by the majority of spectra at lower energy typically around 320 to 330 nm was assigned to the spin allowed ^{1}MLCT transition of dπ (Re(I))$\rightarrow\pi^*$ (N^N).

The incorporation of the coumarin moiety onto the chain resulted in dual-emissive species. Upon photoexcitation at 340 nm all of the complexes exhibit two emission maxima centred on 420 nm and 540 nm. The emission band around 420 nm was assigned as the ^{3}IL ($\pi\rightarrow\pi^*$) of the coumarin and the structureless emission band at about 535-550 nm was assigned as the ^{3}MLCT transition of dπ (Re(I))$\rightarrow\pi^*$ (NN). Through comparing the intensity of emission maxima, IL:^{3}MLCT, it was hoped to be possible to determine the proximity of the coumarin to the $[Re(CO)_3(N\text{^}N)]^+$ unit; if the coumarin moiety is in close proximity to the central $[Re(CO)_3(N\text{^}N)]^+$ unit an increase in ^{3}MLCT intensity would be expected, this coupled with the lifetime data (an increase is expected if the excited state is shielded from solvent) will allow for the amount of hydrophobic interaction to be assessed.

Table 2.2 The absorption and emission data for L8-10, $[Re(CO)_3(bipy)L^{8-10}]^+$ and $[Re(CO)_3(phen)L^{8-10}]^+$. Spectra recorded in both acetonitrile and water. λ_{exc} = 345 nm.

Compounds	Abs (nm)	Em(MeCN) (nm)	Lifetime MeCN (ns)	Em (H_2O) (nm)	Lifetime H_2O (ns)
L^8	290	417	-	421	-
	331				
L^9	291	416	-	420	-
	330				
L^{10}	289	415	-	417	-
	335				
Re-bipy-L^8	223	419	150	422	**108**
	288	549		549	
Re-bipy-L^9	251	414	146		**151**
	288	547			
	320				
Re-bipy-L^{10}	268	416	147	413	**152**
	320	548			
Re-Phen-L^8	277	412	321	408	**183**
	328	539		386	
Re-Phen-L^9	278	420	290	418	**403**
	331	540		536	
Re-Phen-L^{10}	**273**	**410**	**218**	**421**	**177**
	435	**536**		**538**	

Through a comparison of both the emission intensities of ^{3}MLCT-based emission at 550 nm with coumarin-based emission at 420 nm and the lifetimes of the complexes, we can attempt to differentiate between the complex conformations (whether the coumarin unit is close to or further away from the $[Re(CO)_3(N\text{^}N)]^+$ unit). These comparisons are discussed in detail in the following sections.

2.6.3.2. Luminescent properties of $[Re(CO)_3(bipy)L^{8-10}]^+$

In acetonitrile dual emission profiles were observed for all three complexes. The spectra of $[Re(CO)_3(bipy)L^8]^+$ (C_2) (Figure 2.22) depicts how energy transfer is dependent on distance; $[Re(CO)_3(bipy)L^8]^+$ (C_2) is the shortest chain length and in both acetonitrile and water ^{3}MLCT-based signal intensity was greater than the coumarin-based emission intensity. In acetonitrile, for complexes $[Re(CO)_3(bipy)L^{9/10}]^+$, the C_6 and C_{12} chain length respectively, coumarin-based emission was dominant for $[Re(CO)_3(bipy)L^9]^+$ (C_6) and ^{3}MLCT-based emission was dominant for $[Re(CO)_3(bipy)_3L^{10}]^+$ (C_{12}). It is unlikely that chain 'wrapping' occurred for $[Re(CO)_3(bipy)L^{10}]^+$ (C_{12}) in the organic solvent and so it is assumed that the

chain 'folds' into a conformation that brought the coumarin unit into closer contact to the $[Re(CO)_3(bipy)]^+$ unit.

Literature reports have shown that coumarin can act as a sensitizer of $[Re(CO)_3(N^N)]^+$ based emission;[34] coumarin-based emission energy can be 'transferred' to rhenium thus coumarin emission is quenched. However, in water, two out of the three complexes show coumarin-based fluorescence only; there is no evidence for the ^{3}MLCT-based emission for the C_6 and C_{12} chain. Earlier examples of $[Re(CO)_3(N^N)L]^+$complexes (discussed in part 1), in the absence of a coumarin chromophore, reported observed ^{3}MLCT-based emission in water, which suggests quenching of the ^{3}MLCT-based emission is occurring for the C_6 and C_{12} chained $[Re(CO)_3(bipy)]^+$complexes (Figure 2.19).

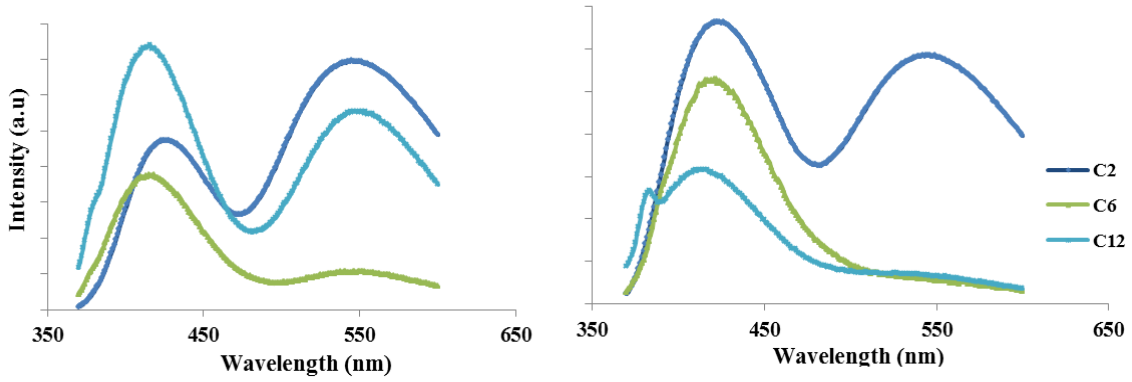

Figure 2.22 Spectra displaying emission of $[Re(CO)_3(bipy)L^{8\text{-}10}]^+$ in acetonitrile (LHS) and water (RHS). (λ_{exc} 340 nm).

2.6.3.3.Luminescent properties of $[Re(CO)_3(phen)L^{8\text{-}10}]^+$

Unlike the $[Re(CO)_3(bipy)L^{8\text{-}10}]^+$, the $[Re(CO)_3(phen)L^{8\text{-}10}]^+$ complexes showed dual emission profiles when in both MeCN and H_2O with more pronounced changes in the emission intensity being observed. In acetonitrile, the ^{3}MLCT-based emission was dominating over that of coumarin-based emission for all three chain lengths, the effect was maximised for $[Re(CO)_3(phen)L^9]^+$ (C_6). The difference in the ^{3}MLCT:coumarin ratio of emission intensities for the different chain lengths followed $C_6 > C_2 > C_{12}$. Coumarin has a much greater quantum yield when compared to $[Re(CO)_3(N^N)]^+$,[1,34b] and so the presence of a dominating ^{3}MLCT-based emission peak illustrated efficient energy transfer from the coumarin to the Re(I) unit (Figure 2.23). Efficient energy transfer suggests the orientation of the coumarin chromophore was in close proximity to the $[Re(CO)_3(N^N)]^+$ central unit, however, these spectra were recorded in acetonitrile so can assume chain wrapping is not causing the closeness.

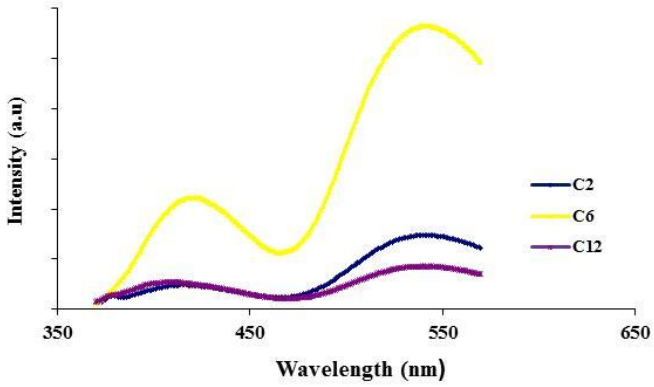

Figure 2.23 Spectra displaying emission of $[Re(CO)_3(phen)L^{8\text{-}10}]^+$ in acetonitrile. (λ_{exc} 340 nm)

When the solvent was changed to water the ^{3}MLCT-based emission was still more dominating than the coumarin-based emission, but the effect was maximised for the $[Re(CO)_3(phen)L^{10}]^+$ (C_{12}), following the trend $C_{12} > C_2 / C_6$ for the different chain lengths. The C_{12} chain showed the most efficient energy transfer (Figure 2.24) suggesting hydrophobic interactions were occurring bringing the coumarin and the $[Re(CO)_3(phen)]^+$ unit into closer proximity than the C_2 chain.

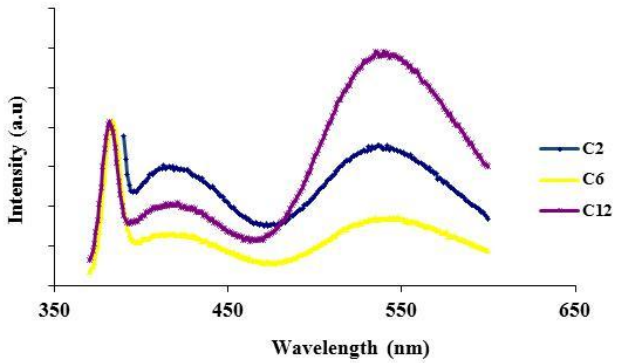

Figure 2.24 Spectra displaying emission of $[Re(CO)_3(phen)L^{8\text{-}10}]^+$ in water. (λ_{exc} 340 nm)

2.6.3.4. Variable temperature measurements

Variable temperature measurements were carried out for $[Re(CO)_3(phen)L^{10}]^+$, (Figure 2.25). The data showed that as the temperature was decreased, the ^{3}MLCT:coumarin intensity ratio increased. The increase in ^{3}MLCT-based emission intensity suggests the favoured conformation brings the coumarin unit into closer proximity of the $[Re(CO)_3(phen)]^+$ unit. The absence of both a blue-shift in emission maxima and an increase in lifetime, as the solvent was changed from acetonitrile to water for the C_{12} species, suggests that chain-

wrapping around the central unit was not responsible for the proximity of coumarin to $[Re(CO)_3(phen)]^+$ unit.

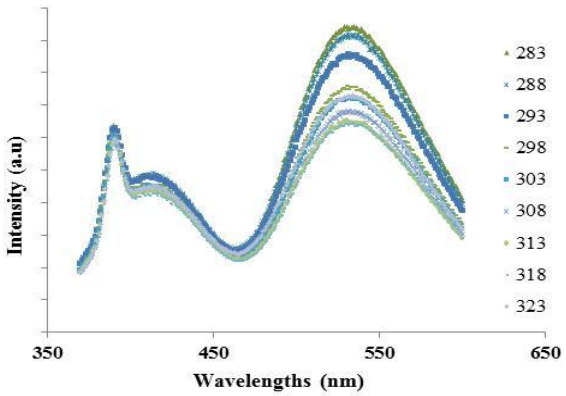

Figure 2.25 VT emission spectra for $[Re(CO)_3(phen)L^{10}]^+$ recorded in water. (λ_{exc} 340 nm).

It was hoped that the inclusion of a the coumarin chromophore moiety would allow greater insight into the conformation of the aliphatic chain with respect to the $[Re(CO)_3(N^N)]^+$ central unit, however, not all the results obtained herein are conclusive; for the $[Re(CO)_3(bipy)L^{8\text{-}10}]^+$ complexes ^{3}MLCT based emission was shown to dominate the coumarin based emission in acetonitrile only but for the phen based complexes, $[Re(CO)_3(phen)L^{8\text{-}10}]^+$, ^{3}MLCT based emission was shown to dominate the coumarin based emission in both solvent systems. These results suggest that the $[Re(CO)_3(phen)]^+$ based complexes are more sensitive to the effects of solvent than $[Re(CO)_3(bipy)]^+$ based complexes but further research is required to determine the orientation of the aliphatic chain in polar solvent.

2.7. Biotinylation of the complexes

To further probe the phenomenon of energy transfer which occurs *via* the aforementioned intramolecular hydrophobic interactions, application of the avidin-biotin binding model was investigated. Avidin can bind up to four biotin units in a 1:4 ratio and so any intermolecular hydrophobic interactions can lead to energy transfer between biotinylated photoactive units. In this case a $[Re(CO)_3(bipy)L(biotin)]^+$ species and a coumarin-biotin species, were to be bound to the surface of avidin, allowing investigation of any inherent energy transfer processes. As already discussed, C_6 is the optimum chain length for linkers to biotin. $[Re(CO)_3(bipy)L(biotin)]^+$ and biotin-coumarin compounds were synthesised with the units linked by a C_6 chain, and for comparison, $[Re(CO)_3(bipy)L(biotin)]^+$ linked by a C_{12} chain was also synthesised. The increase in chain length, from the optimised C_6 chain to the longer C_{12} chain, was expected to bring the hydrophobic $[Re(CO)_3(bipy)]^+$ unit into closer contact to the avidin, which could also result in closer contact to the coumarin allowing energy transfer to occur more efficiently.

2.7.1. Ligand design

Conveniently, there are commercially available, functionalised biotin compounds, such as biotinyl-*N*-hydroxysuccinimydyl ester, but herein the more cost effective, unmodified biotin is used (Figure 2.26). The presence of the carboxylic acid group at the terminal position of the biotin chain allows the stepwise addition of a ligand to biotin *via* a condensation reaction (seen in the ligand synthesis for part 1). The starting material for ligand synthesis should include a C_6 or C_{12} chain appended with an OH/NH_2 terminal functional group for ester or amide linkages. Any ligand chosen should also be suitable for Re(I) co-ordination and thus include a pyridine donor for this purpose.

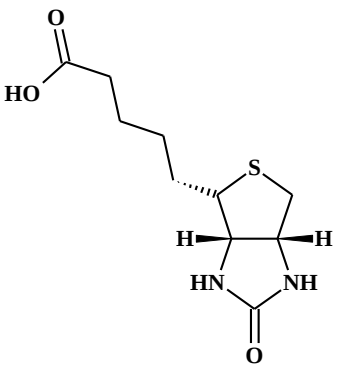

Figure 2.26 Biotin

2.8. Results and discussion (part 3)

2.8.1. Synthesis and reactivity of biotin chloride

Literature precedent was followed for the formation of biotin chloride.[37] Biotin was added to a small Schlenk flask followed by freshly distilled oxalyl chloride and the reaction mixture was stirred at room temperature until complete dissolution of biotin. The excess oxalyl chloride was then removed *in vacuo* and the solid residue was washed with dried toluene. When reacted with 6-amino-1-hexanol in the presence of triethylamine TEA (Figure 2.27) a poorly soluble product was recovered. The absence of a peak in the ^{1}H NMR spectrum corresponding to the formation of an amide/ester group indicated that the reaction was unsuccessful. Additionally, poorly resolved integration for the biotin species in the ^{1}H NMR spectrum suggests possible breakdown of the biotin species.

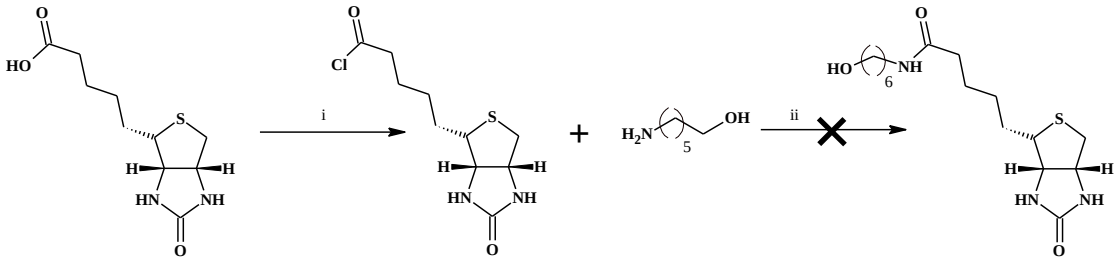

Figure 2.27 Attempted synthesis of functionalised biotin. Reagents; i) oxalyl chloride, toluene; ii) 6-amino-1-hexanol, TEA, $CHCl_3$, Δ.

2.8.2. Synthesis and reactivity of a biotin ester

As the use of biotin chloride had been unsuccessful, an alternative method was used to form a 'reactive' biotin moiety *via* an activated biotin ester.[38] Biotin was dissolved in warm, anhydrous DMF and after the solution was cooled to room temperature, TEA was added followed by drop wise addition of tetrafluorophenyl trifluoroactate (Figure 2.28). The reactivity of the activated biotin ester was tested using both octanol and 1,6-di-amino hexane. The reactants were heated to 50 ˚C in a small amount of DMF in the presence of TEA for 3 days. No reaction was seen using octanol with only starting materials observed in the ^{1}H NMR spectrum.

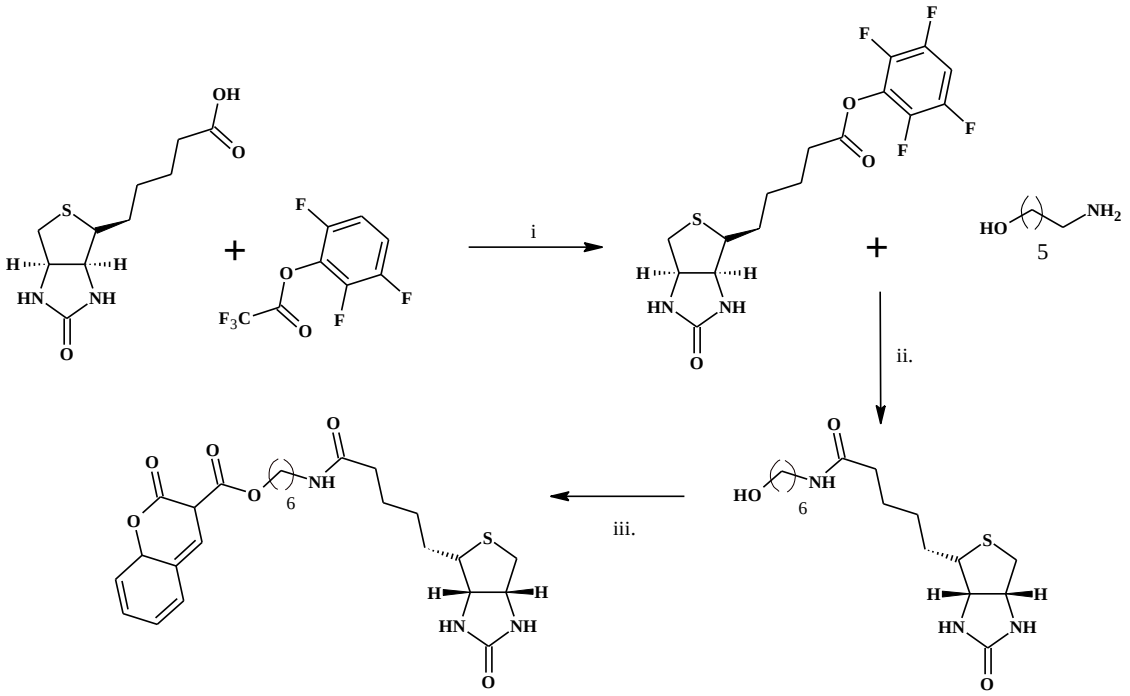

Figure 2.28 The formation of biotin ester (i), pro-ligand 11 (ii) and L^{11} (iii). Reagents; DMF, TEA, Δ.

When using1,6-di-amino hexane, evidence of an amide group was observed in the ^{1}H NMR spectrum with a peak at +3.51 ppm. This led to an attempted reaction using 6-amino-hexan-1-ol, intended to give **pro-ligand 11** (Figure 2.28). The successful formation of **pro-ligand 11** was confirmed using ^{1} H NMR spectroscopy in which the signal corresponding to the CH_2NH$_2$ was shifted to higher frequency from +2.51 ppm to +3.49 ppm. Additional characterisation was carried out using MS (ES) and HRMS analysis, with observed peaks corresponding to the parent ion, [M+Na$^+$] and [M+K$^+$]. **Pro-ligand 11** was formed with a good yield of 76 % and when added to a solution of coumarin acid chloride in chloroform in the presence of TEA, following an aqueous work up, it afforded the pure product **L^{11}** in a 68 % yield (Figure 2.28). This successful synthesis of a biotin–coumarin conjugate suggested that the use of an activated ester of biotin could lead to mixed ester and amide linked biotinylated ligands and/or fluorophores.

2.8.2.1. Synthesis of $L^{12,13}$ using the biotin ester

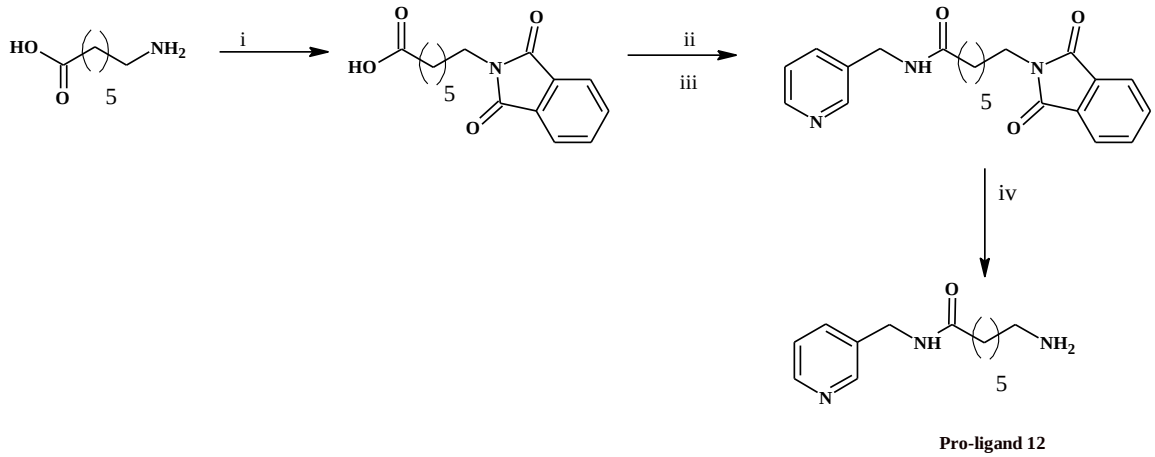

Figure 2.29 Synthesis of pro-ligand 12. Reagents (i) pthalic anhydride, Δ; (ii) $SOCl_2$; (iii) 3-aminomethyl pyridine; (v) hydrazine hydrate, Δ.

Pro-ligand 12 is a ligand precursor similar in nature to that of L^7 (pyridine-spacer-OH) and was synthesised using 6-amino-caproic acid. 6-amino-caproic acid was heated in the presence of phthalic anhydride producing the phalimido-acid **X.** The acyl chloride of the phthalimide protected amino acid was formed by treatment of phalimido-acid **X** with thionyl chloride. Acid chloride **X**, was then reacted with 3-amino methyl pyridine in chloroform and in the presence of TEA to form the starting material for **pro-ligand 12**. The phthalimide protecting group of the starting material was cleaved using hydrazine in ethoxyethanol producing the bi-product phthalazine and the desired primary amine, **pro-ligand 12** in a 68 % yield (Figure 2.29). **Pro-ligand 13** was synthesised following the same methodology but using 12-aminolauric acid. $L^{12,13}$ were then synthesised from their pro-ligands by reacting with biotin activated ester following the same procedure as L^{11} in yields of 65 % and 56 % respectively (Figure 2.30).

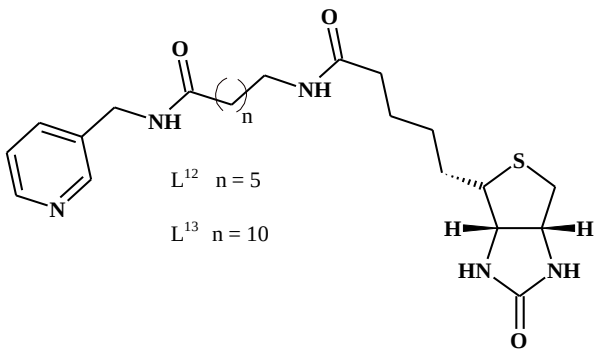

Figure 2.30 $L^{12/13}$

2.8.3. Synthesis of $[Re(CO)_3(bipy)L^{12/13}]^+$

Due to the limited solubility of biotin-based ligands, bipyridine was chosen as the diimine for the rhenium-precursor as the $[Re(CO)_3(bipy)]^+$ analogues are notably more soluble than their phen/neoc analogues. The synthesis of the cationic rhenium complexes, $[Re(CO)_3(bipy)L^{12/13}]^+$, was achieved following literature precedent; 1.1 equivalent of the ligand was reacted with $[Re(CO)_3(bipy)MeCN]^+$ in DMF at 75 ˚C for 7 days. The solution was filtered to yield an orange precipitate. Following additional purification by precipitation, the pure $[Re(CO)_3(bipy)L^{12/13}]^+$ complexes were isolated as their tetrafluoroborate salts in low yields of 18 % and 19 % respectively (Figure 2.31). ^{1}H NMR spectra were obtained for each complex and comparison of the spectra to the free ligand confirmed the successful co-ordination of the ligands to the $[Re(CO)_3(bipy)]^+$ units.

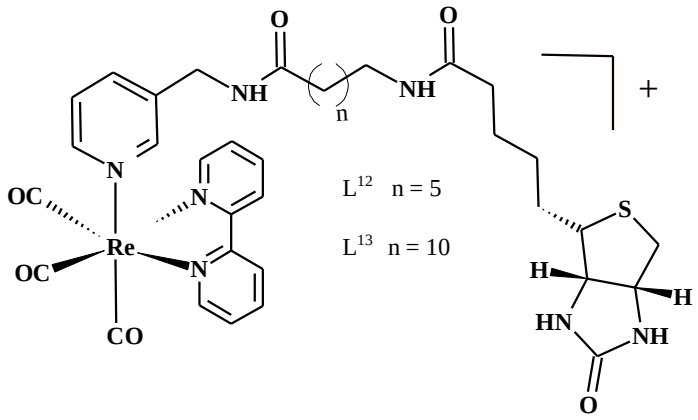

Figure 2.31 $[Re(CO)_3(bipy)L^{12/13}]^+$

2.8.4. Avidin:biotin binding properties of L^{11} and $[Re(CO)_3(bipy)L^{12}]^+$

2.8.4.1.HABA Assay

The avidin:binding activity of both $\mathbf{L^{11}}$ and $[Re(CO)_3(bipy)L^{12}]^+$ were studied by 2-(4'-hydroxyazobenzene) benzoic acid (HABA) assays. HABA when bound to avidin has an absorption feature at 500 nm and a binding constant of K_d = 6 x10^{-6} M.[25] Due to the stronger binding affinity of biotin (K_d = 10^{-15} M)[25] biotin should displace the HABA resulting in a decrease in the absorbance at 500 nm. Solutions of unmodified biotin, $\mathbf{L^{11}}$ and $[Re(CO)_3(bipy)L^{12}]^+$ of known concentrations were prepared and UV-vis titrations of each with avidin-HABA solutions were carried out. Avidin-unmodified biotin binding is known and well documented; the titrations using unmodified biotin not only act as a control for the modified biotin species but also ensure the standard of the avidin starting material is good. For the three UV-vis titrations a decrease in the absorbance at 500 nm was observed which indicates successful avidin-boitin binding in all three samples. A plot of $-\Delta Abs_{500\ nm}$ versus the [biotin] : [avidin] can be seen in Figure 2.32. The equivalence point is show at three-four in all three plots; [biotin] : [avidin] 4:1 which suggests that both the modified and unmodified biotin compounds bind to the avidin with a stoichiometry of 4:1. Figure 2.32 depicts modified biotin, $\mathbf{L^{11}}$, displacing HABA more efficiently than the unmodified biotin. This would suggest coumarin-biotin, $\mathbf{L^{11}}$, binds to avidin more strongly than pure biotin (although the difference in binding strength is small).

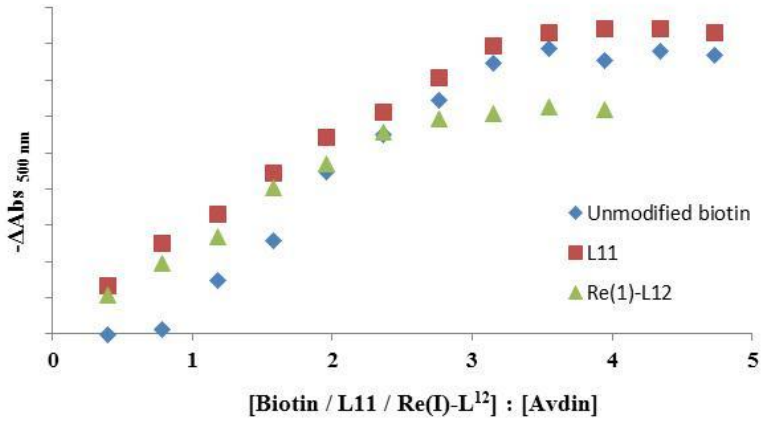

Figure 2.32 Absorption titration curves for the titration of biotin / L11/ $[Re(CO)_3(bipy)L^{12}]^+$ with avidin-HABA.

2.8.4.2. Luminescent spectroscopy titrations

The avidin-binding activity of a molecule can also be investigated using luminescence spectroscopy titrations. This analytical technique is of particular interest when exploring any intermolecular energy tranfer between compounds **L^{11}** and [Re(CO)$_3$(bipy)L^{12}]$^+$ as avidin can bind up to four biotin molecules at one given time. The HABA-titrations of both compounds showed adequate binding to avidin (seperately) with equivalence points of four being observed. When both compounds are added to avidin in solution simultaneously, it is possible to have the two different compounds bound to one molecule of avidin. Although a method to control the binding ratio of the two compounds is unknown, if the two compounds are bound to avidin, any intermolecular energy transfer occuring is expected to be viewed in the luminescence spectra with a difference in the intensity between coumarin-based and ^{3}MLCT-based emissions.

Emission titrations of compounds **L^{11}** and [Re(CO)$_3$(bipy)L^{12}]$^+$ were carried out seperately as well as together (as a 50:50 mix) to allow any changes seen in the mixture to be efficiently analysed. Following a similar procedure to the HABA titrations, solutions of i) a blank solution of PBS (no avidin) and ii) avidin containing solution, was titrated into a known concentration and volume of **L^{11}**. This was repeated for both and [Re(bipy)(CO)$_3$L^{12}]$^+$ and then a mixture of **L^{11}** and [Re(bipy)(CO)$_3$L^{12}]$^+$.

2.8.4.2.1. Solvent effect/ hydrophobic interactions

The first part of this chapter discusses the effect of different solvents on the photophysical properties of complexes with long aliphatic chains, taking the effect of the solvent into consideration, when attempting to analyse energy transfer between long chained aliphatics, the nature of the solvent needs to be analysed and so titrations of blank solutions of PBS were included in the analysis.

Due to the limited solubility of the compounds in aqueous media initial titrations (UV-vis and fluorescence) were carried out using a solvent system of MeOH:PBS (1:1). The data obtained for the UV-vis spectra was as expected, with a decrease in absorbance at 500 nm indicative of the successful biotin-avidin binding. However, the data obtained from the fluorescence titrations showed little change between the standard (blank solution of PBS:MeOH) and avidin for all three compounds (unmodified biotin, **L^{11}** and [Re(CO)$_3$(bipy)L^{12}]$^+$. The titrations were repeated using minimal MeOH in PBS in a ratio of 0.1:3 and more pronounced changes in the luminescence were observed; these changes are discussed in detail in the following sections.

2.8.4.2.2. Emission titrations of L^{11}

An enhancement in the emission intensity at 420 nm was seen for the coumarin-biotin compound, $\mathbf{L^{11}}$, when known quantities of avidin were added to the sample (Figure 2.33). This enhancement was not present in the control (the addition of pure PBS only) and so it is attributed to avidin-biotin binding. The increased emission intensity suggests $\mathbf{L^{11}}$ is shielded from the solvent within the hydrophobic avidin pocket and so any quenching effects that are occuring within the PBS titration are minimised. No blue-shift was observed in the emission maxima when $\mathbf{L^{11}}$ binds to avidin.

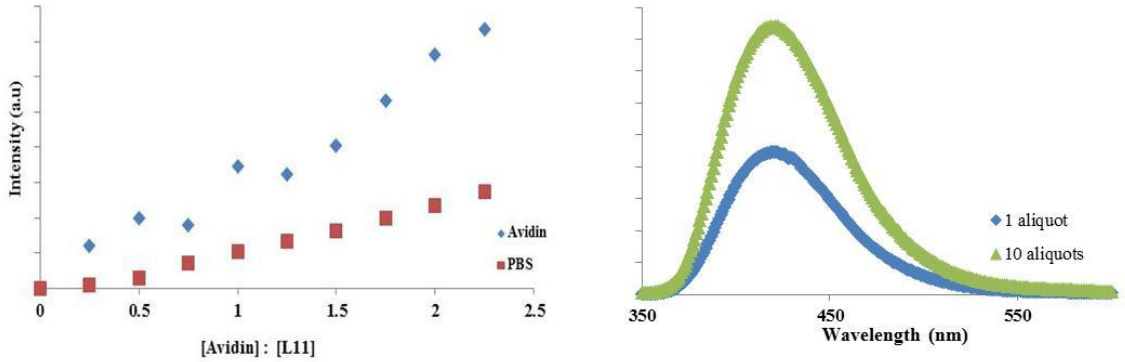

Figure 2.33 Emission titration curves for the titration of i) blank pbs solution with L^{11} [0.3mM] & ii) [0.075mM] aliquots of avidin with L^{11} [0.3 mM]. (λ_{em} = 420 nm). RHS steady state emission of L^{11}. (λ_{exc} = 310 nm).

2.8.4.2.3. Emission titrations of $[Re(CO)_3(bipy)L^{12}]^+$

For both the control, PBS $[Re(CO)_3(bipy)L^{12}]^+$ and avidin $[Re(CO)_3(bipy)L^{12}]^+$, the same change in emission intensity at 552 nm was observed; no change in the luminescence for avidin : $[Re(CO)_3(bipy)L^{12}]^+$ (Figure 2.34). The binding of $[Re(CO)_3(bipy)L^{12}]^+$ (modified biotin) to avidin was confirmed *via* UV-vis avidin-HABA titrations and so the the absence of an increase in emission intensity, the lack of blue-shift in the emission maxima, and the absence of an extension in emission lifetime (Table 3) suggests there is little or no protection of the $[Re(CO)_3(bipy)L^{12}]^+$ unit when it is bound to avidin.

Table 2.3 Lifetimes of $[Re(CO)_3(bipy)L^{12}]^+$ in different media

	Lifetime (ns)
Re(I)-L^{12}	101
Re(I)-L^{12} PBS	108
Re(I)-L^{12} Avidin	104

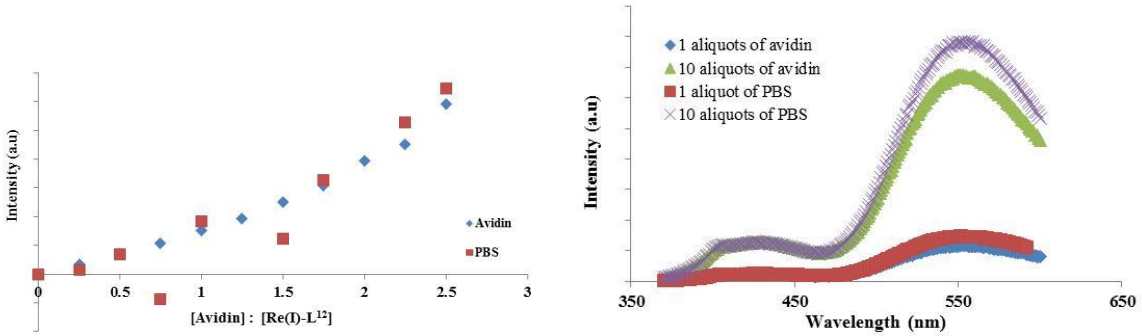

Figure 2.34 LHS; Emission titration curves for the titration of i) blank PBS solution with $[Re(CO)_3(bipy)L^{12}]^+$ [0.3mM] & ii) [0.075mM] aliquots of avidin with $[Re(CO)_3(bipy)L^{12}]^+$ [0.3 mM]. (λ_{em} = 552 nm). RHS steady state emission of $[Re(CO)_3(bipy)L^{12}]^+$. (λ_{exc} = 310 nm).

2.8.4.2.4. Emission titrations of mixed L^{11} and $[Re(CO)_3(bipy)L^{12}]^+$

Despite no effect of avidin-binding being observed for $[Re(CO)_3(bipy)L^{12}]^+$, titrations were carried out using a 50:50 mixture of **L^{11}** and $[Re(CO)_3(bipy)L^{12}]^+$ and avidin/PBS to examine the possibility of intermolecular energy transfer. The intensities of the bands at 420 nm and 552 nm, which correspond to ligand based and ^{3}MLCT-based emission respectively, were analysised at different quantities of avidin/PBS (Figure 2.35). At 420 nm, no enhancement in emission intensity was seen for the ligand based emission when compared to the standard (PBS), this observation is dis-similar to that of the isolated **L^{11}** seen above (Figure 2.33). At 552 nm no change in emission intensity from the standard to the avidin-bound compound was observed, similarly to the behaviour of isolated $[Re(CO)_3(bipy)L^{12}]^+$ seen above (Figure 2.34).

The absence of an increase in ligand based-emission intensity for avidin-bound coumarin-biotin compound, **L^{11}**, in the presence of $[Re(CO)_3(bipy)L^{12}]^+$ (Figure 2.35), suggests that the enhancement in coumarin-based emission previously seen for this compound (Figure 2.33) was being quenched and so it is likely that energy transfer was occuring. The lack of an increase in emission at 552 nm (which would be expected for efficient transfer of

ligand based energy) suggests that the energy transferred is not re-emitted, and so overall the enhancement of coumarin emission which occurs upon avidin binding is simply being quenched by the presence of the rhenium complex in the avidin macromolecule, with no associated extra emission at a different wavelength. The emissivity of the ^{3}MLCT state will be dictated by those processes that dominate quenching of that specific excited state.

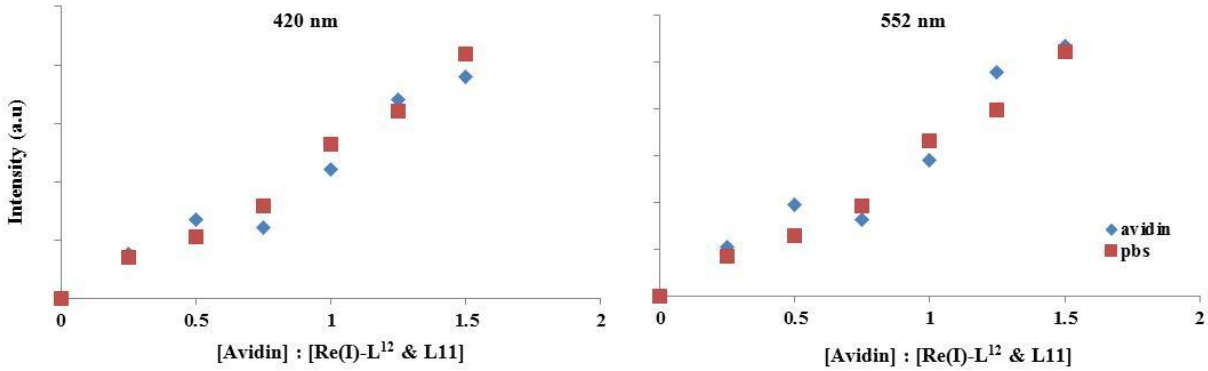

Figure 2.35 Emission titration curves for the titration of i) blank pbs solution with (L^{11} and $[Re(CO)_3(bipy)L^{12}]^+$) [0.3mM] & ii) [0.075mM] aliquots of avidin with (L^{11} and $[Re(CO)_3(bipy)L^{12}]^+$) [0.3 mM]. LHS, (λ_{em} = 420 nm); RHS (λ_{em} = 552 nm). (λ_{exc} = 310 nm).

2.9. Conclusion

L^{11}-L^{13} were successfully synthesised *via* the activated biotin esters and the formation of $[Re(CO)_3(bipy)L^{12/13}]^+$ was achieved following literature precedent.[30] Avidin-biotin binding of coumarin-biotin, **L^{11}** and $[Re(CO)_3(bipy)L^{12}]^+$ was confirmed using UV-vis titrations; the Uv-vis data reported that both compounds have efficient binding to avidin. The flourescence data, acccumulated from the emission titrations, indicate an enhancement in the emission intensity for coumarin-biotin**,** **L^{11}**, when bound to avidin. This increase in emission was absent in a mixed system of coumarin-biotin, **L^{11}** and $[Re(CO)_3(bipy)L^{12}]^+$ which is suggestive of the occurance of energy transfer/quenching. Any effect of Re(I)-biotin avidin binding and/or energy transfer was not observed in the intensity of ^{3}MLCT-based emission which could suggest that any increase in the fluorescence as a result of avidin binding and/or energy transfer was being quenched. To prove this further investigation into the lifetimes of the coumarin and rhenium species is required. If energy transfer is occuring, the lifetime of coumarin in the presence of Re(I) should decrease, additionally, if the lifetime of rhenium decreases in the presesence of the coumarin, quenching would be implied. As coumarin lifetime is short this would be a lot of work, and as the desired result (enhancement of Re(I)) was not observed, no further investigations were carried out.

2.10. Experimental

2.10.1. Synthesis of complexes Re(I)-L^{1-6}

***fac*-[Re(CO)$_3$(bipy)L^1]$^+$** To a round bottom flask L^1 (43 mg, 1.8×10^{-4} mol) and [Re(CO)$_3$(bipy)MeCN]$^+$ (50 mg, 1.07×10^{-4} mol) in toluene (10 mL) were added and heated to 100 ˚C for 24 hours. The solution was filtered through Celite and column chormatography was used to purify the crude product (silica, DCM:MeOH 95:5). Yield: 27 mg, 38 %. ^{1}H NMR ($CDCl_3$, 400 MHz, 298 K) δ_H: 0.82 (3H, t, $^3J_{HH}$ = 6.8 Hz, (*H13*)), 1.15-1.18 (8H, m, (*H9-H12*)), 1.57-1.62 (2H, m, (*H8*)) 2.01-2.04 (2H, m, (*H7*)), 4.10 (2H, d, $^3J_{HH}$ = 5.9 Hz, (*H5*)), 7.02-7.07 (1H, m, (*H3*)) , 7.45 (1H, t, $^3J_{HH}$ = 6 Hz, (*H6*)), 7.65-7.74 (4H, m (*H16, H17*)), 7.76 (1H, d, $^3J_{HH}$ = 7.9 Hz, (*H4*)), 8.13-8.21 (2H, m, (*H1, H2*)), 8.42-8.48 (2H, m, (*H15*)), 9.0-9.08 (2H, m, (*H14*)) ppm. ^{13}C{^{1}H} NMR ($CDCl_3$, 101 MHz, 298 K) δ_C: 12.0, 20.0, 23.5, 26.6, 28.7, 29.2, 33.9, 38.0, 123.5, 124.5, 127.0, 137.5, 138.0, 139.0, 140.1, 148.5, 150.9, 153.8, 172.1 ppm. MS (ES$^+$) *m/z*: 661.26 [M-BF_4^-]$^+$, HRMS (ES$^+$) found *m/z* 659.1784; [$^{185}ReC_{27}H_{30}O_4N_4{}^{10}BF_4$]$^+$ requires 659.1791. IR (nujol) υ: 1670 (CO), 1934 (CO), 2036 (CO) cm^{-1}. UV-vis (ε / M^{-1} cm^{-1}) (MeCN) λ_{max}: 273 (7874) nm.

***fac*-[Re(CO)$_3$(bipy)L^2]$^+$** To a round bottom flask L^2 (38 mg, 1.18×10^{-4} mol) and [Re(CO)$_3$(bipy)MeCN] (50 mg, 1.07×10^{-4} mol) were added and heated to 100 ˚C for 24 hours. Worked up as before. Yield: 36 mg, 45 %. ^{1}H NMR ($CDCl_3$, 400 MHz, 298 K) δ_H: 0.81-0.85 (3H, m, (*H19*)), 1.14-1.27 (20H, m, (*H9-H18*)), 1.42-1.51 (2H, m, (*H8*)), 2.01 (2H, t, (*H7*)), 4.10 (2H, d, (*H5*)), 7.15 (1H, t, (*H3*)) , 7.52-7.56 (1H, m, (*H6*)), 7.62-7.69 (4H, m, (*H22,H23*)), 7.72 (1H, d, (*H4*)), 8.15-8.19 (2H, m, (*H1,H2*)), 8.49-8.52 (2H, m, (*H21*)), 9.01-9.05 (2H, m, (*H20*)) ppm. ^{13}C{^{1}H} NMR ($CDCl_3$, 101 MHz, 298 K) δ_C: 14.9, 22.3, 25.2, 28.9, 29.0, 31.1, 32.6, 36.5, 40.8, 126.8, 129.0, 139.8, 140.1, 141.0, 150.0, 150.8, 153.8, 154.2, 156.1, 174.8 ppm. MS (ES$^+$) *m/z*: 745.34 [M-BF_4^-]$^+$, HRMS (ES$^+$) found *m/z* 743.2728; [$^{185}ReC_{33}H_{42}O_4N_4{}^{10}BF_4$]$^+$ requires 743.2730. IR (nujol) υ: 1560 (CO), 1926 (CO) 2036 (CO) cm^{-1}. UV-vis (ε / M^{-1} cm^{-1}) (MeCN) λ_{max}: 274 (3953) nm.

***fac*-[Re(CO)$_3$(bipy)L^3]$^+$** To a round bottom flask L^3 (44 mg, 1.18×10^{-4} mol) and [Re(CO)$_3$(bipy)MeCN] (50 mg, 1.07×10^{-4} mol) in toluene (10 mL) were added and heated to 100 ˚C for 24 hours. Work up same as before. Yield: 43 mg, 54 %. ^{1}H NMR ($CDCl_3$, 400 MHz, 298 K) δ_H: 0.82 (3H, t, $^3J_{HH}$ =3.5 Hz, (*H23*)), 1.12-1.29 (28H, m, (*H9-H22*)), 1.43-1.49 (2H, m, (*H8*)) 1.99 (2H, t, (*H7*)), 4.11 (2H, d, $^3J_{HH}$ = 6 Hz, (*H5*)), 7.12 (1H, t, (*H3*)) , 7.41 (1H, t, (*H6*)), 7.61-7.81 (5H, m, (*H4, H26, H27*)), 8.16-8.21 (2H, m, (*H1, H2*)), 8.48-8.52

(2H, m, (*H25*)), 9.05 (2H, d, $^{3}J_{HH}$ = 5.4 Hz (*H24*)) ppm. MS (ES^{+}) *m/z*: 745.27 [M-2CO-BF_4]$^{+}$, HRMS (ES^{+}) found *m/z* 745.2744 [M-2CO]$^{+}$; [$^{185}ReC_{35}H_{50}O_2N_4{}^{10}BF_4$]]$^{+}$ requires 745.3486. IR (nujol) υ: 1603 (CO), 1928 (CO), 2036 (CO) cm^{-1}. UV-vis (ε / M^{-1} cm^{-1}) (MeCN) λ_{max}: 275 (8548) nm.

***fac*-[Re(CO)$_3$(phen)L^1]$^{+}$** To a round bottom flask encased in foil, L^1 (44 mg, 1.89×10^{-4} mol), [Re(CO)$_3$(phen)Br] (50 mg, 9.43×10^{-5} mol) and silver tetrafluoroborate (28 mg, 1.44×10^{-4} mol) in toluene (10 mL) were added and heated to 100 °C for 24 hours. The solution was filtered through Celite and washed repeatedly with acetonitrile. The removal of the solvent under high vacuum afforded a yellow solid. Column chromotography was then used to purify the crude product (silica, DCM:MeOH, 95:5). Yield: 14 mg, 22 %. ^{1}H NMR ($CDCl_3$, 400 MHz, 298 K) δ_H: 0.8 (3H, t, (*H13*)), 1.08-1.21 (8H, m, (*H9-H12*)), 1.45 (2H, t, $^{3}J_{HH}$ = 7.1 Hz, (*H8*)), 2.01 (2H, t, $^{3}J_{HH}$ =7 Hz, (*H7*)), 4.01 (2H, s, (*H5*)), 7.11-7.15 (1H, m, (*H3*)), 7.58-7.61 (1H, m, (*H4*)) , 8.10-8.19 (4H, m, (*H14*, *H15*)), 8.21-8.26 (1H, m, (*H2*)), 8.25 (1H, s, (*H1*)), 8.85 (2H, d, (*H16*)), 9.05 (2H, d, (*H17*)) ppm. $^{13}C\{^{1}H\}$ NMR ($CDCl_3$, 101 MHz, 298 K) δ_C: 13.8, 22.2, 25.0, 29.0, 28.9, 31.5, 36.0, 40.0, 125.0, 124.9, 127.5, 128.0, 131.2, 138.0, 141.1, 146.5, 149.3, 151.9, 153.1, 154.2 ppm. MS (ES^{+}) *m/z*: 685.2 [M-BF_4^{-}]$^{+}$. HRMS (ES^{+}) found *m/z* 683.1749 [M]]$^{+}$; [$^{185}ReC_{29}H_{30}O_4N_4{}^{10}BF_4$]]$^{+}$ requires 683.1791. IR (nujol) υ: 1598 (CO), 2024 (CO), 2036 (CO) cm^{-1}. UV-vis (ε / $M^{-1}cm^{-1}$) (MeCN) λ_{max}: 223 (1673), 276 (643) nm.

***fac*-[Re(CO)$_3$(phen)L^2]$^{+}$** To a round bottom flask encased in foil, L^2 (60 mg, 1.89×10^{-4} mol), [Re(CO)$_3$(phen)Br] (50 mg, 9.43×10^{-5} mol) and silver tetrafluoroborate (28 mg, 1.44×10^{-4} mol) in toluene (10 mL) were added and set to sub reflux at 100 °C for 24 hours. Work-up was as described above. Yield: 18 mg, 25 %. ^{1}H NMR ($CDCl_3$, 400 MHz, 298 K) δ_H: 0.81 (3H, t, (*H19*)), 1.11-1.23 (22H, m, (*H8-H18*)), 2.01 (2H, t, (*H7*)), 4.01 (2H, s, (*H5*)), 7.12-7.15 (1H, m, (*H3*)), 7.49 (1H, d, (*H4*)), 8.08-815 (4H, m, (*H22*, *H23*)), 8.17-8.23 (1H, m, (*H2*)), 8.25 (1H, s, (*H1*)), 8.82 (2H, d, (*H21*)), 9.59 (2H, d, (*H20*)) ppm. $^{13}C\{^{1}H\}$ NMR ($CDCl_3$, 101 MHz, 298 K) δ_C: 12.2, 21.1, 22.3, 23.0, 24.1, 27.9, 28.0, 28.5, 29.2, 31.0, 33.2, 37.1, 49.0, 27.8, 124.5, 126.1, 127.1, 130.1, 138.9, 139.5, 145.4, 148.0, 150.8, 153.0, 173.1, 206.0 ppm. MS (ES^{+}) *m/z*: 769.25 [M-BF_4^{-}]$^{+}$, 319.26 [M-Re(CO)$_3$PhenBF$_4$+H]$^{+}$. HRMS (ES^{+}) found *m/z* 769.2757; [$^{185}ReC_{35}H_{42}O_4N_4{}^{10}BF_4$]]$^{+}$ requires 767.2730. IR (nujol) υ: 1599 (CO), 1926 (CO), 2036 (CO) cm^{-1}. UV-vis (ε / M^{-1} cm^{-1}) (MeCN) λ_{max}: 206 (923), 270 (153) nm.

***fac*-Re(CO)$_3$(phen)L^3]$^+$** To a round bottom flask encased in foil L^3 (71 mg, 1.89 × 10^{-4} mol), [Re(CO)$_3$(phen)Br] (50 mg, 9.43 × 10^{-5} mol) and silver tetrafluoroborate (28 mg, 1.44 × 10^{-4} mol) in toluene (10 mL) were added and heated to 100 °C for 24 hours. Work-up as before. Yield: 27 mg, 35%. ^{1}H NMR (CDCl$_3$, 400 MHz, 298 K) δ_H: 0.82 (3H, t, $^3J_{HH}$ = 6.8 Hz, (*H23*)), 1.01-1.24 (28H, m, (*H19-H22*)), 1.38-1.42 (2H, m, (*H8*)), 1.97 (2H, t, $^3J_{HH}$ = 7.7 Hz, (*H7*)), 4.05 (2H, d, $^3J_{HH}$ =6.1 Hz, (*H5*)), 7.01-7.09 (1H, m, (*H3*)), 7.18 (1H, t, (*H6*)), 7.65 (1H, d, (*H4*)), 8.04-8.08 (1H, m, (*H2*)), 8.11-8.15 (4H, m, (*H26,H27*)), 8.25 (1H, s, (*H1*)), 8.69 (2H, d, (*H25*)), 9.57 (2H, d, (*H24*)) ppm. ^{13}C{^{1}H} NMR (CDCl$_3$, 101 MHz, 298 K) δ_C: 14.0, 22.8, 25.8, 29.1, 32.0, 36.0, 40.9, 126.0, 128.2, 129.4, 131.7, 139.2, 146.5, 146.8, 149.9, 152.0, 155.1, 174.5, 195.6 ppm. MS (ES$^+$) *m/z*: 825.33 [M-BF4$^-$]$^+$, 375.33 [M-Re(CO)$_3$PhenBF$_4$]+H]$^+$. HRMS (ES$^+$) found *m/z* 825.3381; [^{185}ReC$_{39}$H$_{50}$O$_4$N$_4$^{10}BF$_4$]$^+$ requires 823.3356. IR (nujol) υ: 1668 (CO), 1923 (CO), 2034 (CO) cm^{-1}. UV-vis (ε / M^{-1}cm^{-1}) (MeCN) λ_{max}: 214 (1628), 273 (785) nm.

***fac*-[Re(CO)$_3$(phen)L^4]$^+$** To a round bottom flask encased in foil L^4 (45 mg, 1.89 × 10^{-4} mol), [Re(CO)$_3$(phen)Br] (50 mg, 9.43 × 10^{-5} mol) and silver tetrafluoroborate (28 mg, 1.44 × 10^{-4} mol) in toluene (10 mL) were added and heated to 100 °C for 24 hours. Work-up as before. Yield 37 mg, 58 %. ^{1}H NMR (CDCl$_3$, 400 MHz, 298 K) δ_H: 0.75 (3H, t, $^3J_{HH}$ = 6.2 Hz, (*H12*)), 1.15-1.28 (8H, m, (*H8-H11*)), 1.42 (2H, t, $^3J_{HH}$ = 6.9 Hz, (*H7*)), 2.14 (2H, t, $^3J_{HH}$ = 7.6 Hz, (*H6*)), 4.85 (2H, s, (*H5*)), 7.29 (1H, t, $^3J_{HH}$ = 4.5 Hz, (H3)), 7.61 (1H, d, $^3J_{HH}$ = 7.9 Hz, (*H4*)), 8.10 (2H, s, (*H16*)), 8.12-8.26 (3H, m, (*H2*, *H15*)), 8.33 (1H, s, (*H1*)), 8.75-8.78 (2H, m, (*H14*)), 9.57 (2H, d, $^3J_{HH}$ = 4.9 Hz, (*H13*)) ppm. ^{13}C{^{1}H} NMR (CDCl$_3$, 101 MHz, 298 K) δ_C: 22.0, 22.9, 24.2, 27.0, 29.8, 30.2, 33.0, 61.0, 126.2, 126.9, 129.8, 130.0, 134.5, 138.2, 139.1, 144.7, 150.0, 152.5, 171.5, 193.5 ppm. MS (ES$^+$) *m/z*: 686.15 [M-BF$_4$$^-$]$^+$. HRMS (ES$^+$) found *m/z* 684.1361; [^{185}ReC$_{29}$H$_{29}$O$_5$N$_3$^{10}BF$_4$]$^+$ requires 684.1631. IR (nujol) υ: 1740 (CO), 2024 (CO), 2037 (CO) cm^{-1}. UV-vis (ε / M^{-1}cm^{-1}) (MeCN) λ_{max}: 221 (6308) 273 (5096) nm.

***fac*-[Re(CO)$_3$(phen)L^5]$^+$** To a round bottom flask encased in foil L^5 (47 mg, 1.89 × 10^{-4} mol), [Re(CO)$_3$(phen)Br] (50 mg, 9.43 × 10^{-5} mol) and silver tetrafluoroborate (28 mg, 1.44 × 10^{-4} mol) in toluene (10 mL) were added and heated to 100 °C for 24 hours. Work-up as before. Yield: 15 mg, 21 %. ^{1}H NMR (CDCl$_3$, 400 MHz, 298 K) δ_H: 0.79 (3H, t, $^3J_{HH}$ = 6.6 Hz, (*H18*)), 1.15-1.33 (20H, m, (*H8-H17*)), 1.49 (2H, t, (*H7*)) 2.13 (2H, t, (*H6*)), 4.85 (2H, s, (*H5*)), 7.23-7.29 (1H, m, (*H3*)), 7.62 (1H, d, (*H4*)) , 8.03-8.17 (5H, m, (*H2*, *H21*, *H22*)) 8.30 (1H, s, (*H1*)), 8.75 (2H, d, $^3J_{HH}$ = 8.2 Hz, (*H20*)), 9.53 (2H, d, $^3J_{HH}$ = 4.7 Hz, (*H1*)) ppm.

$^{13}C\{^{1}H\}$ NMR ($CDCl_3$, 101 MHz, 298 K) δ_C: 13.8, 23.0, 25.2, 28.9, 32.2, 34.1, 62.2, 127.0, 127.5, 128.3, 130.8, 135.7, 139.5, 140.7, 146.6, 151.8, 154.4, 173.5, 195.2 ppm. MS (ES^+) *m/z*: 770.23 $[M\text{-}BF_4]^+$. HRMS (ES^+) found *m/z* 768.2521; $[^{185}ReC_{35}H_{41}O_5N_3{}^{10}BF_4]^+$ requires 768.2570. IR (nujol) υ: 1735 (CO), 1935 (CO), 2035 (CO) cm^{-1}. UV-vis (ε / M^{-1} cm^{-1}) (MeCN) λ_{max}: 216 (3063), 274 (2093) nm.

***fac*-[Re(CO)$_3$(phen)L^6]$^+$** To a round bottom flask encased in foil L^6 (71 mg 1.89×10^{-4} mol), $[Re(CO)_3(phen)Br]$ (50 mg, 9.43×10^{-5} mol) and silver tetrafluoroborate (28 mg, 1.44×10^{-4} mol) in toluene (10 mL) were added and heated to 100 °C for 24 hours. Work-up as before. Yield: 10 mg, 13 %. ^1H NMR ($CDCl_3$, 400 MHz, 298 K) δ_H: 0.83 (3H, t, (*H22*)), 1.08-1.24 (28H, m, (*H8*-*H21*)), 1.45 (2H. t, (*H7*)), 2.24 (2H, t, (*H6*)), 4.2 (2H, s, (*H5*)), 7.13 (1H, t, (*H3*)), 7.37 (1H, d, (*H4*)), 7.92-7.97 (2H, m, (*H24*)), 8.21 (2H, s, (*H26*)), 8.78-8.83 (2H, m, (*H1*, *H2*)), 8.88-8.91 (2H, m, (*H25*)), 9.55 (2H, d, ((*H23*)) ppm. MS (ES^+) *m/z*: 826.29 $[M\text{-}BF4]^+$. IR (nujol) υ: 1795 (CO), 2013 (CO), 2039 (CO) cm^{-1}. UV-vis (ε / M^{-1} cm^{-1}) (MeCN) λ_{max}: 207 (1408), 262 (483) nm.

***fac*-[Re(CO)$_3$(neoc)L^1]$^+$** To a round bottom flask encased in foil L^1 (41 mg, 1.78×10^{-4} mol), $[Re(CO)_3(neoc)Br]$ (50 mg, 8.9×10^{-5} mol) and silver tetrafluoroborate (28 mg, 1.44×10^{-4} mol) in toluene (10 mL) were added and heated to 100 °C for 24 hours. Work-up as before. Yield: 19 mg, 30 %. ^1H NMR ($CDCl_3$, 400 MHz, 298 K) δ_H: 0.74-0.78 (3H, m, (*H13*)), 1.19-1.26 (8H, m, (*H9*-*H12*)), 1.47 (2H, t, $^3J_{HH}$ = 7.3 Hz, (*H8*)), 1.95 (2H, t, $^3J_{HH}$ = 7.7 Hz, (*H7*)), 3.29 (6H, s, (*H14*)), 3.97 (2H, d, (*H5*)), 6.92 (1H, t, (*H3*)) , 7.05 (1H, t, (H6)), 7.48-7.55 (1H, m, (*H4*)), 7.63-7.66 (2H, m, (*H16*)), 7.80 (2H, s, (*H17*)), 7.91 (2H, d, $^3J_{HH}$ = 8.3 Hz, (*H15*)), 8.37-8.41 (2H, m, (*H1*,*H2*)) ppm. $^{13}C\{^{1}H\}$ NMR ($CDCl_3$, 101 MHz, 298 K) δ_C: 13.0, 21.5, 24.2, 27.8, 28.7, 30.0, 30.9, 34.8, 124.8, 124.9, 126.0, 126.9, 128.1, 138.1, 139.0, 146.0, 149.1, 150.2, 163.5, 172.8 ppm. MS (ES^+) *m/z*: 713.15$[M\text{-}BF4]^+$. HRMS (ES^+) found *m/z* 713.2129 $[M]^+$; $[^{185}ReC_{31}H_{34}O_4N_4{}^{10}BF_4]^+$ requires 711.2099. IR (nujol) υ: 1598 (CO), 1970 (CO), 2023 (CO) cm^{-1}.UV-vis (ε / M^{-1} cm^{-1}) (MeCN) λ_{max}: 277 (6528) nm.

***fac*-[Re(CO)$_3$(neoc)L^2]$^+$** To a round bottom flask encased in foil L^2 (57 mg, 1.71×10^{-4} mol), $[Re(CO)_3(neoc)Br]$ (50 mg, 8.9×10^{-5} mol) and silver tetrafluoroborate (28 mg, 1.44×10^{-4} mol) in toluene (10 mL) were added and heated to 100 °C 24 hours. Work-up as before. Yield: 28 mg, 39 %. ^1H NMR ($CDCl_3$, 400 MHz, 298 K) δ_H: 0.78 (3H, t, $^3J_{HH}$ = 6.5 Hz, (*H19*)), 1.17-1.29 (20H, m, (*H9*-*H18*)), 1.45-1.49 (2H, m, (*H8*)), 1.97-1.99 (2H, m, (*H7*)), 3.29 (6H, s, (*H20*)), 4.02 (2H, s, (*H5*)), 6.90-6.95 (1H, m, (*H3*)), 7.51-7.56 (1H, m, (*H6*)),

7.60-7.68 (1H, m, (*H4*)), 7.75 (2H, s, (*H23*)), 7.93-7.97 (2H, m, (*H22*)), 8.28 (2H, d, $^{3}J_{HH}$ = 8.2 Hz, (*H21*)), 8.44-8.47 (2H, m, (*H1*,*H2*)) ppm. MS (ES^{+}) *m/z*: 797.77 $[M\text{-}BF_4]^{+}$. HRMS (ES^{+}) found *m/z* 797.3065; $[^{185}ReC_{37}H_{46}O_4N_4{}^{10}BF_4]^{+}$ requires 795.3043. IR (nujol) υ:1589 (CO), 1961 (CO), 2034 (CO) cm^{-1}. UV-vis (ε / M^{-1} cm^{-1}) (MeCN) λ_{max}: 275 (7447) nm.

***fac*-[Re(CO)$_3$(neoc)L^3]$^+$** To a round bottom flask encased in foil L^3 (67 mg, × 10^{-4} mol), [Re(CO)$_3$(neoc)Br] (50 mg, 8.9 × 10^{-5} mol) and silver tetrafluoroborate (28 mg, 1.44 × 10^{-4} mol) in toluene (10 mL) were added and heated to 100 °C 24 hours. Work-up as before. Yield: 17 mg, 22 %. ^{1}H NMR ($CDCl_3$, 400 MHz, 298 K) δ_H: 0.82 (3H, t, (*H23*)), 1.12-1.28 (30H, m, (*H8*-*H22*)), 1.91-1.95 (2H, m, (*H7*)), 3.31 (6H, s, (*H24*)), 3.97 (2H, s, (*H5*)), 6.89-6.93 (1H, m, (*H3*)) , 7.19 (1H, s, (*H6*)), 7.43-7.49 (1H, m, (*H4*)), 7.56-7.61 (2H, m, (*H25*)), 7.75-7.79 (2H, m, (*H26*)), 8.88 (2H, s, (*H27*)), 8.42-8.47 (2H, m, (*H1*,*H2*)) ppm.$^{13}C\{^{1}H\}$ NMR ($CDCl_3$, 101 MHz, 298 K) δ_C: 12.7, 15.1, 16.0, 16.4, 16.5, 17.1, 17.7, 18.3, 20.5, 24.8, 27.4, 27.9, 28.6, 29.8, 30.8, 54.1, 61.8, 134.0, 139.8, 145.5, 147.1, 149.6, 150.6, 153.2, 162.7, 173.4 ppm. MS (ES^{+}) *m/z*: 853.43 $[M\text{-}BF_4]^{+}$. HRMS (ES^{+}) found *m/z* 853.3700; $[^{185}ReC_{41}H_{54}O_4N_4{}^{10}BF_4]^{+}$ requires 851.3669. IR (nujol) υ: 1597 (CO), 1932 (CO), 2035 (CO) cm^{-1}. UV-vis (ε / M^{-1} cm^{-1}) (MeCN) λ_{max}: 275 (7447) nm.

***fac*-[Re(CO)$_3$(neoc)L^4]$^+$** To a round bottom flask encased in foil L^4 (42 mg, 1.79 × 10^{-4} mol), [Re(CO)$_3$(neoc)Br] (50 mg, 8.9 × 10^{-5} mol) and silver tetrafluoroborate (28 mg, 1.44 × 10^{-4} mol) in toluene (10 mL) were added and heated to 100 °C 24 hours. Work-up as before. Yield: 14 mg, 23 %. ^{1}H NMR ($CDCl_3$, 400 MHz, 298 K) δ_H: 0.80 (3H, t, $^{3}J_{HH}$ = 6.2 Hz, (*H12*)), 1.11-1.28 (8H, m, (*H8*-*H11*)), 1.49 (2H, t, (*H7*)) 2.15 (2H, t, $^{3}J_{HH}$ = 7.6 Hz, (*H6*)), 3.25 (6H, s, (*H13*)), 4.73 (2H, s, (*H5*)), 7.55-7.61 (1H, m, (*H3*)), 7.65 (1H, d, $^{3}J_{HH}$ = 8 Hz, (*H4*)) , 7.89 (2H, $^{3}J_{HH}$ = 8.3 Hz, (*H14*)), 7.92 (2H, s, (*H16*)), 8.25 (2H, d, $^{3}J_{HH}$ = 8.3 Hz, (*H15*)), 8.48-8.52 (2H, m, (*H1*,*H2*)) ppm.$^{13}C\{^{1}H\}$ NMR ($CDCl_3$, 101 MHz, 298 K) δ_C:14.5, 22.0, 25.1, 29.2, 29.3, 30.7, 31.5, 34.2, 62.0, 126.4, 126.5, 127, 127.5, 127.5, 128.7, 129.5, 135.2, 138.0, 139.9, 140.0, 147.1, 151.8, 152.1, 164.0, 164.8, 174.1, 196.2 ppm. MS (ES^{+}) *m/z*: 714.13 $[M\text{-}BF_4]^{+}$. HRMS (ES^{+}) found *m/z* 714.1996; $[^{185}ReC_{31}H_{33}O_5N_4{}^{10}BF_4]^{+}$ requires 712.1944. IR (nujol) υ: 1740 (CO), 1935 (CO), 2036 (CO) cm^{-1}.UV-vis (ε / M^{-1} cm^{-1}) (MeCN) λ_{max}: 221 (1691), 280 (1049) nm.

***fac*-[Re(CO)$_3$(neoc)L^5]$^+$** To a round bottom flask encased in foil L^5 (57 mg, 1.74 × 10^{-4} mol), [Re(CO)$_3$(neoc)Br] (50 mg, 8.9 × 10^{-5} mol) and silver tetrafluoroborate (28 mg, 1.44 × 10^{-4} mol) in toluene (10 mL) were added and heated to 100 °C 24 hours. Work-up as before.

Yield: 28 mg, 39 %. ^{1}H NMR ($CDCl_3$, 400 MHz, 298 K) δ_H: 0.78 (3H, t, $^{3}J_{HH}$ = 7.3 Hz, (*H18*)), 1.10-1.28 (18H, m, (*H9-H17*)), 1.46 (2H, t, (*H8*)), 2.12 (2H, t, (*H7*)), 3.28 (6H, s, (*H19*)), 4.73 (2H, s, (*H6*)), 7.16-7.21 (1H, m, (*H3*)), 7.54 (1H, d, (*H4*)), 7.61 (2H, s, (*H22*)), 8.30-8.37 (2H, m, (*H21*)), 7.90 (2H, d, $^{3}J_{HH}$ = 8.4 Hz, (*H20*)), 8.51-8.53 (2H, m, (*H1*, *H2*)) ppm. $^{13}C\{^{1}H\}$ NMR ($CDCl_3$, 101 MHz, 298 K) δ_C: 2.0, 13.1, 21.9, 23.8, 28.0, 28.0, 28.1, 28.5, 28.5, 28.7, 28.8, 30.0, 31.1, 33.1, 116.2, 124.0, 124.9, 125.8, 126.0, 126.0, 126.2, 128.7, 134.0, 137.5, 137.5, 138.5, 139.7, 145.4, 150.5, 157.5, 163.5, 172.1 ppm. MS (ES^+) *m/z*: 798.38 $[M\text{-}BF_4]^+$. HRMS (ES^+) found *m/z* 798.2902 $[M]^+$; $[^{185}ReC_{37}H_{45}O_5N_3{}^{10}BF_4]^+$ requires 796.2883. IR (nujol) υ: 1739 (CO), 1936 (CO), 2036 (CO) cm^{-1}. UV-vis (ε / M^{-1} cm^{-1}) (MeCN) λ_{max}: 229 (10440), 272 (8240) nm.

***fac*-$[Re(CO)_3(neoc)L^6]^+$** To a round bottom flask encased in foil L^6 (66 mg, 1.78×10^{-4} mol), $[Re(CO)_3(neoc)Br]$ (50 mg, 8.9×10^{-5} mol) and silver tetrafluoroborate (28 mg, 1.44×10^{-4} mol) in toluene (10 mL) were added and heated to 100 °C 24 hours. Work-up as before. Yield: 29 mg, 38 %. ^{1}H NMR ($CDCl_3$, 400 MHz, 298 K) δ_H: 0.78 (3H, m, (*H22*)), 1.13-1.31 (28H, m, (*H8-H21*)), 1.48-1.54 (2H, m, (*H7*)) 2.12 (2H, t, (*H6*)), 3.22 (6H, s, (*H23*)), 4.22 (2H, s, (*H5*)), 7.12-7.16 (1H, m, (*H3*)), 7.55 (1H, d, (*H4*)) , 7.62 (2H, d, (*H25*)), 7.83 (2H, s, (*H26*)), 7.89 (2H, d, (*H24*)), 8.48-8.51 (2H, m, (*H1*, *H2*)) ppm. $^{13}C\{^{1}H\}$ NMR ($CDCl_3$, 101 MHz, 298 K) δ_C: 14.0, 22.2, 24.8, 29.0, 29.0, 29.0, 29.1, 29.1, 29.1, 29.1, 29.1, 29.2, 29.2, 30.8, 31.9, 34.2, 62.0, 125.8, 125.9, 126.0, 126.9, 126.9, 127.8, 130.0, 135.4, 135.5, 139.0, 140.5, 141.3, 147.7, 151.9, 153.5, 164.5, 173.6 ppm. MS (ES^+) *m/z*: 854.33 $[M\text{-}BF_4]^+$. HRMS (ES^+) found *m/z* 854.3537; $[^{187}ReC_{41}H_{53}O_5N_4{}^{10}BF_4]^+$ requires 854.3509 IR (nujol) υ: 1597 (CO), 1924 (CO), 2036 (CO) cm^{-1}. UV-vis (ε / M^{-1} cm^{-1}) (MeCN) λ_{max}: 228 (1041), 277 (725.8) nm.

2.10.2. Synthesis of ligand and $[Re(CO)_3(N\hat{}N)L^{8\text{-}10}]^+$

L^7 1,12 dodecandiol (10 g, 4.99×10^{-2} mol) in chloroform was added slowly to a solution of nicotinyl chloride (1 g, 7.07×10^{-3} mol) and TEA (3.23 mL, 2.2×10^{-2} mol) in chloroform (50 mL). The solution mixture was left to stir at 60 °C for 3 hours. The solution was washed with water (3 × 10 mL) and sat. aq. Ammonium chloride (10 mL). The organic layer was dried and the solvent evaporated to dryness, yielding a cream solid. Yield: 0.940 g, 43 %. ^{1}H NMR ($CDCl_3$, 400 MHz, 298 K) δ_H: 1.49-1.32 (16H, m, (*H7-H14*)), 1.50-1.55 (2H, m, (*H15*)), 1.62-1.69 (2H, m, (*H6*)), 3.58 (2H, t, $^3J_{HH}$ =6.6 Hz , (*H16*)), 4.75 (2H, t, $^3J_{HH}$ =6.6 Hz, (*H5*)), 7.39-7.43 (1H, m, (*H3*)), 8.18-8.22 (1H, m, (*H4*)), 8.67 (1H, d, $^3J_{HH}$ =3.3 Hz, (*H2*)), 9.10 (1H, s, (*H13*)) ppm. ^{13}C{^{1}H} NMR ($CDCl_3$, 101 MHz, 298 K) δc: 24.7, 25.0, 27.6, 28.2, 28.4, 28.5, 28.5, 31.8, 61.9, 64.6, 122.3, 125.4, 136.1, 149.7, 152.2, 164.3 ppm. MS (ES^+) *m/z*: 308.23 $[M+H]^+$, HRMS (ES^+) found *m/z* 308.2218; $[C_{18}H_{30}O_3N]^+$ requires 308.2220. IR (nujol) υ: 1711 (CO) cm^{-1}. UV-vis (ε / M^{-1} cm^{-1}) (MeCN) λ_{max}: 264 (3096) nm.

Pro-L^8 Ethylene glycol (2.8 mL, 4.9×10^{-2} mol) in chloroform was added slowly to a solution of nicotinyl chloride (1 g, 7.07×10^{-3} mol) and TEA (3.23 mL, 2.2×10^{-2} mol) in chloroform (40 mL). The solution was left to stir at 60 °C for 3 h. Work-up as before. Yield: 0.350 g, 30 %. ^{1}H NMR ($CDCl_3$, 400 MHz, 298 K) δ_H: 3.82 (2H, t, $^3J_{HH}$ = 4.7 Hz, (*H6*)), 4.32 (2H, t, $^3J_{HH}$ = 4.5 Hz, (*H5*)), 7.31-7.36 (1H, m, (*H3*)), 8.13 (1H, d, $^3J_{HH}$ = 7.6 Hz, (*H4*)), 8.58-8.64 (1H, m, (*H2*)), 9.22 (1H, s, (*H1*)) ppm. ^{13}C{^{1}H} NMR ($CDCl_3$, 101 MHz, 298 K) δc: 60.4, 67.1, 137.4, 150.5, 153.0, 165.3 ppm. MS (ES^+) *m/z*: 168 $[M+H]^+$, 124.03 $[M-C_2H_5O+H)]^+$. IR (nujol) υ:1734 (CO) cm^{-1}. UV-vis (ε / M^{-1} cm^{-1}) (MeCN) λ_{max}: 230 (2331), 250 (2023), 268 (1940) nm. **L^8** Coumarin acid chloride (0.412 g, 1.98×10^{-3} mol) was dissolved in chloroform (10 mL) and TEA (0.5 mL, 3.96×10^{-3} mol) and added slowly to pro-L^8 (0.300 g, 1.8×10^{-3} mol) in chloroform (25 mL). The solution was left to stir at 60 °C for 3 hours. The solution was washed using sat. aq. sodium bicarbonate (3 × 10 mL) and sat. aq. ammonium chloride (2 x 10 mL) and the organic layer dried and solution evaporated. The crude product was purified using column chromatography eluting with DCM:MeOH (90:10). Yield: 0.100 g, 16 %. ^{1}H NMR ($CDCl_3$, 400MHz, 298K) δ_H: 4.59-4.68 (4H, m, (*H5, H6*)), 7.27-7.33 (2H, m, (H9, H10)), 7.42-7.45 (1H, m, (*H3*)), 7.52-7.62 (2H, m, (*H8, H11*)), 8.24 (1H, d, (*H4*)), 8.49 (1H, s, (H7)), 8.22 (1H, s, (*H2*)), 9.18 (1H, s, (*H1*)) ppm. ^{13}C{^{1}H} NMR ($CDCl_3$, 101 MHz, 298K) δc: 61.9, 62.3, 115.8, 116.6, 116.7, 123.9, 128.7, 133.6, 136.3, 148.1, 149.9, 152.5, 154.2, 156.0, 161.8, 164.0 ppm. MS (ES^+) *m/z*: 362 $[M+Na]^+$, 378 $[M+K]^+$, 403 $[M+MeCNNa]^+$, HRMS (ES^+) found *m/z* 340.0820 $[M+H]^+$; $[C_{18}H_{14}O_6N]^+$

requires 340.0816. IR (nujol) υ: 1642 (CO) cm^{-1}. UV-vis (ε / M^{-1} cm^{-1}) (MeCN) λ_{max}: 330 (2953) nm.

***fac*-[Re(CO)$_3$(bipy)L^8]$^+$** To a round bottom flask, L^8 (35 mg, 1.03 × 10^{-4} mol) and [Re(CO)$_3$(bipy)MeCN] (48 mg, 1.03 × 10^{-4} mol) in chloroform (2 mL) were added and heated at 60 °C for 24 hours. Work up as before. Yield: 25 mg, 32 %. ^{1}H NMR ($CDCl_3$, 400 MHz, 298 K) δ_H: 4.53-4.62 (4H, m, (*H5, H6*)), 7.28-7.32 (2H, m, (*H9, H10*)), 7.51 (1H, t, $^3J_{HH}$ = 4.5 Hz, (*H3*)), 7.56-7.63 (2H, m, (*H8, H11*)), 7.75 (2H, t, $^3J_{HH}$ = 4.5 Hz, (*H15*)), 8.22 (2H, t, (*H14*)), 8.30-8.38 (2H, m, (*H7, H4*)), 8.52-8.56 (3H, m, (*H2, H13*)), 8.65 (1H, s, (*H1*)). 9.18 (2H, d, $^3J_{HH}$ =5 Hz, (*H12*)) ppm. ^{13}C{^{1}H} NMR ($CDCl_3$, 101 MHz, 298 K) δc: 29.9, 52.5, 61.8, 115.7, 116.0, 116.5, 124.1, 124.6, 126.5, 127.3, 128.2, 129.0, 133.8, 139.6, 140.8, 148.7, 151.9, 152.2, 153.5, 153.5, 154.6, 156.1, 162.0 ppm. MS (ES^+) *m/z*: 766.05 [M-BF_4^-]$^+$, HRMS (ES^+) found *m/z* 766.0840 [M]$^+$; [$^{187}ReC_{31}H_{21}O_9N_3{}^{10}BF_4$]$^+$ requires 766.0809. IR (nujol) υ: 1609 (CO), 1732.73 (CO), 1916.41 (CO), 2033.09 (CO) cm^{-1}. UV-vis (ε / M^{-1} cm^{-1}) (MeCN) λ_{max}: 223 (4492.5), 288 (5342.5), 345 (3615) nm.

***fac*-[Re(CO)$_3$(phen)L^8]$^+$** To a round bottom flask, L^8 (43 mg, 1.23 × 10^{-4} mol) and [Re(CO)$_3$(phen)MeCN] (60 mg, 1.1 × 10^{-4} mol) in chloroform (2 mL) were added and heated at 60 °C for 24 hours. Work up as before. Yield: 16 mg, 18 %. ^{1}H NMR ($CDCl_3$, 400 MHz, 298 K) δ_H: 4.52-4.68 (4H, m, (*H5, H6*)), 7.28-7.39 (2H, m, (*H9, H10*)), 7.44-7.47 (1H, m, (*H3*)), 7.60-7.73 (2H, m, (*H8, H11*)), 8.09-8.18 (2H, m, (*H7, H4*)), 8.21-8.32 (3H, m, (*H2, H14*)), 8.48-8.53 (2H, m, (*H15*)), 8.77-8.90 (3H, m, (*H1, H13*)), 9.65 (2H, d, (*H12*)) ppm. ^{13}C{^{1}H} NMR ($CDCl_3$, 101 MHz, 298 K) δc: 77.2, 116.7, 124.2, 127.9, 128.6, 131.3, 135.2, 140.7, 146.3, 149.9, 154.6 ppm. MS (ES^+) *m/z*: 790.09 [M-BF_4^-]$^+$. HRMS (ES^+) found *m/z* 790.0824; [$^{187}ReC_{33}H_{21}O_9N_3{}^{10}BF_4$]$^+$ requires 790.0809. IR (nujol) υ: 1653 (CO). 1733 (CO), 1761 (CO), 1916 (CO), 2031 (CO) cm^{-1}. UV-vis (ε / M^{-1} cm^{-1}) (MeCN) λ_{max}: 277 (5048), 328 (1821) nm.

Pro-L^9 1,6 hexandiol (4.1 g, 3.4 × 10^{-2} mol) in chloroform was added slowly to a solution of nicotinyl chloride (1 g, 7.07 × 10^{-3} mol) and TEA (3.23 mL, 2.2 × 10^{-2} mol) in chloroform (40 mL). The solution mixture was left to stir at 60 °C for 3 hours. Work up as before. Yield: 0.93 g, 59 %. ^{1}H NMR ($CDCl_3$, 400 MHz, 298 K) δ_H: 1.32-1.46 (4H, m, (*H7, H8*)), 1.7 (2H, t, (*H9*)), 2.42-2.46 (2H, m, (*H6*)), 3.61 (2H, t, (*H10*)), 4.34 (2H, t, (*H5*)), 7.39-7.41 (1H, m, (*H3*)), 8.28 (1H, dd, (*H4*)). 8.72-8.75 (1H, m, (*H2*)). 9.11-9.17 (1H, m, ((*H1*)) ppm. **L^9** Coumarin acid chloride (0.250 g, 1.2 × 10^{-3} mol) was dissolved in chloroform (10 mL) and TEA (0.37 mL, 2.6 × 10^{-3} mol) and added slowly to pro-L^9 (0.225 g, 1.01 × 10^{-3} mol) in

chloroform (25 mL). Work up as before. Yield: 0.375 g, 94 %. ^{1}H NMR ($CDCl_3$, 400 MHz, 298 K) δ_H: 1.42-1.50 (4H, m, (*H7, H8*)), 1.69-1.79 (4H, m, (*H6, H9*)), 4.25-4.34 (4H, m, (*H5, H10*)), 7.17-7.20 (3H, m, (*H3, H13, H14*)), 7.52-7.61 (2H, m, (*H12, H15*)), 8.23 (1H, d, (*H4*)), 8.47 (1H, s, (*H11*)). 8.68-8.74 (1H, m, (*H2*)), 9.21 (1H, s, (*H1*)) ppm. ^{13}C{^{1}H} NMR ($CDCl_3$, 101 MHz, 298 K) δc: 25.6, 25.7, 28.5, 28.5, 65.6, 65.8, 116.7, 117.9, 123.2, 124.9, 129.7, 134.4, 137.2, 148.7, 150.7, 153.2, 155.1, 156.7, 163.2, 163.3 ppm. MS (ES^+) *m/z*: 396.13 $[M+H]^+$, 418.12 $[M+Na]^+$, 434 $[M+K]^+$. HRMS (ES^+) found *m/z* 396.1440; $[C_{22}H_{22}O_6N]^+$ requires 396.1442. IR (nujol) υ: 1608.82 (CO), 1721.16 (CO), 1763.58 (CO) cm^{-1}. UV-vis (ε / M^{-1} cm^{-1}) (MeCN) λ_{max}: 292 (30632) nm.

***fac*-[Re(CO)$_3$(bipy)L^9]$^+$** To a round bottom flask, L^9 (52 mg, 1.25×10^{-4} mol) and $[Re(CO)_3(bipy)MeCN]^+$ (45 mg, 9.6×10^{-5} mol) in chloroform (2 mL) were added and heated at at 60 °C for 24 hours. Work up as before. Yield: 28 mg, 35 %. ^{1}H NMR ($CDCl_3$, 400 MHz, 298 K) δ_H: 1.38-1.51 (4H, m, (*H7, H8*)), 1.59-1.71 (4H, m, (*H6, H9*)), 4.24-4.36 (4H, m, (*H5, H10*)), 7.29-7.33 (2H, m, (*H19*)), 7.49 (1H, t, (*H13*)), 7.53-7.59 (2H, m, (*H3, H14*)), 7.75 (2H, t, $^3J_{HH}$ = 6.5 Hz, (*H17*)), 8.21-8.32 (3H, m, (*H4, H18*)), 8.39-6.44 (2H, m, (*H12,H15*)), 8.48-8.53 (1H, m, (*H2*)), 8.61-8.65 (2H, m, (*H1, H11*)). 9.09 (2H, d, (*H16*)) ppm. ^{13}C {^{1}H} NMR ($CDCl_3$, 101 MHz, 298 K) δc: 14.5, 22.8, 23.0, 25.9, 28.8, 29.5, 31.4, 34.5, 66.1, 66.8, 117.2, 118.0, 118.5, 125.4, 126.5, 128.7, 129.3, 129.5, 130.1, 134.9, 141.7, 142.4, 152.6, 149.0, 149.3, 153.0, 153.2, 156.2, 157.4, 163.1, 165.0 ppm. MS (ES^+) *m/z*: 822.09 $[M\text{-}BF_4^-]^+$. HRMS (ES^+) found *m/z* 822.1437; $[^{187}ReC_{35}H_{29}O_9N_3{}^{10}BF_4]^+$ requires 822.458. IR (nujol) υ:1608.82 (CO), 1717.78 (CO), 1817.86 (CO), 2031.64 (CO) cm^{-1}. UV-vis (ε / M^{-1} cm^{-1}) (MeCN) λ_{max}: 251 (1095), 288 (1706), 320 (1027) nm.

***fac*-[Re(phen)(CO)$_3$L^9]$^+$** To a round bottom flask, L^9 (36 mg, 8.7×10^{-5} mol) and $[Re(CO)_3(phen)MeCN]$ (45 mg, 7.9×10^{-5} mol) in chloroform (2 mL) were added and heated at 60 °C for 24 hours. Work up as before. Yield: 29 mg, 43 %. ^{1}H NMR ($CDCl_3$, 400 MHz, 298 K) δ_H: 1.18-125 (4H, m, (*H7, H8*)), 1.50-1.59 (4H, m, (H6, H9)), 4.25 (2H, t, (*H5*)), 4.35 (2H, t, (*H10*)), 7.28-7.34 (2H, m, (*H12, H15*)), 7.54-7.68 (1H, m, (*H3*)), 7.62-7.68 (2H, m, (*H13, H14*)), 8.03-8.22 (5H, m, (*H2, H4, H11, H17*)), 8.51-8.56 (2H, m, (*H19*)), 8.80-8.91 (3H, m (*H1,H18*)), 9.59 (2H, d, (*H16*)) ppm. MS (ES^+) *m/z*: 846.1 $[M\text{-}BF_4^-]^+$. HRMS (ES^+) found *m/z* 846.1450; $[^{187}ReC_{37}H_{29}O_9N_3{}^{10}BF_4]^+$ requires 846.1428. IR (nujol) υ: 1632 (CO), 1688 (CO), 1767 (CO), 1987 (CO), 2031.2 (CO) cm^{-1}. UV-vis (ε / M^{-1} cm^{-1}) (MeCN) λ_{max}: 274 (28123), 318 (30932) nm.

L[10]Coumarin acid chloride (0.112 g, 5.37 × 10^{-4} mol) was dissolved in chloroform (10 mL) and TEA (0.137 mL, 9.8 × 10^{-4} mol) and added slowly to L^7 (0.150 g, 4.88 × 10^{-4} mol) in chloroform (25 mL), then heated at 60 °C for 3 hours. Work up as before. The crude product was purified using column chromatography eluting with DCM. Yield: 0.118 g, 50 %. ^{1}H NMR ($CDCl_3$, 400 MHz, 298 K) δ_H: 1.17-1.32 (12H, m, (*H8-H13*)), 1.42-1.49 (4H, m, (*H7, H14*)), 1.68-1.75 (4H, m, (*H6, H15*)), 4.29-4.36 (4H, m, (*H5, H16*)), 7.23-7.27 (2H, m, (*H18, H21*)), 7.36-7.43 (1H, m, (*H3*)), 7.54-7.59 (2H, m, (*H19, H20*)), 8.29-8.35 (1H, m, (*H4*)), 8.48 (1H, s, (*H17*)), 8.52-8.57 (1H, m, (*H2*)), 9.12-9.18 (1H, m, (*H1*)) ppm. ^{13}C {^{1}H}NMR ($CDCl_3$, 101 MHz, 298 K): δc: 24.9, 25.0, 27.6, 27.6, 28.2, 28.5, 64.6, 65.1, 115.8, 116.9, 117.4, 123.8, 128.5, 133.3, 136.1, 147.4, 154.0, 155.3, 162.2 ppm. MS (ES^+) *m/z*: 480 $[M+H]^+$, 502 $[M+Na]^+$, 518 $[M+K]^+$, 543 $[M+MeCNNa]^+$. IR (nujol) υ: 1706 (CO), 1717 (CO), 1759 (CO) cm^{-1}.UV-vis (ε / M^{-1} cm^{-1}) (MeCN) λ_{max}: 289 (1410), 334.9 (6829) nm.

***fac*-[Re(bipy)(CO)$_3$L[10]]$^+$** To a round bottom flask, L^{10} (33 mg, 6.82 x 10^{-4} mol) and $[Re(CO)_3(bipy)]MeCN$ (29 mg, 4.07 × 10^{-5} mol) in chloroform (2 mL) were added and heated at 60 °C for 24 hours. Work up as before. Yield: 14 mg, 38 %. ^{1}H NMR ($CDCl_3$, 400 MHz, 298 K) δ_H: 1.18-1.42 (16H, m, (*H7- H14*)), 1.59-1.73 (4H, m, (*H6, H15*)), 4.19-4.30 (4H, m, (H5, H16)), 7.25-7.31 (2H, m, (*H19, H20*)), 7.49-7.63 (3H, m, (*H3, H18, H21*)), 7.79 (2H, t, (*H25*)), 8.19-8.32 (3H, m, (*H2, H24*)), 8.46-8.49 (2H, m (*H4, H17*)), 8.73-8.76 (2H, m, (*H23*)), 8.84 (1H, s, (*H1*)). 9.12 (2H, d, (*H22*)) ppm. ^{13}C{^{1}H} NMR ($CDCl_3$, 101 MHz, 298 K) δc: 24.1, 26.7, 26.8, 27.4, 27.5, 27.5, 27.8, 28.0, 30.2, 51.8, 64.4, 64.9, 115.0, 116.2, 121.6, 123.2, 124.3, 125.5, 125.9, 127.3, 127.6, 127.9, 132.7, 137.5, 138.5, 140.0, 147.1, 151.0, 151.0, 151.4, 153.1, 153.9, 154.1, 155.1, 160.9, 161.5 ppm. MS (ES^+) *m/z*: 906.24 $[M-BF_4^-]^+$. HRMS (ES^+) found *m/z* 906.2387; $[^{187}ReC_{41}H_{41}O_9N_3]^+$ requires 906.2353. IR (nujol) υ: 1609.31 (CO), 1732.73 (CO), 1760.59 (CO), 1916.9 (CO), 2033.57 (CO) cm^{-1}. UV-vis (ε / M^{-1} cm^{-1}) (MeCN) λ_{max}: 290 (14193), 317 (8666), 335 (5949), 350 (3707) nm.

***fac*-[Re(CO)$_3$(phen)L[10]]$^+$** To a round bottom flask, L^{10} (22 mg, 4.58 × 10^{-5} mol) and $[Re(CO)_3(phen)MeCN]$ (20 mg, 4.16 × 10^{-5} mol) in chloroform (2 mL) were added and heated at 60 °C for 24 hours. Work up as before. Yield: 10 mg, 26 %. ^{1}H NMR ($CDCl_3$, 400 MHz, 298 K) δ_H: 1.17-1.33 (16H, m, (*H7-H14*)), 1.51-1.54 (2H, m, (*H15*)), 1.71 (2H, m, (*H6*)), 4.14-4.17 (2H, m, (*H16*)), 4.25-4.31 (2H, m, (*H5*)), 7.21-7.24 (1H, m, (*H3*)), 7.39-7.44 (2H, m, (*H19, H20*)), 7.56-7.68 (2H, m, (*H18, H21*)), 7.81-7.94 (3H, m, (*H24, H4*)), 8.02-8.09 (3H, m, (*H25, H17*)), 8.68 (2H, d, (*H23*)), 8.71 (1H, d, (*H2*)), 9.21 (2H, d, (*H22*)). 9.49-9.55 (1H, m, (*H1*)) ppm. ^{13}C{^{1}H} NMR ($CDCl_3$, 101 MHz, 298 K) δ_C: 24.9, 26.4, 26.7, 26.9,

27.0, 27.1, 27.2, 28.9, 30.5, 51.8, 64.5, 64.9, 65.0, 116.7, 125.0, 125.8, 127.9, 128.1, 131.8, 141.7, 146.6, 150.7, 156.2, 161.0 ppm. MS (ES^+) *m/z*: 930.25 $[M\text{-}BF_4^-]^+$. HRMS (ES^+) found *m/z* 928.2366; $[^{185}ReC_{43}H_{41}O_9N_3{}^{10}BF_4]^+$ requires 928.2367. IR (nujol) υ: 1730 (CO), 1912 (CO), 2034 (CO) cm^{-1}.UV-vis (ε / $M^{-1}cm^{-1}$) (MeCN) λ_{max} : 273 (4148), 435 (1667) nm.

2.10.3. Experimental-Biotin

HABA-assay of modified and unmodified biotin

Typically, to a mixture of HABA (300 Mm) and avidin (0.0075 mM) in 50 mM potassium phosphate buffer pH 7.4 were added 5 μL aliquots of the biotin/modified biotin compounds (0.3 mM) in 1-min intervals. The formation of biotin-avidin adduct was indicated by a decrease in the absorbance at 500 nm due to the displacement of HABA from the avidin. By plotting $-\Delta A_{500\ nm}$ versus [biotin]:[avidin], the binding stoichiometry of the biotin compounds was determined

Emission titrations

In a typical procedure, avidin (0.0075 mM) in 50 μM PBS buffer pH 7.4 was titrated with the modified biotin compounds (0.3 mM) by accumulative additions of 5 μL aliquots at 1-min intervals. The solutions were excited at 310 nm, and the emission intensity was monitored at the emission maxima of the compounds.

Pro-L[11] To a solution of biotin-ester (150 mg, 0.383 mmol) in DMF (2 mL) was added 6-amino-1-hexanol (58 mg, 0.497 mmol) and TEA (0.01 mL). The solution was heated at 50 ˚C for 3 days. Yield: 95 mg, 73 %. ^{1}H NMR ($CDCl_3$, 400 MHz, 298 K) δ_H: 1.2-1.62 (14H, m, (*H2-H5, H8-H10*)), 2.09 (2H, t, $^3J_{HH}$ = 7.3 Hz, (*H1*)), 2.61 (1H, d, $^3J_{HH}$ = 12.3 Hz, (*H12a*)), 2.83 (1H, dd, (*H12b*)), 3.05 (2H, t, (*H7*)), 3.49 (2H, t, $^3J_{HH}$ = 6.6 Hz, (*H6*)), 4.12-4.18 (1H, m, (*H14*)), 4.30-4.39 (1H, m, (*H13*)) ppm. ^{13}C NMR (($CDCl_3$) 400 MHz, 298K) δ_c: 25.3, 25.6, 26.5, 28.5, 29.1, 32.3, 35.5, 39, 39.7, 55.7, 60.3, 61.6, 62.1, 78.2 ppm. MS (ES^+) *m/z*: 344.25 $[M+H]^+$, 366.23 $[M+Na]^+$, 367.24 $[M+K]^+$**.** HRMS (ES^+) found *m/z* 344.1995 $[M+H]^+$; $[C_{16}H_{30}O_3N_3S_1]^+$ requires 344.2002, HRMS (ES^+) found *m/z* 366.1812 $[M+Na]^+$; $[C_{16}H_{29}O_3N_3S_1Na]^+$ requires 366.1822. IR (nujol) υ: 1636 (CO), 1675 (CO), 1698 (CO) cm^{-1}. UV-vis (ε / M^{-1} cm^{-1}) (MeCN) λ_{max}: 208 (30895), 234 (14683) nm. **L[11]** Pro-L[11] (125 mg, 0.364 mmol) was added to a solution of coumarin acid chloride (76 mg, 0.4 mmol) in chloroform (15 mL) followed by TEA (0.1 mL, 0.56 mmol) and reaction left stirring at RT for 4 days. The solution was washed with water (3 × 5 mL) and sat. aq. Ammonium chloride (10 mL). The organic layer was dried and the solvent evaporated to dryness, yielding a cream solid. Yield: 127 mg, 68 %. ^{1}H NMR ($CDCl_3$, 400 MHz, 298 K) δ_H: 1.1-1.82 (14H, m, (*H2-H5, H8-H10*)), 2.18 (2H, t, (*H7*)), 2.61-2.64 (1H, m, (*H12b*)), 2.87-2.95 (1H, m, (*H12a*)), 3.08-3.12 (1H, m, (*H11*)), 3.21-3.26 (2H, m, (*H1*)), 4.27-4.36 (3H, m, (*H14, H6*)), 4.49-4.55 (2H, m, (*H13*)), 6.12-6.18 (2H, m, (*NH*)), 7.20-7.27 (2H, m, (*H17*)), 7.58-7.63 (2H, m,

(*H16*)), 8.49 (1H, s, (*H15*)) ppm. MS (ES^+) *m/z*: 516 $[M+H]^+$, 538 $[M+Na]^+$, 554 $[M+K]^+$. HRMS (ES^+) found m/z 516.2157 $[M+H]^+$; $[C_{26}H_{34}O_6N_3S_1]^+$ requires 516.2163. IR (nujol) υ: 1640 (CO), 1708 (CO), 1755 (CO), 1798 (CO) cm^{-1}. UV-vis (ε / M^{-1} cm^{-1}) (MeCN) λ_{max}: 290 (1719), 330 (9252.57) nm.

Pro-L[12] 6-amino caproic acid (1.5 g, 11.43 mmol) and phthalic anhydride (1.7 g, 11.43 mmol) were added to a shlenk and heated until no more vapour was seen to be given off. Yield: 2.1 g, 67 %. ^1H NMR ($CDCl_3$, 400 MHz, 298 K) δ_H: 1.39-1.42 (4H, m, (*H6, H5*)), 1.62-1.66 (4H, m, (*H4,H7*)), 2.32-2.35 (2H, m, (*H3*)), 3.61-3.66 (2H, m, (*H8*)), 7.80-7.83 (2H, m, (*H2*)), 7.91-7.97 (2H, m, (*H1*)) ppm. The acyl chloride (700 mg, 2.54 mmol) was dissolved in chloroform (10 mL) and TEA (0.54 mL, 3.82 mmol) then added to 3-amino methyl pyridine (0.26 mL 2.54 mmol) in chloroform (10 mL). The solution was left to stir at 61 ˚C for 3 h. The solution was washed with water (3 × 5 mL) and sat. aq. Ammonium chloride (10 mL). The organic layer was dried and the solvent evaporated to dryness. The crude product was purified using column chromatography eluting with DCM:MeOH (90:10). Yield: 0.78 g, 84 %. ^1H NMR ($CDCl_3$, 400 MHz, 298 K) δ_H: 1.28-1.32 (4H, m, (*H5, H6*)), 1.68-1.71 (4H, m, (*H4, H7*)), 2.21 (2H, t, $^3J_{HH}$=7.55 Hz, (*H3*)), 3.62 (2H, t, $^3J_{HH}$=7.42 Hz, (*H8*)), 4.39 ((2H, d, $^3J_{HH}$=5.94 Hz, (*H9*)), 6.2 (1H, m, (*NH*)), 7.15-7.19 (1H, m, (*H13*)), 7.59 (1H, d, $^3J_{HH}$=8.13 Hz, (*H13*)), 7.61-7.66 (2H, m, (*H2*)), 7.73-7.76 (2H, m, (*H1*)), 8.42-8.47 (2H, m, (*H1, H2*)) ppm. ^{13}C NMR (($CDCl_3$) 400 MHz, 298K) δ_c: 25, 26.4, 28.2, 36.3, 37.7, 121, 123.2, 132.1, 134, 135.8, 168.5, 172.8 ppm. IR (nujol) υ: 1715 (CO), 1772 (CO) cm^{-1}.UV-vis (ε / M^{-1} cm^{-1}) (MeCN) λ_{max}: 257 (5744) nm. Hydrazine (0.18 mL, 3.9 mmol) was added and solution left at 70 ˚C overnight. ^1H NMR ($CDCl_3$, 400 MHz, 298 K) δ_H: 1.18-1.25 (8H, m, (*H7, H10*)), 2.12 (2H, t, (*H11*)), 2.54 (2H, t, (*H6*)), 4.22 (2H, d, (*H5*)), 7.05-7.13 (1H, m, (*H3*)), 7.56 (1H, d, (*H4*)), 8.25-8.33 (2H, m, (*H1, H2*)) ppm. ^{13}C NMR (($CDCl_3$) 400 MHz, 298K) δ_c: 25.4, 26.4, 29.7, 36.4, 40.9, 134.9, 184.3, 173.1 ppm. IR (nujol) υ: 1647.9 (CO) cm^{-1}. **L[12]** Biotin-ester (125 mg, 0.319 mmol) in DMF (2 mL) was added to a solution of pro-L[12] (98 mg, 0.415 mmol) and TEA (0.01 mL). The solution was stirred at 50 ˚C for 5 days. (95 mg, 65 %) ^1H NMR ($CDCl_3$, 400 MHz, 298 K) δ_H: 1.25-1.41 (8H, m, (*H8- H11*)), 1.47-1.56 (6H, m, (*H15-H17*)), 2-2.08 (2H, m, (*H14*)), 2.23-3.01 (2H, m, (*H7*)), 2.6 (1H, s, (*H19a*)), 2.65 (1H, s, (*H19b*)), 2.82-2.85 (2H, m, (*H12*)), 3.05 (1H, s, (*H18*)), 4.12-4.15 (1H, m, (*H20*)), 4.31-4.36 (3H, m, (*H5, H21*)), 6.32 (1H, s, (*H23*)), 6.49 (1H, s, (*H22*)), 7.36-7.40 (1H, m, (*H3*)), 7.62 (1H, d, (*H4*)), 7.78 (1H, s, (*H6*)), 8.42-8.49 (2H, m, (*H1, H2*)) ppm. ^{13}C NMR (($CDCl_3$) 400 MHz, 298K) δ_c: 25.3, 26, 26.3, 28.2, 28.5, 28.6, 35.5, 38.8, 39.6, 39.9, 55.7, 60.3, 62.1, 135.4,

147, 147.5, 163.2 ppm. IR (nujol) υ: 1633.4 (CO), 1697 (CO), 2057.7 (CO) cm^{-1}. UV-vis (ε / M^{-1} cm^{-1}) (MeCN) λ_{max}: 260 (3002) nm.

[$Re(CO)_3$(bipy)L^{12}] [$Re(CO)_3$BipyMeCN] (50 mg, 0.107 mmol) and L^{12} (49 mg, 0.107 mmol) in DMF (2 mL) was heated at 50 ˚C 7 days. The solution was filtered and the filtrate evaporated yielding an orange precipitate. Yield: 17 mg, 18 %. ^{1}H NMR ($CDCl_3$, 400 MHz, 298 K) δ_H: 1.15-1.67 (12H, m, (*H7-H10, H13,H14*)), 2.02-2.2 (4H, m, (*H6, H12*)), 3-3.17 (4H, m, (*H11, H17*)), 3.48-3.55 (1H, m, (*H16*)), 4.12 (2H, s, (*H5*)), 4.41-4.62 (2H, m, (*H18, H19*)), 7.21-7.24 (1H, m, (*H3*)), 7.63-7.81 (3H, m, (*H4, H24*)), 8.14-8.32 (4H, m, (*H1, H2, H22*)), 8.53 (2H, d, (*H21*)), 9.22 (2H, d, (*H20*)) ppm. ^{13}C NMR (($CDCl_3$) 400 MHz, 298K) δ_c: 25 (x2), 25.1, 26, 29, 34, 34.1, 34.5, 38.4, 38.9, 39.5, 54, 56.5, 58, 58.2, 70, 124.2, 126, 128.8, 138.6, 141, 150, 150.5, 153.5, 155.3, 184.8, 185.1 ppm. MS (ES) *m/z*: 890.24 $[M]^+$.

L^{13} Biotin-ester (125 mg, 0.319 mmol) in DMF (2 mL) was added to a solution of Pro-L^{13} (126 mg, 0.415 mmol) and TEA (0.01 ml). The solution was left to stir at 50 ˚C for 5 days. Yield: 95 mg, 56 %. ^{1}H NMR ($CDCl_3$, 400 MHz, 298 K) δ_H: 1.18-1.29 (20H, m, (*H8- H17*)), 1.37-1.43 (6H, m, (*H21-H23*)), 2.04-2.08 (2H, m, (*H20*)), 2.18 (2H, t, (*H7*)), 2.55 (1H, s, (*H25a*)), 2.60 (1H, s, (*H25a*)), 3.01-3.04 (2H, m, (*H18*)), 3.32 (1H, s, (*H24*)), 4.13 (1H, s, (*H26*)), 4.28-4.36 (3H, m, (*H5, H27*)), 6.32 (1H, s, (*H29*)), 6.46 (1H, s, (*H28*)), 7.36-7.39 (1H, m, (*H3*)), 7.62 (1H, d, (*H4*)), 7.65 (1H, s, (*H6*)), 8.42-8.49 (3H, m, (*H1, H2, H19*)) ppm. ^{13}C NMR (($CDCl_3$) 400 MHz, 298K) δ_c: 27.4, 28.4, 29.9, 30.2, 30.7, 30.9, 31, 37.3, 37.4, 40.8, 41.5, 41.9, 49.2, 49.4, 49.6, 49.9, 50.1, 55.3, 57.5, 62, 63.8, 125.7, 138.1, 149.2, 149.8, 176.4 ppm. MS (ES): 531.33 $[M+H]^+$. UV-vis (ε / M^{-1} cm^{-1}) (MeCN) λ_{max}: 229 (3316), 259 (910) nm.

[$Re(CO)_3$(bipy)L^{13}] [$Re(CO)_3$bipyMeCN] (50 mg, 0.107 mmol) amd L^{13} (57 mg, 0.107 mmol) in DMF (2 mL) was heated at 50 ˚C 7 days. The solution was filtered and filtrate evaporated yielding an orange precipitate. Yield: 19 mg, 19 %. ^{1}H NMR ($CDCl_3$, 400 MHz, 298 K) δ_H: 1.22-1.6 (24H, m, (*H8-H16, H21-H23*)), 1.9-2.05 (4H, m, (*H7, H20*)), 2.53-2.56 (1H, m, (*H25a*)), 2.79-2.85 (1H, m, (*H25b*)), 3.02-3.07 (2H, m, (*H17*)), 3.99 (2H, d, (*H5*)), 4.08-4.10 (1H, m, (*H27*)), 4.78-4.82 (1H, m, (*H26*)), 7.08-7.11 (1H, m, (*H3*)), 7.55 (2H, d, (*H4*)), 7.61.7.64 (2H, m, (*H31*)), 7.92-8.03 (2H, m, (*H1, H2*)), 8.12-8.19 (2H, m, (*H30*)), 8.2-8.23 (2H, m, (*H29*)), 9.12-9.17 (2H, m, (*H28*)) ppm. ^{13}C NMR (($CDCl_3$) 400 MHz, 298K) δ_c: 24.2, 25.5, 29, 34, 34.2, 48.2, 48.8, 53.1, 66, 67, 70, 124.1, 125.8, 137.9, 138, 138.2, 140.8, 149.5, 152, 154 ppm. MS (ES) *m/z*: 974.34 $[M+NH_3]^+$. HRMS (ES^+) found *m/z* 974.3270 $[M+NH_3]^+$; $[ReC_{41}H_{53}O_7N_7]^+$ requires 974.3280.

2.11. References

1. V. Fernández-Moreira, F. L. Thorp-Greenwood and M. P. Coogan, *Chem. Commun*., 2010, **46**, 186.
2. A. J. Amoroso, M. P. Coogan, J. E. Dunne, V. F-Moreira, J. B. Hess, A. J. Hayed, D. Llloyd, C. Milliet, S. J. A. Pope and C. Williams, *Chem. Commun*., 2007, 3066.
3. J. Liddle, S. V. Lindeman, D. L. Reger and J. R. Gardinier, *Inorg. Chem*., 2007, **46**, 8484.
4. A. J. Stufkens and A. Vicek, Jr, *Coord. Chem. Rev*., 1988, **177**, 127.
5. M. S. Wrighton and D. L. Morse, *J. Am. Chem. Soc*., 1974, **96**, 998.
6. L. Lui, X. Li, Y. Xue, Y. Ma, X. Feng, S. He, Y. Lu, Y. Wang amd X. Zeng, *Chem. Commun*., 2009, 6759.
7. E. Ferri, D. Donghi, M. Panigati, G. Prencipe, L. D'Alfonso, I. Zanoni, C. Baldoni, S. Maiorana, G. D'Alfonso and E. Licandro, *Chem. Commun*., 2010, **46**, 6255.
8. A. E. Nahhas, C. Consani, A. M. B-Rodriguez, K. M. Lancaster, O. Bream, A. Cannizzo, M. Towrie, I. P. Clark, S. Zalis, M. Chergui and A. Vicek. Jr, *Inorg. Chem*., 2011, **50**, 2932.
9. A. J. Amoroso, R. J. Arthur, M. P. Coogan, J. B. Court,V. Fernandez-Moreira, A. J. Hayes, D. Lloyd, C. Millet and S. J. A. Pope, *New J. Chem.*, 2008, **32**, 1097.
10. *members.multimania.co.uk/lucarz/Projects/ErSRSO/**Chapter3**.pdf* accessed 10/5/2012.
11. S. Speiser, *Chem. Rev*., 1996, **96**, 1953.
12. I. B. Berlman, *Energy Transfer Parameters of Aromatic Compounds*; Academic Press: New York, 1973.
13. T. S. Levy, S. Speiser, *J. Chem. Phys.*, 1992, **96**, 3585.
14. J. Jortner, J. Rice, S. A. Katz, and J. L. Choi. *J. Chem. Phys.*, 1965, **42**, 309.
15. www.openlearn.open.ac.uk. accessed 11/05/2012.
16. A. Coleman, C. Brennan, J. G. Vos and M. T. Pryce, *Coord. Chem. Rev.*, 2008, **252**, 2585.
17. O.H. Laitinent, A. T. Marttila, K. J. Airenne, T. Kulik, O. Livnah, E. A. Bayer, M. Wilchek and M.S. Kulomaa, *A. Soc. Biochem. Mol. Biol*., 2001, **11**, 8219.
18. A. Chilkoti and P. S. Stayton, *J. Am. Chem. Soc*, 1995, **117**, 10622. (b) P. C. Weber, D. H. Ohelendorf, J. J. Wendoloski and F. R. Salaemme, *Science*., 1989, **243**, 85.
19. E. P. Diamandis and T. K. Christopoulos, *Clin. Chem. (Washington, D. C.)*., 1991, **37**, 625.
20. A. Piffetau and M. Gaudry, *Biochim. Biophys. Acta*., 1985, **816**, 77.
21. P. Hebbeln, D. A. Rodionov, A. Alfandega and T. Eitinger, *Proc. Natl. Acad. Sci. U. S. A*., 2007, **104**, 2909.
22. K. K. –W. Lo, W.-K. Hui, C.-K. Chung, K. H.-K. Tsang, D. C.-M. Ng. N. Zhu and K.. Cheung, *Coord. Chem. Rev*., 2005, **249**, 1434.
23. K. K. –W. Lo, K. H.-K. Tsang, K.-S. Sze, C.-K. Chung, T. K.-M. Lee, K. Y. Zhang, W.-K. Hui, C.-K. Li, J. S.-Y. Lau, D. C.-M. Ng and N. Zhu, *Coord. Chem. Rev*., 2007, **251**, 2292.
24. K. A. King and R. J. Watts, *J. Am. Chem. Soc.*, 1987, **109**, 1589.
25. K. K.-W. Lo, K. Y. Zhang, S.-K. Leung and M.-C, Tang, *Angew. Chem., Int. Ed*., 2008, **47**, 2213.
26. K. K-W. Lo, C.-K. Li and J. S.-Y. Lau, *Organometallics*., 2005, **24**, 4594.
27. K. K-W. Lo and W.-K. Hui, *Inorg. Chem*., 2005, **44**, 1992; (b) K. Y. Zhang and K-W. Lo, *Inorg. Chem*., 2009, **48**, 6011.
28. K. K –W. Lo, K. H.-K. Tsang, and K.-S. Sze, *Inorg. Chem*., 2006, **45**, 1714.
29. K. K –W. Lo, M.-W. Louie, K.-S. Sze and S.-Y. Lau, *Inorg. Chem*., 2008, **47**, 602.
30. H. Van Dijk, D. J. Stukens and A. Oskam, *Inorg. Chem*., 1989, **28**, 28.

31. A. F. Morales, G. Accorsi, N. Armardi. F. Barigelletti, S. J. A. Pope and M. D. Ward, *Inorg Chem*., 2002, **41**, 6711.
32. M. Ezoe, T. Minami, Y. Ogawa, S. Yagi, H. Nakazumi, T. Matsuyama, K. Wada and H. Horinaka, *Photochem. Photobiol. Sci.*, 2005, **4**, 641; (b) C. S. Choi, L. Mishra, T. Mutai and K. Araki, *Bull. Chem. Soc. Jpn.*, 2000, **73**, 2051; (c) R. Wang, Y. Liang and R. H.Schmehl, *Inorg. Chim. Acta*., 1994, **225**, 275.
33. E. G. Moore, P. V. Bernhardt, A. Furstenburg, M. J. Riley and E.Vauthey, *J. Phys. Chem*., 2005; (b) D. C. Magri, J. F. Callan, A. P.de Silva, D. B. Fox, N. D. McClenaghan and K. R. A. S. Sandanayake, *J. Fluoresc.*, 2005, **15**, 769; (c) T. Gunnlaugsson, T. C. Lee and R. Parkesh, *Tetrahedron*., 2004, **60**, 11239.
34. M. I. Sluch, I. D.W. Samuel, A. Beeby andM. C. Petty, *Langmuir*., 1998, **14**, 3346; (b) F. C. Bos and J. Schmidt, *J. Chem. Phys.*, 1986, **84**,584.
35. H. S. G. Roh, N.S. Baek, K. S. Hong and H. K. Kim., *Korean Chem. Soc.*, 2004, **25**, 343; (b) J. R. Lacowicz. *Principles of Fluorescence spectroscopy*, 3rd ed., Springer. 2006.
36. T. A. -Matsumoto, A. Takama and K. -I. Mizuno, *Elsevier*., 2009, **129**, 1531.
37. D. E. Wolfe, J. Valiant and K. Folkers, *J. Am. Chem. Soc*., 1951, **73**, 4142.
38. F. J. Munoz, A. Rumbero, J. V. Sinisterra, J. I. Santos, S. Andre, H. J. Gabius, J. Jimenez-Barbero and M. J.Hernaiz, *Glycoconjugate. Jourmal*., 2008, **23**, 633.

Chapter 3. Hydrophobic Modulation of Emission Lifetimes For Both Mono- and Di-Metallic Re(I) Complexes Linked Through Functionalized Alkyl Chains Towards Cellular Imaging Applications.

3.1. Introduction

In Chapter 2 the effect of the chain length, linking units and varying diimines on the photophysical properties of a Re(I) species in different media were reported. Continuing with the same objective, Chapter 3 focuses on the hydrophobic modulation of emission lifetimes for a novel series of both mono- and di-metallic Re(I) complexes, additionally, reported herein is the first application of di-metallic rhenium complexes in cellular imaging. For the complexes described in this chapter, a series of monomeric ligands with varying chromophoric 'linking' units, along with a series of dimeric ligands suitable for the co-ordination to two metal ions, were synthesised.

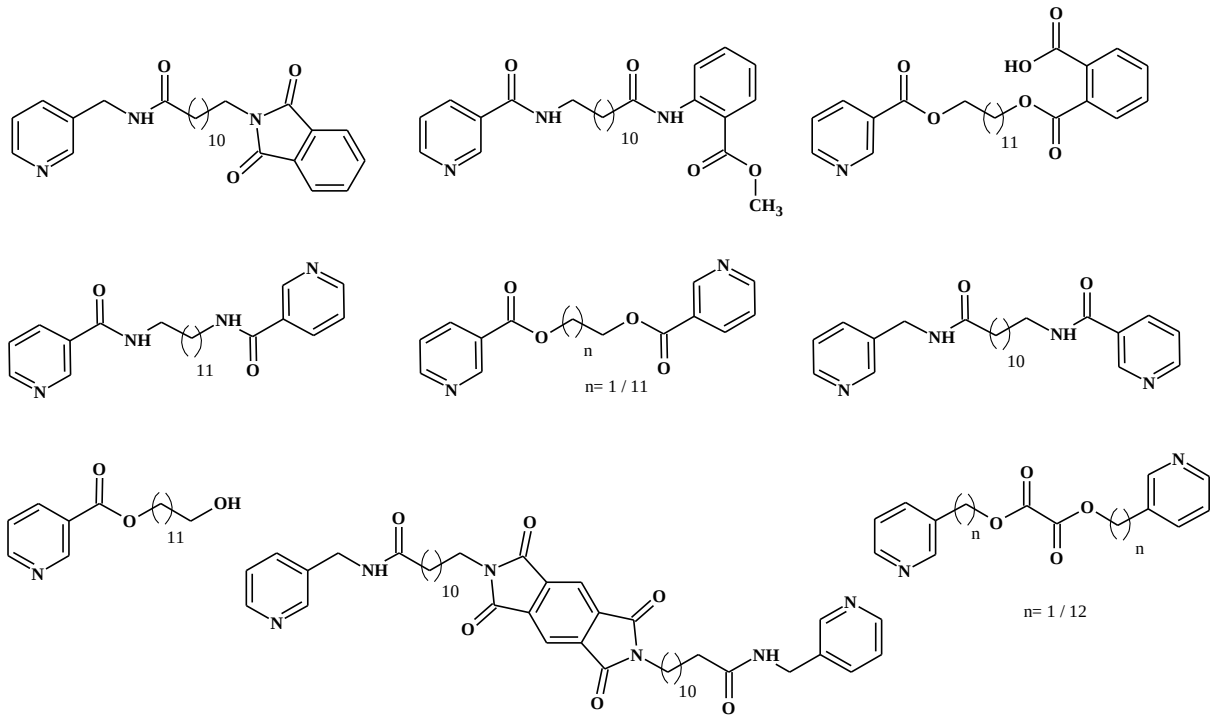

Figure 3.1 Ligands discussed herein.

3.2. Ligand Design

For the complexes described in this chapter, the ligand design will take into account variables such as chain length, the nature of linking units and the incorporation of chromophores into, or at, the terminus of the chain.

3.2.1. Variations in the alkyl chain length

The photophysical findings for the fifteen analogous Re(I) diimine complexes reported in Chapter 2, suggests that when the solvent is changed from acetonitrile to water, the C_{12} chain is the optimum chain length for chain-wrapping / fold-back to occur. This data complements the findings from the original investigation into the effect of solvent on the photophysical properties of a luminescenct rhenium complex reported in 2009 (Figure 3.2).[1,2] Chapter 2 also highlighted how the nature of the linker functionality to pyridine (amide/ester), in the case of bipyridine-based complexes had an effect on the degree of intramolecular hydrophobic chain wrapping. Therefore, when looking to further probe the hydrophobic modulation of emission lifetimes it is logical to include the C_{12} alkyl chain and vary the linker units used.

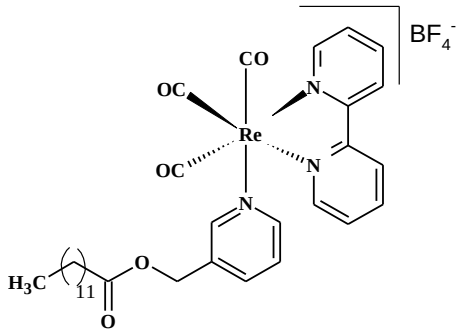

	λ_{max} / nm	τ / ns
MeCN	**555**	**176**
H_2O	**523**	**688**

Figure 3.2 Preliminary results discussed in Chapter 2. [1,2]

3.2.2. Variations in the chromophore unit

The addition of a chromophore unit to an aliphatic chain could, potentially, allow for a better understanding of the chain wrapping phenomena helping to deduce the extent of hydrophobic interactions. The proximity of the chromophore to the ^{3}MLCT-based excited state may be detectable through the photophysical observations; the variation in emission intensity and lifetimes for the two luminescent centres will be dependent on the quenching processes and energy transfer mechanisms, which in turn will be dependent on the nature, position and number of chromophore units employed.

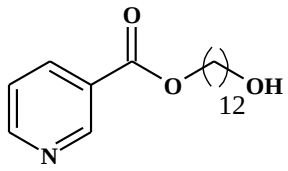

Figure 3.3 Ligand precursor A

The incorporation of a chromophoric unit requires a ligand precursor adaptable for the stepwise addition of functional groups providing easy variation in the ligand design. The synthesis of ligand precursor **A** (Fig. 3.3), from 1,12-dodecandiol, was described in Chapter 2, and provided a small degree of control in the ligand synthesis. This allowed six analogous coumarin-appended complexes, which varied in both the diimine (phen/bipy) and in chain lengths ($C_{2/6/12}$), to be synthesised (Fig 3.4).

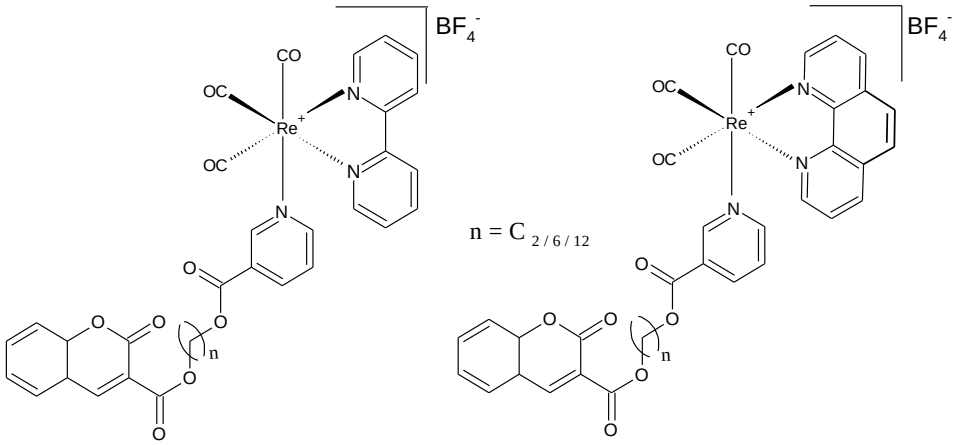

Figure 3.4 $[Re(CO)_3(bipy/phen)L^{8\text{-}10}]^+$

Although a conclusive model of the interaction of the chain/chromophore unit with the ^{3}MLCT excited state could not be drawn from the photophysical data of the complexes, the emission intensities were shown to vary in different media. The varying intensities demonstrated that a chromophoric unit within a complex does provide some additional insight into the position of the chain and so perhaps variation in the chromophore unit could allow further insight into the chain wrapping phenomena. The electronic nature of the choromophoric moiety (*e.g.* a sensitizer or quencher or excited states) and its spatial position within the complex are areas that require further investigation. The phthalimide unit was selected as a chromophore for additional study in this way (Figure 3.5).

3.2.2.1. Phthalimide

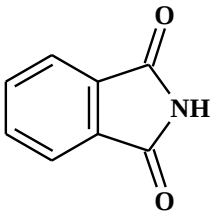

Figure 3.5 Phthalimide

Phthalimides are a group of compounds described as imides; a functional group with two acyl groups bound to a nitrogen centre, and are generally synthesised from a condensation reaction with a dianhydride. The best known example of phthalimide is the well documented thalidomide. Thalidomide is well documented for the adverse effects encountered during its use in the treatment of morning sickness. Thalidomide was prescribed without any clinical trials (and so without being teratogenically tested) which resulted in a huge number of babies being born with birth defects. *In vivo* the *R*-thalidomide, prescribed for the treatment of morning sickness, racemises forming *S*-thalidomide which has since been shown to be responsible for the teratogenic effects. The adverse effects of thalidomide resulted in much stricter testing for drug and pesticide licencing and nowadays it is used safely for the treatment of cancers (bone marrow), leprosy and used as an anti-inflammatory.[3-5]

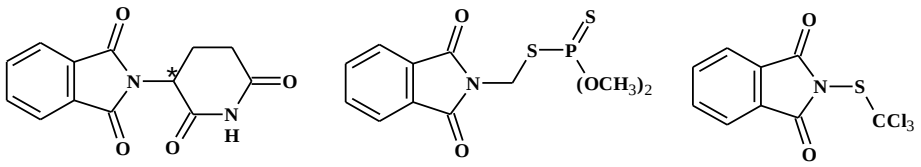

Figure 3.6 Thalidomide with chiral centre marked (LHS), Imidan (centre) and Folpet (RHS).

Phthalimide is used in the synthesis of a range of important products including: pharmaceuticals (discussed above); pesticides; fungicides and dyes. For instance, Imidan (Figure 3.6) is an insecticide derived from phthalimide, it is a cholinesterase inhibitor that kills insect pests on crops whilst having low toxicity for humans; another phthalimide derivative, Folpet (Figure 3.6) is a leaf fungicide;[6] phthalimide is also used as a chromophore in photochemistry and for many synthetic applications, some of which are shown below.[7]

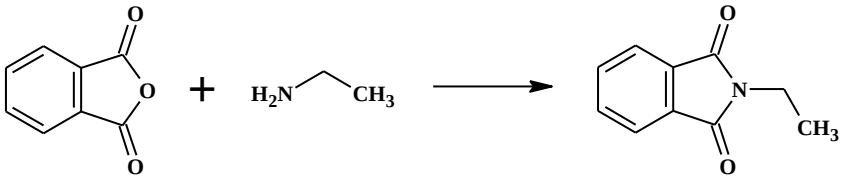

Figure 3.7 An example of phthalimide used as a protecting group; phthalic anhydride used as a protecting group for an amine or amino acid.

Potassium phthalimide is a precursor used in the preparation of primary amines using Gabriel synthesis. Gabriel synthesis is limited to the formation of primary amines from primary alkyl halides.[8,9] There are few gentle deprotection methods for cleaving the 'amide' bond with the more common methods using hydrazine or 2 eq. NaOH (Figure 3.8).[10]

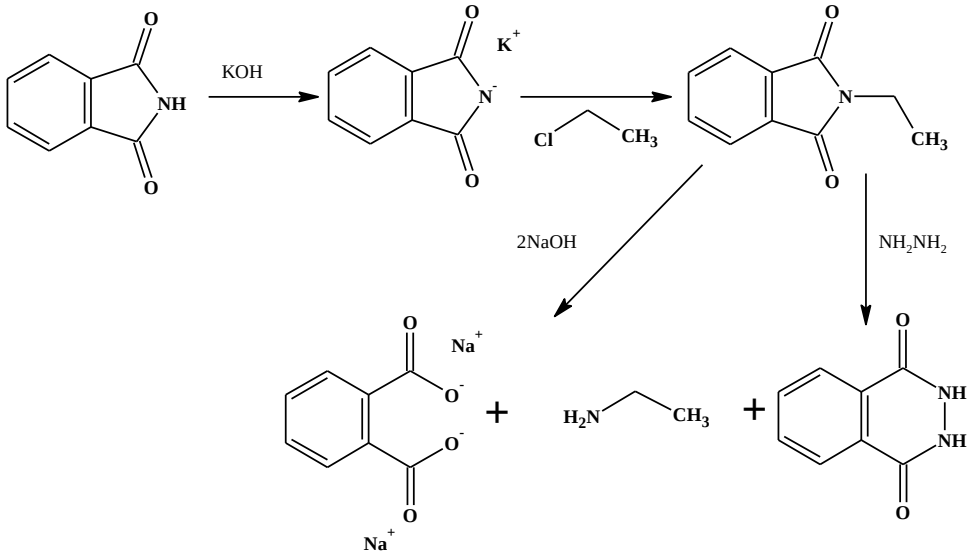

Figure 3.8 An example of Gabriel synthesis

3.2.2.2. Pyromellitic centre

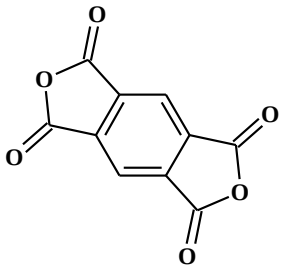

Figure 3.9 PMDA Unit

Polyimides are polymers of the imide monomer. Following the same synthetic approach described in Figure 3.7, a polyimide can be incorporated into the centre of two aliphatic chains. Benzol 1,2,4,5-benzenetetracarboxylicdianhydride otherwise known as

pyromellitic dianhydride and herein referred to as PMDA (Figure 3.9) is a well-known, cheap, commercially available dianhydride. It is used in the production of thermostable polyimides (PI's), for example, Kapton.[10-15] The rigid backbone and strong inter-chain interactions of PMDA have been reported to have an effect on both the solubility and the charge transfer fluorescence intensity within a compound.[16,17]

3.2.2.3. Di-metallic rhenium complexes

Although the number of complexes reporting the effect of solvent on the photophysical properties of a complex is increasing,[1,2,18] no statement on the specific interaction of the aliphatic chain with the excited state species can be made. The incorporation of an additional rhenium unit to the terminal position of the alkyl chain, synthesising a di-metallic rhenium complex (Re(I)-spacer-Re(I)), may provide further insight as to how the chain interacts.

If the two rhenium centres are brought within close proximity, shielding each other from the effect of the aqueous solvent, a blue shift in emission maxima along with an increase in emission lifetime and intensity should be seen. It is possible, in an aqueous environment, that the two different rhenium centres within a complex will have different degrees of shielding from the quenching effect of a solvent, essentially resulting in two inequivalent emitting states, and therefore two different emission lifetimes would be expected. If it is in fact only the initial carbons in the chain involved in the 'wrapping' of the excited state (this was a suggestion made in Chapter 1), the two rhenium centres should be in the same environments and so no difference in lifetimes would be expected.

3.3. Results and discussion

3.3.1. Ligand synthesis

3.3.1.1. Synthesis of symmetrical ligands equipped to form di-metallic complexes

The simplest ligands, which allow the co-ordination of two rhenium units to an alkyl chain (one at each end) can be synthesised by reacting symmetrical functionalised aliphatic chains, such as 1,12-dodecandiol, with acid chlorides, such as nicotinoyl chloride. An acid chloride enables 'activation' of a carbon promoting more facile nucleophillic substitution. In a ^{1}H NMR spectrum, the frequency of the CH_2 group adjacent to the functional group (*e.g.* OH or NH_2) on the aliphatic chain can be used, in most cases, to distinguish the products from starting material.

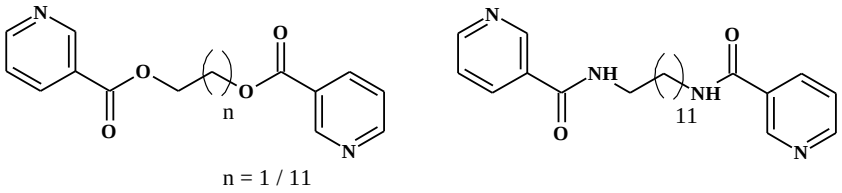

Figure 3.10 Symmetrical ligands, $L^{1,2}$ (LHS) and L^3 (RHS).

The synthesis of the symmetrical esters, $\mathbf{L^{1,2}}$, and the symmetrical amide, $\mathbf{L^3}$, was achieved using an excess of commercially available nicotinic acid which was converted to the derived nicotinoyl chloride by stirring at 70 ˚C in thionyl chloride for 1 hour (Figure 3.10). Nicotinoyl chloride was then reacted with either commercially available 1,12-dodecandiol, ethylene glycol, or the synthesised 1,12-diaminododecane (for its synthesis see Chapter 2). The observation of a shift to higher frequency for the CH_2OCO / CH_2NHCO in the ^{1}H NMR spectra confirms the formation of the ether/amide units, which were achieved in low to excellent yields; $\mathbf{L^1}$ 68 %, $\mathbf{L^2}$ 93 %, $\mathbf{L^3}$ 27%. The lowest yield was for the C_{12} chained di-amide based ligand, $\mathbf{L^3}$, this was the only ligand that required purification by column chromatography recovering: starting material, mono (in very low yield) and di-substituted products. The difference in the reactivity of $\mathbf{L^1}$-$\mathbf{L^3}$ was attributed to the presence of different functional groups (ester *vs.* amide); the presence of an NH functional group in the precursor of $\mathbf{L^3}$ can promote intra- and intermolecular hydrogen bonding which could potentially inhibit the reactivity of the terminal groups.

An alternative route for the synthesis of symmetrical ligands equipped to co-ordinate to two rhenium di-imine units was taken *via* a reaction with oxalyl chloride. The di-ester

ligands, $\mathbf{L^4}$ and $\mathbf{L^5}$ were formed by reacting hydroxymethyl pyridine or ligand precursor **A** (in a slight excess) with oxalyl chloride (Figure 3.11). The reaction was left to stir at room temp for 30 minutes. $\mathbf{L^4}$, the di-ester equipped with a C_1 aliphatic chain, was formed in a 53 % yield requiring no further purification; however $\mathbf{L^5}$, the di-ester equipped with a C_{12} aliphatic chain, required purification *via* column chromatography which resulted in a low yield of 12 %. The low yield of $\mathbf{L^5}$ was attributed to the change in chain length (C_1 *vs*. C_{12}), again, the increased chain length can allow intra- as well as intermolecular hydrophobic interactions whilst the C_1 chain length omits intramolecular interactions completely.

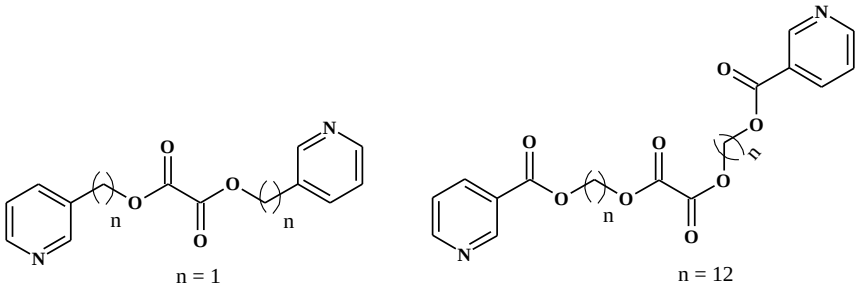

Figure 3.11 Symmetrical ligands, L^4 (LHS) and L^5 (RHS).

The use of symmetrical ligand precursors limits the variation of (and within) the possible ligands which can be produced with the majority of symmetrical starting materials forming only symmetrical products (di-alcohols seem to be one of the few exceptions to this trend).

3.3.1.2. Synthesis of unsymmetrical ligands derived from laurolactam

A dual functional starting material which allowed variation in both the symmetry and functionality within the ligands it synthesised was laurolactam. Laurolactam otherwise known as 12-aminododecanolactam, is a cheap, commercially available starting material which has been reported to readily undergo acid or base promoted ring opening hydrolysis to produce 12-aminolauric acid. Both routes (acid/base) were attempted; HCl (6 M) displayed enhanced reactivity with the better yield of 73 %, as opposed to the lower yield of 35 % with the base. The two different functional groups (amine and carboxylic acid) in 12-aminolauric acid allowed the stepwise addition of functional groups allowing a variety of ligands to be produced.

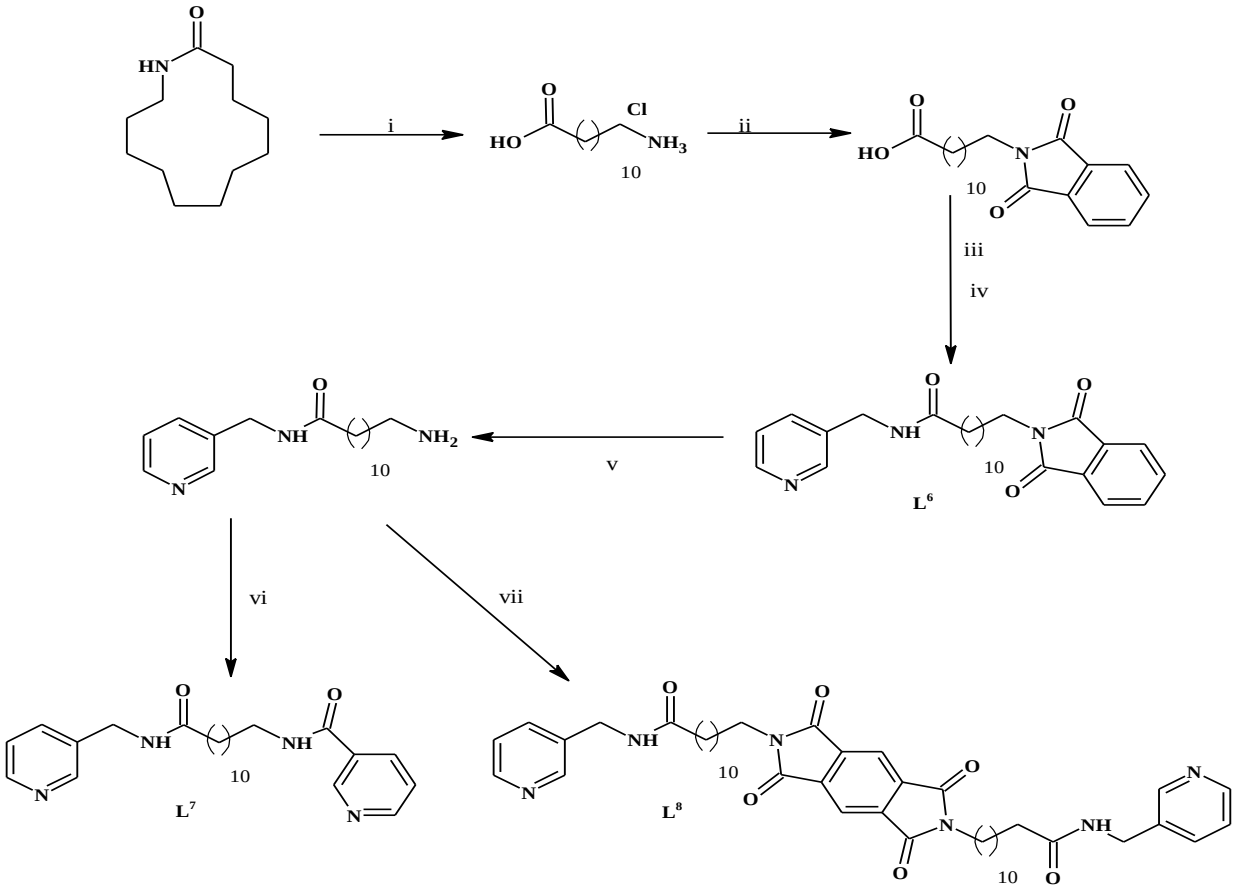

Figure 3.12 Reagents (i) 6M HCl; (ii) phthalic anhydride, Δ; (iii) $SOCl_2$; (iv) 3-aminomethyl pyridine; (v) hydrazine hydrate, Δ; (vi) nicotinyl chloride; (vii) pyromellitic dianhydride, Δ.

3.3.1.2.1. Synthesis of L^{6-8}

The incorporation of a phthalimide unit to one end of the 12-aminolauric acid allowed greater control in reactivity and led to the formation of the chromophore appended ligand, **L^6,** in an excellent yield of 95 %. **L^6** was formed from a series of reactions; 12-aminolauric acid was heated (neat) with phthalic anhydride until no further vapour was given off producing the phalimido-acid**.** The acyl chloride of the phthalimide appended chain was formed by treatment of phalimido-acid with thionyl chloride. The acid chloride was then reacted with 3-amino methyl pyridine, in chloroform and TEA to form the amide **L^6** (Figure 3.12).

The phthalimide protecting group of **L^6** was cleaved using hydrazine in ethoxyethanol to produce the bi-product phthalazine and the desired primary amine, ligand precursor **B** in a 58 % yield. Finally, ligand precursor **B** was reacted with an excess of nicotinoyl chloride in chloroform in the presence of TEA to produce **L^7**, the first unsymmetrical dimer accessed in this work. **L^7** was distinguished from its precursor by the expected downfield shift of the signal corresponding to the CH_2 adjacent to NH_2 from +2.55ppm to +3.35ppm in the ^{1}H NMR

spectrum. Additionally, two separate singlet peaks integrating to one proton each, at +6.1ppm and +6.48ppm, were displayed for the two inequivalent N*H*'s. **L**^{7} was formed in an excellent yield of 93 % (Figure 3.12).

3.3.1.3. Synthesis of a symmetrical chromophore centred dimer

The bi-functional analogue of phthalic anhydride, PMDA, can provide a central chromophore to link two C_{11} alkyl chains; PMDA, when reacted with an excess of ligand precursor **B** produces a dimeric ligand, **L**^{8}, in an excellent yield of 98 %. Again, the characteristic change in chemical shift of the CH_2 adjacent to NH_2 was observed (Figure 3.12).

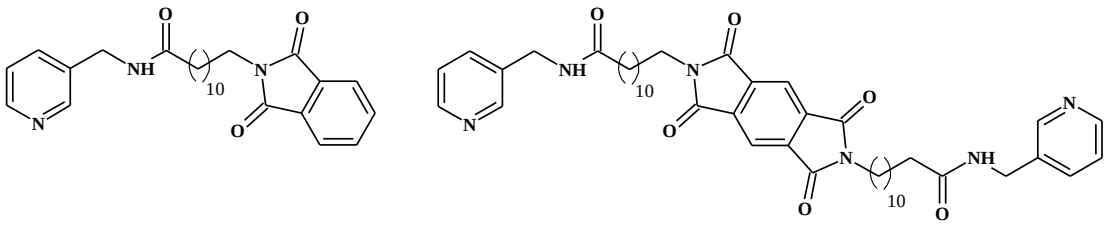

Figure 3.13 L^{6} (LHS), L^{8} (RHS).

L^{8} is structurally related to the previously discussed phthalimide appended pyridine C_{11} ligand, **L**^{6} (differing in the additional anhydride unit and a C_{11} chain) (Figure 3.13). The structural relationship between the ligands, **L**^{6} and **L**^{8}, allowed a comparison of the effects of the chromophore unit on the photophysical properties of the molecule.

Following the successful preparation of **L**^{8} the synthesis of a range of ligands which incorporated the PMDA centre and could add additional functionality within the aliphatic chain was attempted following the same solvent-free method discussed above. The incorporation of a C_3 chain to the chromophore, using 1-amino-3-propanol, resulted in a product of low solubility which inhibited ease of characterisation. The reaction of a C_6 chain (using 1-amino-6-hexanol with PMDA) produced a product with a mixture of amide and ester bonds as indicated in the ^{1}H NMR spectrum. In an attempt to initiate some control in the reaction (slow the reaction so the more kinetically favourable product would form) a solvent was introduced; 1-amino-6-hexanol and PMDA were heated in DMF at 160 ˚C for 6 hours. The solution was cooled and poured into ice water and the white precipitate that formed was filtered and recrystallized using methanol giving **L**^{9} in a good yield of 84 % (Figure 3.14).

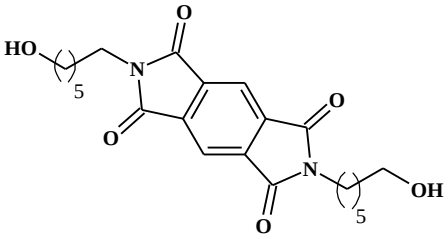

Figure 3.14 L^9 formed using PMDA centre and 1-amino-6-hexanol.

As with other PMDI derivatives, the limited solubility of **L^9** in common organic solvents required any reactions using it as a starting material to be carried out in DMF at high temperatures. Following a succession of unsuccessful reactions using the di-chloro alkyl of **L^9** in the presence of a phthalimide unit and catalytic amounts of KI at 150 ˚C, the reaction time was extended to 3 weeks. The extension of reaction time resulted in a single phthalimide unit being appended to **L^9** forming **L^{10}** in low yield (Figure 3.15). This limited reactivity meant that no further work on this set of compounds was attempted and an alternative route was sought for the synthesis of unsymmetrical chromophore centred ligands.

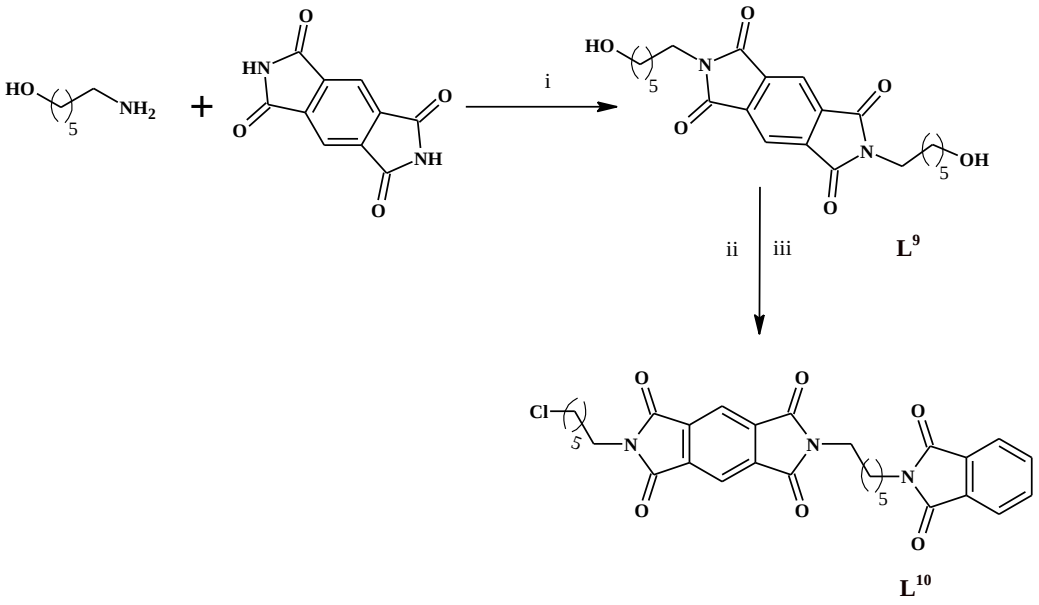

Figure 3.15 Formation of L^{10}. Reagents: (i) DMF; (ii) thionyl chloride, Δ; (iii) potassium phthalimide, KI, DMF, Δ.

3.3.1.4. Synthesis of unsymmetrical chromophore centred ligands

A bi-functionalised centred chromophore presents an alternative route to introduce more variation within the ligand design. Through the synthesis of ligands with varying

terminal functional groups appended to the aliphatic chain, a wider scope of bi-functionalised chromophores could be included.

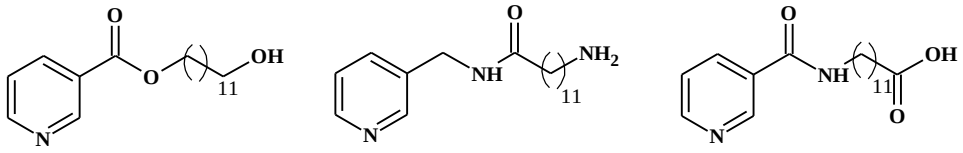

Figure 3.16 Ligand Precursors A (LHS), B (centre) and C (RHS).

An additional ligand precursor to ligand precursor **A** (with a terminal hydroxy group), and ligand precursor **B** (with a terminal amine group), which have both been well documented herein, was synthesised from the reaction of dried 12-amino lauric acid with nicotinoyl chloride. Precursor ligand **C**, equipped with a terminal acid group was synthesised in a 55 % yield.

3.3.1.4.1. 3-hydroxy, 2-napthoic acid

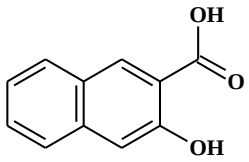

Figure 3.17 3-hydroxy, 2-naphtoic acid

3-hydroxy, 2-naphthoic acid (3-HNA) is a commercially available, bi-functionalised chromophore whose photophysical properties have been well documented.[19-24]It has two different functional groups and thus represents an ideal ligand precursor to allow the synthesis of an unsymmetrical, chromophore centred ligand. When the acyl chloride of 3-hydroxy, 2-naphthoic acid was reacted with ligand precursor **B** (following same procedure as above) there was little evidence of product formation. The absence of naphthol aromatic protons in the final ^{1}H NMR spectrum indicated that either the reaction was unfavourable or the chromophore/final product was soluble in water.

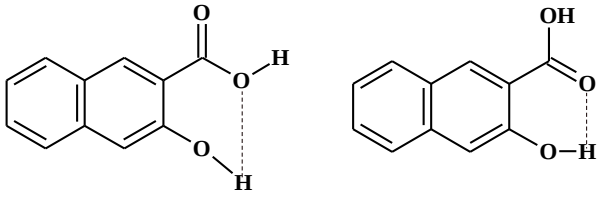

Figure 3.18 Two ground state conformers known for 3-HNA, R (left) and P (right).[19]

There are several observations which could account for the limited reactivity between the two starting materials, including; the presence of two groups on the chromophore moiety which can become chlorinated providing additional reaction/intermediate forming pathways than those predicted; the presence of an amide bond within ligand precursor **B** which could allow hydrogen bonding to the chromophore, slowing the reaction; or, the more likely, intramolecular interactions between the hydroxyl group and the assumed chlorinated carboxylic acid in the chromophore. The latter is a well-known photophysically observed interaction that is deemed responsible for excited state intramolecular proton transfer (ESIPT). 3-HNA has a large Stokes shift resulting from the translocation of the hydroxyl proton to the carboxylic acid group (Figure 3.18) which leads to ESIPT.[19] TEA is a proton acceptor thus promotes ESIPT,[24] the reaction between 3-HNA and ligand precursor **B** was repeated varying conditions such as the concentration of TEA used, omitting the TEA completely and changing the chlorinating reagent from thionyl chloride to the less aggressive oxalyl chloride, but only starting material was recovered (no shift in the resonance of CH_2NH$_2$). The strong interactions between the hydroxy and the carboxylic acid groups are believed to have hindered the reaction and thus an alternative type of chromophore was subsequently investigated.

3.3.1.4.2. Methyl anthranilate

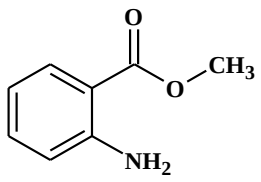

Figure 3.19 Methyl anthranilate

Methyl anthranilate (MA) is a naturally occurring compound that is found in cocoa, coffee and a variety of fruits such as grapes and limes, and is a well-known chromophore. It contains both an ester and amine functional group at the 1,2-position. The two different functional groups can potentially allow control in the reactivity of the bi-functionalised chromophore unit (MA) when compared to the previously investigated 3-HNA, and although there is still the possibility of hydrogen bonding within the MA chromophore, it is weaker. Methyl anthranilate was reacted with the acyl chloride of ligand precursor **C** to produce **L**^{11} in a moderate yield of 37 % (Figure 3.20).

To further functionalise the central unit of **L**^{11}, an attempt was made to form a six membered heterocyclic moiety (*via* an imine formation) using hydrazine in ethanol in a one

pot synthesis (Figure 3.20). The ^{1}H NMR spectrum of the product showed the absence of the methyl group, but with further characterisation (MS and IR) it was evident that hydrolysis of the ester bond had occurred with no evidence to suggest the presence of hydrazine unit within the ligand. The incorporation of an acid (*i.e.* catalytic HCl) can, in some cases, accelerate reactions of this type,[25]however, although the predicted product was not produced, the hydrolysis of **L^{11}** presents an alternative route for the synthesis of an unsymmetrical dimer unit with a chromophore centre.

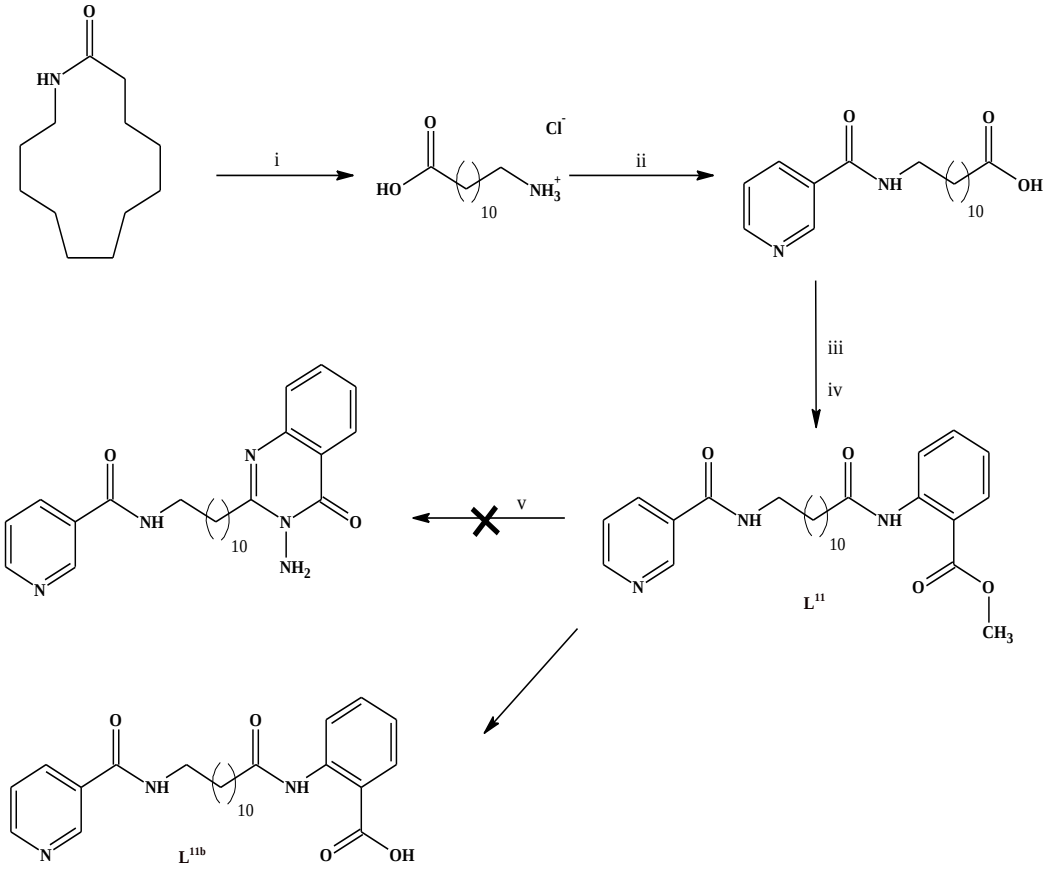

Figure 3.20 Synthesis of L^{11} and hydrolysed L^{11b}. Reagents: (i) 6M HCl; (ii) nicotinoyl chloride; (iii) $SOCl_2$, Δ; (iv) methyl anthranilate; (v) hydrazine hydrate, Δ.

3.3.1.4.3. Ring Opening

Following the unpredicted synthesis of hydrolysed **L^{11}** (Figure 3.20) a simpler, alternative synthetic route that resulted in a similar end product was carried out using partial ring opening chemistry. Ring opening reactions of phthalic anhydride and PMDA in the presence of various metal salts[29,30] and Lewis acids[26-28] have been well documented with the latter being more common. Ring opening of phthalic anhydride with different alcohols in the presence of a Lewis acid leads to the mono-ester of the alcohol forming under mild conditions.[31] The Lewis acid acts as a catalyst and accelerates the reaction by co-ordinating to

the carbonyl oxygen, the partially positive charge located on a carbon accelerates the likelihood of a nucleophilic attack which will proceed to open the ring.

Ligand precursor **A** was reacted with phthalic anhydride in DMF and in the presence of acid. Through trial and error it was found that the acid catalyst chosen should be such that is unlikely to react with the cleaved CO or COO, for example, trifluoroacetic acid (TFA). When acetic acid was used the formation of methyl ester was observed; the presence of the singlet peak at +2 ppm accurately integrating to three protons in the ^{1}H NMR spectrum was primary evidence for this formation, confirmed with the mass spectrum displaying a dominant *m/z* peak for the $[M+H]^{+}$ acetyl ester. In the presence of TFA the desired product was formed with the ^{1}H and ^{13}C NMR spectra, as well as the mass spectrum results all in agreement. The formation of the symmetrical dimeric ligand proved kinetically un-favourable, however, the low and limiting yield of this reaction has led to no further reactions having taken place to date.

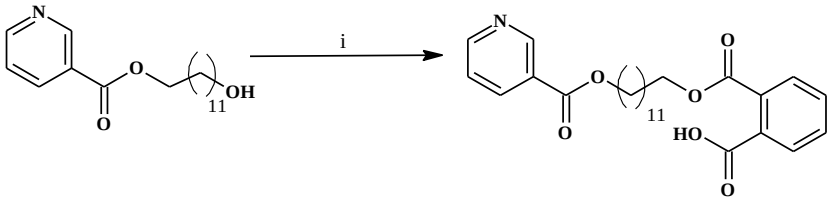

Figure 3.21 L[12]. Reagents (i) phthalic anhydride, TFA, Δ.

3.3.2. Synthesis and characterisation of the complexes

With a variety of novel ligands having been synthesised, the formation of the corresponding rhenium complexes was attempted. From the data reported in Chapter 2 it was noted that the choice of diimine is crucial for the photophysical properties. The phenanthroline diimine consistently exhibits more pronounced changes in the photophysical properties of a complex when the solvent is changed from acetonitrile to water in comparison to its analogues and therefore this diimine was to be used in further investigations. The synthesis of the following cationic rhenium complexes was achieved following literature precedent, with 1.1 equivalents of the ligand reacted with [$Re(CO)_3$PhenBr] (1 eq per pyridine present in ligand)) in the presence of silver tetrafluoroborate (1.2 eq) in chloroform at 55 ˚C for 12 hours. The solution was filtered through Celite and the filtrate dried *in vacuo.* Following additional purification by column chromatography the pure mono- and di-metallic complexes were isolated as their tetrafluoroborate/hexafluoroborate salts in low to moderate yields of 16% to 65 % (Figure 3.22).

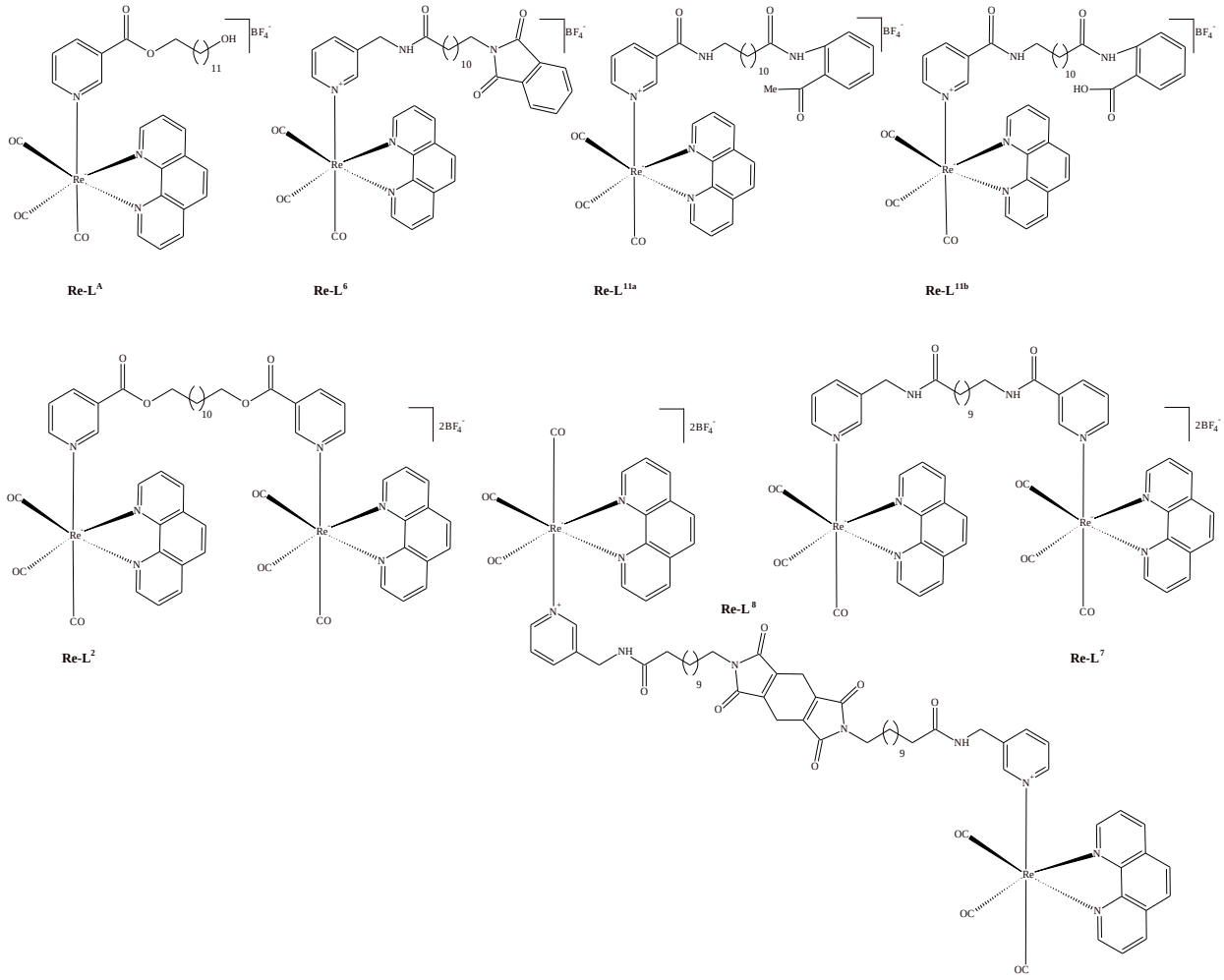

Figure 3.22 The complexes discussed herein.

^{1}H NMR spectra were obtained for each complex and comparison of the spectra to the free ligand confirmed the successful co-ordination of the ligands to the Re(I) units *e.g.* For $[Re(CO)_3(phen)L^6]^+$ a shift of the C*H*$_2$NH to a lower frequency, +4.32 ppm to +4.09 ppm was displayed.

Solid state IR studies were carried out for all complexes which show subtle changes in the ν(CO) in comparison to the rhenium precursor. Complexes show two carbonyl stretching frequencies at around 2030 and 1921 cm^{-1} with very slight variation in wavenumbers directly relating to the electron density available at the metal centre.

MS and HRMS analysis for each of the complexes was carried out and gave good mass ions in all cases. For the dimeric complexes, fragmentation occurred in all three complexes which resulted in a loss of the $[Re(CO)_3Phen]^+$ unit. The dimeric complex ion was visible only in $\{[Re(CO)_3(phen)]_2L^8\}^{2+}$, in the spectra the dominant mass ion was that of [M-$Re(CO)_3Phen]^+$

3.3.3. UV-Vis absorption spectroscopy

The electronic absorption spectra were obtained in acetonitrile for the Re(I) complexes and their ligands are the data shown in Table 3.1 and are discussed in the following sections.

Table 3.1 UV-vis data for the ligands and their complexes

Compound	λ_{abs} / nm (ε)
L^A	264 (30960)
Re-phen-L^A	367 (1711), 324 (3191), 273 (14639)
L^6	294 (6394), 259 (14699)
Re-phen-L^6	365 (3421), 275 (29552)
L^{11a}	311 (4442), 252 (14839)
Re-Phen-L^{11a}	348 (1253), 272 (2911), 252 (8949)
L^{11b}	255 (9260)
Re-Phen-L^{11b}	255 (11424)
$[[Re(phen)]_2$-L^2	377 (2946)
L^7	260 (9859)
$[Re(phen)]_2$-L^7	324 (5760), 272 (5520)
L^8	234 (17545)
$[Re(phen)]_2L^8$	375 (5085), 274 (17451)

The high energy band (below 330nm) was visible for all complexes and is typically assigned to spin-allowed intra ligand (IL) ($\pi \rightarrow \pi^*$) transitions. The transitions in the region of 340-400nm are assigned to the spin allowed charge transfer (^{1}MLCT) (d $\pi \rightarrow \pi^*$). As the conjugation within a ligands increases the energy required to promote an electron into the excited state is decreased (the π^* orbital energy is lowered.). This accounts for the additional adsorption peaks seen within the ligands with more than one chromophore moiety.

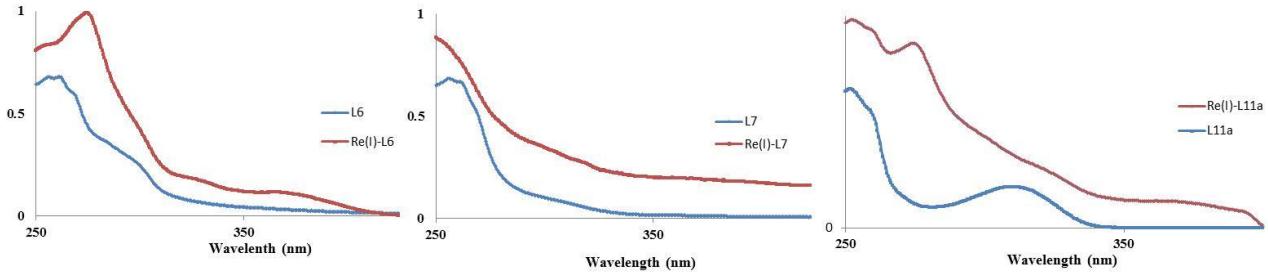

Figure 3.23 UV-vis graph, each displaying ligand (--) and their complex (--).

The high energy absorption of complex $[Re(CO)_3(phen)L^6]^+$ displayed a red-shifted, less structured profile in comparison to the phthalimide-appended-free ligand, with an additional peak at 365 nm, which was assigned to the addition of the rhenium unit (^{1}MLCT). A prominantly structured peak at 310 nm in the unsymmetrical dimer, $\mathbf{L^{11a}}$ indicated the presence of a chromophore moiety, ^{1}IL ($\pi \rightarrow \pi^*$). A less structured profile was displayed by the $[Re(CO)_3(phen)L^{11a}]$ complex with a broad shoulder at 377 nm indicating a ^{1}MLCT transition (Figure 3.23).

3.3.4. Luminescence spectroscopy

Luminescence spectra were obtained in aerated acetonitrile solutions following irradiation at λ_{exc} 340 nm. Complexes displayed the expected broad, structureless emission band around 536-546 nm that corresponds to ^{3}MLCT emission (Table 3.2). With excitation at 345 nm and detection at 540 nm respectively, time-resolved lifetime measurements detected lifetimes in the range of 46-248 ns corresponding to the expected values for the varying diimines. When the solvent was changed from acetonitrile to water, a slight blue shift in emission wavelength was seen in most cases, this was accompanied with an increase in emission lifetime for all complexes with some complexes showing an increase of more than 100 %. The luminescence data for the Re(I) complexes are shown in Table 3.2 and are discussed in detail in the following section.

Table 3.2 Luminescence data for complexes discussed in Chapter 3 recorded in both water and acetonitrile. λ_{exc} = 340 nm.

Compound	λ_{em} MeCN (nm)	τ/ns MeCN	ϕ MeCN	λ_{em} H_2O (nm)	τ/ns H_2O
Re-phen-L^A	532	248	0.02	531	623
Re-phen-L^6	546	248	0.08	543	338
Re-phen-L^{11a}	536	221	0.06	538	318
Re-phen-L^{11b}	395,543	122	0.01	385, 539	383
$[Re\text{-}phen]_2\text{-}L^2$	541	248	0.064	546	444
$[Re\text{-}phen]_2\text{-}L^7$	547	215	0.048	540	510
$[Re\text{-}phen]_2\text{-}L^8$	405,541	46,202	0.050	415,537	27,332

3.3.4.1. Luminescence properties of $\{[Re(CO)_3(phen]_2L^{2/7}]^{2+}$ and $[Re(CO)_3(phen)L^A]^+$

Upon excitation at 340nm, in acetonitrile, $[Re(CO)_3(phen)L^A]^+$ (monomeric complex of ligand precursor **A**, C_{12} chain with a terminal OH group) displayed a single broad emission band around 532 nm, which is blue-shifted emission when compared to the emission maxima of the di-metallic ester and amide complexes, $\{[Re(CO)_3(phen)]_2L^{2/7}\}^{2+}$, at 541 nm and 547 nm respectively. When the solvent was changed to water, a blue-shift in emission maxima was observed for the unsymmetrical di-amide, $\{[Re(CO)_3(phen)]_2L^7\}^{2+}$ only. All three complexes displayed dramatic extensions in lifetime with increases from 79 % for the unsymmetrical di-amide di-rhenium, $\{[Re(CO)_3(phen)]_2L^7\}^{2+}$, to 151 % for the monomeric rhenium complex, $[Re(CO)_3(phen)L^A]^+$.

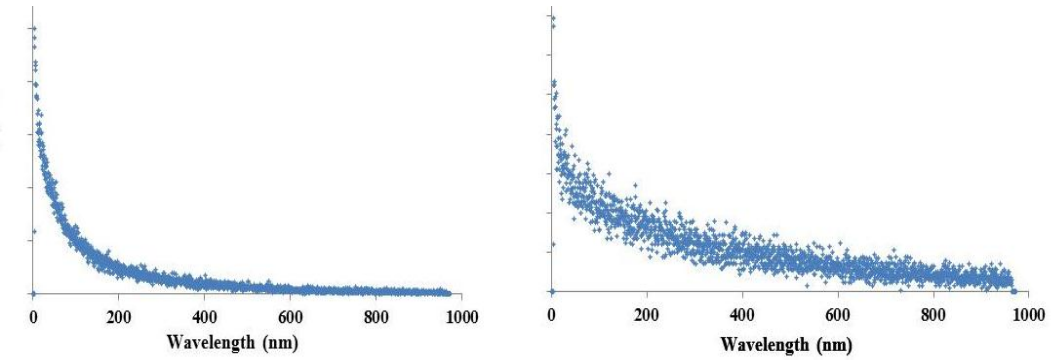

Figure 3.24 Lifetime graphs of $\{[Re(CO)_3(phen)]_2L^2\}^{2+}$ in MeCN (LHS) and H_2O (RHS).

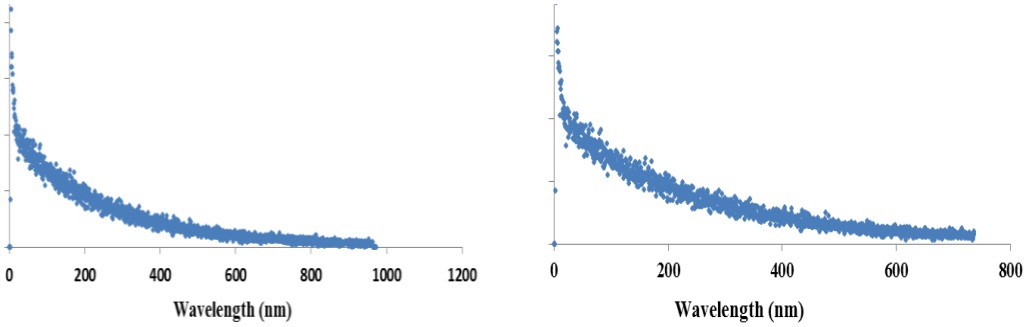

Figure 3.25 Lifetime graphs of $[Re(CO)_3(phen)]L^A\}^+$ in MeCN (LHS) and H_2O (RHS).

These extensions in lifetime were similar to those displayed in the preliminary studies with a $C_{12,}$ ester linker chain, suggesting that the excited state, localised on the $[Re(CO)_3Phen]^+$ central unit, is shielded from the quenching effect of the water solvent.[1,2] With the effect for the mono-rhenium complex mimicking the effects of the dimers it is assumed that the additional rhenium moiety had little or no effect on the change in the photophysical properties of these complexes. The lifetimes, which best fit to a single exponential decay, suggested that both the $[Re(CO)_3(phen)]^+$ moieties are in the same excited state environment. These findings imply that the 'start' of the chain (the methylene units in the chain closest to rhenium) is responsible for the shielding of the excited state from the solvent. These findings are in agreement with the behaviour of the coumarin complexes studied in Chapter 1.

Variable temperature measurements were carried out on the symmetrical ester, $\{[Re(CO)_3(phen)]_2L^2\}^{2+}$ (Figure 3.26). An increase in the intensity of the emission maximum was seen as the temperature decreased which was attributed to an enhancement in the shielding of the excited state. As the temperature is lowered the conformations of the chain is more restricted (less freedom to move) and the average conformation resides around the $[Re(CO)_3(phen)]^+$ centre resulting in the enhancement of the emission intensity.

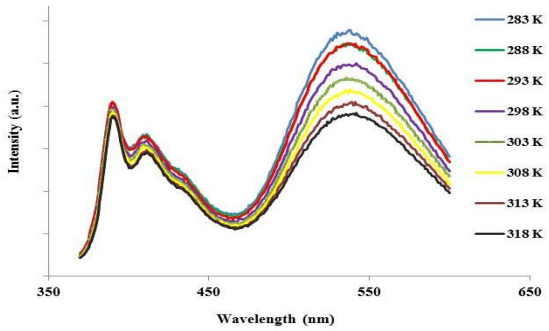

Figure 3.26 Steady state emission spectra for $\{[Re(CO)_3(phen)]_2L^2\}^{2+}$ recorded in water (λ_{exc} 345 nm).

3.3.4.2. Luminescence properties of $[Re(CO)_3(phen)L^6]^+$ and $\{[Re(CO)_3(phen)]_2L^8\}^{2+}$

$\{[Re(CO)_3(phen)]_2L^8\}^{2+}$ is a symmetrical di-metallic compound incorporating a chromophoric centre. The presence of the additional chromophore moiety results in a dual emissive compound exhibiting two emission bands; in acetonitrile, the emission band at 405 nm is attributed to the PMDA fluorophore with a wavelength which is very similar to that of the free ligand, the second, more broader emission band, at 541 nm is attributed to the ^{3}MLCT. The decay profile for $\{[Re(CO)_3(phen)]_2L^8\}^{2+}$ was best fit to a bi-exponential decay giving two distinct lifetimes; 46 and 202 ns which were assigned to PMDA-based fluorescence and ^{3}MLCT-based phosphorescence respectively. The ^{3}MLCT-based emission for $\{[Re(CO)_3(phen)]_2L^8\}^{2+}$ followed the same trend as $\{[Re(CO)_3(phen)]_2L^{2/7}\}^{2+}$ and $[Re(CO)_3(phen)L^A]^+$; when the solvent is changed from acetonitrile to water a slight blue-shift in emission maxima and an increase in lifetime of 65 % was observed (Figure 3.27).

The PMDA-based fluorescence presents the opposite trend to the ^{3}MLCT based emission. For the PMDA-based fluorescence, the results depict those predicted by a simple solvation model (the lowering of the π^* orbital and the decrease in the $\pi \rightarrow \pi^*$ energy gap with more polar solvent). When the solvent was changed from acetonitrile to water a red-shift of 10 nm of the emission maxima was viewed, this bathochromic shift was presented in the emission lifetime data with a decrease 41 % in the more polar solvent.

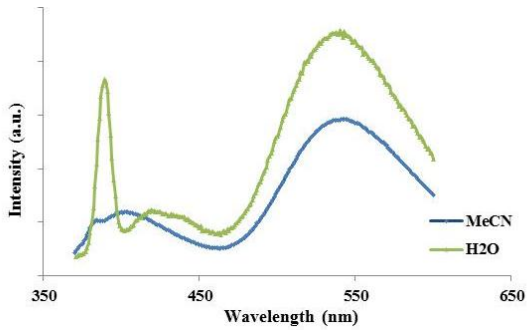

Figure 3.27 $\{[Re(CO)_3(phen)]_2L^8\}^{2+}$ in different solvents.

Further evaluation of the lifetime data in acetonitrile showed the fluorescence lifetime of the PMDA-based emission in the free ligand to be longer than the PMDA-based emission in the complex (2.6 *vs* 4.9 ns) suggesting some quenching of PMDA-based emission had occurred in the presence of the rhenium units. When the lifetime and the quantum yield values for $\{[Re(CO)_3(phen)]_2L^8\}^{2+}$ and the structurally similar reference complex $[Re(CO)_3(phen)L^6]^+$ for acetonitrile were compared, the data suggest quenching of the rhenium emission *via* the PMDA centre. The lifetimes of both, chromophore (PMDA) and rhenium in the complex, decreased in comparison to the starting materials or structural isomers.

The PMDA centred $^3\pi\rightarrow\pi^*$ state of $\mathbf{L^8}$ (recorded at 77 K; 1:1, EtOH : MeOH glass) showed structured emission at 467 nm (21400 cm^{-1}) and at 490 nm (20400 cm^{-1}), these values are higher that the reported PMDA triplet state energy of 19700 cm^{-1} [32] suggesting that the PMDA-based emission in the complex may have some spectral overlap with the ^{3}MLCT-based emission profile which could account for the decrease in both the lifetime attributed to ^{3}MLCT emission and the shorter PMDA-based lifetime when compared to its free ligand.

Variable temperature measurements were carried out for the symmetrical complex, $\{[Re(CO)_3(phen)]_2L^8\}^{2+}$. Again, an increase in the intensity of the ^{3}MLCT emission maximum was seen as the temperature was decreased indicative of increased shielding of the excited state at lower temperatures (Figure 3.28).

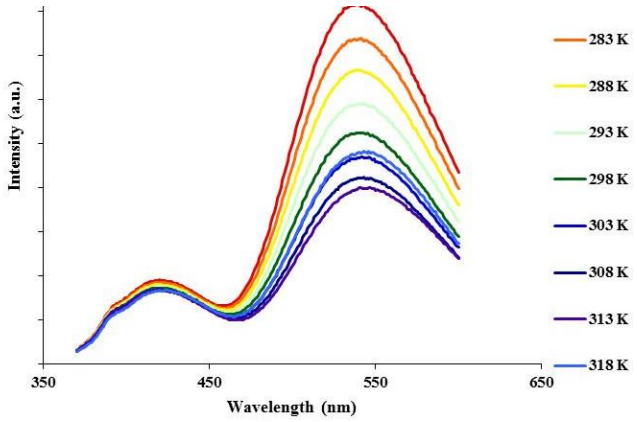

Figure 3.28 Steady state emission spectra for $\{[Re(CO)_3(phen)]_2L^8\}^{2+}$ recorded in water (λ_{exc} 345 nm).

3.3.4.3. Luminescence properties of $[Re(CO)_3(phen)L^{11a}]^+$ and $[[Re(CO)_3(phen)]L^{11b}]^+$

$\mathbf{L^{11a}}$ and $\mathbf{L^{11b}}$ differ only in the functional group appended to the aromatic chromophore, be it an ester or carboxylic acid, respectively. When co-ordinated to the $[Re(CO)_3(phen)]^+$ unit, in acetonitrile, (although the data reported in Table 3.2 shows little

change in the standard emission in comparison to $[Re(CO)_3(phen)L^{11a}]$, $[Re(CO)_3(phen)L^{11b}]^+$ showed an increase in the ratio of intensity of the ligand based emission to ^{3}MLCT emission. This increase was accompanied by a decrease in the emission lifetime in comparison to the complexes previously reported. The difference was observed in acetonitrile only and so, similarly to the unpredictable photophysical properties of the Re(I)-coumarin type complexes discussed in Chapter 2, no conclusive statement concerning the difference in the photophysical properties of the analogous complexes $[Re(CO)_3(phen)L^{11a/11b}]^+$ could be made.

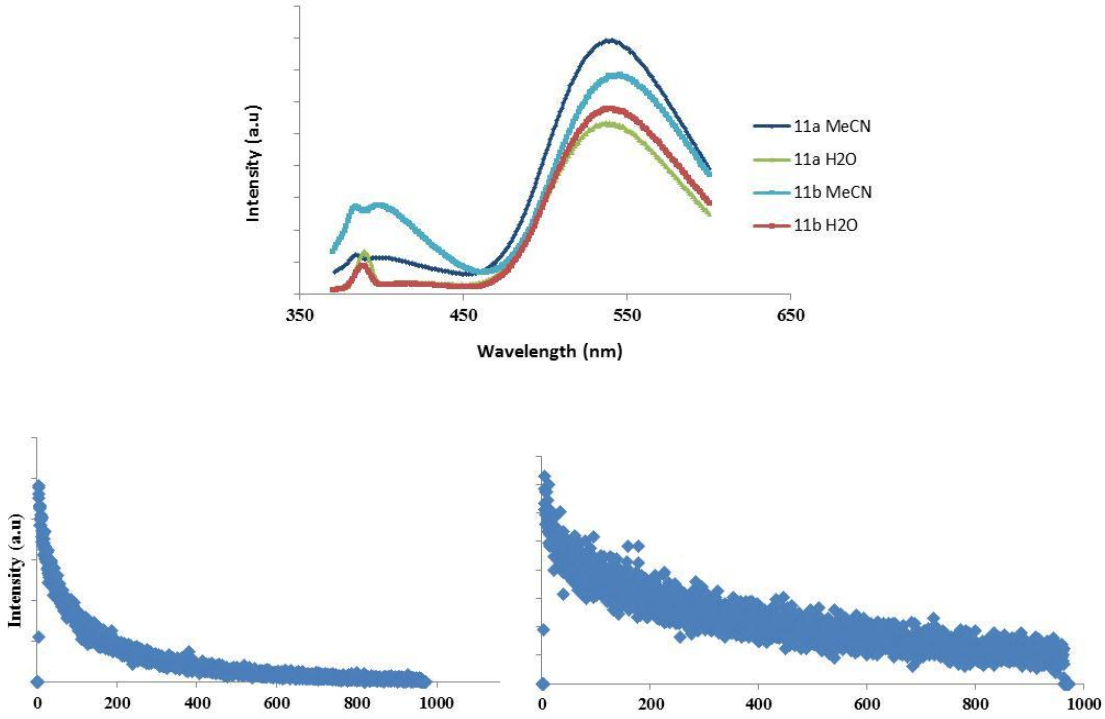

Figure 3.29 Steady state emission of $[Re(CO)_3(phen)L^{11a/11b}]^+$ in different solvents & lifetime graphs of $[Re(CO)_3(phen)L^{11b}]^+$.

3.4. Cellular imaging

The photophysical studies show that for all the complexes reported each possess suitable excitation and emission characteristics for cellular imaging applications. The cellular imaging properties of $[Re(CO)_3(phen)L^6]^+$ and $\{[Re(CO)_3(phen)]_2L^{2,7,8}]^{2+}$ were investigated and are discussed below.

Cationic, highly lipophilic complexes are known to accumulate in cells due to passive diffusion across a lipid membrane assisted by the membrane potential (the inside of the cell is negative compared to the outside). The favourable photophysical properties (Stokes shift/lifetime) and tuneable properties (lipophilicity/charge) of $[Re(CO)_3(N\text{^}N)pyridine]^+$ type complexes have resulted in complexes of this type being heavily investigated for applications as luminophores in cellular imaging. A catalogue of complexes based around the $[Re(CO)_3(N\text{^}N)]^{0/+}$ central unit, suitable for roles as cellular imaging agents, have already been reported (Chapter 1/2), however, the application of *fac*-$\{[Re(CO)_3(phen)]_2L]^{2+}$ (di-metallic) type species in this role has yet to be explored.

Rhenium complexes functionalised with a long chain aliphatic have reported enhanced lipophilicity thus a high degree of cellular uptake.[1,2] Both the di-cationic charge and the aliphatic chain length situated on $\{[Re(CO)_3phen]_2\text{-}L^{2,7,8}]^{2+}$ present characteristics, such as favourable concentration gradient/ lipophilicity to promote an increase in the uptake of the complexes through the outer cell membrane and possibly uptake through the inner cell membranes leading to more specific localisation in organelles. (*Note: In some cases an increase in lipophilicity has led to an increase in toxicity*). To test the viability of these complexes as cellular imaging agents the selected complexes were incubated with the MCF-7 cell line and then the cells examined by confocal fluorescence microscopy.

The mono-metallic $[Re(CO)_3(phen)L^6]^+$ and di-metallic $\{[Re(CO)_3(phen)]_2\text{-}L^{2,7,8}\}^{2+}$ were each incubated with MCF-7 cells over a 30 minute period at 4 ˚C. The low temperature allows energy-dependent uptake processes, such as endocytosis, to be repressed.[33,34] Following the removal of excess agent, the cells were allowed to warm to room temperature. At room temperature the cells functions normalise; energy-dependent pathways are no longer repressed allowing the accumulation and toxicity of the investigated complexes to be viewed.

The samples were imaged by confocal microscopy using an excitation wavelength of 405 nm (providing effective sensitisation of the ^{1}MLCT band) and a detection range between 530-580 nm in accordance to the ^{3}MLCT emission reported in Table 3.2 thus effectively eliminating autofluorescence. All four of the complexes viewed showed successful uptake with > 80 % of cells showing rhenium based emission for complexes

$\{[Re(CO)_3(phen)]_2L^{7,8}\}^{2+}$,$[Re(CO)_3(phen)L^6]^+$ and > 90 % of cells showing rhenium based emission for $\{[Re(CO)_3(phen)]_2L^2\}^{2+}$. Good cell morphology was maintained for each of the four samples. Further localisation details are discussed in detail in the following sections.

3.4.1. Cell imaging with $[Re(CO)_3(phen)]L^6]^+$

The mono-metallic complex, $[Re(CO)_3(phen)L^6]^+$, equipped with a phthalimide moiety showed invariable rhenium based emission. The absence of intense spots (seen in later examples) confirms non-specific localisation within the cell. Non-specific localisation was displayed with the plasma membrane, internal membrane and the perinuclear region of the cytoplasm all showing strong emission (Figure 3.30).

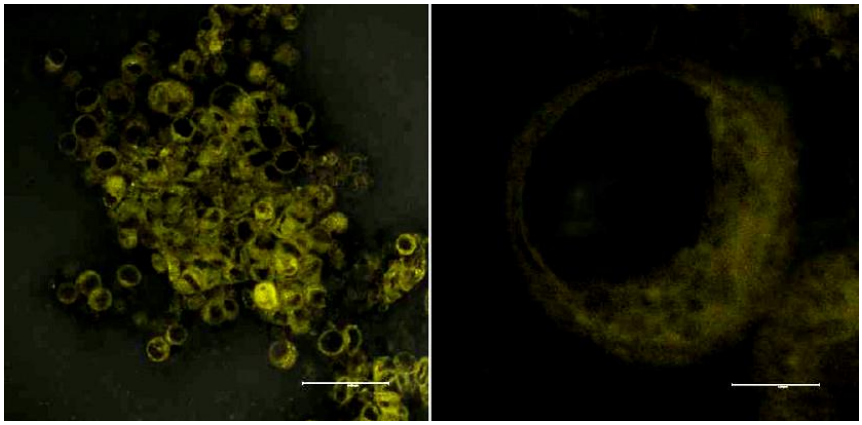

Figure 3.30 $[Re(CO)_3(phen)L^6]^+$ uptake (left, scale bar = 48 µm) and localization (right, scale bar = 5 µm).

3.4.2. Cell imaging with $\{[Re(CO)_3(phen)]_2L^8\}^{2+}$

Unlike the monometallic complex, $[Re(CO)_3(phen)L^6]^+$ (Figure 3.30) the emission intensity of the chromophore-centred, di-rhenium complex was variable from cell to cell; general background emission from the membrane and cytoplasm was observed along with distinct bright spots, which are indicative of specific localisation. The increase in the specificity of localisation from the monomer to the dimer can be attributed to the increase in lipophilicity and charge on the $\{[Re(CO)_3(phen)]_2L^8\}^{2+}$ complex allowing the dimer to diffuse across inner-membranes to accumulate within the organelles. The diffuse nature of the bright spots argues against specific mitochondrial staining but can be attributed to ER and Golgi apparatus staining (Figure 3.31).

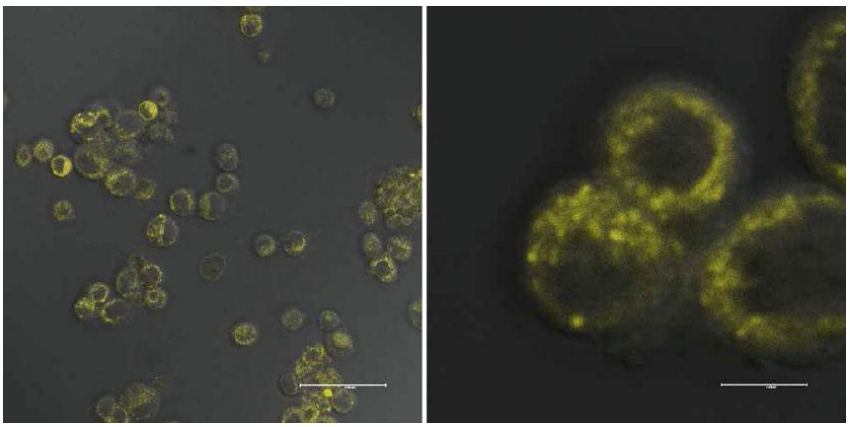

Figure 3.31 $\{[Re(CO)_3(phen)]_2L^8\}^{2+}$ uptake (left, scale bar = 48 µm) and localization (right, scale bar = 10 µm).

3.4.3. Cell imaging with $\{[Re(CO)_3(phen)]_2L^7\}^{2+}$

Similarly to the previous example, $\{[Re(CO)_3(phen)]_2L^8\}^{2+}$ (Figure 3.31), this non-symmetrical, di-rhenium complex showed variable emission intensity from cell to cell, however, unlike the chromophore, centred dimer, $\{[Re(CO)_3(phen)]_2L^7\}^{2+}$ showed a decrease in the intensity of the rhenium based emission with visible staining of the cytoplasm only (Figure 3.32). The absence of bright spots is indicative of non-specific localisation.

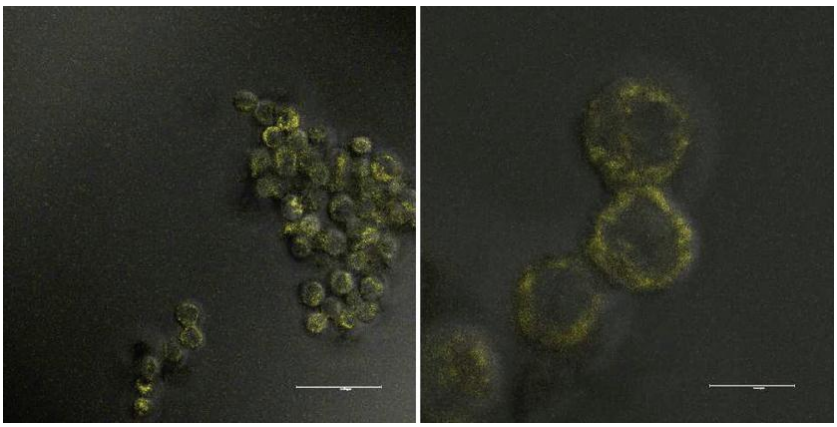

Figure 3.32 $\{[Re(CO)_3(phen)]_2L^7\}^{2+}$ Uptake Uptake (left, scale bar = 48 µm) and localization (right, scale bar = 10 µm).

3.4.4. Cell imaging with $\{[Re(CO)_3(phen)]_2L^2\}^{2+}$

The symmetrical, di-rhenium ester species, $\{[Re(CO)_3(phen)]_2L^2\}^{2+}$, displayed invariable intensity with non-specific, diffuse cytoplasmic and membrane staining of higher intensity than the unsymmetrical amide analogue, $\{[Re(CO)_3(phen)]_2L^7\}^{2+}$. Additionally, intense spots could be viewed from the centre of a small number of cells; this emission is attributed to specific staining of the nucleolar. Z-stacks were taken confirming the presence of intra-nuclear staining as oppose to cell surface staining. The increased lipophilic nature of

this complex in comparison to previous mono and di-rhenium complexes herein is evident in the accumulation of the ester in the nucleolar *via* permeation of the nuclear membrane (Figure 3.33). This increased lipophilicity is attributed to the linker unit (amides show lower uptake than esters, *see Chapter 1*).

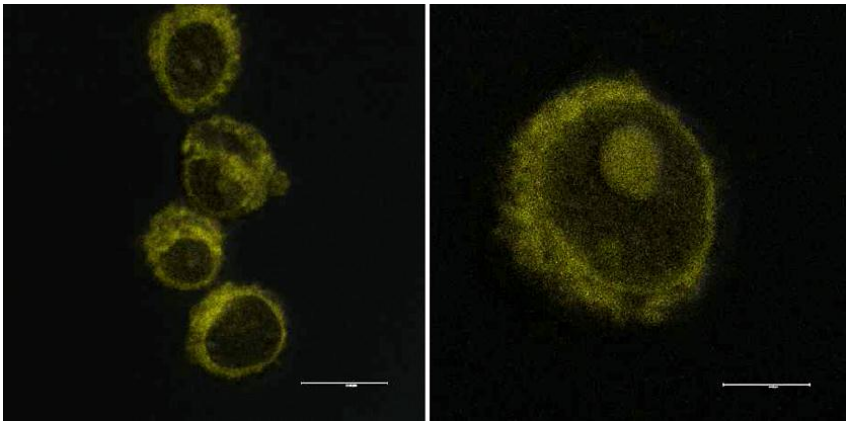

Figure 3.33 $\{[Re(CO)_3(phen)]_2L^2\}^{2+}$ uptake (left, scale bar = 14 µm) and localization (right, scale bar = 10 µm).

3.4.4.1. SYTORNASelect (SRS)

The low number of cells displaying nucleolar staining made confirmation of the specific organelle staining *via* co-localization experiments impossible. To demonstrate the accumulation of the di-rhenium ester in the nucleolei, SRS was used (Figure 3.34). SRS is a cell permeable nucleic acid known to selectively stain the nucleolei, but more specifically it stains the RNA found in the nucleolei. When incubated with MCF-7s SRS displayed emission distribution very similar to that shown in Figure 3.33. Both the Z stacks and SRS localisation indicate the assignment for the bright emissive spot to nucleolar staining is highly probable.

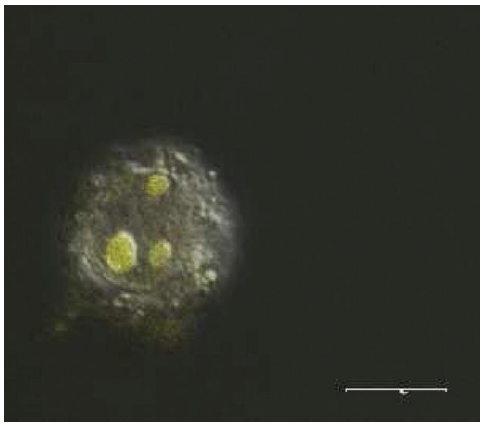

Figure 3.34 Localization of SRS (scale bar = 9 µm) in MCF7s

3.5. Cytotoxicity investigation

Propidium iodide (PI) is a cell impermeable fluorophore that can only be taken up into cells with damaged membranes and it is commonly used to test the number of dead cells in a given sample and thus can be used to test the toxicity of the complexes after incubation. Following incubation of MCF-7's with $\{[Re(CO)_3(phen)]_2L^{2/7}\}^{2+}$ and $[Re(CO)_3(phen)L^6]^+$, the cells were incubated with PI. The results are shown in Table 3.3.

A control made up of MCF-7 cells, PI and DMSO showed 3 % of cells took up the PI indicator. The symmetrical, di-rhenium ester species, $\{[Re(CO)_3(phen)]_2L^2\}^{2+}$, gave the highest toxicity value of 7 % indicating a relationship between toxicity and lipophilicity as reported previously. Despite the increase in toxicity of the dimer ester in comparison to the control all three complexes tested showed low-cytotoxicity with 1-7% of samples taking up the PI indicator. The low toxicity values of all four complexes favour their use as cellular imaging agents.

Table 3.3 Cytotoxicity data for$\{[Re(CO)_3(phen)]_2L^{2/7}\}^{2+}$ and $[Re(CO)_3(phen)L^6]^+$

Compound	% of dead cells
Control	3 ± 2.92
$[Re\text{-}phen\text{-}L^{51b}]^+$	4 ± 3.51
$[[Re\text{-}phen]_2\text{-}L^{42}]^{2+}$	7 ± 4.66
$[[Re\text{-}phen]_2\text{-}L^{62}]^{2+}$	1 ± 1.79

3.6. Conclusion

From the photophysical data discussed it was clear that each of the complexes reported herein are sensitive to the nature of the solvent environment. The inclusion of an additional rhenium moiety in complexes $\{[Re(CO)_3(phen)]_2L^{2/7/8}\}^{2+}$, showed an appreciable difference in the photophysical results of the complex when the solvent is changed from acetonitrile to water with both a dramatic increase in emission intensity and lifetime seen in the majority of compounds investigated. The monomer species, $[Re(CO)_3(phen)L^{A}]^{+}$, mimics the photophysical changes with solvent seen in both the di-metallic complexes and the mono-rhenium complex reported in the preliminary studies. The monomers, $[Re(CO)_3(phen)L^{6/11a/11b}]^{+}$ showed a much smaller increase in lifetime when the solvent was changed in comparison to $[Re(CO)_3(phen)L^{A}]^{+}$ thus linker units and functional groups appended to the end of the chains must have an effect on the extent of chain wrapping.

Similar to the results in Chapter 2, the inclusion of a chromophore moiety to the centre and end of a ligand chain does show an effect on the solvent-dependent photophysical properties with changes in emission intensities. As only a small number of complexes have been investigated no conclusive statement on the role of the chromophore in hydrophobic interactions can be drawn.

Four complexes were investigated for their suitability as cellular imaging agents, the monomer $[Re(CO)_3(phen)L^{6}]^{+}$, and the di-metallic complexes $\{[Re(CO)_3(phen)]_2L^{2/7/8}]^{2+}$. All four complexes displayed low toxicity and good cellular uptake. More specific localisation was viewed for the di-rhenium, di-ester complex, $\{[Re(CO)_3(phen)]_2L^{2}]^{2+}$ with specific localisation in the nucleolar and for the di-rhenium chromophore centred complex, $\{[Re(CO)_3(phen)]_2L^{8}]^{2+}$, with probable ER and Golgi apparatus localisation.

3.7. Experimental

3.7.1. Synthesis of ligands

L[1] Nicotinoyl chloride (0.5 g, 3.5 mmol) in chloroform was added slowly to a solution of ethylene glycol (4 mL, 7 mmol) and TEA (1.6 mL, 11 mml) in chloroform (40 mL) and the solution was left to stir at 60 °C for 5 h. The solution was washed with water (3 × 10 mL) and sat. aq. ammonium chloride (10 mL). The organic layer was dried and solvent evaporated to dryness, yielding a cream solid. Yield: 1.3 g, 68 %. ^{1}H NMR ($CDCl_3$, 400 MHz, 298K) δ_H: 4.61 (4H, s, (*H5*)), 7.32-7.35 (2H, m, (*H3*)), 8.21-8.26 (2H, m, (*H4*)), 8.68-8.73 (2H, m, (*H2*)), 9.13 (2H, s, (*H12*)) ppm. ^{13}C{^{1}H} NMR ($CDCl_3$, 101 MHz, 298K) δc: 61.9, 122.4, 136.2, 149.9, 152.6, 164 ppm. MS (ES^+) *m/z*: 272 $[M+H]^+$. HRMS (ES^+) found *m/z* 273.0872 $[M+H]^+$; $[C_{14}H_{13}O_4N_2]^+$ requires 273.0791**.** IR (nujol) υ: 1651 (CO) cm^{-1}. UV-vis (ε / M^{-1} cm^{-1}) (MeCN) λ_{max}: 261 (3488), 332 (558) nm. Mp= 112-115.

L[2] Nicotinoyl chloride (1.77 g, 12.48 mmol) in chloroform was added slowly to a solution of 1,12-dodeacanediol (1 g, 4.99 mmol) and TEA (2.1 mL, 14.97 mml) in chloroform (40 mL) and the solution was left to stir at 60 °C for 5 h. Same work up as above. Yield: 1.90 g, 93 %. ^{1}H NMR ($CDCl_3$, 400 MHz, 298K) δ_H: 1.13 (12H, s, (*H8-H10*)), 1.43-1.48 (4H, m, (*H7*)), 1.69-1.79 (4H, m, (*H6*)), 4.75 (4H, t, $^{3}J_{HH}$ = 6.7 Hz, (*H5*)), 7.30-7.36 (2H, m, (*H3*)), 8.21-8.27 (2H, m, (*H4*)), 8.68-8.72 (2H, m, (*H2*)), 9.12 (2H, s, (*H1*)) ppm. ^{13}C{^{1}H} NMR ($CDCl_3$, 101 MHz, 298K) δc: 24.9, 27.6, 28.2, 28.5, 28.9, 64.6, 122.3, 125.4, 136.2, 149.7, 152.1, 164.2 ppm. MS (ES^+) *m/z*: 413.2 $[M+H]^+$.

L[4] To a solution of hydroxy methyl pyridine (0.8 mL, 92 mmol) in DCM (30 mL) was added oxalyl chloride (0.3 mL, 3.7 mmol) dropwise at room temperature. The reaction was left to stir for 30 mins. The white precipitate formed was filtered and dried under reduced pressure. Yield 800 mg, 53 %. ^{1}H NMR ($CDCl_3$, 400 MHz, 298K) δ_H: 5.31 (4H, s, (*H5*)), 7.29-7.36 (2H, m, (*H3*)), 7.71-7.75 (2H, m, (*H4*)), 8.78-8.80 (2H, m, (*H2*)), 8.62 (2H, s, (*H1*)) ppm. ^{13}C{^{1}H} NMR ($CDCl_3$, 101 MHz, 298K) δc: 66.2, 110, 123.7, 129.7, 136.7, 150, 150.3, 157 ppm. MS (ES^+): 273 $[M+H]^+$. HRMS (ES^+) found *m/z* 273.08 $[M+H]^+$; $[C_{14}H_{13}O_4N_2]^+$ requires 273. IR (nujol) υ: 1732.7 (CO) cm^{-1}. UV-vis (ε / M^{-1} cm^{-1}) (MeCN) λ_{max}: 209 (367), 224 (681), 250nm, (1090) nm.

L[5] To a solution of ligand precursor A (1 g, 3.26 mmol) and TEA (0.69 mL, 4.89 mmol) in DCM (30 mL) was added oxalyl chloride (0.201 g, 1.63 mmol) dropwise at room temperature. The reaction was left to stir for 30 mins. The crude product was purified

using column chromatography, eluting with dichloromethane:methanol (96:4). Yield: 0.136 mg, 12 %. ^{1}H NMR ($CDCl_3$, 400 MHz, 298 K) δ_H: 1.15-1.29 (28H, m, (*H8-H14*)), 1.29-1.41 (4H, m, (*H7*)), 1.53-1.62 (4H, m, (*H15*)), 1.68-1.77 (4H, m, (*H6*)), 4.08 (4H, t, $^{3}J_{HH}$ = 6.8 Hz, (*H16*)), 4.29 (4H, t, $^{3}J_{HH}$ = 6.7 Hz, (*H5*)), 7.27-7.36 (2H, m, (*H3*)), 8.18 (2H, dd, (*H4*)), 8.13-8.25 (2H, m, (*H2*)), 9.11-9.19 (2H, m, (*H1*)) ppm. ^{13}C{^{1}H} NMR ($CDCl_3$, 101 MHz, 298 K) δc: 25.6, 25.8, 26.2, 26.8, 27.1, 28.5, 28.9, 28.6, 29, 29.3, 29.6, 42.3, 65.7, 123.3, 137.1, 151.2, 153.4, 164.6 ppm. MS (ES^+) *m/z*: 682.41 $[M]^+$. HRMS (ES^+) found m/z 682.4181 $[M]^+$; $[C_{30}H_{58}O_8N_2]^+$ requires 682.4188. IR (nujol) υ: 1751 (CO), 1756 (CO) cm^{-1}. UV-vis (ε / $M^{-1}cm^{-1}$) (MeCN) λ_{max} : 261 (6067), 363 (610) nm.

L^6 12-aminolauric acid (1 g, 3.98 mmol) and phthalic anhydride (0.589 mg, 3.98 mmol) were added to a shlenk and heated until no vapour was given off. ^{1}H NMR (MeOD, 400 MHz, 298 K) δ_H: 1.25 (12H, s, (*H5-H10*)), 1.5-1.62 (4H, m, (*H4,H11*)), 2.23 (2H, t, $^{3}J_{HH}$ = 6.8 Hz, (*H12*)), 3.26 (2H, m, (*H3*)), 3.63 (2H, t, $^{3}J_{HH}$ = 6.3 Hz, (*H13*)), 7.7-7.82 (4H, m, (*H1,H2*)) ppm. Thionyl chloride (2 mL) was added and solution was left at 71 °C for 1 h. The excess thionyl chloride was removed under vacuum and chloroform (20 mL), TEA (1.14 mL, 11.14 mmol) and amino-methyl pyridine (0.76 mL, 7.43 mmol) were added and mixture heated to 59 ˚C for 3 h. The product was washed with sat. aq. ammonium chloride (3 × 10 mL), the organic layer dried and solution evaporated. Yield: 1.48 g, 95 %. ^{1}H NMR ($CDCl_3$, 400 MHz, 298 K) δ_H: 1.21 (14H, s, (*H5-H11*)), 1.58-1.65 (4H, m, (*H4, H12*)), 2.19 (2H, t, $^{3}J_{HH}$ = 7.3 Hz, (*H3*)), 3.58 (2H, t, $^{3}J_{HH}$ = 7.5 Hz, (*H13*)), 4.32 (2H, d, $^{3}J_{HH}$ = 4.3 Hz, (*H14*)), 6.47 (1H, s, (*NH*)), 7.13-7.18 (1H, m, (*H17*)), 7.50-7.53 (1H, m, (*H16*)), 7.61-7.64 (2H, m, (*H2*)), 7.72-7.76 (2H, m, (*H1*)), 8.46-8.49 (2H, m, (*H15,H18*)) ppm. ^{13}C{^{1}H} NMR ($CDCl_3$, 101 MHz, 298K) δc: 25.7, 26.8, 28.6, 29.1, 29.2, 29.4, 36.7, 38.1, 40.9, 123.1, 123.5, 132.2, 133.9, 134.2, 135.6, 148.7, 149, 168.5, 173.3 ppm. MS (ES^+) *m/z*: 435.33 $[M+H]^+$. HRMS (ES^+) found m/z 436.2588 $[M+H]^+$; $[C_{26}H_{33}O_3N_3]^+$ requires 436.2695. IR (nujol) υ: 1715 (CO), 1772 (CO) cm^{-1}. UV-vis (ε / M^{-1} cm^{-1}) (MeCN) λ_{max}: 259 (14699), 294 (6394) nm.

Ligand precursor B: L^6 (1.2 g, 2.84 mmol) was dissolved in methoxyethanol (20 mL), hydrazine (0.41 mL, 0.854 mmol) was added and the solution left at 115 ˚C for 12 h. The solution cooled and the white precipitate was filtered and filtrate evaporated. Yield: 0.5 g, 58 %. ^{1}H NMR ($CDCl_3$, 400 MHz, 298 K) δ_H: 1.21 (14H, s, (*H8-H15*)), 1.59 (2H, t, $^{3}J_{HH}$ = 6.2 Hz, (*H16*)),1.63 (2H, t, $^{3}J_{HH}$ = 7.5 Hz, (*H7*)), 2.55 (2H, t, $^{3}J_{HH}$ = 12.5 Hz, (*H17*)), 4.44 (2H, d, $^{3}J_{NH}$ = 5 Hz, (*H5*)), 7.1-7.19 (1H, m, (*H3*)), 7.53 (1H, d, $^{3}J_{HH}$ = 7.5 Hz, (*H4*)), 8.44-8.49 (2H, m, (*H1,H2*)) ppm. ^{13}C{^{1}H} NMR ($CDCl_3$, 101 MHz, 298K) δc: 24.5, 24.7, 25.8, 28.2, 28.3,

28.4, 28.5, 32.5, 33.5, 35.6, 39.9, 41.1, 122.6, 134.6, 147.7, 148.1 ppm. MS (ES^+) *m/z*: 306.26 $[M+H]^+$, HRMS (ES^+) found *m/z* 306.2537 $[M+H]^+$; $[C_{18}H_{32}ON_3]^+$ requires 306.2540. IR (nujol) υ: 3292 (NH), 1632 (CO) cm^{-1}. UV-vis. (ε / M^{-1} cm^{-1}) (MeCN) λ_{max}: 259 (759) nm.

L^7 : To nicotinoyl chloride (55 mg, 0.39 mmol) was added Ligand precursor B (100 mg, 0.38 mmol) and TEA (0.14 mL, 0.93 mmol) in chloroform (30 mL) and the solution heated to 59 ˚C for 3 h. Work-up was the same as above. Yield: 125 mg, 93 %. ^1H NMR ($CDCl_3$, 400MHz, 298K) δ_H: 1.22-1.45 (12H, m, (*H9-H15*)), 1.49-1.62 (4H, m, (*H8,H16*)), 2.15 (2H, t, $^3J_{HH}$ = 7.6 Hz, (*H17*)), 3.36-3.41 (2H, m, (*H7*)), 4.45 (2H, d, $^3J_{HH}$ = 5.9 Hz, (*H5*)), 6.1 (1H, s, (*NH*)), 6.48 (1H, s, (*NH*)), 7.12-7.15 (1H, m, (*H21*)), 7.21-7.27 (1H, m, (*H3*)), 7.50 (1H, d, $^3J_{HH}$ = 7.8 Hz, (*H20*)), 8.00 (1H, d, (*H4*)), 8.32-8.39 (2H, m, (*H2,H22*)), 8.49-8.55 (1H, m, (*H19*)), 8.82-8.96 (1H, m, (*H1*)) ppm. ^{13}C NMR ($CDCl_3$, 400 MHz, 298K) δc: 25.7, 26.9, 29.2, 29.3, 29.5, 36.7, 40.1, 49, 65.2, 123.6, 123.7, 135.3, 135.9, 147.8, 148.8, 149.1, 156.8 ppm. MS (ES^+) *m/z*: 411.3 $[M+H]^+$, 433.3 $[M+Na]^+$. HRMS (ES^+) found *m/z* 411.2749 $[M+H]^+$; $[C_{24}H_{35}O_2N_4]^+$ requires 411.2755. IR (nujol) υ:1633 (CO) cm^{-1}. UV-vis (ε / M^{-1} cm^{-1}) (MeCN) λ_{max}: 260 (9859) nm. Mp=74-82

L^8: Ligand precursor B (200 mg, 0.655 mmol) and benzol-1,2,4,5 benzenetetracarboxylic-dianhydride (71 mg, 0.323 mmol) were heated together in a Schlenk until no vapour was given off producing a brown solid. Yield: 251 mg, 98 %. ^1H NMR (MeOD, 250 MHz, 298 K) δ_H: 1.11-1.42 (32H, m, (*H9-H16*)), 1.49-1.62 (8H, m, (*H17,H18*)), 2.18 (4H, t, $^3J_{HH}$ = 15 Hz, (*H7*)), 3.17 (4H, t, $^3J_{HH}$ = 1.5 Hz, (*H18*)), 4.41 (4H, d, $^3J_{NH}$ = 6.3 Hz, (*H5*)), 7.2-7.24 (2H, m, (*H3*)), 7.57 (2H, d, $^3J_{HH}$ = 7.5 Hz, (*H4*)), 8.22 (2H, d, (*H19*)), 8.41-8.61 (4H, m, *(H1,H2*)) ppm. $^{13}C\{^1H\}$ NMR (MeOD, 101 MHz, 298K) δc: 24.7, 25.7, 27.4, 28, 28.2, 28.3, 28.4, 35.6, 37.7, 38.7, 39.9, 117.1, 117.4, 122.7, 122.8, 133.4, 134.9, 135.8, 135.9, 136.2, 136.4, 147.5, 147.8, 148.5, 149, 164.7, 165.1, 165.3, 172.3 ppm. MS (ES^+) *m/z*: 793.5 $[M+H]^+$, 815.5 $[M+Na]^+$. HRMS (ES^+) found *m/z* 793.4634 $[M+H]^+$; $[C_{46}H_{61}O_6N_6]^+$ requires 793.4647. IR (nujol) 1696 (CO), 1740 (CO) cm^{-1}. UV-vis (ε / M^{-1} cm^{-1}) (MeCN) λ_{max}: 234 (17545) nm.

L^9 6-amino, 1-hexanol (1.07 g) was added drop wise to a solution of benzol-1,2,4,5 benzenetetracarboxylicaciddianhydride (1 g) in DMF (4.5 mL) The mixture was set to sub reflux at 160 ˚C. After 6 h the solution was cooled and poured into ice water. The white precipitate that formed was filtered and recrystallized using methanol. Yield: 1.6 g, 84 %. ^1H NMR ($CDCl_3$, 400MHz, 298K) δ_H: 0.82-0.88 (8H, m, (*H3,H4*)), 1.52-1.57 (4H, m, (*H2*)), 1.68-1.71 (4H, m, (*H5*)), 3.52 (4H, t, $^3J_{HH}$ = Hz, (*H1*)), 3.69 (4H, t, $^3J_{HH}$ = Hz, (*H6*)), 8.15 (2H, s, (*H7*)) ppm. MS (ES) *m/z*: 855.31 $[2M+Na^+]$. **L^{10}** The white precipitate (1 g) thionyl

chloride (2 mL) was added and the reaction was left at 71 ˚C for 4 h. The excess thionyl chloride was then removed using a second vacuum chamber. ^{1}H NMR ($CDCl_3$, 400MHz, 298K) δ_H: 1.42-1.48 (4H, m, (*H3*)), 1.49-1.57 (4H, m, (*H4*)), 1.75-1.80 (8H, m, (*H2, H5*)), 3.48 (4H, t, $^{3}J_{HH}$ =6.6 Hz, (*H1*)), 3.72 (4H, t, $^{3}J_{HH}$ = 7.3 Hz, (*H6*)), 8.19 (2H, s, (*H7*)) ppm. To the precursor (100 mg, 0.22 mmol) in DMF (20 mL) was added potassium pthalimide (101 mg, 0.56 mmol) in DMF (10 mL) drop wise followed by catalytic amount of KI. The reaction was left at 150 ˚C for 3 weeks. The resulting solution was evaporated to yield a orange oil. Recrystalised using chloroform and petrol. ^{1}H NMR ($CDCl_3$, 400MHz, 298K) δ_H: 1.43-1.46 (8H, m, (*H3, H4, H12, H13*)), 1.65-1.75 (8H, m, (*H2, H5, H11, H15*)), 3.51 (2H, t, (*H15*)), 3.59 (2H, t, (*H6*)), 3.68-3.72 (4H, m, (*H1, H10*)), 7.62-7.66 (2H, m, (*H7*)), 7.79-7.84 (2H, m, (*H8*)), 8.15-8.19 (2H, m, (*H9*)) ppm. ^{13}C NMR ($CDCl_3$, 400 MHz, 298K) δc: 36.1, 41.2, 44.1, 44.4, 44.8, 45, 45.7, 55.8, 127.9, 138.7 ppm. MS (ES^+) *m/z*: 545.22 [M]. IR (solid) υ: 1661.86 (CO), 1716.82 (CO), 1769.85 (CO), 3414.83 (OH), cm^{-1}. UV-vis (ε / M^{-1} cm^{-1}) (MeCN) λ_{max}: 237 (5377) nm.

Ligand precursor C: Nicotinoyl chloride (1.96 g, 15.9 mmol) in chloroform (10 mL) was added slowly to a solution of 12-amino lauric acid (2 g, 7.95 mmol) and TEA (5.6 ml, 39.8 mmol) in chloroform (20 mL) and the solution was left to stir at 60 °C for 5 h. The solution was washed with water (3 × 10 mL) and sat. aq. ammonium chloride (10 mL). The organic layer was dried and solvent evaporated to dryness, yielding a cream solid Yield: 1.6 g, 55 %. ^{1}H NMR (MeOD, 400 MHz, 298 K) δ_H: 1.17-1.25 (14H, m, (*H7-H13*)), 1.55-1.58 (4H, m, (*H6,H14*)), 2.22 (2H, t, $^{3}J_{HH}$ = 7.4 Hz, (*H5*)), 3.34 (2H, t, $^{3}J_{HH}$ = 7.2 Hz, (*H15*)), 7.49-7.54 (1H, m, (*H3*)), 8.18-8.21 (1H, m, (*H4*)), 8.62-8.68 (1H, m, (*H2*)), 8.91-8.93 (1H, m, (*H1*)) ppm. ^{13}C{^{1}H} NMR (MeOD, 101 MHz, 298K) δc: 26, 28.1, 30, 30.1, 35, 41.2, 48, 49.7, 50.1, 125.2, 132.3, 137.2, 148.9, 152.4, 167.7, 177.7 ppm. MS (ES^+) *m/z*: 321.33 $[M+H]^+$, 343.20 $[M+Na^+]$, 359.18 $[M+K^+]$, 384.22 $[M+MeCNNa^+]$. HRMS (ES^+) found *m/z* 319.2035 $[M-H]^+$; $[C_{18}H_{27}O_3N_2]^+$ requires 319.2035. IR (nujol) υ: 1650 (CO), 1807 (CO), 3306 (NH) cm^{-1}. UV-vis (ε / M^{-1} cm^{-1}) (MeCN) λ_{max}: 213 nm (10891), 257 (16758) nm.

L^{11a}: Ligand precursor C (1.2 g, 3.75 mmol) was dissolved thionyl chloride (2 mL and left at 71 ˚C for 1 h. The excess thionyl chloride was removed under vacuum. Methyl anthranilate (1.45 mL, 11.25 mmol) in chloroform (30 mL) was added and reaction left at 59 ˚C for 3 h. The precipitate in solution was filtered. The solution was concentrated and petrol added to precipitate out a cream solid. Yield: 600 mg, 37 %. ^{1}H NMR ($CDCl_3$, 400 MHz, 298 K) δ_H: 1.12-1.37 (16H, m, (*H7-H14*)), 1.52 (2H, t, $^{3}J_{HH}$ = 7.4 Hz, (*H15*)), 1.67 (2H, t, $^{3}J_{HH}$ = 7.1 Hz,

(*H6*)), 2.35 (2H, t, $^{3}J_{HH}$ = 7.3 Hz, (*H5*)), 3.31-3.38 (2H, m, (*H15*)), 3.82 (3H, s, (*H20*)), 6.12 (1H, s, (*NH*)), 6.92 (1H, t, $^{3}J_{HH}$ = 7.5 Hz, (*H19*)), 7.22-7.27 (1H, m, (*H3*)), 7.42 (1H, t, $^{3}J_{HH}$ = 7.3 Hz, *(H18*)), 7.79 (1H, d, $^{3}J_{HH}$ = 7.5 Hz (*H4*)), 8.00 (1H, d, $^{3}J_{HH}$=8 Hz, (*H20*)), 8.49-8.51 (2H, m, (*H1*,*H2*)), 8.81-8.87 (1H, m, (*H17*)) ppm. $^{13}C\{^{1}H\}$ NMR $CDCl_{3,}$ 101 MHz, 298 K) δc: 25.5, 27, 29.2, 29.3, 29.4, 29.6, 38.7, 40.3, 52.3, 114.8, 120.2, 122.3, 130.8, 134.7, 135.3, 141.7, 147.7, 151.8, 168.8, 172.4 ppm. MS (ES^{+}) *m/z*: 454.28 $[M+H]^{+}$, 476.35 $[M+Na^{+}]$, 493.23 $[M+K^{+}]$, HRMS (ES^{+}) found *m/z* 454.2692 $[M+H]^{+}$; $[C_{26}H_{36}O_4N_3]^{+}$ requires 454.2700. IR (nujol) ν: 1650 (CO), 1683 (CO) cm^{-1}. UV-vis (ε / M^{-1} cm^{-1}) (MeCN) λ_{max}: 223 (31383) 252.4 (14839), 310.5 (4442) nm.

L^{l1b}: 11a (600 mg, 1.38 mmol) was dissolved in ethanol (30 mL) and hydrazine (0.05 mL, 1.65 mmol) was added drop-wise. The reaction mixture was left to heat at 70 ˚C for 3 h. Water was then added to the mixture and product was extracted using chloroform and ethyl acetate. Organic layer dried and solution evaporated to yield a dark cream ppt. Yield: 400 mg, 66 %. ^{1}H NMR ($CDCl_{3,}$ 400 MHz, 298 K) δ_H: 1.19-1.35 (14H, m, (*H8-H14*)), 1.48-1.52 (2H, m, (*H15*)), 1.57-1.63 (2H, m, (*H7*)), 2.30 (2H, t, $^{3}J_{HH}$ = 7.5 Hz, (*H16*)), 3.41 (2H, t, $^{3}J_{HH}$ = 7.2 Hz, (*H6*)), 6.94 (1H, t, $^{3}J_{HH}$ = 7.6 Hz, (*H20*)), 7.29 (1H, dt, (*H19*)), 7.42-7.46 (1H, m, (*H3*)), 8.0 (1H, d, $^{3}J_{HH}$ = 7.6 Hz , (*H4*)), 8.11 (1H, d, $^{3}J_{HH}$ = 8 Hz, (*H21*)), 8.40 (1H, d, $^{3}J_{HH}$ = 8.3 Hz, (*H18*)), 8.51-8.55 (1H, m, (*H2*)), 8.79-8.83 (1H, m, (*H1*)) ppm. $^{13}C\{^{1}H\}$ NMR ($CDCl_{3,}$ 101 MHz, 298 K) δc: 25.1, 26.4, 26.8, 28.9, 29, 29.2, 29.3, 38.7, 41.2, 119.4, 122.2, 131.6, 135.6, 166.2, 172.9 ppm. IR (nujol) ν: 1656 (CO), 3440 (CO) cm^{-1}. UV-vis (ε / M^{-1} cm^{-1}) (MeCN) λ_{max}: 254.5 (926) nm.

L^{12}: Ligand precursor A (150 mg, 0.488 mmol) and phthalic anhydride (72 mg, 0.488 mmol) were dissolved in chloroform (20 mL) and added to RBF where they were heated to 56 ˚C. TFA was added drop wise until pH was acidic and reaction left to heat and stir at room temperature for 48 h. The resulting solution was washed with $NaH(CO)_3$ (2 × 5 mL), dried and solution evaporated. Yield: 39 mg, 18 %. ^{1}H NMR ($CDCl_{3,}$ 400 MHz, 298 K) δ_H: 1.21 (16H, m, (*H7-H14*)), 1.54-1.71 (4H, m, (*H6*,*H15*)), 4.21 (2H, t, $^{3}J_{HH}$ = 6.7 Hz, *(H5*)), 4.31 (2H, t, $^{3}J_{HH}$ = 6.7 Hz, (*H16*)), 7.78 (2H, m, (*H18*)), 7.91 (2H, m, (*H17*)), 8.72 (1H, d, $^{3}J_{HH}$ = 7.3 Hz, (*H4*)), 8.89 (1H, m, (*H2*)), 9.31 (1H, s, *(H1*)) ppm. $^{13}C\{^{1}H\}$ NMR ($CDCl_3$, 101 MHz, 298 K) δc: 20.9, 25.4, 25.8, 28, 28.4, 29, 29.1, 29.3, 29.4, 65, 67.4, 68.4, 125.7, 127.1, 131.2, 136.1, 143.7, 145.4, 145.6, 161.7, 162.8 ppm. MS (ES^{+}) *m/z*: 456.25 $[M+H]^{+}$. HRMS (ES^{+}) found *m/z* 456.2378 $[M+H]^{+}$; $[C_{26}H_{34}O_6N]^{+}$ requires 456.2378. IR (nujol) ν: 1687 (CO), 1732 (CO), 1810 (CO) cm^{-1}. UV-vis (ε / M^{-1} cm^{-1}) (MeCN) λ_{max}: 264 (2212) nm.

3.7.2. Synthesis of Complexes

[Re(CO)$_3$(phen)L^{A}]$^+$ To a round bottom flask encased in foil ligand precursor A (36 mg, 1.25 × 10^{-4} mol), [Re(CO)$_3$(phen)Br] (60 mg, 1.1 × 10^{-4} mol), and silver tetrafluoroborate (33 mg, 1.7 × 10^{-4} mol) in toluene (10 mL) were added and heated to 100 ˚C for 24 h. The solution was filtered through Celite and washed repeatedly with acetonitrile. The removal of the solvent under high vacuum afforded a yellow solid. Column chromatography was then used to purify the crude product. Yield: 22 mg, 27 %. ^{1}H NMR ($CDCl_3$, 400 MHz, 298 K) δ_H: 1.17-1.21 (14H, s, (*H12-H18*)), 1.40-1.43 (2H, m, (*H11*)), 1.55-1.57 (2H, m, (*H19*)), 2.12-2.17 (2H, m, (*H10*)), 3.39 (2H, t, $^3J_{HH}$ = 6.6 Hz, (*H20*)), 4.08 (2H, t, $^3J_{HH}$ = 6.6 Hz, (*H9*)), 7.24-7.26 (1H, m, (*H7*)), 7.99-8.04 (2H, m, (*H3*)), 8.05-8.09 (1H, m, (*H8*)), 8.17 (2H, s, (*H4*)), 8.79-8.86 (3H, m, (*H2*,*H6*)), 9.32-9.40 (2H, m, (*H1*)), 9.51-9.57 (1H, m, (*H5*)) ppm. ^{13}C{^{1}H} NMR ($CDCl_3$, 101 MHz, 298 K) δc: 6.96, 23.8, 24, 26.4, 26.7, 27.3, 27.5, 30.9, 45.5, 61.1, 65.6, 120.5, 124.9, 125.7, 126.4, 126.8, 129.4, 129.5, 138.3, 138.9, 144.4, 144.9, 152, 191.3 ppm. MS (ES$^+$) *m/z*: 758.23 [M+H]$^+$. HRMS (ES$^+$) found m/z 758.2132 [M+H]$^+$; [$ReC_{33}H_{37}O_6N_3$]$^+$ requires 758.22. IR (nujol) υ: 1765 (COO), 1924 (CO), 2025.85 (CO), 3404 (OH) cm^{-1}. UV-vis (ε / M^{-1} cm^{-1}) (MeCN) λ_{max}: 251.2 (12228), 273.4 (14639), 323.6 (3191),366.7 (1711) nm.

[Re(CO)$_3$(phen)L^{6}]$^+$ To a round bottom flask encased in foil L^6 1(50 mg, 0.12 mmol), [Re(CO)$_3$(phen)Br] (57 mg, 0.1 mmol) and silver tetrafluoroborate (31 mg, 0.14 mmol) in toluene (10 mL) were added and heated to 100 ˚C for 24 h. Work-up as before. Yield 29 mg, 33 %. ^{1}H NMR ($CDCl_3$, 400 MHz, 298 K) δ_H: 1.11-1.17 (16H, m, (*H12-H19*)), 1.36-1.46 (2H, m, (*H12*)), 1.53-1.64 (2H, m, (*H20*)), 1.96 (2H, t, $^3J_{HH}$ = 7.7 Hz , (*H11*)), 3.59 (2H, t, $^3J_{HH}$ = 7.3 Hz, (*H21*)), 4.09 (2H, t, $^3J_{HH}$ = 6 Hz, (*H9*)), 6.88-6.91 (1H, m, (*H7*)), 7.56-7.59 (4H, m, (*H3, H23*)), 7.69-7.71 (2H, m, (*H22)*), 8.0 (2H, s, (*H4*)), 8.01-8.09 (1H, m, (*H8*)), 8.06-8.13 (2H, m, (*H2*)), 8.60-8.64 (2H, m, (*H5, H6*)), 9.51-9.54 (2H, m, (*H1*)) ppm. ^{13}C NMR (($CDCl_3$) , 101 MHz, 298K): δc: 22.8, 23, 25.9, 26.1, 27.3, 29, 29.6, 29.8, 29.9, 34.5, 36.4, 38.5, 40.6, 53.9, 123.6, 124.1, 126.5, 128.1, 128.8, 131.5, 131.8, 132.5, 134.3, 135.1, 139.9, 140.5, 146.8, 150, 152, 154.6, 168.9, 174.6 ppm. MS (ES$^+$) *m/z*: 886.40, HRMS (ES$^+$) found m/z 884.2570 [M-BF_4^-]$^+$; [$^{185}ReC_{41}H_{41}O_6N_5$]$^+$ requires 884.2581. IR (nujol) ν: 1711 (CO), 1781 (CO), 1921 (CO), 2032 (CO) cm^{-1}. UV-vis (ε / M^{-1} cm^{-1}) (MeCN) λ_{max}: 275.3 (29552), 365 (3421) nm.

[Re(CO)$_3$(phen)L^{11a}]$^+$ To a round bottom flask encased in foil L^{11a} (50 mg, 0.11 mmol), [Re(CO)$_3$(phen)Br] (50 mg, 0.09 mmol) and silver tetrafluoroborate (30 mg, 0.15 mmol) in

toluene (10 mL) were added and heated to 100 ˚C for 24 h. Work-up as before. Yield: 21 mg, 26 %. ^{1}H NMR ($CDCl_3$, 400 MHz, 298 K) δ_H: 1.17-1.40 (14H, m, (*H8-H14*)), 1.41-1.47 (2H, m, (*H15*)), 1.62-1.69 (2H, m, (*H7*)), 2.48 (2H, t, (*H16*)), 3.19-3.25 (2H, m, (*H6*)), 4.38 (3H, s, (*H21*)), 6.68 (1H, t, (*H19*)), 7.32-7.38 (1H, m, (*H3*)), 7.41-7.49 (1H, m, (*H18*)), 7.91-8.03 (2H, m, (*H24*)), 8.04 (2H, s, (*H25*)), 8.02-8.09 (1H, m, (*H20*)), 8.31 (1H, d, (*H4*)), 8.51 (1H, s, (*H1*)), 8.67-8.92 (3H, m, (*H2*, *H23*)), 9.29 (1H, d, (*H17*)), 9.48-9.53 (2H, m, (*H22*)) ppm. MS (ES^+) *m/z*: found 903.33 $[M\text{-}BF_4^-]^+$, HRMS (ES^+) found m/z 902.2675 $[M\text{-}BF_4^-]^+$; $[^{185}ReC_{41}H_{43}O_7N_5]^+$ requires 902.2665. IR (nujol) ν: 1710 (CO), 1921 (CO), 2034 (CO) cm^{-1}. UV-vis λ_{max} (ε / M^{-1} cm^{-1}) (MeCN): 252.4 (8949), 272.32 (7911), 348 (12536) nm.

$[Re(CO)_3(phen)L^{11b}]^+$ To a round bottom flask encased in foil L^{11b} (50 mg, 0.11 mmol), $[Re(CO)_3(phen)Br]$ (50 mg, 0.09 mmol), and silver tetrafluoroborate (30 mg, 0.15 mmol) in toluene (10 mL) were added and heated to 100 ˚C for 24 h. Work-up as before. Yield: 14 mg, 18 mg. ^{1}H NMR ($CDCl_3$, 400 MHz, 298 K) δ_H: 1.09-1.42 (14H, m, (*H8-H14*)), 1.44 (2H, t, $^{3}J_{HH}$ = 6.7 Hz, (*H15*)), 1.68 (2H, t, $^{3}J_{HH}$ = 6.9 Hz, (*H7*)), 2.32 (2H, t, $^{3}J_{HH}$ = 7.1 Hz, (*H16*)), 3.18-3.25 (2H, m, (*H6*)), 6.73 (1H, t, $^{3}J_{HH}$ = 7.5 Hz, (*H5*)), 7.11-7.13 (1H, m, (*H3*)), 7.22 (1H, t, $^{3}J_{HH}$ = 7 Hz, (*H18*)), 7.72 (1H, d, $^{3}J_{HH}$ = 6.8 Hz, (*H20*)), 7.91 (2H, s, (*H24*)), 8.04-8.07 (3H, m, (*H19*, *H23*)), 8.21 (1H, d, $^{3}J_{HH}$ = 5.6 Hz, (*H4*)), 8.45-8.56 (4H, m, (*H2*, *H17*, *H22*)), 8.86 (1H, s, (*H1*)), 9.2 (2H, d, $^{3}J_{HH}$ = 5.2Hz, (*H21*)) ppm. MS (ES^+) *m/z*: found 890.26 $[M\text{-}BF_4^-]^+$. IR (nujol) ν: 1690 (CO), 1895 (CO), 1920 (CO), 2049 (CO) cm^{-1}. UV-vis (ε / M^{-1} cm^{-1}) (MeCN) λ_{max}: 239 (18984), 255 (11424) nm.

$\{[Re(CO)_3(phen)]_2L^2\}^{2+}$ To a round bottom flask encased in foil L^2 (14 mg, 3.69×10^{-5} mol), $[Re(CO)_3PhenBr]$ (30 mg, 7.39×10^{-5} mol), and silver tetrafluoroborate (8.5 mg, 4.4×10^{-5} mol) in toluene (10 mL)) were added and heated to 100 ˚C for 24 h. Work-up as before. Yield: 19 mg, 26 %. ^{1}H NMR (CD_3CN, 400 MHz, 298 K) δ_H: 1.13-1.31 (12H, s, (*H12-H14*)), 1.50-1.58 (4H, m, (*H11*)), 1.92- 2.05 (4H, m, (*H10*)), 4.04 (4H, t, $^{3}J_{HH}$ = 6.6 Hz, (*H9*)), 7.23-7.42 (2H, m, (*H7*)), 7.97-7.99 (4H, m, (*H3*)), 8.02-8.06 (6H, m, (*H4*, *H8*)), 8.31 (2H, d, (*H6*)), 8.48 (2H, s, (*H5*)), 8.72 (4H, d, (*H2*)), 9.51-9.54 (4H, m, (*H1*)) ppm. $^{13}C\{^{1}H\}$ NMR ($CDCl_3$, 400 MHz, 298K) δc: 28.1, 29.4, 29.9, 66, 126.7, 127.2, 128.3, 129.2, 131.4, 140.4, 140.6, 146.7, 152, 154.6, 155.6, 162.9 ppm. MS (ES^+) *m/z*: 863.3 $[M\text{-}(Re(CO)_3Phen)+H]^+$. HRMS ($ES^+$) found *m/z* 861.2404 $[M\text{-}(Re(CO)_3Phen)]^+$; $[^{185}ReC_{39}H_{40}O_7N_4]^+$ requires 861.2421. IR (nujol) ν: 1722 (CO), 1917 (CO), 2034 (CO) cm^{-1}. UV−vis (ε / M^{-1} cm^{-1}) (MeCN) λ_{max}: 252 (24400), 275 (26600), 377 (2900) nm. Anal. calcd (%) for $B_2C_{54}F_8H_{48}N_6O_{10}Re_2 \cdot 0.75CH_2Cl_2$: C, 42.40; H, 3.22; N, 5.42. Found (%): C, 42.13; H, 3.87; N, 5.80.

{[Re(CO)$_3$(phen)]$_2$L^7 }$^{2+}$ To a round bottom flask encased in foil L^7(27 mg, 0.06 mmol), [Re(CO)$_3$PhenBr] (70 mg, 0.13 mmol), and silver tetrafluoroborate (40 mg, 0.2 mmol) in toluene (10 mL)) were added and heated to 100 ˚C for 24 h. Work-up as before. Yield: 21 mg, 24 %. ^{1}H NMR (CD$_3$CN, 400 MHz, 298 K) δ_H: 1.18-1.35 (16H, m, (*H7-H14*)), 1.36-1.42 (2H, m, (*H15*)), 1.51-1.55 (2H, m, (*H6*)), 3.90-3.92 (2H, m, (*H16*)), 4.31 (2H, d, (*H5*)), 6.61 (1H, s, (*NH*)), 6.92 (1H, s, (*NH*)), 7.02-7.09 (1H, m, (*H19*)), 7.11-7.17 (1H, m, (*H3*)), 7.52 (1H, d, (*H18*)), 7.60-7.65 (1H, m, (*H4)*), 8.01-8.09 (8H, m, (*H23*, *H24*, *H27*, *H28*)), 8.20-8.25 (1H, m, (*H20*)), 8.44-8.49 (1H, m, (*H2*)), 8.71-8.78 (5H, m, (*H17*, *H22*, *H26*)), 9.49-9.53 (5H, m, (*H1*, *H21*, *H25*)) ppm. MS (ES$^+$) *m/z*: 861.29 [M-Re(CO)$_3$(phen)]$^+$. HRMS (ES$^+$) found *m/z* 859.2743 [^{185}ReC$_{39}$H$_{42}$O$_5$N$_6$]$^+$; [^{185}ReC$_{39}$H$_{42}$O$_5$N$_6$]$^+$ requires 859.2741$^+$. IR (nujol) υ: 1675 (CO), 1910 (CO), 2031 (CO) cm^{-1}. UV-vis (ε / M^{-1}cm^{-1}) (MeCN) λ_{max}: 252.4 (5760), 272 (5520) nm. Anal. calcd (%) for B$_2$C$_{54}$F$_8$H$_{50}$N$_8$O$_8$Re$_2$·3CH$_2$Cl$_2$ C, 39.35; H, 3.24; N, 6.44. Found (%): C, 39.24; H, 3.60; N, 6.69.

{[Re(CO)$_3$(phen)]$_2$L^8}$^{2+}$ To a round bottom flask L^8 (40 mg, 0.05 mmol), [Re(CO)$_3$PhenMeCN] (50 mg, 0.1 mmol) in chloroform (10 mL)) were added and heated to 59 ˚C for 12 h. The removal of the solvent under high vacuum afforded an orange colored solid. The crude product was purified using column chromatography, eluting with dichloromethane:methanol (96:4). Yield: 16 mg, 14%. ^{1}H NMR (CD$_3$CN, 400 MHz, 298 K) δ_H: 0.98-1.13 (32H, m, (*H8-H15*)), 1.37 (4H, t, $^3J_{HH}$ = 7 Hz, (*H7*)), 1.65 (4H, t, $^3J_{HH}$ = 6.7 Hz, (*H16*)), 3.57 (4H, t, $^3J_{HH}$ = 7.2 Hz , (*H6*)), 3.93 (4H, d, $^3J_{HH}$ = 6 Hz, *(H5)*), 6.62 (2H, s, (*NH*)), 7.01-7.03 (2H, m, (*H3*)), 7.49 (2H, d, $^3J_{HH}$ = 7.9 Hz, (*H4*)), 8.0-8.08 (12H, m, (*H2*, *H17*, *H20*, *H21*)), 8.1 (2H, s, (*H1*)), 8.72 (4H, d, (*H19*)), 9.46-9.49 (4H, m, (*H18))* ppm. MS (ES$^+$) *m/z*: 846.2 ([M]$^{2+}$, 1243.5 [M-(Re(CO)$_3$Phen)]$^+$, 1779.5 [M+BF$_4$]$^+$. HRMS (ES$^+$) found m/z 845.2345 [M-2BF$_4^-$]$^{2+}$; [^{185}Re$_2$C$_{76}$H$_{76}$0$_{12}$N$_{10}$]$^{2+}$ requires 845.2346. IR (nujol) υ: 2032 (CO), 1917 (CO), 1717 (CO) cm^{-1}. UV-vis (ε / M^{-1} cm^{-1}) (MeCN) λ_{max}: 274 (17451) nm, 375 (5085) nm. Anal. Calcd (%) for the corresponding hexafluorophosphate salt, C$_{76}$F$_{12}$-H$_{76}$N$_{10}$O$_{12}$P$_2$Re$_2$·1.5CH2Cl2: C, 44.08; H, 3.78; N, 6.64. Found (%): C, 44.06; H, 3.80; N, 6.38.

3.8. References

1. J. Amoroso, R. J. Arthur, M. P. Coogan, J. B. Court,V. Fernández-Moreira, A. J. Hayes, D. Lloyd, C. Millet and S. J. A. Pope, *New J. Chem.*, 2008, **32**, 1097.
2. J. Amoroso, M. P. Coogan, J. E. Dunne, V. Fernández-Moreira, J. B. Hess, A. J. Hayes, D. Lloyd, C. Millet, S. J. A. Pope and C. Williams, *Chem. Commun*., 2007, 3066.
3. M. Rouhi, *A. Chem.* Soc., 2006, **83.**
4. M. Tetsuhashi, M.Ishikawa, Y. Hashimoto and H. Aoyama, *Bioinorganic & Medicinal Chemistry*., 2010, **18**, 5325.
5. X. Collin, J. M. Robert, G. Wielgosz, G. Le. Baut, C. Bobin-Dubigeon, B. Grimaud and J. Y. Petit, *J. Med. Chem*., 2001, **36**, 639.
6. J. C. Johnson Jr, R. S. Lowrey, M. C. Bowman, D. B. Leuck, E. W. Beck and J. C. Derbyshire, *J. Dairy Sci*., 1968, **51**, 1219.
7. P. H. Mazzocchi, F. Khachik and P. Wilson, *J. Am. Chem. Soc*., 1981, **103**, 6498.
8. M. S. Gibson and R. W. Bradshaw, *Angew. Chem*., 1968, **7**, 919.
9. F. A Carey, "Organic Chemistry", 4th ed., Chapter 22.
10. S. E. Sen and S. L. Roach, *Synthesis*., 1995, 756.
11. M. Hasegawa and K. Horie, *Prog. Polym. Sci*., 2001, **26**, 259.
12. D. Asthana, M. R. Ajayakumar, R. P. Pant and P. Mukhopadhyay, *Chem. Comm*., 2012, **48**, 6475.
13. W. C. Price, *Chem. Rev*., 1947, **41**, 257.
14. K. J. Watanabe, *Chem. Phys*., 1957, **26**, 542.
15. R. E. Merrifield and W. D. Phillips, *J. Am. Chem. Soc*., 1958, **80**, 2778.
16. H. Hasegawa and K. Horie, *Polym. Sci*., 2001, **26**, 259.
17. L. K. Kong and C. Y. Pan, *Polymer*., 2008, **49**, 5439.
18. R. Balasingham, M. P. Coogan and F. L. Thorp-Greenwood, *Dalton. Trans*., 2011, **40**, 11663.
19. H. Mishra, H. C. Joshi, H. B. Tripathi, S. Maheshwary, N. Sathyamurthy, M. Panda and J. Chandrasekhar, *J. Photochem & Photobiol. A. Chem*., 2001, **139**, 23.
20. G. J. Woolfe and P.J. Thistlewaite, *J. Am. Chem. Soc*., 1980, **102**, 6917.
21. W. R. Ware, P. R. Shukla, P. J. Sullivan and R. V. Bremplis, *J. Chem. Phys*., 1971, **55**, 4048.
22. S. G. Schulman and P. J. Kovi, *Anal. Chim. Acta*., 1973, **67**, 259.
23. G. J. Woolfe and P.J. Thistlewaite, *J. Am. Chem. Soc*., 1981, **103**, 3849.
24. K. Y. Law and J. Shoham, *J. Phys. Chem*., 1994, **98**. 3114.
25. J. Gergely, J. B. Morgan and L. E. Overman, *J. Org. Chem*., 2006, **71**, 9144.
26. J. Otera, "Esterification: Methods, Reactions and Applications"., 2006.
27. J. F. Norris and G. W. Rigny, *J. Am. Chem. Soc*., 1932, 54, 2088.
28. H. S. Rho, S. H. Oh, J. W. Lee, J. Chin and C. E. Song, *Chem. Commun*., 2008, 1208.
29. M. A. Wells and T. C. Bruice, *J. Am. Chem. Soc*., 1977, **99**, 5431.
30. T. H. Fife and T. J. Prystas, *J. Am. Chem. Soc*., 1983, **105**, 1638.
31. K. Deka, N. Barooah, R.J. Sarma and B. J. Baruah, *J. Mol. Struct*., 2007, **827**, 44.
32. (a) S. I. Kato, Y. Nonaka, T. Shinasaki, K. Goto and J. Shinmyozu, *J. Org.Chem*, 2008, **73**, 4063; (b) B. Balan and K. R. Gopidas, *Euro*. J. 2007, 5173.
33. J. B. Pawlet, "Ed.Handbook of Biological Confocal Microscopy"; Springer: New York, 2006.
34. V. Fernández-Moreira, F. L. Thorp-Greenwood and M. P. Coogan, *Chem. Commun*., 2010, **46**, 186.

Chapter 4. Luminescent Di-metallic Au(I) Complexes Bearing Functionalised Alkyl Chains Towards Therapeutic Applications.

4.1. Introduction

Therapeutics is an area of growing interest due to the rising resistance of diseases to known therapeutics such as chloroquinone and cisplatin (Figure 4.1). Cisplatin is a therapeutic agent inclusive of the metal platinum and has been used in the treatment of cancer for over 30 years, but due to the increase of cellular resistance cisplatin has become ineffective in its role as an antitumor agent. With this rise in resistance, the development of new compounds for effective use in the treatment of diseases is needed and so different types of metal-based compounds are now being studied. Through comparing IC_{50} values of a given complex to a standard, such as cisplatin ($IC_{50} = 2$ μM), the potential of a given complex for applications as a therapeutic agent can be assessed. IC_{50} values represent the concentration at which the 'agent' reduces cell survival to 50 % of the control value.[1] The design of metal-based therapeutics is a promising area in this field.

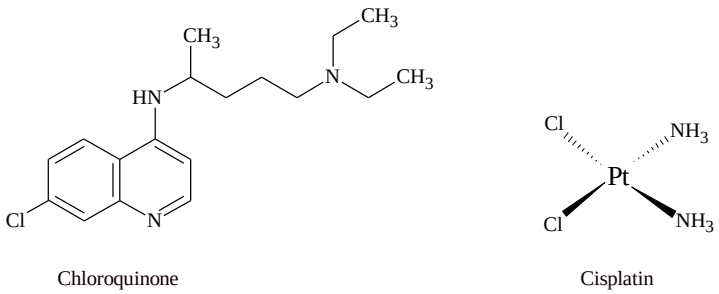

Chloroquinone Cisplatin

Figure 4.1 Structure of chloroquinone (LHS) and cisplatim (RHS).

Gold complexes tend to form aggregates through metal-metal interactions, these weak intra- and intermolecular interactions present between gold centres have attracted increasing interest since they were first reported by Schmidbaur *et al.* in 1988.[2] The rich photophysical properties associated with aurophilic interactions make Au(I) complexes an interesting class of luminescent materials. Additionally, the number of Au(I)-based complexes in therapeutics is increasing.

The design of gold complexes as therapeutic agents has primarily focused on gold analogues of cisplatin and/or the addition of Au(I) or Au (III) to known antitumor agents to form new compounds with enhanced activity.[3,4]There have been several cases where gold complexes have been synthesised for a specific role but have shown enhanced suitability for another. Herein, the synthesis of two different series of di-metallic Au(I) complexes are reported and their photophysical and potential therapeutic properties are discussed.

4.1.1. Aurophilic Interactions

Aurophilicity describes the intra- and intermolecular attractive forces between gold centres. Due to relativistic effects, the strength of these attractive forces are comparable to those of hydrogen bonding. Relativistic effects are caused by the presence of a heavy atom, in this case gold. As the charge on the gold increases (Au(0)→Au(I)) an acceleration in the average velocity of electrons is observed; the high speed electrons lead to an increase in the effective nuclear charge. Both s and p, the less diffuse orbitals contract, increasing the shielding effect, which leads to the expansion of the more diffuse orbitals, d and f. Au(I) has a filled 5d orbital thus exhibits the maximum impact of the relativistic effect.[5,6] Weak bonding interactions can be used to explain the interactions between Au(I) closed shell d^{10} metal centres of the same charge. Metal-metal interactions destabilise the filled $5d_z^2$ orbital. The filled 5d orbitals are stabilised by configuration mixing with the empty molecular orbitals of correct symmetry 6s and 6p orbitals. This lowers the energy difference between the filled d orbital and the empty s and p, leading to a more effective nuclear overlap and stronger metal-metal interactions. Thus these forces are deemed responsible for the structural and so photophysical properties of a complex. Aurophillic interactions are generally observed with a bond distance of 3 Å and a bond energy of 5-10 kcal mol^{-1}.[3]

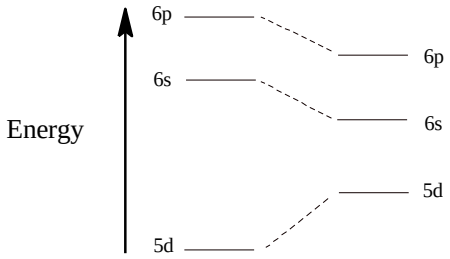

Figure 4.2 Energy-level diagram showing the effect of relativistic effect on the energy of atomic orbitals. [7]

The heavy metal effect (gold in this case) enhances spin orbit coupling which aids in the forbidden transition of singlet to triplet excited state *via* intersystem crossing, which often results in phosphorescence. Emission can arise from intra-ligand (IL), metal centred (MC), [5d(Au)→6p(Au)], and ligand-metal (LM) charge transfer transitions. LMCT can be modified by the presence of Au-Au interactions (intra- and intermolecular) which can lead to a ligand-metal-metal charge transfer (LMMCT) transition. It is not always possible to assign luminescence to one particular charge transfer process.[8] The following sections discuss how the distances vary for intra- and intermolecular molecular interactions and the outcome of these variations.

4.1.2. Au(I) co-ordination chemistry

The most common coordination geometry of Au(I) is a two coordinate, linear geometry (as a result of relativistic effects), however, trigonal planar and tetrahedral have also been reported.[3] Au(I) is a soft Lewis acid and thus prefers to bind to soft Lewis bases such as phosphines and thiolates, although examples of Au(I) bound to pyridines, alkynes and carbenes are also known.[8-13]

4.1.3. Au(I) phosphine co-ordination chemistry

Phosphines, PR_3, are tuneable ligands; they can be strong σ-donors with easily adjustable electronic and steric factors (they can be π-acids or π-bases depending on the R-substituent). Phosphines have a low charge and are highly polarizable, they tend to form stable complexes with low valent, electron rich metal ion's, for example gold.

The electronic and steric factors of phosphine's were determined by Tolman through the use of $Ni(CO)_3(PR_3)$ type complexes. Through the monitoring of the stretching frequency of CO (using infrared spectroscopy) the electronic properties of phosphines could be determined.[14] For example:

$$F_3P\text{-}M^{-}\text{-}C{\equiv}O^{+} > PH_3P\text{-}M{=}C{=}O > Cy_3\text{-}P\text{-}M^{+}{\equiv}C\text{-}O^{-}$$

The steric properties for PR_3 type ligands are determined using the Tolman cone angle, θ. The Tolman cone angle is the standard parameter used when discussing ligand size. The sterics for PR_3 are based on the R group and can be determined through the angle of the cone where the metal atom is situated on the apex, centred 2.28 Å from the centre of the P atom, which touches the van der Waals radii of the outermost atoms of the molecule. [14-16]

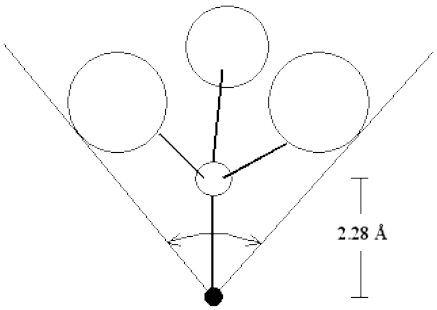

Figure 4.3 Tolman Cone Angle. Reproduced from ref. 14.

Au(I) phosphine chemistry has been well researched with examples of both, mono and bis-chelated phosphine Au(I) complexes and mono- and di-metallic Au(I) phosphine complexes displaying rich luminescent properties and potential as therapeutic agents.[17,18]

4.1.4. Au(I) phosphines in therapeutics

The cytotoxic activity of Au(I) and Au(III) phosphine based complexes was highlighted by Berners-Price *et al.*[11] with reports on auranofin, bis[1,2-bis (diphenyl-phosphino)ethane] gold(I) chloride and bis[1,2-bis(di-n-pyridylphosphino)ethane] gold(I) chloride (Figure 4.4). All three of the complexes were shown to exhibit antitumor activity in murine tumour models *in vivo*. In 2007 this group went on to provide evidence to suggest that the cytotoxic properties of complexes of this type are a result of mitochondrial interaction, more particularly, the triggering of cytochrome C that induces apoptosis. Although the exact mechanism for the triggering of apoptosis is un-known, the inhibition of selenocysteine residues of thioredoxin reductase (TrxR) is believed to be key. TRxR (found in the mitochondria) has been identified as the most relevant target for gold inhibitors.[19]

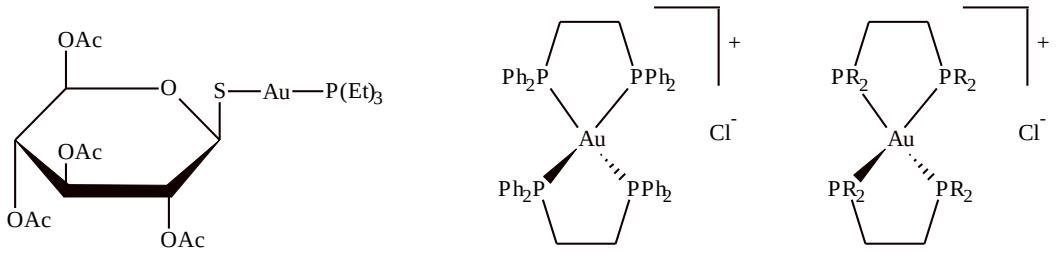

Figure 4.4 Au(I)-complexes 1-3. Auranofin (LHS), bis(1,2-bis(diphenylphosphino)ethane]gold(I)chloride (centre) and bis[1,2-bis(di-n-pyridylphosphino)ethane]gold(I)chloride (RHS); R = pyridine.[11]

Collaborative work between Berners-Price and McKeage[20] on complexes of the type $[Au(dppe)_2]^+$ showed the selectivity of a cytotoxic complex for cancer cells over healthy cells could be tuned by adjustments in the complexes liphophilic and hydrophilic properties. However, despite the complex $[Au(dppe)_2Cl]$ showing potential as an antitumor agent with increased cytotoxic activity against cisplatin resistant cell lines, the observation of hepatotoxicity *in vivo* means complexes of this type require further understanding before they can be of use as an antitumor agent in therapeutics.[8,19,20.]

The luminescent properties of complexes inclusive of Au(I) phosphines are generally dominated by metal perturbed ligand-based emission and/or aurophillic interactions (mainly in the solid state) examples of which are discussed both herein and in Chapter 5. Although intensely studied, we are a long way from realising the true potential of Au(I) phosphine chemistry with reports recently emerging 40 years after originally discussing the antitumor properties of Au(I). The potent reproducible cytotoxic properties of Au(I) phosphines have resulted in them being considered as one of the more promising candidates for therapeutics.[21,22]

4.1.5. Au(I) thiolates

Au(I) thiolates have been the main compounds used in chrysotherapy.[3,22] Since the first report in 1935 displaying the anti-inflammatory properties of Au(I) salts, Au(I) complexes have been well documented for the treatment of arthritis. Au(I) thiolates such as sodium aurothiomalate (Myocrisin) and aurothioglucose (Solganol), which are intramuscular injected, as well as auranofin (Ridaura) which is orally ingested, are the more commonly used Au(I) complexes for the treatment of rheumatoid arthritis (Figure 4.5), however, the exact anti-arthritic mechanism is un-known.[11] Auranofin, although commonly used in the treatment of arthritis, has also shown potential in the treatment of AIDS[23] and malaria[24] and thus research into applications of known therapeutics for the treatment of different diseases is also under investigation.

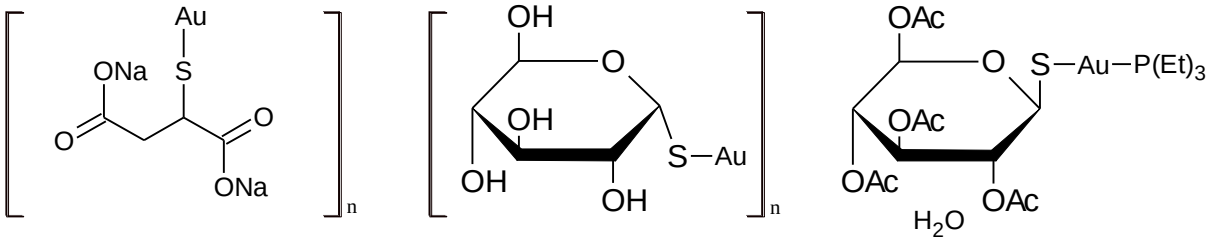

Figure 4.5 Au(I)-complexes 4-6, complexes commonly used in the treatment of arthritis. Sodium aurothiomalate (LHS), Aurothioglucose (centre) and Auranofin (RHS).

The dependency of the luminescent properties of Au(I) thiolate compounds on the Au-Au interactions can be exemplified by reports by Fackler *et al.*[24] and Eisenberg *et al.*[24b] Both groups reported the dependence of the luminescence properties of mono- and di-metallic Au(I) thiolate compounds on the intermolecular Au-Au interactions. Einsburg *et al.*[24b] reported the more interesting luminescent properties with the di-metallic Au(I) compound, $[Au_2\{S_2CN(C_5H_{11})_2\}_2]$.DMSO. Recrystallization of $[Au_2\{S_2CN(C_5H_{11})_2\}_2]$.DMSO produced orange crystals with a λ_{em} = 631 nm, however, when the crystals were dried *in vacuo*, colourless, non-emissive crystals resulted. The orange and the colourless compounds reported intramolecular Au-Au distances of 2.9617 Å and 2.7653 Å respectively, however, the intermolecular separation of the Au centres (for the orange and colourless compounds) were 2.7690 Å and 8.135 Å, respectively. This data suggests the orange colour and hence luminescence properties are dependent on the intermolecular distances more so than the intramolecular distances. Drying the orange compound removes any solvent present, and this in turn increases the Au-Au intermolecular distance suggesting an effect of the solvent on the Au-Au aggregate.

Interestingly, on/off aurophillic based luminescent properties dependent on ion sensing was displayed by Yam *et al.*[25] with a di-metallic-Au(I) phosphine thiolate complex. In absence of K^+ ions, the Au-Au distance was such that no aurophillic interactions were present. On binding of K^+ the two Au(I) centres were brought into closer proximity and a new, red-shifted emission peak at 720 nm was observed (Figure 4.6). The proximity of the two Au(I) centres resulted in LMMCT emission.[25]

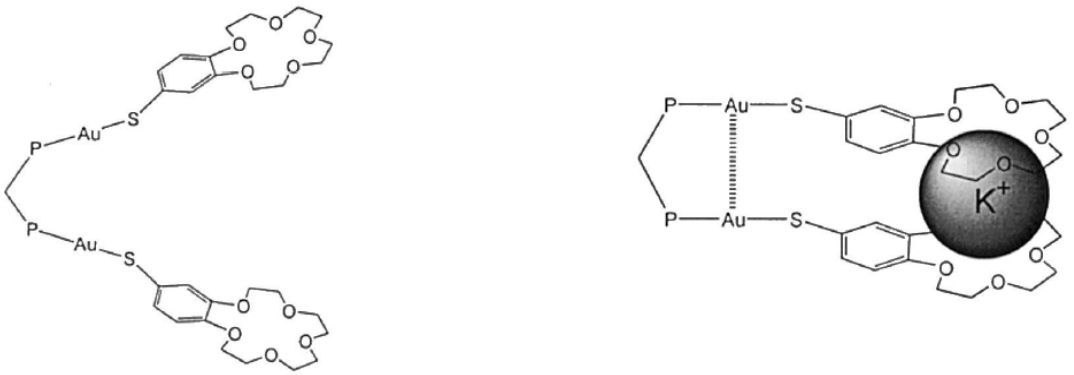

Figure 4.6 Complex 7 (LHS) with its ion sensing capability (RHS). Reproduced from ref. 25.

4.1.6. Au(I) alkynes in therapeutics and luminescence

Au(I) alkyne complexes display linear coordination geometry with the potential to form short Au-Au contacts.[3,27] Both mono and di-metallic alkyne complexes have been reported. The Au(I) centre can bind to two unsaturated alkyne units, one bound *via* a σ bond whereas the second is *via* a π bond. These two types of bonding, coupled with the potential of intermolecular aurophilic interactions between Au(I) centres, can lead to the formation of interesting Au(I)-alkynyl complexes.[4] There exists to date few examples of alkynyl gold complexes as therapeutics.

The synthesis of a novel series of mono-Au(I)-alkyne complexes was reported by Mohr *et al*.[27] (Figure 4.7). These complexes were synthesised primarily for investigation into their activity against malaria; low activity against the malaria parasite strains 3D7 (chloroquine sensitive) and KI (chloroqine resistant) was reported. Their low activity was attributed to the strength of the C-Au bond and the increased lipophilic nature of the complex (when compared to chloroquinone) which is suspected to hinder the complex reaching the target site.[27]

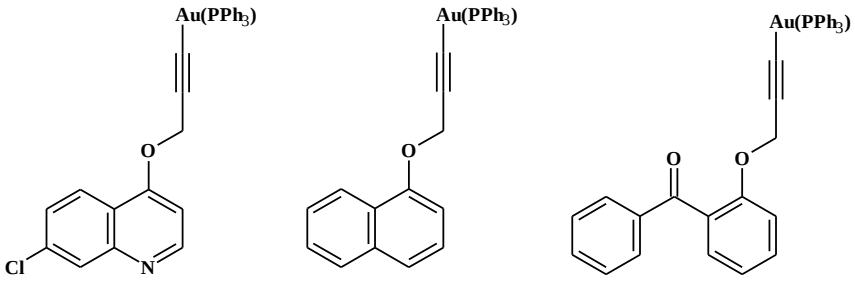

8 **9** **10**

Figure 4.7 Structure of complexes 8-10.

Although limited success against chloroquinone sensitive strains was observed, complexes 8-10 was tested against four tumour cell lines. The results show increased anti-cancer activity of complex 10 (in comparison to 8 and 9) with activity similar to that of cisplatin in ovarian and colon cancer cell lines (Table 4.1). Despite complex 10 showing enhanced activity, the similar nature of all three results suggest that the cytotoxic activity is governed/dominated by the [Au(PPh_3)-alkyne] moiety as oppose to the variable ligands attached.[27]

Table 4.1 In vitro cytotoxicity results[27]

Compound	CH1 ovarian cancer cell line	SW480 colon cancer cell line
10	0.4 ± 0.1	4.5 ± 0.7
Cisplatin	0.16 ± 0.03	3.5 ± 0.3

4.17. Au(I) pyridines

Despite pyridine ligands being considered as one of the more versatile ligands in co-ordination chemistry, there are very few reports of Au(I)-pyridine based complexes when compared to the previously mentioned Au(I)-thiolate or Au(I)-phosphine based complexes.[28,29] The stability of the Au(I)-N unit is dependent on the electronics and sterics of the complex formed.

Schmidbaur *et al.*[30] reported the first Au(I)-pyridine complexes with $[PPh_3Au\text{-pyridine}]^+$ and $[PPh_3Au\text{-2-hydroxypyridine}]^+$. The crystal structures of the two complexes provided evidence that suggested the incorporation of the hydroxyl group in the 2 position of the pyridine had no effect on the donating ability of the nitrogen; N-Au bond length was unchanged for the two complexes reported.[30]

The successful synthesis of six novel complexes incorporating planar aromatic pyridine N-Au(I) bonds in good yields, 49 % to 88 %, was reported by Pope *et al.*[13]. The nature of the fluorophore unit and its position on the pyridine, as well as the spacer length, were varied (Figure 4.8). The luminescent properties of the directly bound phthalimides reported a red-shifted emission which was attributed to increased conjugation within the ligands bound to the $-AuPPh_3$ unit; the lifetimes were short for all complexes reported.[13]

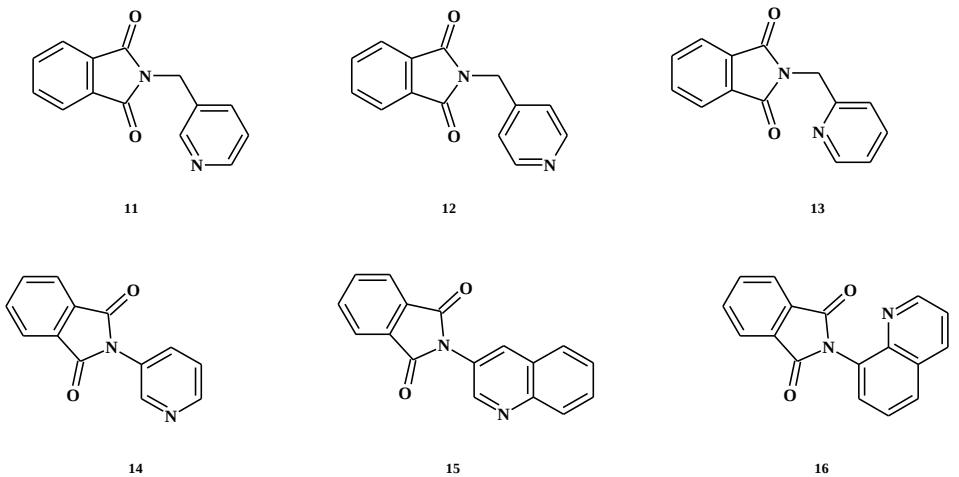

Figure 4.8 Ligands 11-16 reported by Pope *et al.*[13]

4.1.8. Au(I) azolates

An azolate is a 5-membered heterocyclic ring inclusive of a nitrogen, it is included herein due to similar nature of the Au(I)-N bond for pyridine. The cytotoxic analysis of nine novel (PPh_3 / TPA)-Au-(pyrazolates / imindazolates) type complexes was reported by Marzano *et al*.[31] Two out of the nine complexes reported (Figure 4.9) show potent cytotoxic activity with IC_{50} values exceeding those of cisplatin (Table 4.2). The triphenylphosphine based complexes showed increasing cytotoxic activity when compared to the TPA based complexes. With the Trx having been reported as the most relevant molecular target for gold complexes (previously discussed in reports by Berners-Price *et al*.),[19,20] the inhibitor activity of these compounds, compounds 17 and 18 were investigated for TrxR1 and TrxR2 forms of Trx. Compounds 17 and 18 displayed increasing inhibitor potential in TrxR1 in comparison to TrxR2 (Table 4.2). TrxR inhibition was then evaluated in 2008 with complexes 17 and 18 which showed a decrease in cellular activity of TrxR by 85 %.[6,31]

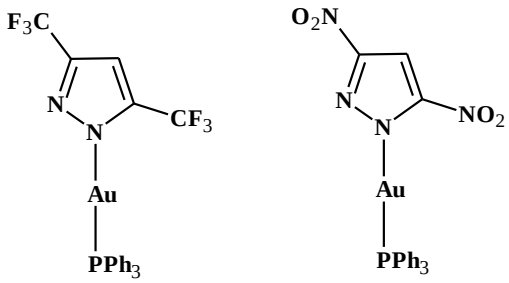

17 18

Figure 4.9 Complex 17 (LHS) and 18 (RHS), both exhibit cytotoxic values > cisplatin[31]

Table 4.2 In vitro cytotoxicity results for complex 17 and 18 for TrxR1/R2, MCF-7, A549 and LoVo cell lines.

Compound	MCF-7	A549	LoVo	TrxR1	TrxR2
17	1.03 ± 0.59	0.96 ± 0.34	0.90 ± 0.52	3.50	38.12
18	0.53 ± 0.35	0.49 ± 0.21	0.73 ± 0.30	15.80	48.12
Cisplatin	10.31 ± 1.36	13.42 ± 1.96	8.03 ± 1.23	-	-

4.2. Overview

The first part of this chapter discusses the attempts to synthesise a series of di-metallic Au(I)-pyridyl complexes, $\{[Au(PPh_3)]_2L\}^{2+}$, with varying aliphatic chain lengths. The synthesis and photophysical properties of the structurally related di-metallic Re(I)-based complexes have been reported in Chapter 3. The second half of this chapter reports a novel series of di-metallic Au(I)-alkyne complexes, based around a malonate centre, inclusive of both aliphatics and/or aromatics. The synthesis, photophysical properties and the application of these complexes as therapeutic agents is discussed herein.

4.3. Results and discussion (part 1)

4.3.1. Syntheses of L^{1-3}

The synthesis of symmetrical ligands suitable for the co-ordination of two metal ions was initially discussed in Chapter 3. Continuing with the same ligand system, three symmetrical pyridyl based ligands with varying aliphatic chain lengths were synthesised for the co-ordination of two gold units. The symmetrical esters, $\mathbf{L^{1-3}}$, varying in chain lengths $C_2/C_6/C_{12}$ respectively, were synthesised using an excess of commercially available nicotinic acid which was converted to the derived nicotinoyl chloride by stirring at 70 ˚C in thionyl chloride for 1 hour. Nicotinoyl chloride was then reacted with either commercially available 1,12-dodecandiol, 1,6 hexanol or ethylene glycol. The observation of a shift to higher frequency for the signal corresponding to the ester methylene unit C*H*$_2$OCO in the ^{1}H NMR spectrum from +3.35 ppm to +4.5 ppm confirmed the formation of the ester units, which were achieved in good yields of 68 %, 78 % and 46 % respectively.

4.3.2. Syntheses of $\{[Au(PPh_3)]_2L^{1-3}\}^{2+}$

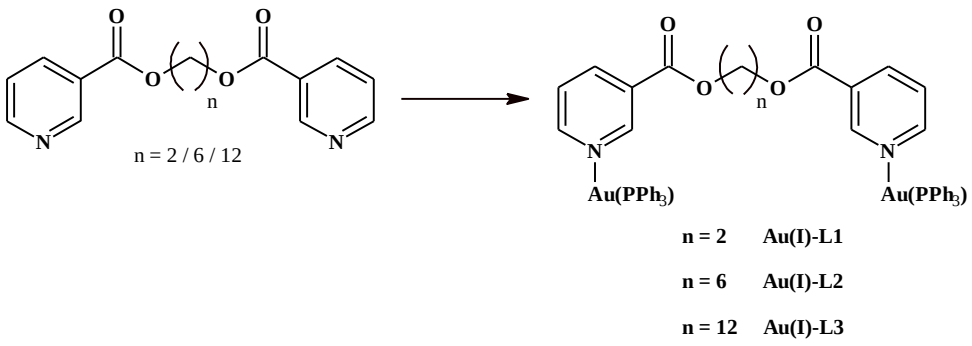

Figure 4.10 Synthesis of $[Au(PPh_3)L^{1-3}]$. Reagents: AgOTf, $[AuClPPh_3]$, DCM, N_2(g)

Having achieved the synthesis of $\mathbf{L^{1-3}}$ in good yields the synthesis of $\{[Au(PPh_3)]_2L^{1-3}\}^{2+}$ was attempted. $[AuClPPh_3]$ was chosen as the gold precursor complex as work within the group had shown successful bonding of the gold unit to the pyridine nitrogen.[13] The synthesis of the gold complexes was carried out using literature precedent. In the absence of light, due to the sensitive nature of the gold precursor, at 0 ˚C, $[AuClPPh_3]$ and silver triflate were stirred in DCM for 20 minutes. Silver triflate was necessary to remove the chloride ion. Following the addition of the symmetrical ligand, $\mathbf{L^{1-3}}$, (0.5 eq) the reaction was left to reach room temperature and was stirred for an additional 16 hours. After the removal AgCl *via* filtration, the product was purified *via* re-precipitation using diethyl ether. Principal

characterisation using ^{1}H and ^{31}P NMR spectroscopies suggested the presence of the predicted products, however there was also the presence of $[Au(PPh_3)_2](OTf)$ (δ_{31P} = +45 ppm) and or the presence of the gold starting material.

Recrystallizations were carried in an attempt to obtain pure products of all three products, $\{[Au(PPh_3)]_2L^{1\text{-}3}\}^{2+}$. Crystals suitable for XRD were obtained for all three reactions however the recrystallized products were not consistent with the proposed products. For both $\{[Au(PPh_3)]_2L^{1}\}^{2+}$ and $\{[Au(PPh_3)]_2L^{2}\}^{2+}$ an unexpected gold trimer cluster biproduct (Figure 4.11) resulted from the recrystallisations. This biproduct was formed as a result, presumably, of ligand dissociation. Structures of this nature have been previously reported[32-34] and so no further data was collected. The driving forces for the formation of these clusters have not been investigated and so are not fully understood.

For $\{[Au(PPh_3)]_2L^{1}\}^{2+}$, the expected product was observed as a linear C_{12} alkyl, di-pyridyl-Au(I) complex. There was no evidence of intra- or intermolecular Au-Au aurophillic interactions in the solid state IR of this complexl. The absence of these interactions can be attributed to the linearity and the sterics of the bulky substituents of the complex. The co-ordination of the gold unit was linear with the N-Au-P bond angle of 177 ˚, the Au-N and Au-P bond distances of 2.069 Å and 2.25 Å are in accordance with related compounds.[11] The presence of crystalline starting material, $[AuClPPh_3]$, within the sample (which was not present in the initial characterisation *via* ^{31}P NMR spectroscopy) indicated that decomposition of the product in solution had occured, this resulted in incomplete characterisation. These findings are reported further in the following section.

4.3.3. Single crystal X-ray diffraction studies

Re-crystallisation of complexes $\{[Au(PPh_3)]_2L^{1\text{-}3}\}^{2+}$ yielded pale orange crystals suitable for X-ray diffraction studies. The crystals were obtained *via* vapour diffusion of diethyl ether into a concentrated THF solution (Figure 4.11).

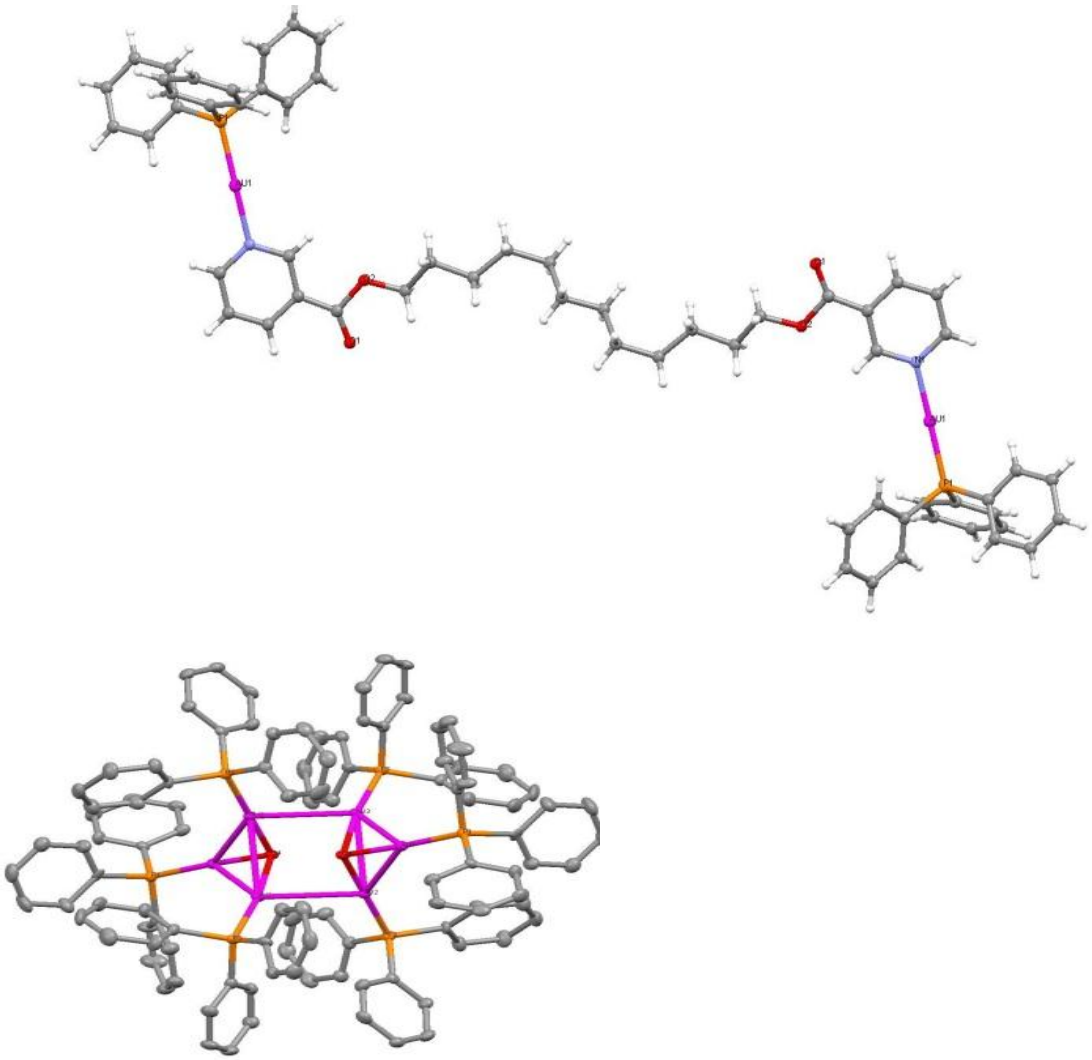

Figure 4.11 Structural representations of the bi-product of $\{[Au(PPh_3)]_2L^1$ and $L^2\}^{2+}$ (bottom) and $\{[Au(PPh_3)]_2L^3\}^{2+}$ (top) (H atoms omitted for clarity).

The parameters associated with the data collections of the novel complex $\{[Au(PPh_3)]_2L^3\}^{2+}$ and the gold trimer cluster biproduct (Table 4.3) and the selected bond lengths and bond angles (Table 4.4) are shown below.

Table 4.3 Crystal data collection and refinement details for the crystal structures of $\{[Au(PPh_3)]_2L^3\}^{2+}$ and the gold trimer cluster biproduct.

	$\{[Au(PPh_3)]_2L^3\}^{2+}$	Cluster
Empirical formula	$C_{62}H_{62}Au_2F_6N_2O_{10}P_2S_2$	$C_{56}H_{47}Au_3Cl_2F_3O_4P_3S$
Formula weight	1629.13	1627.71
Temperature	293 K	150 K
Wavelength	0.71013Å	0.71013Å
Crystal system	Monocyclic	Triclinic
Space group	P2(1)/n	P-1(2)
Unit cell dimensions	a = 12.0014 (15) Å	a = 12.7242 (2) Å
	α = 90.00 ˚	α = 63.8380 (10) ˚
	b = 27.888 (4) Å	b = 14.5427 (2) Å
	β = 104.048˚	β = 81.6950 (10)˚
	c = 19.133 (2)	c = 16.2111 (3) Å
	ϒ =90.00˚	ϒ =89.6090 (10)˚
Volume	6212.2 $Å^3$	2658.75 $Å^3$
Z	4	2
Density (calculated)	1.742 g/cm^3	2.033 g/cm^3
F(000)	3208	1548
Crystal size	0.10 × 0.04 × 0.04	0.12 × 0.10 × 0.10
Theta range for data collection	38	55
All reflections	9107	17979
Independent reflections	4906	12118
Observed reflections	3666	10074
Goodness-of-fit-on F	1.353	1.033
R_{int}	0.0864	0.0367
Final R indices [I>2sigma(I)]	R_1 = 0.1565	R_1 = 0.0453
	wR_2 = 0.3030	wR_2 = 0.1065
R indices (all data)		

Table 4.4 Selected bond lengths and bond angles for the complexes: $\{[Au(PPh_3)]_2L^3\}^{2+}$ and the gold trimer cluster biproduct.

$\{[Au(PPh_3)]_2L^3\}^{2+}$		Cluster	
$C_{62}H_{62}Au_2F_6N_2O_{10}P_2S_2$		$C_{56}H_{47}Au_3Cl_2F_3O_4P_3S$	
Bond Lengths (Å)			
Au-N	2.069 (3)	Au1-Au2	3.184 (3)
Au-P	2.25 (1)	Au1-Au3	2.967 (4)

The labile nature of Au(I)-pyridyls can be rationalised in terms of the donating properties of the pyridine unit. Pyridine is a 'borderline' soft donor and therefore is less well matched to the soft Au(I) ion than sulfur or phosphine donors. This mismatch, coupled with the electron-withdrawing ester functional group reducing the donor ability of the pyridine, decreases the stability of the complex; the donating ability of the pyridyl nitrogen is reduced and the Au(I)-N bond becomes increasing labile. The most stable Au(I) complexes are seen when 'softer' donors such as thiolates, phosphines or even alkynes are used.[35,36] A new di-metallic Au(I) complex series based around Au(I) alkynes was synthesised to further probe the potential of Au(I) complexes as both therapeutic and cellular imaging agents. Additionally, the effect of aurophilic interactions on the luminescent properties of Au(I) are explored.

4.4. Results and discussion (part 2)

4.4.1. Ligand Design

Having shown the labile nature of the Au(I)-N unit, an alternative approach to the synthesis of di-metallic Au(I) complexes for investigation into their photophysical and therapeutic properties was made. There have been an increasing number of reports on the syntheses of Au(I)-alkyne units and for this reason these units were investigated. Several commercially available functionalised alkynes exist, including propargyl alcohol and propargyl bromide, both of which are equipped to act as 'building blocks' providing additional functionality to the compound.

4.4.1.1.Malonates

Malonate is a commercially available compound. It is also a known competitive inhibitor of the enzyme succinate dehydrogenase; an enzyme that is bound to the inner mitochondrial membrane. The incorporation of a malonate unit within a di-metallic Au(I) alkyne complex allows additional functionality within the compound and also offers the potential to allow cellular functions to be monitored *via* imaging.

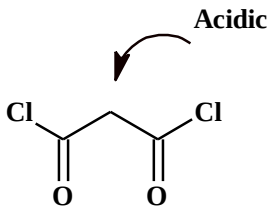

Figure 4.12 Malonyl chloride

Malonyl chloride is an organic compound with an acidic α carbon. This carbon provides a second, alternative route for the addition of functionality to the compound. A reaction of the acyl unit of the compound with propargyl alcohols allows the addition of two alkyne units suitable for the co-ordination of gold units, the presence of the acidic α carbon allows the synthesis of more complicated ligand systems, for example, the addition of an aromatic group.

4.4.2 Ligand synthesis

4.4.2.1.Synthesis of L^4

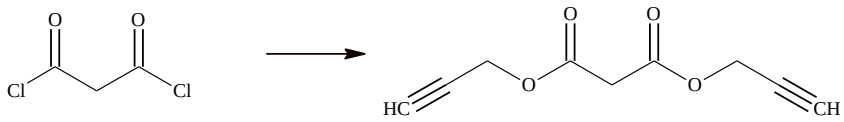

Figure 4.13 Synthesis of L^4(RHS). Reagents: propargyl chloride, TEA and DCM.

The addition of two alkyne units to a malonyl chloride precursor resulted in the formation of **L^4** (Figure 4.13). **L^4** was synthesised *via* the drop-wise addition of malonyl choride to a solution of propargyl alcohol and TEA in DCM. After stirring at room temperature for 15 minutes, following an aqueous work up, **L^4** was produced in a moderate yield 41 %. The acidic nature of the central CH_2 in **L^4** was a suggested route to further functionalise the compound whilst keeping the alkynes 'intact' for the co-ordination of two Au(I) units. The 'removal' of the acidic proton on **L^4**, using a base, produces a carbanion suitable to undergo nucleophilc substitution with an alkyl halide. The presence of excess base in this reaction can lead to both mono- and di-substitution reactions taking place. The addition of a di-halide species can lead to the synthesis of an alicyclic compound.

4.4.2.2. Synthesis of L^{5-6}

To further functionalise **L^4**, it was reacted with benzaldehyde following literature precedent using ammonium acetate[37] and/or potassium tertiary butoxide[38] however, in both cases no reaction was evident with only starting material observed in the ^{1}H NMR spectra. An alternative base is proline; proline is a zwitterionic, α amino acid (Figure 4.14). The lack of a proton on the amide group means it cannot act as a proton donor, only as a hydrogen bond acceptor, thus can be used as a base for the removal of the acidic proton.

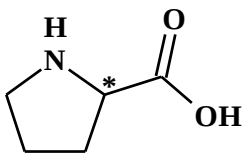

Figure 4.14 Proline

L^{4} was reacted with both benzaldehyde and anisaldehyde in the presence of proline in DMSO at room temperature for 24 hours to produce **L**^{5} and **L**^{6} in low to moderate yields of 21 % and 33 % respectively (Figure 4.15). Nitro-benzaldehyde was also reacted with **L**^{4} following the same procedure, however, only starting material was recovered.

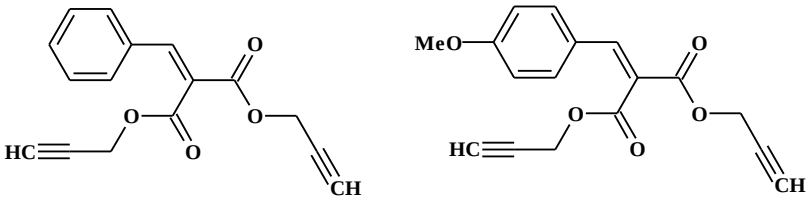

Figure 4.15 L^{5} **(LHS) and L**^{6} **(RHS),**

The unsuccessful formation of a ligand inclusive of nitro-benzaldehyde resulted in an alternative synthetic route being attempted. Benzaldehyde was reacted with malonoic acid (as opposed to **L**^{4}), following the same reaction conditions as above, to form ligand precursor 2 with a very low yield of 3.5 %. For the synthesis of compounds of this type, the nature of the substituent in the para position of the benzaldehyde was shown to dictate the reaction yield / outcome; EDG > H > EWG. The limited reactivity of **L**^{4} resulted in an alternative synthetic approach being taken where the alkyne units were situated on the acidic CH_2 and the compounds further functionalised *via* the terminal positions of the malonate.

4.4.2.3. Synthesis of L$^{7\text{-}15}$

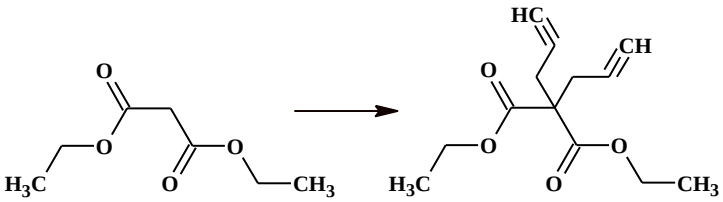

Figure 4.16 Synthesis of L^{7}**. Reagents: propargyl bromide, potassium tertiary butoxide, ethanol.**

Diethyl malonate (DEM) is the most common malonic ester. Following literature precedent propargyl bromide was added to a solution of diethyl malonate and potassium tertiary butoxide in ethanol, to form **L**^{7} with an 82 % yield (Figure 4.16).[39] Continuing with the same reaction conditions used for both **L**^{4} and **L**^{7}, a novel series of alkyne based ligands with varying aliphatic chain lengths and aromatic substituents were synthesised; **L**^{8}**-L**^{15} precursors were synthesised following the same procedure as **L**^{4} using ethyl malonyl chloride or malonyl chloride resulting in yields ranging from 12 % to 78 %. The addition of the

alkynes to the ligand precursors *via* nucleophilic substitution reactions (following the same procedure used for $\mathbf{L^4}$) resulted in the formation of $\mathbf{L^8}$-$\mathbf{L^{15}}$ in yields ranging from 5 % to 59 %.

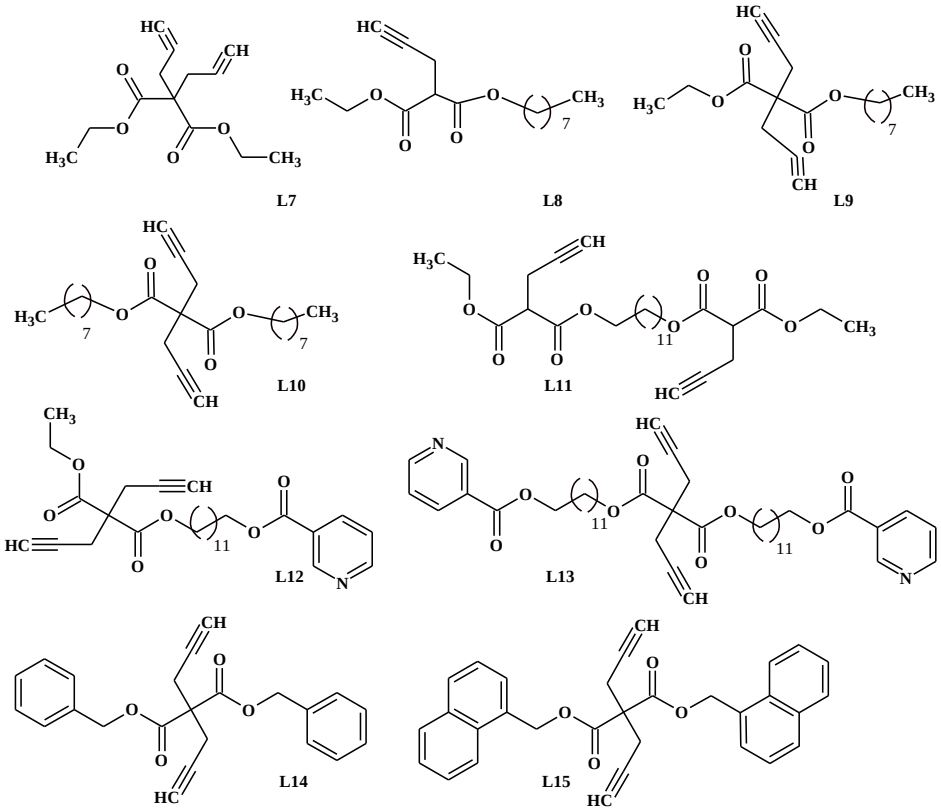

Figure 4.17 Ligands L^7-L^{15} discussed herein.

4.4.2.4.Synthesis of $L^{8\text{-}10}$

Ligand precursors of $\mathbf{L^9}$ and $\mathbf{L^{10}}$ were formed from the addition of octanol to the unsymmetrical starting material ethyl malanoate and the symmetrical starting material malonate respectively and purified *via* distillation with a Kugelrohr apparatus (removing excess butanol). The shift in the ^{1}H NMR spectra of the octanol CH_2OH to the higher frequencies of +4.01ppm or +4.18 ppm was attributed to product formation in ligand precursors $\mathbf{L^9}$ and $\mathbf{L^{10}}$ respectively. The addition of the alkyne units was achieved using propargyl bromide. Purification of $\mathbf{L^9}$ *via* chromatography isolated both unsymmetrical mono- and di-alkyne ligands, $\mathbf{L^8}$ and $\mathbf{L^9}$ respectively. For $\mathbf{L^9}$, the absence of the peak at +3.32 ppm (acidic CH_2 in the ligand precursor) and the appearance of two new peaks, a triplet at +2.08 ppm and a doublet at +2.98 ppm in the ^{1}H NMR spectrum, both with intensities fitting the addition of two alkyne units, confirmed its formation. In the ^{1}HNMR spectrum of $\mathbf{L^8}$, a multiplet peak at +2.72 ppm, at lower frequency when compared to that of the CH_2 peak in the ligand precursor was observed as-well as peaks similar in frequency to those of the di-alkyne

L[9]. MS analyses confirmed the addition of one alkyne unit only for **L**[8]. The symmetrical, di-alkyne ligand, **L**[10] was formed in a 59 % yield with peaks in the ^{1}H NMR spectrum similar in nature to the unsymmetrical di-alkyne ligand, **L**[9]. No bi-products were isolated.

4.4.2.5. Synthesis of L[11-13]

Ligand precursor **A** was documented in both Chapters 2 and 3 and consists of a pyridine-spacer-OH. When reacted with ethyl malonyl chloride, following the same procedure as **L**[7] and purification *via* column chromatography, the ligand precursor **L**[12] was formed in a good yield of 69 %. The number of signals in the ^{1}H NMR spectrum and their intensities fit well for the predicted product, characterization by MS (ES^+) showed the presence of $[M+H]^+$ at 422.25, $[M+Na]^+$ at 444.23 and $[M+K]^+$ at 460.21. Despite the high yielding nature of its ligand precursor, **L**[12] was formed in a very low yield; following purification of **L**[12] *via* column chromatography isolated both **L**[7] , **L**[12] and bi-product **L**[11] (Figure 4.18). The bi-product **L**[11] was fully characterized and similarly to the bi-product, **L**[8], in the ^{1}H NMR spectrum, a multiplet peak at +2.72 ppm was observed.

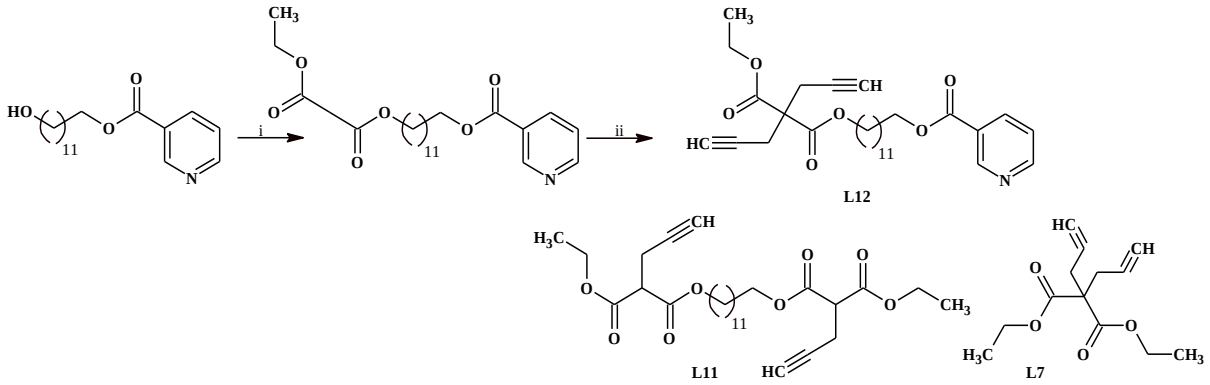

Figure 4.18 Synthesis of ligand L[12] with bi-products L[11] and L[7]. Reagents: (i) ligand precursor A, ethyl malonoate, TEA, DCM, RT; (ii) Propargyl bromide, K^+ ^{t}BuO, EtOH, N_2(g).

The isolation of the two bi-products, **L**[8] and **L**[11], indicated the breakdown of the ligand precursor and/or **L**[12] during their reactions. Intra- or intermolecular breakdown of ligand precursor A has not been seen previous chapters, but it is possible that with the additional ester groups present on the ligand precursor, and in the presence of potassium tertiary butoxide, intra- or intermolecular breakdown of the product was promoted. The low yield of the unsymmetrical, di-alkyne pyridine ligand, **L**[12], resulted in the synthesis of the analogous

symmetrical di-alkyne pyridine $\mathbf{L^{13}}$ in a more favorable yield of 37 % (Figure 4.19). $\mathbf{L^{13}}$ was again purified *via* column chromatography with no isolation of bi-products.

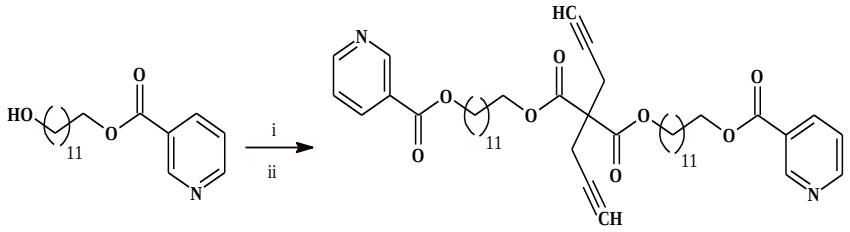

Figure 4.19 Synthesis of ligand L^{13}. Reagents: (i) ligand precursor A, malonyl chloride, TEA, DCM, RT; (ii) propargyl bromide, K^tBuO, EtOH, N_2(g).

4.4.2.6. Synthesis of L^{14-15}

Having synthesized a series of di-alkyne ligands with varying aliphatic chained ligands, aromatic di-alkyne ligands were synthesized to add additional functionality to ligands of this type. Benzyl-alcohol and naphthyl alcohol were reacted with malonyl chloride and then propargyl bromide following the same procedures as above to produce $\mathbf{L^{14}}$ and $\mathbf{L^{15}}$ in yields of 37 % and 16 % respectively (Figure 4.20).

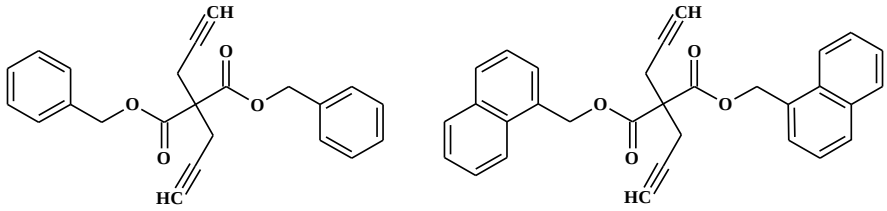

Figure 4.20 L^{14} (LHS) and L^{15} (RHS).

4.4.3. Complex synthesis

The gold precursor [AuClPPh$_3$] was synthesised *via* literature methodology from H[AuCl$_4$], as this is known to be useful in the synthesis of gold alkynes.[40] Omitting the bi-products formed during the ligand synthesis, the di-alkyne ligands, **L^7**, **L^{9,10}** and **L$^{12\text{-}15}$** , were reacted with [AuClPPh$_3$] (1.2 eq of gold per alkyne present in ligand) in the absence of light under a N_2 atmosphere and in the presence of potassium tertiary butoxide in ethanol. The reaction mixture was left to stir at room temperature for 16 hours. Due to the production of potassium chloride salt; the filtrate was dried under reduced pressure, re-dissolved in chloroform and filtered. The work up was slightly modified in the cases where precipitate was visible in the reaction mixture; the precipitate was filtered, dissolved in DCM and re-filtered to remove the salt. Each complex was purified by recrystallization using vapour diffusion of diethyl ether into a concentrated THF solution. The use of THF proved necessary as prolonged exposure to chlorinated solvents resulted in the breakdown of complexes to the Au(I)- starting material [AuClPPh$_3$]. The complexes, {[Au(PPh$_3$)]$_2$L^7}, {[Au(PPh$_3$)]$_2$L^9}, {[Au(PPh$_3$)]$_2$L^{10}}, {[Au(PPh$_3$)]$_2$L^{15}}, were isolated in yields ranging from 57 % to 87 %.

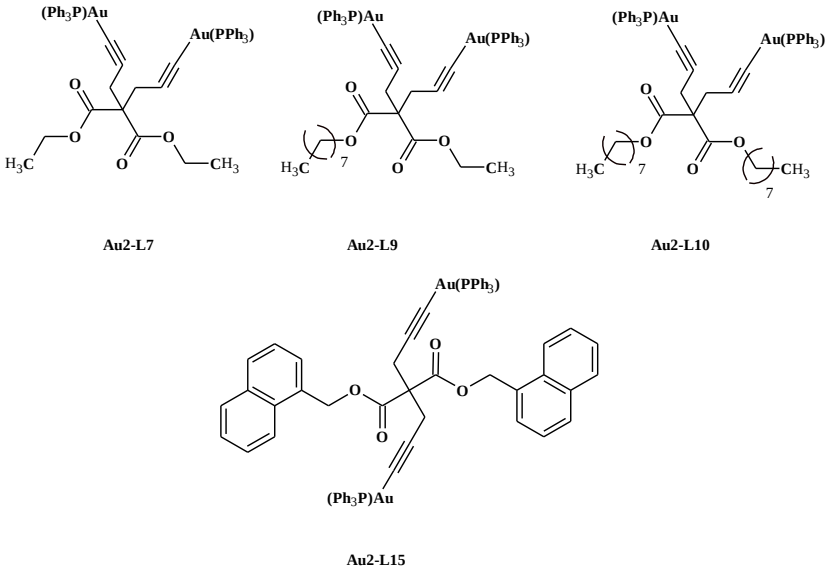

Figure 4.21 Complexes discussed herein.

^{1}H NMR spectra for all complexes were obtained in CDCl$_3$. For each complex there was an absence of the $CH_2CC\mathit{H}$ peak seen in the free ligand and a characteristic shift of the H_2CC- to higher frequency from around +2.92 ppm in the free ligand to around +3.21 ppm in the complexes. The addition of the phenyl ligands was also apparent in all four NMR spectra. For the aliphatic based, di-alkyne Au(I)$_2$ complexes, {[Au(PPh$_3$)]$_2$L^7}, {[Au(PPh$_3$)]$_2$L^9},

{[Au(PPh_3)]$_2$L^{10}}, a broad proton resonance in the region of 7.21-7.62 ppm integrating to 30H for the triphenyl phosphine proton resonances was observed. For the aromatic based, di-alkyne Au(I)$_2$ complex, {[Au(PPh_3)]$_2$L^{15}}, the triphenyl phosphine proton resonances were typically broad and super imposed with co-ordinated ligand aromatic protons in the region of 7.22-7.52 ppm.

The ^{31}P{^{1}H} NMR spectra for complexes{[Au(PPh_3)]$_2$L$^{7/9/10/15}$} gave a signal in a range with agreement to literature around +42.8 ppm. All of the complexes gave a single peak in the ^{31}P NMR which indicated the di-metallic complexes were symmetrical. Solid state IR studies were carried out for all complexes which showed subtle changes in the ν(CC) in comparison to ligand. The ligands displayed an IR stretch similar to the precursors, propargyl alcohol and propargyl bromide with a shift at 2120 cm^{-1} whereas the complexes displayed a weaker IR absorption band ranging from 2168-2329 cm^{-1} for the alkyl stretch; for the aliphatic, di-alkyne Au(I)$_2$ complexes the lower stretching frequency was observed. This slight shift to a higher frequency for the aromatic, di-Alkyne Au(I)$_2$ complex, {[Au(PPh_3)]$_2$L^{15}}, corresponds to a stronger CC bond. MS analysis for each of the complexes gave a peak at 721 only which is attributed to the breakdown of the complex within the mass spectrometer and then recombination to form [Au(PPh_3)$_2$]$^+$.

The synthesis of {[Au(PPh_3)]$_2$L$^{12-14}$} was attempted, but in all three cases, despite evidence in the ^{1}H NMR and ^{31}P NMR spectra to support product formation, when purification *via* recrystallization was attempted breakdown of the product was observed; starting materials were observed in both ^{1}H NMR and ^{31}P NMR spectra following recrystallization.

4.4.3.1. Single crystal X-ray diffraction studies

Re-crystallisation of complexes {[Au(PPh_3)]$_2$$L^7$}, {[Au($PPh_3$)]$_2$$L^9$} and {[Au($PPh_3$)]$_2$$L^{15}$} yielded pale crystals suitable for X-ray diffraction studies. The crystals were obtained *via* vapour diffusion of diethyl ether into a concentrated THF solution.

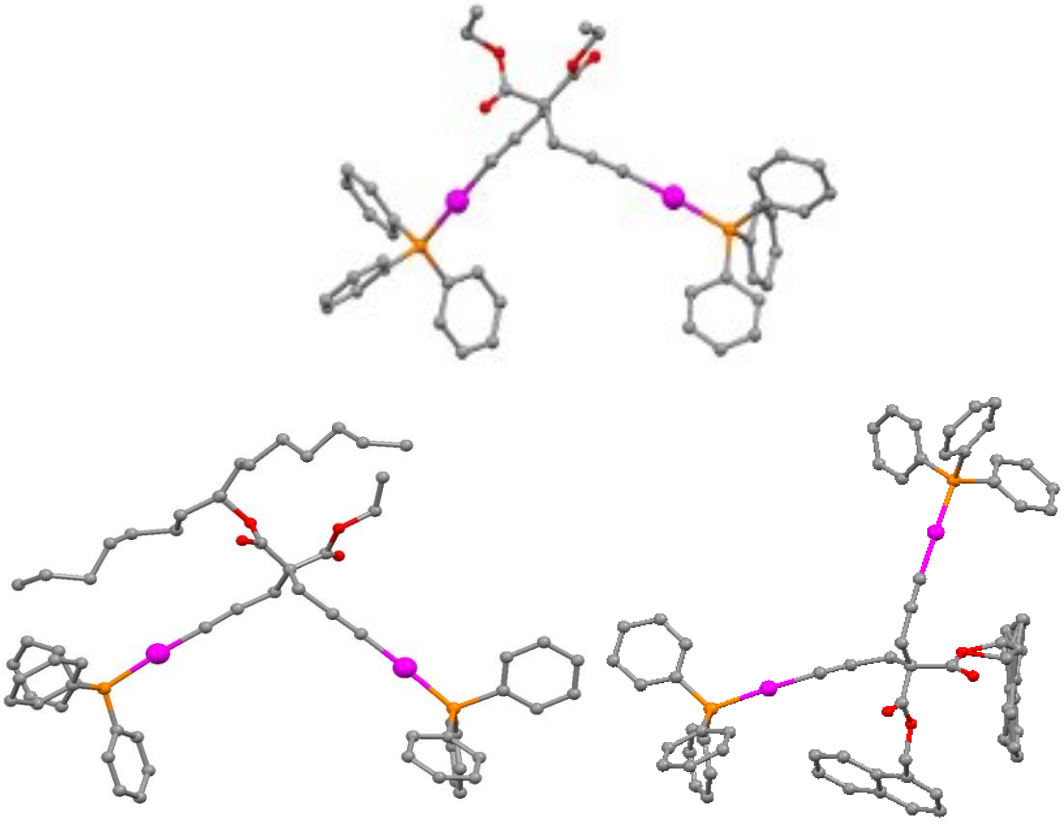

Figure 4.22 Structural representations of complexes {[Au(PPh_3)]$_2$$L^7$}, {[Au($PPh_3$)]$_2$$L^9$} and {[Au($PPh_3$)]$_2$$L^{15}$}, (H atoms omitted for clarity).

The parameters associated with the data collection of the novel complexes {[Au(PPh_3)]$_2$$L^7$}, {[Au(P Ph$_3$)]$_2$$L^9$} and {[Au($PPh_3$)]$_2$$L^{15}$}, (Table 4.5) and the selected bond lengths and bond angles (Table 4.6) are shown below.

For the diethyl malonate based di-alkyne Au(I)$_2$ structure of {[Au(PPh_3)]$_2$$L^7$}, the C-Au-P bond angle did not show substantial deviations from linearity, 176 °. The Au-P bond lengths have an average length of 2.28 Å and the Au-C bond lengths, 2.00 Å, which are both consistent with other gold(I)-acetylide complexes reported, additionally, both bond lengths are longer than those of the [AuClPPh_3] starting material, consistent with the stronger *trans* influence of the acetylene group when compared to the chloride.[41-43] The C≡C bond lengths in the complex have an average length of 1.19 Å, and are again normal for complexes of this

type. There was no evidence of intra- or intermolecular contacts between the Au(I) units. Similarly to the {[Au(PPh_3)]$_2$$L^7$}, both the unsymmetrical and symmetrical di-alkyne Au(I)$_2$ structures of {[Au(PPh_3)]$_2$$L^9$} and of {[Au($PPh_3$)]$_2$$L^{15}$}, respectively, showed no deviation from the expected literature values for gold(I)-acteylide complexes and again no intra- or intermolecular contacts between the Au(I) units were observed.[18,44] Both complexes however did display dis-ordered structures; for {[Au(PPh_3)]$_2$$L^9$} disorder was modelled with in the C_7 alkyl chain; for {[Au(PPh_3)]$_2$$L^{15}$} disorder modelled in one napthyl ring (C10 to C19). All atoms refined as split over two sites with occupancies refined to 0.60(2) and 0.40(2) for the two components.

Table 4.5 Crystal data collection and refinement details for the crystal structures of {[Au(PPh_3)]$_2$$L^7$} and {[Au($PPh_3$)]$_2$$L^9$} and {[Au($PPh_3$)]$_2$$L^{15}$}.

	{[Au(PPh)$_3$]$_2$$L^7$}	**{[Au(PPh)$_3$]$_2$$L^9$}**	**{[Au(PPh$_3$)]$_2$$L^{15}$}**
Empirical formula	$C_{49}H_{44}Au_2O_4P_2$	$C_{55}H_{56}Au_2O_4P_2$	$C_{67}H_{52}Au_2O_4P_2$
Formula weight	1152.71	1236.87	1376.96
Temperature	150(2)K	293(2)K	120(2)K
Wavelength	0.71013Å	0.71013Å	0.71013Å
Crystal system	Monoclinic	Monoclinic	Triclinic
Space group	P2(1)/*a*	P2(1)/*a*	P-1
Unit cell dimensions	a = 18.3922 (7) Å α = 90.00 ˚ b = 12.7687 (4) Å β = 112.362˚ c = 22.6554 (8) ϒ =90.00˚	a = 18.6917 (16) Å α = 90.00 ˚ b = 12.9506 (13) Å β = 110.571˚ c = 22.7648 (12) ϒ =90.00˚	a = 13.2177 (12) Å α = 72.055 ˚ b = 13.2371 (11) Å β = 77.650 ˚ c = 17.0686 (18) ϒ =83.635 ˚
Volume	4920.39 (3) Å^3	5159.23 () Å^3	2772.1 (4) Å^3
Z	4	4	2
Density (calculated) F(000)	1.556 g/cm^3	1.592 g/cm^3	1.650 Mg/m^3
Crystal size	0.40 × 0.28 × 0.122	0.25 × 0.15 × 0.02	0.53 × 0.34 × 0.02
Theta range for data collection			3.11 – 27.46 °
All reflections	14715	9411	29975
Independent reflections	8086	5271	11299
Observed reflections	5461	2885	
Goodness-of-fit on F	1.035	1.394	0.975
R_{int}	0.067	0.1260	0.1704
Final R indices [I>2sigma(I)]	R_1 = 0.1107	R_1 = 0.1535	R_1 = 0.1424
	wR_2 = 0.2657	wR_2 = 0.3603	wR_2 = 0.2173
R indices (all data)			

Table 4.6 Selected bond lengths and bond angles for the complexes: {[Au(PPh$_3$)]$_2$L^7} and {[Au(PPh$_3$)]$_2$L^9} and {[Au(PPh)$_3$]$_2$L^{15}}.

{[Au(PPh)$_3$]$_2$L^7}		{[Au(PPh)$_3$]$_2$L^9}		{[Au(PPh)$_3$]$_2$L^{15}}	
$C_{49}H_{44}Au_2O_4P_2$		$C_{55}H_{56}Au_2O_4P_2$		$C_{67}H_{52}Au_2O_4P_2$	
		Av. Bond Lengths (Å)			
Au-P	2.28 (6)	Au-P	2.2 (2)	Au-P	2.28 (3)
Au-C	2.00 (2)	Au-C	1.94 (2)	Au-C	1.9 (13)
C-C	1.19 (3)	C-C	1.23 (8)	C-C	1.20 (15)

4.4.3.2. Promoting aurophilic interactions

Following the successful crystallisation of the three complexes, {[Au(PPh$_3$)]$_2$L$^{7/9/15}$}, a better insight into the solid state interactions of the Au(I) centres was gained. In all three complexes the Au(I) centres were orientated away from each-other and there was no evidence to suggest intra- or even intermolecular interactions were occurring. An attempt was made to bring the two Au(I) centres into a closer proximity to each-other, *i.e.* 'lock' the two Au(I) centres in a position that could result in aurophillic interactions. Both dppm and dppe were used in an attempt to lock the Au(I) centres and to promote and investigate any aurophillic interactions that may be occurring.

4.4.3.2.1. Synthesis of [Au(I)$_2$-dppm-L^7]

Dppm was reacted with {[Au(PPh$_3$)]$_2$L^7}; to a solution of {[Au(PPh$_3$)]$_2$L^7} in toluene, under nitrogen, was added dppm. After 12 hours, the resulting solution was dried *in vacuo.*[45] In the ^{31}P NMR spectra, peaks at +21.7 ppm, +33.1 ppm and +43.4 ppm were observed which were attributed to oxidised dppm, gold starting material and potential product respectively. The presence of the gold starting material [AuClPPh$_3$] in the spectra indicated breakdown of the complex, {[Au(PPh$_3$)]$_2$L^7}. A second synthetic approach was taken to synthesise the same product. [(Au-dppm)$_2$] was reacted with **L^7** following literature precedent,[46] however, peaks attributed to oxidised phosphines were observed in the ^{31}P NMR spectra only (Figure 4.23).

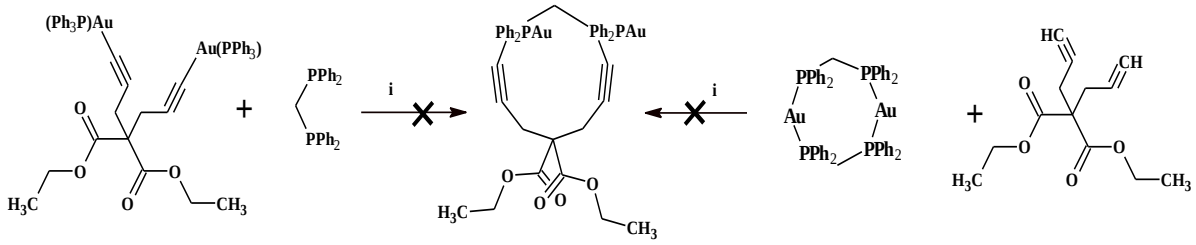

Figure 4.23 Attempted synthesis of [Au(I)$_2$-dppm-L^4]

The oxidation of the phosphine units, even in an inert atmosphere, indicated the stability of the product and/or the intermediate (where one dppe unit is bound) was poor. The distance required to 'lock' the two Au(I) centres, whilst attached to the alkynes, may also have been a hindering factor in these reactions.

4.4.3.2.2 Synthesis of [Au(I)$_2$-dppe-L^7]

In an attempt to overcome the issues discussed above, dppe was reacted following the same reaction pathways as previous; {[Au(PPh$_3$)]$_2$L^7} with dppe and [(Au-dppe)$_2$] with **L^7**, using completely anhydrous, deoxygenated conditions. The reaction of [(Au-dppe)$_2$] with **L^7** resulted in starting material and oxidised dppe being recovered only. The reaction of {[Au(PPh$_3$)]$_2$L^7} with dppe produced the desired product. In the ^{31}P NMR spectrum peaks at +21.3 ppm and +39.7 ppm were observed for the oxidised dppe and product respectively. The ^{1}H NMR spectra revealed the C*H*$_2$ dppe peak at a higher frequency, from +2.02 ppm to +2.55 ppm, which is attributed to its successful co-ordination to the Au(I) unit. The absence of peaks at a lower frequency in the ^{1}H NMR spectrum suggests, firstly, that the two CH$_2$ groups on dppe are equivalent, and both are bonded to a Au(I) unit, and secondly, with one peak present at +3.25 ppm for the CH$_2$ alkyne, the Au(I) units remain co-ordinated to the alkynes.

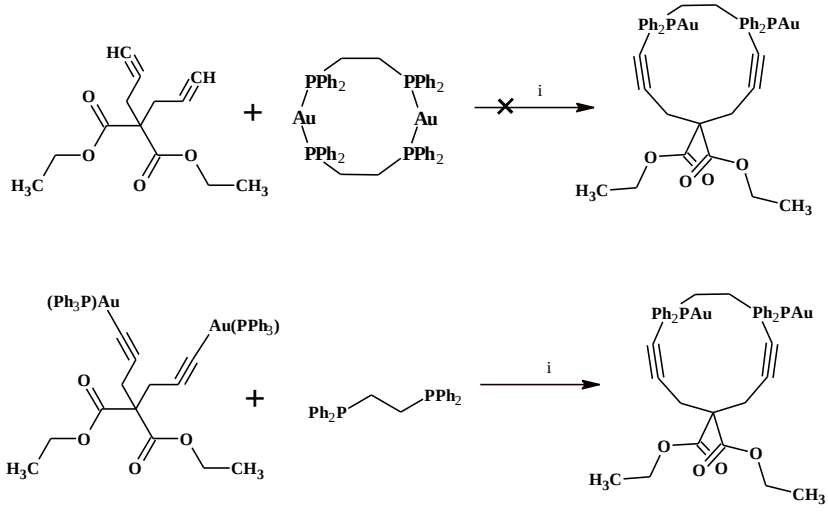

Figure 4.24 Attempted synthesis of [Au(I)$_2$-dppe-L^4]. Reagents: (i) toluene.

4.4.4 UV-Vis absorption spectroscopy

The UV-Vis data are summarised in Table 4.7. The high energy transitions around 250 nm are attributed to ^{1}IL ($\pi \rightarrow \pi^*$) or metal perturbed ^{1}IL transitions. The low energy absorptions in the regions of 330 nm are indicative of ligand to ligand charge transfer (^{1}LLCT) transitions from the π orbital on the alkyne ligands.

4.4.5. Luminescence spectroscopy

There have been a number of reports discussing the luminescent properties of Au(I) complexes resulting from aurophilic interactions. To investigate the potential aurophilic interactions of the malonate, di-alkyne Au(I) both solution and solid state spectra were recorded with irradiation at λ_{exc} 340 nm. The results of these measurements can be seen in Table 4.7 and are discussed in the following sections.

Table 4.7 Solid and solution photophysical data for {[Au(PPh$_3$)]$_2$L$^{7/9/10/15}$} and [Au$_2$–dppe L^7] complexes, λ_{exc} 340 nm and solid state IR data.

Compound	Abs	ε dm^3 mol^{-1} cm^{-1}	Em(MeCN)	Em(Solid)	CC (Cm^{-1})
{[Au(PPh$_3$)]$_2$L^7}	250	14608			
	271	4939	403-420	405-438	2168
	297	1497			
{[Au(PPh$_3$)]$_2$L^9}	250	14608			
	271	4939	407-429	414-448	2168
	297	1497			
{[Au(PPh$_3$)]$_2$L^{10}}	251	20779			
	306	5000	383-415	405-453	2182
	326	4429			
{[Au(PPh$_3$)]$_2$L^{15}}	253	1076	407-438	410-458	2329
	273	831			
[Au$_2$–dppe L^7]	241	11788			
	285	6100	403-455	404-440	2166
	315	1246		500-540	

4.4.5.1. Luminescent properties of {[Au(PPh$_3$)]$_2$L$^{7/9/10/15}$}

Upon excitation at 340nm all four complexes, {[Au(PPh$_3$)]$_2$L$^{7/9/10/15}$} displayed a very similar, single, broad emission band ranging between 403 nm and 438 nm. The luminescence lifetimes of the three aliphatic based, di-alkyne Au(I)$_2$-complexes, {[Au(PPh$_3$)]$_2$L$^{7/9/10}$} were < 2 ns, which is suggestive of emission of a singlet excited state, and is attributed to ^{1}IL/^{1}LLCT with possible mixed character of CC ($\pi \rightarrow \pi^*$) and Au-P ($\sigma \rightarrow \pi^*$)CC (the π^* may be localised on the alkyne/aryl group). As the conjugation within the ligands is increased, {[Au(PPh$_3$)]$_2$L$^{7/9/10}$} to [[Au(PPh$_3$)]$_2$L^{15}] a small red-shift in the emission maxima is observed (Figure 4.25). The variation in the emission maxima of the naphthalene-based, di-alkyne Au(I) complex was compared to the emission maxima of the free ligand, **L^{15}** (Figure 4.25).

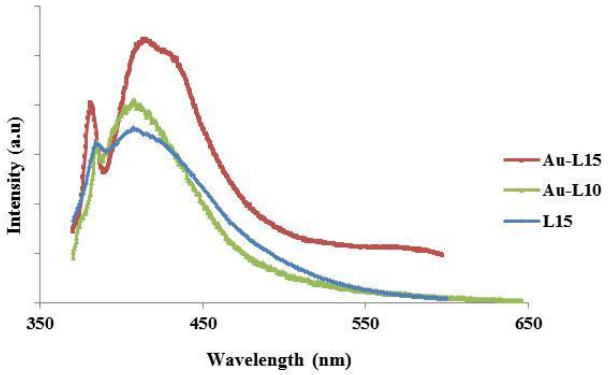

Figure 4.25 Emission spectra of L^{15}, {[Au(PPh$_3$)]$_2$L^{10}} and {[Au(PPh$_3$)]$_2$L^{15}} (λ_{exc} = 340 nm).

The more extensively conjugated, {[Au(PPh$_3$)]$_2$L^{15}} displayed a more structured, red-shifted emission profile when compared to that of **L^{15}**, 407-438 nm and 395-426 nm respectively. The red-shifted emission in {[Au(PPh$_3$)]$_2$L^{15}} was attributed to the effect of the [AuPPh$_3$]$^+$ unit. The luminescence lifetimes of {[Au(PPh$_3$)]$_2$L^{15}} was < 2 ns and so again is suggestive of emission singlet in origin; the emission is attributed to ^{1}IL/^{1}LLCT possibly with mixed character of CC ($\pi \rightarrow \pi^*$) and Au-P $\sigma \rightarrow \pi^*$CC.

4.4.5.2. Aurophillic Interactions

Au-Au interactions have been reported to lead to the observation of a red-shift in the emission maxima in the solid state emission when compared to the solution state. The solid and solution state emission for the Au(I) malonate complexes are compared in the following sections.

4.4.5.3. Luminescent properties of both the solid and solution state of {[Au(PPh$_3$)]$_2$L$^{10/15}$}.

In both the solution and solid state spectra the same emission maxima were observed for {[Au(PPh$_3$)]$_2$L^{15}} (Figure 4.26) however, for the symmetrical, aliphatic based complex [[Au(PPh$_3$)]$_2$L^{10}] a more dramatic difference was seen. When changing from solution to solid state measurements, a red-shifted, more-structured emission spectra was observed; 383-415 nm in solution to 405-453 nm. The tail of the emission profile in the solid state is more structured than that in solution; this increased resolution could suggest the presence of aurophilic interactions between Au-Au centres. The absence of an increase in emission lifetime make the MMLCT dσ (Au-Au)→π^* PPh$_3$/CC transition unlikely.

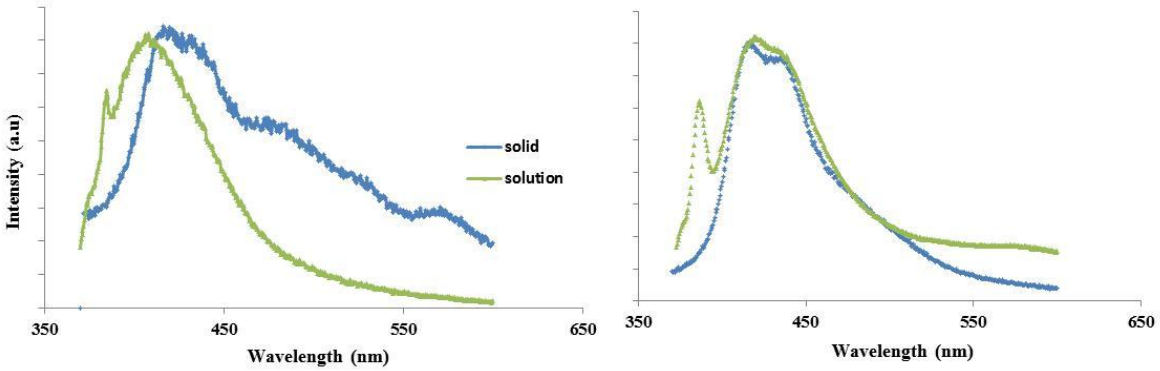

Figure 4.26 Solution and solid state emission spectra of {Au(PPh$_3$)]$_2$L^{10}} (LHS) and {Au(PPh$_3$)]$_2$L^{15}} (RHS) (λ_{exc} = 340 nm).

4.4.5.4. Luminescent properties of both the solid and solution state of {[Au(PPh$_3$)]$_2$L^7} & [Au$_2$-dppe-L^7]

In both the solid and solution state spectra the same emission maxima were observed for {[Au(PPh$_3$)]$_2$L^7} (Figure 4.27). More interesting results are seen when changing to the dppe-linked complex [Au$_2$-dppe-L^7]. A red-shifted emission maximum in the was observed when compared to the spectra ran in solution with a shift of *ca.* 100 nm (404-440 nm in solution to 500-540 nm in the solid state) (Figure 4.27). This red-shift may be indicative of aurophilic interactions occurring. The absence of a red-shift in emission maxima of [Au$_2$-dppe-L^7] in the solution state suggests the red-shifted emission seen in the solid state is a result of intermolecular interactions only, however, the lack of an increase in the emission lifetime suggest the emission is singlet state in origin as opposed to the suggested triplet state.

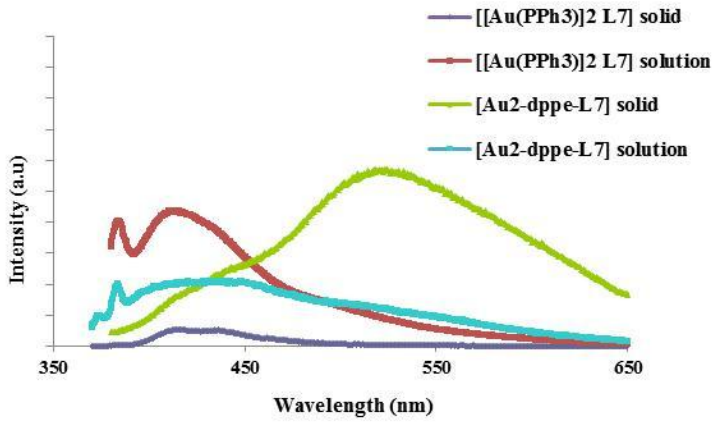

Figure 4.27 Steady state emission spectra of {$Au(PPh_3)]_2L^7$} and [Au_2-dppe-L^7] in solid and solution (λ_{exc} = 340 nm).

4.5. Cytotoxicity investigation

A preliminary study of the cytotoxicity was undertaken for **L^{15}** and {$[Au(PPh_3)]_2L^{15}$} using the MTT assay with four different cancer cell lines: MCF-7 (breast adenocarcinoma), A549 (lung adenocarcinoma), PC3 (prostate adenocarcinoma) and LOVO (colon adenocarcinoma). For the MTT assay, the compounds were initially dissolved in DMSO, and doses of 0.1, 1, 10 and 100 μm were tested to analyse the activity of different concentrations and then compared to a control medium with no treatment. The approximate IC_{50} values for these compounds are shown in table 4.8.

Table 4.8 Cytotoxicity data for L^{15} and {$[Au(PPh_3)]_2L^{15}$}

Ligand / Complex	IC_{50} MCF-7	IC_{50} PC3	IC_{50} A549	IC_{50} Lovo
L^{15}	>100	>100	>100	>100
$[Au(PPh_3)]_2L^{15}$	5	>100	>100	>100

A comparison of the IC_{50} values in Table 4.8, showed that the Au(I) complex of {$[Au(PPh_3)]_2L^{15}$} is significantly more toxic than the corresponding free ligand towards the MCF-7 cell line and so the increase in the cytotoxicity of the complex is attributed to the presence of the Au(I) alkynyl unit, as opposed to the presence of the naphthalene unit. The MCF-7 cell line is the most sensitive cell line to this complex with an IC_{50} value of 5 μM. For the other three cell lines (A549, PC3 and LOVO) no sensitivity to the complex is observed. Despite the increased sensitive nature of the MCF-7 cell line, when compared to the IC_{50} value of *cis*-platin (IC_{50} = 2.0 μM) these values are not sufficiently active to suggest applications solely as a therapeutic agent. The cellular imaging application of {$[Au(PPh_3)]_2L^{15}$} could not be assessed as the excitation wavelength for this complex is too high in energy and cellular damage would be expected.

4.6. Conclusion

A novel series of mono-and di-alkyne malonate ligands were synthesized followed by their $\{[Au(PPh_3)]_2\}^+$ complexes. Crystal structures were obtained for $\{[Au(PPh_3)]_2L^7\}$, $\{[Au(PPh_3)]_2L^9\}$ and $\{[Au(PPh_3)]_2L^{15}\}$, but no intra- or intermolecular Au-Au interactions were observed in the solid state of these structures. A novel dppe containing complex was synthesized using dppe and $\{[Au(PPh_3)]_2L^7\}$, which 'locked' the Au(I) units in a fixed position. Luminescence measurements were recorded for all five complexes in both solution and solid state to investigate the presence of aurophilic interactions. There was no evidence of Au-Au interactions for $\{[Au(PPh_3)]_2L^7\}$, $\{[Au(PPh_3)]_2L^9\}$ or $\{[Au(PPh_3)]_2L^{15}\}$ with the same emission maxima being observed for both solution and solid state. More interestingly, for $\{[Au(PPh_3)]_2L^{10}\}$ and $\{[Au_2\text{-dppe-}L^7\}$, when changing from the solution to solid state, a red-shifted, more structured emission profile is viewed. The red-shift is more dramatic for $[Au_2\text{-dppe-}L^7]$ with a shift of *ca.*100 nm. The absence of an increase in lifetime suggests that the luminescent transitions occurring in $\{[Au(PPh_3)]_2L^{10}\}$ and $[Au_2\text{-dppe-}L^7]$ in the solid state are singlet in nature and therefore not a result of aurophilic interactions.

Cytotoxicity measurements were carried out for the naphthalene-based complex $\{[Au(PPh_3)]_2L^{15}\}$ and its ligand, $\mathbf{L^{15}}$. No sensitivity to the ligand was seen in any of the cell lines tested. The only cell line to show sensitivity to the complex $\{[Au(PPh_3)]_2L^{15}\}$ was that of MCF-7. The absence of sensitivity to the ligand suggests the toxicity of the complex is attributed to the gold unit. MCF-7's are high in mitochondria, given that the mitochondria are believed to be the key intracellular target of gold agents (see the earlier discussion of TrxR), this is a promising route for the synthesis of a gold-based therapeutic agent. The dual functionality of complexes of this type (cellular and therapeutic agents) could not be assessed as the excitation wavelength of the malonate based complex is of high energy and therefore would damage the cells if used.

4.7. Experimental

4.7.1. Crystallography

{[Au(PPh$_3$)]$_2$L^3}: $C_{62}H_{62}Au_2F_6N_2O_{10}P_2S_2$, M = 1629.13, 0.10 × 0.04 × 0.04 mm^3, monoclinic, space group $P2_1/n$ (No. 14), a = 12.0014(15), b = 27.888(4), c = 19.133(2) Å, β = 104.048(7)°, V = 6212.2(14) Å^3, Z = 4, D_c = 1.742 g/cm^3, F_{000} = 3208, MoKα radiation, λ = 0.71073 Å, T = 293(2)K, $2\theta_{max}$ = 38.0º, 9107 reflections collected, 4906 unique (R_{int} = 0.0864). Final *GooF* = 1.355, *R1* = 0.1565, *wR2* = 0.3030, *R* indices based on 3666 reflections with I >2sigma(I) (refinement on F^2), 321 parameters, 46 restraints. Lp and absorption corrections applied, μ = 4.913 mm^{-1}.

Au cluster: $C_{56}H_{47}Au_3Cl_2F_3O_4P_3S$, M = 1627.71, 0.12 × 0.10 × 0.10 mm^3, triclinic, space group P-1 (No. 2), a = 12.7242(2), b = 14.5427(2), c = 16.2111(3) Å, α = 63.8380(10), β = 81.6950(10), γ = 89.6090(10)°, V = 2658.75(7) Å^3, Z = 2, D_c = 2.033 g/cm^3, F_{000} = 1548, MoKα radiation, λ = 0.71073 Å, T = 150(2)K, $2\theta_{max}$ = 55.0º, 17979 reflections collected, 12118 unique (R_{int} = 0.0367). Final *GooF* = 1.033, *R1* = 0.0453, *wR2* = 0.1065, *R* indices based on 10074 reflections with I >2sigma(I) (refinement on F^2), 650 parameters, 9 restraints. Lp and absorption corrections applied, μ = 8.544 mm^{-1}.

{[Au(PPh$_3$)]$_2$L^7} $C_{49}H_{44}Au_2O_4P_2$, M = 1152.71, colourless plate, 0.40 × 0.28 × 0.12 mm^3, monoclinic, space group $P2_1/a$ (No. 14), a = 18.3922(7), b = 12.7687(4), c = 22.6554(8) Å, b = 112.362(2)°, V = 4920.4(3) Å^3, Z = 4, D_c = 1.556 g/cm^3, F_{000} = 2232, KappaCCD, MoKa radiation, l = 0.71073 Å, T = 150(2)K, $2q_{max}$ = 49.1º, 14715 reflections collected, 8086 unique (R_{int} = 0.0670). Final *GooF* = 1.035, *R1* = 0.1107, *wR2* = 0.2657, *R* indices based on 5461 reflections with I >2sigma(I) (refinement on F^2), 444 parameters, 7 restraints. Lp and absorption corrections applied, m = 6.060 mm^{-1}.

{[Au(PPh$_3$)]$_2$L^9} $C_{55}H_{56}Au_2O_4P_2$, M = 1236.87, 0.25 × 0.15 × 0.02 mm^3, monoclinic, space group $P2_1/a$ (No. 14), a = 18.6917(16), b = 12.9506(13), c = 22.7648(12) Å, β = 110.571(4)°, V = 5159.3(7) Å^3, Z = 4, D_c = 1.592 g/cm^3, F_{000} = 2424, MoKα radiation, λ = 0.71073 Å, T = 293(2)K, $2\theta_{max}$ = 41.8º, 9411 reflections collected, 5271 unique (R_{int} = 0.1260). Final *GooF* = 1.394, *R1* = 0.1535, *wR2* = 0.3603, *R* indices based on 2885 reflections with I >2(I)

(refinement on F^2), 198 parameters, 37 restraints. Lp and absorption corrections applied, μ = 5.785 mm^{-1}.

{[Au(PPh$_3$)]$_2$L^{15}} $C_{67}H_{52}Au_2O_4P_2$, M = 1376.96, 0.53 × 0.34 × 0.02 mm^3, triclinic, space group *P-1*, a = 13.3177 (12), b = 13.2371 (11), c = 17.0686 (18) Å, β = 77.650 (6)°, V = 2772.1 (4) $Å^3$, Z = 2, D_c = 1.650 Mg/m^3, F_{000} = 1348, MoKα radiation, λ = 0.71075 Å, T = 120(2)K, $2\theta_{max}$ = 41.8º, 29975 reflections collected, 11299 unique (R_{int} = 0.1704). Final *GooF* = 0.975, *R1* = 0.1424, *wR2* = 0.1846,

4.7.2. Synthesis of ligands:

L^1: Ethylene glycol (4 mL, 7 mmol) was added to a solution of nicotinoyl chloride (0.5 g, 3.5 mmol) in chloroform (30 mL) and TEA (1.6 mL, 11 mmol). The solution was left at stir at 60 ˚C for 3 h. The solution was washed using sat. aq. sodium bicarbonate (3 × 10 mL) and sat. aq. ammonium chloride (2 × 10 mL). The organic layer was dried and the solvent evaporated to dryness, yielding a cream solid. Yield: 1.3 g, 68 %. ^{1}H NMR ($CDCl_3$, 300 MHz, 298 K) δ_H: 4.61 (4H, s, (*H5*)), 7.32-7.35 (2H, m, (*H3*)), 8.11-8.19 (2H, m, (*H4*)), 8.63-8.68 (2H, m, (*H2*)), 9.13 (2H, s, (*H12*)) ppm. ^{13}C{^{1}H} NMR ($CDCl_3$, 101 MHz, 298 K) δ_C: 164, 152.6, 149.9, 136.2, 122.4, 61.9 ppm. MS (ES^+) *m/z*: 272.08 $[M+H]^+$. IR (nujol) υ: 1651 (CO) cm^{-1}.

L^2: 1,6 hexan-diol (0.380 g, 3.23 mmol) was added to a solution of nicotinoyl chloride (1 g, 7.07 mmol) in chloroform (50 mL) and TEA (3.23 mL, 22 mmol). The solution was left at stir at 60 ˚C for 3 h. The solution was washed using sat. aq. sodium bicarbonate (3 × 10 mL) and sat. aq. ammonium chloride (2 × 10 mL). The organic layer was dried and the solvent evaporated to dryness, yielding a white solid. Yield: 0.831 g, 78 %. ^{1}H NMR ($CDCl_3$, 300 MHz, 298 K) δ_H: 1.38-1.45 (4H, m, (*H8, H9*)), 1.7 (2H, t, (*H7*)), 2.42-2.48 (2H, m, (*H6*)), 3.61 (2H, t, (*H10*)), 4.34 (2H, t, (*H5*)), 7.38-7.42 (2H, m, (*H3*)), 8.28 (2H, dd, (*H4*)). 8.68-8.72 (2H, m, (*H2*)). 9.18 (2H, m, ((*H1*)) ppm.

L^4: To a solution of propargyl alcohol (2.085 g, 37.24 mmol) and TEA (12.3 mL, 89.4 mmol) in DCM (15 mL) was added malonyl chloride (2.5 g, 17.73 mmol) drop wise. The solution was left to stir at room temperature for 15 mins. The solution was washed using sat. aq. sodium bicarbonate (3 × 10 mL) and sat. aq. ammonium chloride (2 × 10 mL). The organic layer was dried and the solvent evaporated to dryness, yielding orange oil. Yield: 1.3 g, 41 %.

^{1}H NMR ($CDCl_3$, 400 MHz, 298 K) δ_H: 2.5 (2H, t, (*H1*)), 3.41 (4H, s, (*H3*)), 4.59 (4H, t, (*H2*)) ppm.

L^5: To a solution of benzaldehyde (0.112 mL, 1.11 mmol) in DMSO (5 mL) was added proline (0.128 g, 1.11 mmol). L^4 (0.200 g, 1.11 mmol) was added after 5 minutes. The solution was stirred at room temperature for 24 h. EtOAc (20 mL) was added and then the solution was washed with water (2 × 10mL). The organic layer was dried and the solvent evaporated to dryness, yielding light orange oil. The crude product was purified using column chromatography eluting with DCM. Yield: 0.063 g, 21 %. ^{1}H NMR ($CDCl_3$, 400 MHz, 298 K) δ_H: 2.41-2.46 (2H, t, $^{3}J_{HH}$ = 2.5 Hz, (*H1*)), 4.74 (4H, d, $^{3}J_{HH}$ = 2.8 Hz, (*H2*)), 7.2-7.43 (3H, m, (*H3, H4*)), 7.38-7.43 (2H, m, (*H5*)), 7.71 (1H, s, (*H6*)) ppm. $^{13}C\{^{1}H\}$ NMR ($CDCl_3$, 101 MHz, 298 K) δ_C: 53.1, 75.2, 124, 129, 130, 131.2, 132.3, 144.6, 163.1, 165.4 ppm. MS (ES^+) *m/z*: 213.05 $[M\text{-}C_3H_3O]^+$, 268.07 $[M]^+$. HRMS (ES^+) found *m/z* 268.0730; $[C_{16}H_{12}O_4]^+$ requires 268.0730. IR (nujol) υ: 1626 (CO), 1735 (CO), 2130 (CC) cm^{-1}. UV-vis λ_{max} (ε / $M^{-1}cm^{-1}$) (MeCN) λ_{max} : 280 (4874) nm.

L^6: To a solution of anisaldehyde (0.126 mL, 1.11 mmol) in DMSO (5 mL) was added proline (0.128 g, 1.11 mmol). L^4 (0.200 g, 1.11 mmol) was added after 5 minutes. The solution was stirred at room temperature for 24 h. Work-up as before. Yield: 0.108 g, 33 %. ^{1}H NMR ($CDCl_3$, 400 MHz, 298 K) δ_H: 2.43-2.59 (2H, t, $^{3}J_{HH}$ = 2.6 Hz, (*H1*)), 3.76 (3H, s, (*H6*)), 4.71-4.85 (4H, d, $^{3}J_{HH}$ = 2.4 Hz, (*H2*)), 6.73 (2H, d, $^{3}J_{HH}$ = 8.8 Hz, (*H4*)), 7.78 (2H, d, $^{3}J_{HH}$ = 8.8 Hz (*H5*)), 7.62 (1H, s, (*H3*)) ppm. $^{13}C\{^{1}H\}$ NMR ($CDCl_3$, 101 MHz, 298 K) δ_C: 51.9, 52, 54.4, 74.7, 75.9, 76.1, 113.4, 120, 123.7, 131.1, 143.1, 161.1, 162.4, 164.8 ppm. MS (ES^+) *m/z*: 243.05 $[M\text{-}C_3H_3O]^+$, 298.07 $[M]^+$, HRMS (ES^+) found *m/z* 298.0775; $[C_{17}H_{14}O_5]^+$ requires 298.0836. IR (nujol) υ: 1651 (CO),1737 (CO), 2129 (CC) cm^{-1}. UV-vis λ_{max} (ε / $M^{-1}cm^{-1}$) (MeCN) λ_{max} : 311 (18419) nm.

L^7: To a solution of diethyl malonate (4.74 mL, 31.2 mmol), potassium tertiary butoxide (8.4 g, 74.88 mmol), in ethanol (200 mL) was added propargyl bromide (9.8 mL, 74.99 mmol) slowly. The solution was stirred at room temperature, under N_2(g) for 5 h. The solution was washed with water (3 × 50 mL). The organic layer was dried and the solvent evaporated to dryness, yielding orange oil. Yield: 4.21 g, 82 %. ^{1}H NMR ($CDCl_3$, 400 MHz, 298 K) δ_H: 1.22 (6H, t, $^{3}J_{HH}$ = 7.25 Hz, (*H1*)), 1.99 (2H, t, $^{3}J_{HH}$ = 2.6 Hz, (*H4*)), 2.92 (4H, d, $^{3}J_{HH}$ = 2.6 Hz, (*H3*)), 4.17 (4H, q, $^{3}J_{HH}$ = 7.1 Hz, (*H2*)) ppm. $^{13}C\{^{1}H\}$ NMR ($CDCl_3$, 101 MHz, 298 K) δ_C:

53.1, 75.2, 124, 129, 130, 131.2, 132.3, 144.6, 163.1, 165.4 ppm. MS (ES^+) *m/z*: 163 $[M-H]^+$. IR (nujol) *υ*: 1740 (CO), 1995 (CC) cm^{-1}.

Ligand precursor $L^{8/9}$: To a solution octanol (0.716 g, 5.5 mmol) and TEA (1.17 mL, 9 mmol) in DCM (15 mL) was added ethyl malonyl chloride (0.750 g, 5 mL) drop wise. The solution was left to stir at room temperature for 15 mins. The solution was washed using sat. aq. sodium bicarbonate (3 × 10 mL) and sat. aq. ammonium chloride (2 × 10 mL). The organic layer was dried and the solvent evaporated to dryness, yielding colourless oil. Yield: 0.434 g, 36 %. ^{1}H NMR ($CDCl_3$, 400 MHz, 298 K) δ_H: 0.82 (3H, t, $^3J_{HH}$=6.7 Hz, (*H11*)), 1.18-1.32 (13H, m, (*H1*,*H6-H10*)), 1.53-1.72 (2H, m, (*H5*)), 3.32 (2H, s, (*H3*)), 4.01-4.18 (4H, m, (*H2, H4*)) ppm. **$L^{8/9}$** To a solution of ligand precursor (0.167 g, 0.684 mmol), potassium tertiary butoxide (0.183 g, 1.64 mmol), in ethanol (50 mL) was added propargyl bromide (0.18 mL, 2.05 mmol) slowly. The solution was stirred at room temperature, under N_2(g) for 5 h. The solution was washed with water (3 × 50 mL). The organic layer was dried and the solvent evaporated to dryness, yielding a colourless oil. Yield L^8 : 0.029 g, 15 %. ^{1}H NMR ($CDCl_3$, 400 MHz, 298 K) δ_H: 0.82 (3H, t, (*H11*)), 1.12-1.34 (13H, m, (*H1, H6-H10*)), 1.62-1.66 (2H, m, (*H5*)), 2.08 (1H, t, (*H3b*)), 2.72-2.75 (1H, m, (*H3*)), 2.98 (2H, d, (*H3a*)), 4.12-4.29 (4H, m, (*H2*,*H4*)) ppm. $^{13}C\{^1H\}$ NMR ($CDCl_3$, 101 MHz, 298 K) δ_C: 14.1, 14.2, 18.6, 22.7, 25.9, 28.6, 19.2, 29.3, 31.9, 52.3, 56.5, 61.8, 62.2, 70.5, 71.8, 78.6, 168.8, 168.9 ppm. MS (ES^+) *m/z*: 282 $[M+H]^+$. Yield L^9: 0.129 g, 59 %. ^{1}H NMR ($CDCl_3$, 400 MHz, 298 K) δ_H: 0.82 (3H, t, (*H11*)), 1.18-1.43 (13H, m, (*H1, H6-H10*)), 1.52-1.68 (2H, m, (*H5*)), 2.08 (2H, t, $^3J_{HH}$ = 2.4 Hz, (*H3b*)), 2.98 (4H, d, $^3J_{HH}$ = 2.6 Hz, (*H3a*)), 4.12-4.29 (4H, m, (*H2*,*H4*)) ppm. $^{13}C\{^1H\}$ NMR ($CDCl_3$, 101 MHz, 298 K) δ_C: 14.0, 14.1, 22.5, 22.6, 25.7, 28.4, 29.1, 29.2, 31.6, 31.8, 40.1, 56.3, 62.1, 66.2, 71.7, 76.6, 78.4, 168.6, 168.7 ppm. MS (ES^+) *m/z*: 321.2 $[M]^+$. HRMS (ES^+) found *m/z* 321.2063; $[C_{19}H_{29}O_4]^+$ requires 321.2065. IR (nujol) *υ*: 1739 (CO), 2124 (CC) cm^{-1}.

Ligand precursor L^{10}: To a solution octanol (2.35 mL, 14.9 mmol) and TEA (2.29 mL, 21.2 mmol) in DCM (15 mL) was added malonyl chloride (0.750 g, 5 mL) drop wise. The solution was left to stir at room temperature for 15 mins. The solution was washed using sat. aq. sodium bicarbonate (3 × 10 mL) and sat. aq. ammonium chloride (2 × 10 mL). The organic layer was dried and the solvent evaporated to dryness. Excess octanol was removed *via* distillation. Yield: 0.987 g, 42 % ^{1}H NMR ($CDCl_3$, 400 MHz, 298 K) δ_H: 0.85 (6H, t, $^3J_{HH}$= Hz, (*H1*)), 1.39-1.98 (20H, m, (*H2-H6*)), 1.65-1.78 (4H, m, (*H7*)), 3.33 (2H, s, (*H9*)), 4.13

(4H, t, (*H8*)) ppm.$^{13}C\{^{1}H\}$ NMR ($CDCl_3$, 101 MHz, 298 K) δ_C: 14.1, 22.7, 25.8, 28.5, 29.2, 29.7, 31.8, 41.7, 65.6, 166.7 ppm. IR (nujol) υ:1651 (CO) 1737 (CO) cm^{-1}. UV-vis λ_{max} (ε / $M^{-1}cm^{-1}$) (MeCN) λ_{max} : 253 (3489) nm. **L^{10}:** To a solution of ligand precursor (0.400 g, 1.22 mmol), potassium tertiary butoxide (0.328 g, 2.92 mmol), in ethanol (50 mL) was added propargyl bromide (0.32 mL, 3.65 mmol) slowly. The solution was stirred at room temperature, under N_2(g) for 5 h. The solution was washed with water (3 × 50 mL). The organic layer was dried and the solvent evaporated to dryness, yielding orange oil. Yield: 0.168 g, 36 %. ^{1}H NMR ($CDCl_3$, 400 MHz, 298 K) δ_H: 0.82 (6H, t, $^{3}J_{HH}$ = 6.8 Hz, (*H1*)), 1.32-1.43 (20H, m, (*H2-H6*)), 1.58 (4H, m, (*H7*)), 2.06 (2H, t, $^{3}J_{HH}$ = 2.6 Hz, (*H10*)), 2.98 (4H, d, $^{3}J_{HH}$ = 2.6 Hz, (*H9*)), 4.18 (4H, t, $^{3}J_{HH}$ = 4.7 Hz, (*H8*)) ppm.

Ligand precursor $L^{11/12}$: To a solution ligand precursor A (0.560 g, 1.7 mmol) and TEA (0.037 mL, 2.3 mmol) in DCM (25 mL) was added ethyl malonyl chloride (0.231 g, 1. 5 mmol) drop wise. The solution was left to stir at room temperature for 15 mins. The solution was washed using sat. aq. sodium bicarbonate (3 × 10 mL) and sat. aq. ammonium chloride (2 × 10 mL). The organic layer was dried and the solvent evaporated to dryness, yielding a dark orange oil. Yield: 0.972 g, 69 %. ^{1}H NMR ($CDCl_3$, 400 MHz, 298 K) δ_H: 1.14-1.44 (19H, m, (*H1*,*H6-H13*)), 1.55-1.69 (2H, m, (*H5*)), 1.67-1.72 (2H, m, (*H14*)), 3.27 (2H, s, (*H3*)), 4.0-4.18 (4H, m, (*H2, H4*)), 4.26 (2H, t, $^{3}J_{HH}$ = 6.5 Hz, (*H15*)), 7.29-7.32 (1H, m, (*H17*)), 8.17-7.24 (1H, m, (*H16*)), 8.69 (1H, d, (*H18*)), 9.17 (1H, s, (*H19*)) ppm. $^{13}C\{^{1}H\}$ NMR ($CDCl_3$, 101 MHz, 298 K) δ_C: 12.3, 25.8, 26.0, 26.2, 26.5, 27.0, 28.1, 28.5, 28.8, 29.3, 29.6, 31.2, 34.3, 42.0, 65.8, 122.9, 137.1, 149.1, 152.3 ppm. MS (ES^+) *m/z*: 422.25 $[M+H]^+$, 444.23 $[M+Na]^+$, 460.21 $[M+K]^+$. HRMS (ES^+) found *m/z* 422.2535; $[C_{23}H_{36}O_6N]^+$ requires 422.2357. IR (nujol) *υ*:1591 (CO), 1658 (CO), 1728 (CO) cm^{-1}. UV-vis (ε / M^{-1} cm^{-1}) (MeCN) λ_{max}: 254 (5214) nm. **$L^{11/12}$** To a solution of ligand precursor (0.560 g, 1.7 mmol), potassium tertiary butoxide (0.04 g, 4.08 mmol), in ethanol (50 mL) was added propargyl bromide (0.8 mL, 4.08 mmol) slowly. The solution was stirred at room temperature, under N_2(g) for 5 h. The solution was washed with water (3 × 50 mL). The organic layer was dried and the solvent evaporated to dryness, yielding a dark orange oil. Yield L^{11}: 0.021 g**.** ^{1}H NMR ($CDCl_3$, 400 MHz, 298 K) δ_H: 1.18-1.39 (22H, m, (*H1*,*H6-H13*,*H18*)), 1.55-1.73 (4H, m, (*H5*,*H14*)), 1.97-2.08 (2H, m, (*H3b, H16b*)), 2.70-2.81 (2H, m, (*H3, H16*)), 2.92-2.98 (4H, m, (*H3a*,*H16a*)), 4.08-4.29 (8H, m, (*H2*,*H4*,*H15*,*H17*)) ppm. $^{13}C\{^{1}H\}$ NMR ($CDCl_3$, 101 MHz, 298 K) δ_C: 14.0, 14.1, 18.5, 22.6, 25.8, 28.5, 29.1, 29.2, 29.5, 29.6, 51.2, 56.4, 61.8, 61.9, 62.2, 66.0, 66.3, 70.5, 70.6, 71.8, 78.5, 78.5, 168.0, 168.9 ppm. MS (ES^+) *m/z*: 507.1 $[M+H]^+$, 529

$[M+Na]^+$, 545 $[M+K]^+$. HRMS (ES^+) found *m/z* 524.3216; $[C_{28}H_{46}O_8N]^+$ requires 524.3218. IR (nujol) *υ*: 1591 (CO), 1658 (CO), 1735 (CO), 2124 (CC) cm^{-1}. UV-vis (ε / M^{-1} cm^{-1}) (MeCN) λ_{max}: 263 (3215), 302 (1653), 352 (528) nm. Yield L^{12}: 0.060 g, 7 %. ^1H NMR ($CDCl_3$, 400 MHz, 298 K) δ_H: 1.18-1.39 (19H, m, (*H1, H6-H13*)), 1.55-1.73 (2H, m, (*H5*)), 1.68-1.75 (2H, m, (*H14*)), 1.97 (2H, t, (*H3a*)), 2.92-2.98 (4H, m, (*H3b*)), 4.0-4.18 (4H, m, (*H2, H4*)), 4.26 (2H, t, $^3J_{HH}$ = 6.5 Hz, (*H15*)), 7.29-7.32 (1H, m, (*H17*)), 8.18-8.24 (1H, m, (*H16*)), 8.69 (1H, d, (*H18*)), 9.17 (1H, s, (*H19*)) ppm. $^{13}C\{^1H\}$ NMR ($CDCl_3$, 101 MHz, 298 K) δ_C: 53.1, 75.2, 124, 129, 130, 131.2, 132.3, 144.6, 163.1, 165.4 ppm. MS (ES^+) *m/z*: 498.28 $[M+H]^+$, 520.26 $[M+Na]^+$. HRMS (ES^+) found m/z 498.2844 $[M+H]^+$; $[C_{29}H_{40}O_6N]^+$ requires 498.2850. IR (nujol) *υ*: 1591 (CO), 1727 (CO) cm^{-1}. UV-vis (ε / M^{-1} cm^{-1}) (MeCN) λ_{max}: 262 (3827) nm.

Ligand Precursor L^{13}: To a solution ligand precursor A (1 g, 3.26 mmol) and TEA (0. 69 mL, 4.89 mmol) in DCM (15 mL) was added malonyl chloride (0.230 g, 1.63 mmol) drop wise. The solution was left to stir at room temperature for 15 mins. The solution was washed using sat. aq. sodium bicarbonate (3 × 10 mL) and sat. aq. ammonium chloride (2 × 10 mL). The organic layer was dried and the solvent evaporated to dryness, yielding orange oil. Yield: 0.136 g, 12 %. ^1H NMR ($CDCl_3$, 400 MHz, 298 K) δ_H: 1.15-1.29 (28H, m, (*H7-H13*)), 1.29-1.41 (4H, m, (*H14*)), 1.53-1.62 (4H, m, (*H6*)), 1.68-1.77 (4H, m, (*H15*)), 3.31 (2H, s, (*H17*)), 4.08 (4H, t, $^3J_{HH}$ = 6.8 Hz, (*H16*)), 4.29 (4H, t, $^3J_{HH}$ = 6.7 Hz, (*H5*)), 7.27-7.36 (2H, m, (*H3*)), 8.18 (2H, dd, (*H4*)), 8.13-8.25 (2H, m, (*H2*)), 9.11-9.19 (2H, m, (*H1*)) ppm. $^{13}C\{^1H\}$ NMR ($CDCl_3$, 101 MHz, 298 K) δ_C: 25.6, 25.8, 26.2, 26.8, 27.1, 28.5, 28.9, 28.6, 29, 29.3, 29.6, 42.3, 65.7, 123.3, 137.1, 151.2, 153.4, 164.6 ppm. MS (ES^+) *m/z*: 682.41 $[M]^+$. HRMS (ES^+) found m/z 682.4181 $[M]^+$; $[C_{30}H_{58}O_8N_2]^+$ requires 682.4188. IR (nujol) υ: 1751 (CO), 1756 (CO) cm^{-1}. UV-vis λ_{max} (ε / $M^{-1}cm^{-1}$) (MeCN) λ_{max} : 261 (6067), 363 (610) nm. **L^{13}** To a solution of ligand precursor (0.100 g, 0.146 mmol), potassium tertiary butoxide (0.05 g, 0.439 mmol), in ethanol (50 mL) was added propargyl bromide (0.1 mL, 0.439 mmol) slowly. The solution was stirred at room temperature, under N_2(g) for 5 h. The solution was washed with water (3 × 50 mL). The organic layer was dried and the solvent evaporated to dryness, yielding orange oil. Yield: 0.04 g, 37 %. ^1H NMR ($CDCl_3$, 400 MHz, 298 K) δ_H: 1.12-1.31 (28H, m, (*H7-H13*)), 1.49-1.56 (4H, m, (*H14*)), 1.62-1.73 (8H, m, (*H6, H15*)), 1.92 (2H, t, $^3J_{HH}$ = 2.3 Hz, (*H17b*)), 2.81 (4H, d, $^3J_{HH}$ = 2.2 Hz, (*H17a*)), 4.08 (4H, t, $^3J_{HH}$ = 6.6 Hz, (*H16*)), 4.27 (4H, t, $^3J_{HH}$ = 6.7 Hz, (*H5*)), 7.25-7.36 (2H, m, (*H3*)), 8.18 (2H, dd, (*H4*)), 8.13-8.25 (2H, m, (*H2*)), 9.11-9.19 (2H, m, (*H1*)) ppm. $^{13}C\{^1H\}$ NMR ($CDCl_3$, 101 MHz, 298 K) δ_C: 21.5,

24.7, 24.9, 27.4, 27.6, 28.1, 28.2, 28.5, 29.3, 55.4, 64.5, 65.2, 70.7, 77.5, 122.3, 125.3, 136, 149.9, 152.3, 164.3, 167.6 ppm. MS (ES^+) *m/z*: 758.45 $[M]^+$. HRMS (ES^+) found m/z 758.4507 $[M+H]^+$; $[C_{45}H_{62}O_8N_2]^+$ requires 758.4501. IR (nujol) υ: 1724 (CO), 1735 (CO) cm^{-1}. UV-vis λ_{max} (ε / $M^{-1}cm^{-1}$) (MeCN) λ_{max} : 261 (10356) nm.

Ligand Precursor L[14]: To a solution benzyl-alcohol (1 g, 9.25 mmol) and TEA (1.86 mL, 13.8 mmol) in DCM (15 mL) was added malonyl chloride (0.620 g, 4.39 mmol) drop wise. The solution was left to stir at room temperature for 15 mins. The solution was washed using sat. aq. sodium bicarbonate (3 × 10 mL) and sat. aq. ammonium chloride (2 × 10 mL). The organic layer was dried and the solvent evaporated to dryness, yielding a colourless oil. Yield: 0.840 g, 68 %. ^{1}H NMR ($CDCl_3$, 400 MHz, 298 K) δ_H: 3.39 (2H, s, (*H5*)), 5.05 (4H, s, (*H4*)), 7.11-7.32 (10H, m, (*H1-H3*)) ppm. **L[14]**:To a solution of ligand precursor (0.840 g, 2.96 mmol), potassium tertiary butoxide (1.16 mL, 10.35 mmol), in ethanol (50 mL) was added propargyl bromide (1.34 mL, 14.8 mmol) slowly. The solution was stirred at room temperature, under N_2(g) for 5 h. The solution was washed with water (3 × 50 mL). The organic layer was dried and the solvent evaporated to dryness, yielding a colourless oil. Yield: 0.625 g, 37 %. ^{1}H NMR ($CDCl_3$, 400 MHz, 298 K) δ_H: 1.98 (2H, t, $^3J_{HH}$ = 2.65 Hz, (*H6*)), 2.92 (4H, d, $^3J_{HH}$ = 2.6 Hz (*H5*)), 5.03 (4H, s, (*H4*)), 7.08-7.29 (10H, m, (*H1-H3*)) ppm. $^{13}C\{^1H\}$ NMR ($CDCl_3$, 101 MHz, 298 K) δ_C: 21.5, 29.3, 65.1, 70.9, 75.5, 77.1, 122.4, 124.1, 124.5, 124.9, 125.5, 126.5, 127.6, 128.4, 129.3, 130.4, 132.5, 167.2 ppm. MS (ES^+) *m/z*: 461.18 $[M+H]^+$, 478.20 $[M+NH_4]^+$, 483.16 $[M+Na]^+$, 499.13 $[M+K]^+$, HRMS (ES^+) found *m/z* 483.1561 $[M+Na]^+$; $[C_{31}H_{24}O_4Na]^+$ requires 483.1567. IR (nujol) υ: 1739 (CO) cm^{-1}. UV-vis λ_{max} (ε / $M^{-1}cm^{-1}$) (MeCN) λ_{max} : 281 (3510) nm.

Ligand Precursor L[15]: To a solution naphthol (1 g, 6.32 mmol) and TEA (1.27 mL, 9.03 mmol) in DCM (15 mL) was added malonyl chloride (0.424 g, 3.01 mmol) drop wise. The solution was left to stir at room temperature for 15 mins. The solution was washed using sat. aq. sodium bicarbonate (3 × 10 mL) and sat. aq. ammonium chloride (2 × 10 mL). The organic layer was dried and the solvent evaporated to dryness, yielding a pale orange oil. Yield: 0.900 g, 78 %. ^{1}H NMR ($CDCl_3$, 400 MHz, 298 K) δ_H: 3.43 (2H, s, (*H9*)), 5.03 (4H, s, (*H8*)), 7.31-7.55 (8H, m, (*H3-H6*)), 7.72-7.9 (6H, m, (*H1, H2, H7*)) ppm. **L[15]:** To a solution of ligand precursor (0.579 g, 1.5 mmol), potassium tertiary butoxide (0.592 mL, 5.29 mmol), in ethanol (50 mL) was added propargyl bromide (0.88 mL, 7.5 mmol)

slowly. The solution was stirred at room temperature, under N_2(g) for 5 h. The solution was washed with water (3 × 50 mL). The organic layer was dried and the solvent evaporated to dryness, yielding a colourless oil. Yield: 0.110 g, 16 %. ^{1}H NMR ($CDCl_3$, 400 MHz, 298 K) δ_H: 1.81 (2H, t, $^3J_{HH}$ = 2.3 Hz (*H10*)), 2.92 (4H, d, $^3J_{HH}$ = 2.3 Hz (*H9*)), 5.38 (4H, s, (*H8*)), 7.21-7.28 (2H, m, (*H4*)), 7.23-7.37 (4H, m, (*H3*, *H5*)), 7.53-7.78 (8H, m, (*H1*, *H2*, *H6*, *H7*)) ppm. ^{13}C{^{1}H} NMR ($CDCl_3$, 101 MHz, 298 K) δ_C: 21.5, 29.3, 65.1, 70.9, 75.5, 77.1, 122.4, 124.1, 124.5, 124.9, 125.5, 126.5, 127.6, 128.4, 129.3, 130.4, 132.5, 167.2 ppm. MS (ES^+) *m/z*: 461.18 $[M+H]^+$, 478.20 $[M+NH_4]^+$, 483.16 $[M+Na]^+$, 499.13 $[M+K]^+$, HRMS (ES^+) found m/z 483.1561 $[M+Na]^+$; $[C_{31}H_{24}O_4Na]^+$ requires 483.1567. IR (nujol) υ: 1739 (CO) cm^{-1}. UV-vis λ_{max} (ε / $M^{-1}cm^{-1}$) (MeCN) λ_{max}: 281 (3510) nm.

4.7.3. Synthesis of Complexes:

{[Au(PPh$_3$)$_2$L^7}: To a round bottom flask encase in aluminium foil L^7 (0.044 g, 0.184 mmol), [AuClPPh$_3$] (0.200 g, 0.404 mmol), potassium tertiary butoxide (0.062 g, 0.552 mmol) and ethanol (2 mL) were added and stirred under nitrogen for 12 h. The solution was concentrated *in vacuo*, re-dissolved in DCM and filtered. The orange solid was recrystallized from THF and diethyl ether. Yield: 0.097 g, 50 %. ^{1}H NMR ($CDCl_3$, 400 MHz, 298 K) δ_H: 1.22 (6H, t, (*H1*)), 3.21 (4H, s, (*H3*)), 4.18 (4H, q, (*H2*)), 7.30-7.62 (30H, m, (*H4*)) ppm. ^{13}C{^{1}H} NMR ($CDCl_3$, 101 MHz, 298 K) δ_C: 14.1, 24.2, 61.4, 129.0, 129.1, 131.4, 134.3, 134.5 ppm. δ ^{31}P 42.73 ppm. IR (nujol) υ: 1732 (CO), 1771 (CO), 2168 (CC) cm^{-1}. UV-vis (ε / M^{-1} cm^{-1}) (MeCN) λ_{max}: 250 (14608), 271 (4939), 297 (1497) nm.

[Au$_2$dppe-L^7]: To degassed toluene (10 mL) was added [[Au(PPh$_3$)]$_2$L^7] (0.076 g, 0.07 mmol), degassed, and dppe (0.026 g, 0.07 mmol) added. The degassed solution was left to stir under N_2(g) for 72 h. The solution was concentrated *in vacuo* and the cream solid was recrystallized from THF and diethyl ether. Yield: 0.027 g, 40 %. ^{1}H NMR ($CDCl_3$, 400 MHz, 298 K) δ_H: 1.25 (6H, t, (*H1*)), 2.55 (4H, s, (H4)), 3.25 (4H, s, (*H3*)), 4.18 (4H, q, (*H2*)), 7.36-7.70 (20H, m, (*H5)*) ppm. ^{13}C{^{1}H} NMR ($CDCl_3$, 101 MHz, 298 K) δ_C: 14.3, 24.1, 61.6, 77.3, 129.6, 131.9, 133.5, 169.4 ppm. δ ^{31}P 39.67 ppm. IR (nujol) υ: 1621 (CC), 1732 (CO), 2166 (CC) cm^{-1}. UV-vis (ε / M^{-1} cm^{-1}) (MeCN) λ_{max}: 241.5 (11788), 285 (6106), 351.5 (1246) nm.

{[Au(PPh$_3$)]$_2$L^9}: To a round bottom flask encase in aluminium foil L^9 (0.021 g, 0.07 mmol), [AuClPPh$_3$] (0.072 g, 0.07 mmol), potassium tertiary butoxide (0.026 g, 0.023 mmol) and

ethanol (2 mL) were added and stirred under nitrogen for 12 h. Work-up as before. Yield: 0.012 g, 48 %. ^{1}H NMR ($CDCl_3$, 400 MHz, 298 K) δ_H: 0.78 (3H, t, (*H11*)), 1.06-1.32 (10H, m, (*H6-H10*)), 3.17 (4H, s, (*H3a*)), 4.02-4.18 (4H, m, (*H2, H4*)), 7.21-7.56 (30H, m, (*H3b)*) ppm. ^{13}C{^{1}H} NMR ($CDCl_3$, 101 MHz, 298 K) δ_C: 14.1, 22.7, 24.2, 44.1, 25.8, 25.9, 37.5, 39, 39.2, 31.8, 62.4, 129.0, 129.1, 129,4, 131.4, 134.3, 134.5 ppm. δ ^{31}P 42.71 ppm. MS (ES) *m/z*: 721 $[Au(PPH_3)_2]^+$. IR (nujol) *υ*: 1732 (CO), 1771 (CO), 2168 (CC) cm^{-1}. UV-vis (ε / M^{-1} cm^{-1}) (MeCN) λ_{max}: 250 (14608), 271 (4939), 297 (1497) nm.

{[Au(PPh$_3$)]$_2$L^{10}}: To a round bottom flask encase in aluminium foil L^{10} (0.012 g, 0.032 mmol), [AuClPPh$_3$] (0.034 g, 0.069 mmol), potassium tertiary butoxide (0.011 g, 0.095 mmol) and ethanol (2 mL) were added and stirred under nitrogen for 12 h. Work-up as before Yield: 0.073 g, 57 %. ^{1}H NMR ($CDCl_3$, 400 MHz, 298 K) δ_H: 1.32 (6H, t, $^{3}J_{HH}$ = 8.3 Hz (*H1*)), 1.12-1.27 (20H, m, (*H2-H6*)), 1.49-1.61 (4H, m, (*H7*)), 3.21 (4H, s, (*H9*), 4.05 (4H, t, $^{3}J_{HH}$ = 6.7 Hz, (*H8*)), 7.22-7.41 (30H, m, (*H10*)) ppm. ^{13}C{^{1}H} NMR ($CDCl_3$, 101 MHz, 298 K) δ_C: 14.2, 22.4, 22.7, 24.8, 28.5, 29.3, 31.8, 33.2, 65.7, 128.9, 129.1, 131.4, 134.8, 134.5. ppm**.** δ ^{31}P 42.75 ppm. IR (nujol) υ: 1724 (CO), 1735 (CO), 2182 (CC) cm^{-1}. UV-vis λ_{max} (ε / $M^{-1}cm^{-1}$) (MeCN) λ_{max} : 251 (20779), 306 (5000), 326 (4429) nm.

{[Au(PPh$_3$)]$_2$L^{15}}: To a round bottom flask encase in aluminium foil L^{15} (0.033 g, 0.071 mmol), [AuClPPh$_3$] (0.080 g, 0.162 mmol), potassium tertiary butoxide (0.024 g, 0.213 mmol) and ethanol (2 mL) were added and stirred under nitrogen for 12 h. Work-up as before. Yield: 0.071 g, 74 %. ^{1}H NMR ($CDCl_3$, 400 MHz, 298 K) δ_H: 3.26 (4H, s, (*H9*)), 5.41 (4H, s, (*H8*)), 7.22-7.52 (38H, m, (*H2, H3, H4, H6, H10*)), 7.62 (2H, d, (*H5)),* 7.68 (2H, d, (*H7*)), 7.93 (2H, d, (*H1*)) ppm. ^{13}C{^{1}H} NMR ($CDCl_3$, 101 MHz, 298 K) , δ_C: 65.2, 76.3, 125.7, 126.7, 126.9, 128.8, 129, 129.1, 131.4, 134.3, 134.5, 169.4 ppm. δ ^{31}P 42.75 ppm. IR (nujol) *υ*: 1736 (CO), 2329 (CC) cm^{-1}.UV-vis (ε / M^{-1} cm^{-1}) (MeCN) λ_{max}: 253 (1076), 273 (831) nm.

4.8. References:

1. J. L. Sebaugh. *Guidelines for accurate EC50/IC50 estimation*. Pharmaceut Statist., 2011, **10**, 128.
2. F. Scherbaum, A. Grohmann, B. Huber, C. Krüger and H. Schmidbaur, *Angew. Chem., Int. Ed. Engl*., 1988, **27**, 1544.
3. N. J. Long and C. K. Williams, *Angew. Chem. Int. Ed.*, 2003, **42**, 2586.
4. P. J. Stang and R. Tykwinski, *J. Am. Chem. Soc*., 1992, **114**, 4411.
5. V. W. W. Yam and S. W. K. Choi, *Chem. Soc. Rev.*, 1996, 4227.
6. A. Vogler and H. Kunkely, *Chem. Phys. Lett*, 1988, **150**, 135.
7. V. W. W. Yam and E. C. -C. Cheng, *Chem. Soc. Rev.*, 2008, **37**, 1806.
8. C.-M. Che and R. W.-Y. Sun, *Chem. Commun*., 2011, **47**, 9554.
9. V. W. W. Yam and K. K. –W. Lo, *Chem. Soc. Rev.*, 1999, **28**, 323.
10. P. J. Barnard, L. E. Wedlock, M. V. Baker, S. J. Berners-Price, D. A. Joyce, B.W. Skelton and J. H. Steer, *Angew. Chem. Int. Ed*., 2006, **45**, 5966.
11. M. J. Mckeage, L. Maharaj and S. J. Berners-Price, *Coord. Chem. Rev.*, 2002, **232**, 127.
12. M. Navarro, *Coord. Chem. Soc. Rev.*, 2009, **253**, 1619.
13. L. A. Mullice, F. L. Thorp-Greenwood, R. H. Laye, M. P. Coogan. B. M. Kariuki and S. J. A. Pope, *Dalton. Trans*., 2009, 6836.
14. C. A. Tolman, *Chem. Rev.*, 1977, **77**, 313.
15. T. E. Müller and D. M. P. Mingos, *Transition Met. Chem.*, 1995, **20**, 533.
16. www.docholliday.homecall.co.uk/research/tolman.html.
17. M. C. Laguanas, C. M. Fierro, A. Pintado-Alba, H. de la Riva and S. Bentanzos-Lara, *Gold Bulletin.*, 2007, **40**, 135.
18. W. J. Hunks, M. A. MacDonald, M. C. Jennings and R. J. Puddephatt, *Organometallics.*, 2000, **19**, 24.
19. P. J. Barnard and S. J. Berners-Price, *Co-ord. Chem. Rev*., 2007, **251**, 1889.
20. J. J. Liua, P. Galettisa, A.Farra, L. Maharaja, H. Samarasinhaa, A. C. McGechana, B. C. Baguleyb, R. J. Bowenc, S. J. Berners-Price and M. J. McKeage, *J. Inorg. Biochem*., 2008, **102**, 303.
21. C. K. Mirabelli, R. K. Johnson, D. T. Hill, L. F. Faucette, G. R. Girard, G. Y. Kuo, C. Sung and S. T. Crooke, *G. Med. Chem*., 1986, **29**, 218.
22. J. Li and P. Pyykko, *Chem. Phys. Lett*., 1992, **197**, 586.
23. O. Gevert, J. Wolf and H.Werner, *Organometallics*., 1996, **15**, 2806.
24. J. M. Forward, D. Bohmann, J. P. Fackler and R. J. Staples., *Inorg. Chem*., 1995, **34**, 6330; (b) M. A. Mansour, W. B. Connick, R. J. Lachicotte, H. J. Gysling and R. Eisenberg, *J. Am. Chem. Soc*., 1998, **120**, 1329.
25. V. W. W. Yam, C. L. Chan, C. K. Li and K. M. C. Wong, *Coord. Chem. Rev*., 2001, **216**, 173.
26. R. J. Puddephatt, *Comprehensiv Coordination Chemistry, Vol. 5.* Pergamon, Oxford, 1987, 861.
27. E. Schuh, S. M. Valiahdi, M. A. Jakupec, B. K. Keppler, P. Chiba and F. Mohr, *Dalton. Trans*., 2009, 10841.
28. J. Strähle, *Gold, Progress in Chemistry, Biochemistry and Technology*, ed. H. Schmidbaur, Wiley, Chichester, 1999.
29. E. J. Fernández, A. Laguna, J. M. López, M. Monge, M. Montiel, M. E. Olmos, J. Pérez and M. Rodriguez-Castillo, *Gold Bulletin*., 2007.
30. S. E. Thwaite, A. Schier and H. Schmidbaur, *Inorg. Chim. Acta*., 2004, **357**, 1549.
31. R. Galassi, A. Burini, S. Ricci, M. Pellei, M. P. Rigobello, A. Citta, A. Dolmella, V. Gandin and C. Marzano, *Dalton. Trans*., 2012, **41**, 5307.
32. V. Ramamorthy, Z. Wu, Y. Yi and P. R. Sharp, *J. Am. Chem. Soc.*, 1992, **114**, 1526.

33. J. Vicente, M. T. Chicote and R. Guerrero, *Inorg. Chem.*, 1997, **36**, 4438.
34. J. J. Li and P. R. Sharp, *Inorg. Chem.*, 1994, **33**, 2.
35. V. W. W. Yam, K. L. Cheung, S. K. Yip and K. K. Cheung, *J. Organomet. Chem*.,2003, **681**, 196.
36. M. V. Baker, P. J. Barnard, S. J. Berners-Price, S. K. Brayshaw, J. L. Hickey, B. W. Skelton and A. H. White, *J. Organomet. Chem*.,2005, 690, 5625.
37. W. Carruthers, *Modern Methods Of Organic Chemistry*., 4th Ed, University of Sheffield. 2004.
38. R. Mosteiro, A. Fernández, M. López-Torres, D. Vázquez-García, J. J. Fernández and J. M. Vila, *N. J. Chem.*,2002, **26**, 1425.
39. R. J. Puddephatt,.*Chem.Commun*., 1998, 105.
40. R. Uson, A. Laguna, M. Laguna, D. A. Briggs, H. H. Murray and J. P. Fackler, *Inorg. Synth*, 1989, **26**, 85; (b) P. Sinah, A. K. Wilson and M. A. Omary, *J. A. Chem. Soc*, 2005, **127**, 12488.
41. F. Caruso, M.Rossi, J. Tanski, C. Pettinari and F. Marchetti *J. Med. Chem*., 2003, **46**, 1737.
42. R. C. Bott, G. A. Bowmaker, R. W. Bucklery, P. C. Healy and M. C. S. Perera, *Aust. J. Chem*., 1999, **52**, 271.
43. P. Pyykkö, J. Li, and N. Runeberg, *Chem. Phys. Lett*., 1994, **218**, 133.
44. R. J. Puddephatt,*Chem.Commun*., 1998, 105.

Chapter 5. Luminescent Mono- and Di-Metallic Au(I) Complexes Incorporating Anthraquinone-Based Ligands Towards Dual-Functional Therapeutic And Cellular Imaging Applications.

5.1. Introduction

Despite the increasing interest in Au(I) species as therapeutic and cellular imaging agents, limited research has been dedicated to combining these properties within a single entity. Following on from the series of alkyl and aryl Au(I) alkyne based complexes discussed in Chapter 4, this chapter looks at the synthesis of a series of aromatic, mono- and di-metallic Au(I) alkyne based complexes for suitability as both therapeutic and cellular imaging agents. Through varying the nature of the aromatic functional groups attached to the alkyne Au(I) units, a novel series of complexes was synthesised and their synthesis, photophysical and cytotoxic properties, as well as their cellular imaging properties are reported herein.

5.1.1. Heterocycles in therapeutics and luminescence

The addition of Au(I) and Au(III) to existing antitumor agents can lead to enhanced antitumor activity, however, there exists several reports highlighting the cytotoxic behaviour of aromatic compounds in the absence of Au(I). Bair *et al*.[1] reported the synthesis of a series of polyaromatic propane diol derivatives which displayed a dependency of antitumor activity on the shape of the aromatic system. A more detailed discussion by Becker *et al*.[2] reporting a series of lipophilic aromatic amines, discussed the effects of varying, aliphatic chain length, aromatic ring size and the terminal heterocyclic ring on the cytotoxicity of the compounds. The more interesting observation within the series was seen with the nature of the linkers, amine and amide. The amines (which were formed *via* a reduction of the amides) displayed increased cytotoxic activity when compared to their precursors. Additionally, this series of complexes reported that the functional groups incorporated inside the heterocyclic ring and the ring size did affect the cytotoxic profile, however the length of the aliphatic chain and the incorporation of a double bond did not.[2]

5.1.2. Anthraquinone

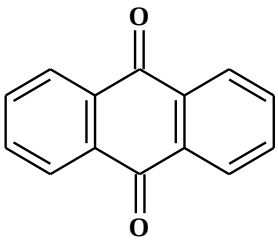

Figure 5.1 Anthraquinone.

Anthraquinones, otherwise referred to as anthracenedione, are used as the building blocks of many important organic compounds; anthraquinones and their derivatives can be found in dyes, as a bird repellent in seeds, but more importantly they are found in abundance in pharmaceuticals.[3] Although anthraquinone based compounds have been extensively studied, studies on their photophysical and therapeutic properties have been conducted separately.

5.1.2.1.Cytotoxic studies of anthraquinones

Cytotoxic studies on anthraquinone based complexes have been conducted with several reports on DHAQ suggesting their potential to act as antitumor agens.[4,5,6] Reports by Ahn *et al*. have documented good antitumor activity for a range of derivatives of anthraquninones including 2-(1-hydroxyalkynyl)- and 2-(1-alkoxy-alkynyl)- 1,4-dihydroxyalkynyl complexes[5] and 2-(1-hydroxyalkyl)-anthracene-1,4,9,10-tetraones complexes.[6] Additionally, this group have reported the incorporation of chlorambucil, a known chemotherapy drug, into a 1,4-DHAQ unit (*via* an ester unit) with varying aliphatic chain lengths and substituents in the 2 position of the aromatic ring (Figure 5.2). From the 12 new complexes investigated, 2 esters (R=H and R=phenyl) gave cytotoxic values higher than that of unmodified chlorambucil. The complexes followed a trend that indicated that the toxicity of compounds of this nature was dependent on the size of the alkyl group.[7] The anti-tumor activity of anthraquinones is thought to be due to the intercalation of the planar ring system between the base pairs of the DNA, resulting in an inhibition of DNA transcription and replication.

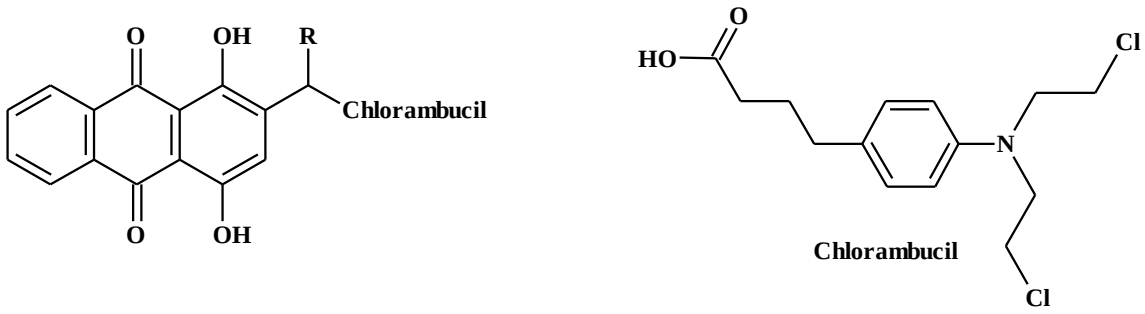

Figure 5.2 1,4 DHAQ incorporating chlorambucil and the structure of chlorambucil (RHS).

5.1.2.2.Luminescent properties of anthraquinones

DHAQ, unlike AQ is a coloured chromophore. The presence of the hydroxyl groups on DHAQ allows intramolecular hydrogen bonding to occur between the donor group (OH) and the accepter group (CO). In the excited state the phenolic OH is more acidic and the carbonyl oxygen is more basic which results in proton transfer. This proton transfer leads to significant changes in the electronics and fluorescent properties of the molecule. Therefore the dual fluorescence properties exhibited by molecules of this type are attributed to ESIPT (excited state, intramolecular proton transfer) from the S1 states of the two tautomer forms, the enol and keto forms (Figure 5.3) The energy barrier for ESIPT increases with polarity of the solvent and varies with the position of the OH; ESIPT does not occur with 1-4-DHAQ.[8,9]

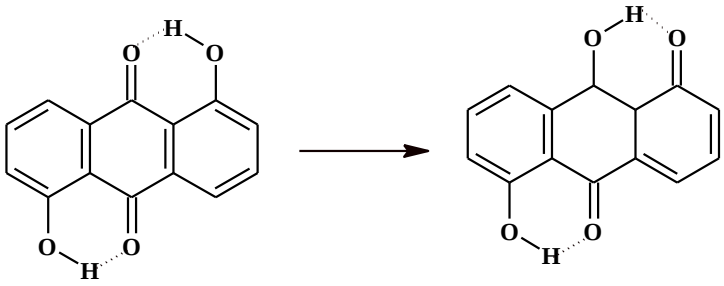

Figure 5.3 1,5 DHAQ, intramolecular hydrogen bonding displayed; enol form (LHS), keto form (RHS).

5.1.3. Cell imaging with Au(I) species

The application Au(I) complexes as cellular imaging agents, when compared to their application as therapeutic agents (discussed in detail in Chapter 1 and Chapter 4), has received considerably less attention with only a few examples to date having been reported, some of which are discussed below.

Ott *et al*.[10] have reported a series of four Au(I) complexes based on the lipophilic, cell growth inhibiting compound, naphthalimide. The four complexes varied *via* the substituent bound to the phosphine (Figure 5.4). All four complexes gave an IC_{50} value in the range of 1.1-3.7 μM. Low cell uptake was observed for the toxic [$AuClPPh_3$] precursor complexes. Cellular biodistribution studies were carried out on the two complexes inclusive of R = $P(CH_2CH_3)_3$ and R=PPh_3 and uptake into the nuclei was observed. [10]

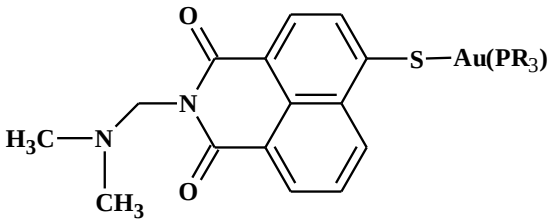

R = CH_3 / CH_2CH_3 / $C(CH)_3$ / C_6H_5

Figure 5.4 Complexes reported by Ott *et al.*[10]

Aswell as reporting a mechanistic explanation for the favourable antitumor properties of Au(I) phosphine complexes (discussed in detail in Chapter 4), Berners-Price *et al.*[11] have reported the first example of an Au(I) NHC based complex in cellular imaging (Figure 5.5); in compound **A** and **B** the Au(I) centres are 'locked' with a separation for **A** of 3.0484 (3) Å and **B** 3.79417 (4) Å. The emissive nature of compound **A** was attributed to the shorter Au-Au distance, however, its luminescence properties are such that they would damage the cells if imaged since high energy irradiation was required; λ_{ex} = 260 nm, λ_{em} = 400 nm. Compound **C** gave the smaller Au-Au distance of 2.9582 (4) Å with the more favourable luminescence properties, λ_{ex} = 355 nm, λ_{em} = 496 nm for cell imaging. Compound **C** was incubated with RAW264.7 cells (a mouse macrophage cancer cell line) and co-localisation studies with both a lysosomal and mitochondrial dye were carried out showing clear localisation of Compound **C** in lysosomes only (Figure 5.6).[11] The cellular distribution of a series of Au(I) alkynyls has also been reported with the distribution of the Au(I)-alkyne complex throughout the cells rather than limited to one area.[11]

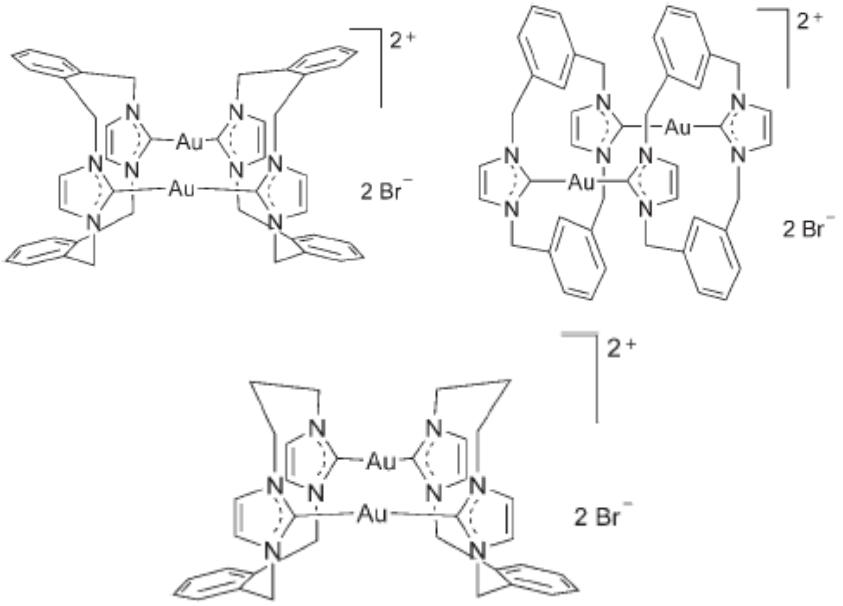

Figure 5.5 Complex A (top LHS), B (top RHS) and C (bottom). Reproduced from ref 11.[11]

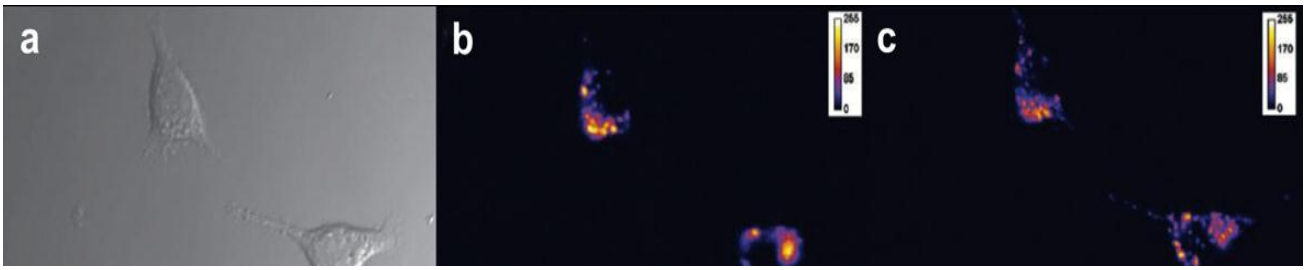

Figure 5.6 Cell imaging with Compound C. Bright field image (LHS), luminescence image (centre) and lysosome stain (RHS). Reproduced from ref. 11.

The cellular imaging and distribution studies of the highly cytotoxic Au(I) complexes discussed above highlight an inconsistency with the proposed mitochondrial pathway to apoptosis in cancer cells discussed in Chapter 4; none of the complexes discussed above reveal mitochondrial staining. As these are only a few examples of cellular imaging with therapeutic agents (allowing the cellular distribution of a complex to be viewed) a noticeable rise in the need for this new method of analysis for the apoptosis mechanism is realised.

5.2. Overview

The exploitation of aurophillic interactions (and thus the luminescent properties which result) can allow the cellular distribution of therapeutic agents to be viewed, but to date, compounds of this type are yet to be fully explored. Taking into account previous reports where-by Au(I) units were added onto already known antitumor aromatics, the initial aromatic compounds chosen for co-ordination onto the Au(I) alkyne unit was coumarin (Chapter 3 reports cytotoxic nature of Re(I)-coumarin to MCF-7 cells) and anthracene. Thereafter, anthraquinones were investigated. The successful synthesis of Au(I)-alkyne based complexes in Chapter 4 resulted in its continued use throughout this chapter. Herein, the synthesis of a novel series of aromatic, mono- and di-metallic Au(I) complexes are reported and their dual suitability as therapeutic and cellular imaging agents discussed.

5.3. Results and discussion

5.3.1. Synthesis and characterisation of ligands

Despite $\mathbf{L^1}$-$\mathbf{L^4}$ being reported previously in research, their photophysical data has been reported herein for easy referral when discussing the novel Au(I) complexes of $\mathbf{L^1}$, $\mathbf{L^2}$ and $\mathbf{L^4}$. The Au(I) complex of $\mathbf{L^3}$ has also been reported previously, however, the cellular imaging properties of the complex have yet to be investigated.

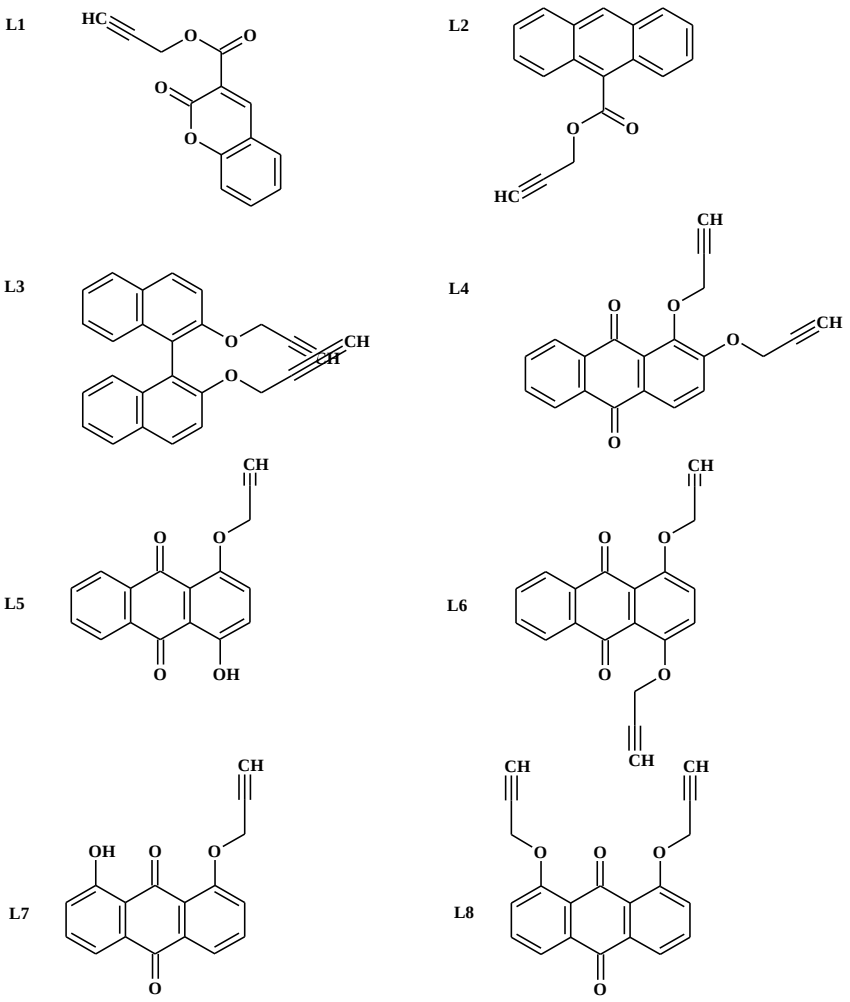

Figure 5.7 Synthesis of ligands: L^1 and L^2, reagents; acid chloride, propargyl alcohol, TEA, $CHCl_3$, 61 ˚C, 3 h: L^{3-8}; propargyl bromide, excess carbonate, acetone, Δ, 2-5 days.

$\mathbf{L^1}$ and $\mathbf{L^2}$ were synthesised *via* the production of coumarin-3- and anthracene-9- acyl chlorides, respectively. These syntheses were achieved by heating coumarin-3-carboxylic acid or anthracen-9-carboxylic acid in excess thionyl chloride (2 mL) and catalytic DMF at 71 ˚C for 3 hours. The precursors were dried thoroughly and added to propargyl alcohol and TEA in chloroform. Purification of the ligands was achieved using column chromatography producing $\mathbf{L^1}$ and $\mathbf{L^2}$ in good-to-excellent yields of 71 % and 86 % respectively.

L^{3} to **L**^{8} were synthesised following literature methodology. The relevant phenolic starting materials, which are all commercially available, were reacted with propargyl bromide, in the presence of excess potassium carbonate *via* an S_N2 nucleophilic substitution reaction. Both the reaction time and the base used had an influence on the nature and yields of the products formed. Since literature reports the use of potassium carbonate as the base, this was incorporated into the production of **L**^{3} and **L**^{4} both of which were formed in moderate yields, 29 % and 40 % respectively, and required no further purification. When changing the base from potassium to sodium carbonate the yields of **L**^{6}, **L**^{7}, and **L**^{8} were increased and these yields are reported herein.

The observation of a shift downfield for the peak in the ^{1}H NMR spectra between +4.51 and +5 ppm corresponding to the *CH*$_2$CCH unit for **L**^{1}-**L**^{8} confirmed the formation of the ether/ester units. MS and HRMS analysis for each of the ligands showed peaks corresponding to the parent $[M]^+$ for **L**^{5}-**L**^{8} and $[M+H]^+$ for **L**^{4}. **L**^{5} also showed a peak corresponding to $[M-C_3H_2]$ and both **L**^{6} and **L**^{8} showed peaks corresponding to $[M-C_3H_3]^+$ resulting from the loss of a propargyl radical. Both the IR and UV-Vis data for each ligand are reported in Table 5.4.

Different isomers of di-hydroxy anthraquinone, when reacted with propargyl bromide, showed varying results with respect to the nature and the yields of the products formed. These results are summarised in Table 5.1. The di-alkyne ligand of the 1,2-isomer, **L**^{4}, required no purification as only the dimer was produced. However, the production of di-alkyne, 1,4- and 1,8- isomer of **L**^{6} and **L**^{8} respectively, under the same conditions produced a mixture of products (using either sodium or potassium carbonate) and so further purification *via* column chromatography was required. Column chromatography isolated both mono- and di-alkyne ligands, in poor yields in both cases. Increasing the reaction time by an additional 48 hours resulted in a yield increase for the production of the di-alkyne ligands, **L**^{6} and **L**^{8} (**L**^{6} 3 days: 5.6 %, 5 days: 31 %) (**L**^{8} 3 days: 14.3 %, 5 days: 54 %). The synthesis of mono- and di-alkyne ligands based around the 1,5-dihydroxy anthraquinone isomer produced **L**^{9} and **L**^{10}, however, due to the poor yields obtained (**L**^{9}, 4 % and **L**^{10}, 3 %) it was decided the synthesis of the complexes would not be attempted. The difference in the reactivity of the di-hydroxy anthraquinones can be attributed to the electronic properties of the compounds and the reactivity of the phenoxide groups.

Table 5.1 Reactivity of anthraquinones; percentage yields varied with time.

Di-hydroxy anthraquinone	% after 3 days		% after 5 days	
1, 2	Dimer	40		
1, 4	Monomer	15	-	
	Dimer	5.6	Dimer	31
1, 5	Monomer	4	Monomer	4
	-		Dimer	3
1, 8	Monomer	13.4	-	
	Dimer	14.3	Dimer	54

5.3.2. Synthesis and characterisation of the complexes

The alkynes were reacted following the same method as Chapter 4, however, the work up was slightly modified in the cases where a di-metallic Au(I) complex was produced as a result of a precipitate being formed; the precipitate was filtered, dissolved in DCM and re-filtered to remove the salt. Each complex was purified by recrystallization using vapour diffusion of diethyl ether into a concentrated THF solution. Again, the use of THF proved necessary as prolonged exposure to chlorinated solvents resulted in the breakdown of complexes to the Au(I)- starting material [AuClPPh$_3$]. The soluble complexes were characterised by ^{1}H and ^{31}P NMR and IR spectroscopies.

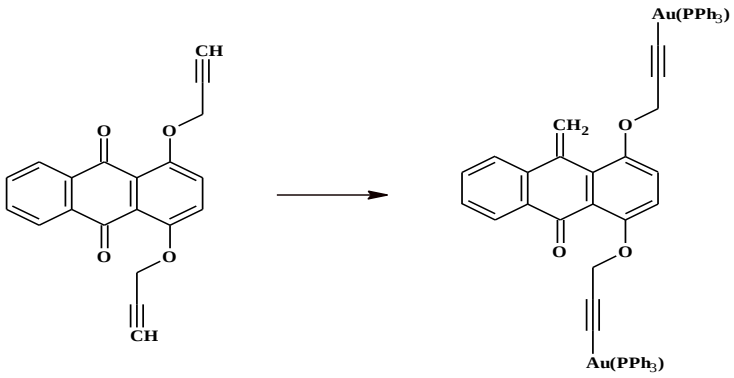

Figure 5.8 Synthesis of {[Au(PPh$_3$)]$_2$L^4}. Reagents: [AuClPPh$_3$], K^{+t}BuO$^-$, ethanol, N$_2$(g), RT.

^{1}H NMR spectra were obtained for each complex in $CDCl_3$. For each complex there was an absence of the terminal alkyne proton $CH_2CC\mathit{H}$ peak seen in the free ligand and a shift of propargyl CH_2, H_2CC-, to higher frequency. The latter peak was seen as a singlet in the region +4.5 to +5.0 ppm. For [Au(PPh$_3$)L$^{1/2}$] a shift in the aromatic protons adjacent to the ester gold unit to lower frequency was also displayed. The tri-phenyl phosphine proton resonances were typically broad and in most cases superimposed with the co-ordinated ligand aromatic protons. For [Au(PPh$_3$)L^{5}] and {[Au(PPh$_3$)]$_2$L$^{6/8}$} broad proton resonances were seen in the region of +7.23 to +7.5 ppm integrating to 15H and 30H respectively.

^{31}P{^{1}H} NMR spectra for [Au(PPh$_3$)L$^{1/2}$] gave a signal in the range of +29 to +30 ppm. For the mono-metallic, [Au(PPh$_3$)L^{5}] and the di-metallic {[Au(PPh$_3$)]$_2$L^{3,4,6,8}} complexes a shift of +42 ppm was displayed. All of the complexes gave a single peak in the ^{31}P NMR spectra indicating the symmetrical nature of the di-metallic Au(I) complexes. The difference in ^{31}P NMR shifts can be explained in terms of the donating ability of the alkyne; [Au(PPh$_3$)L$^{1/2}$] displayed peaks at a lower frequency, which are attributed to the ester oxygen being more electron withdrawing (when compared to the ether unit for **L$^{3-6,8}$**) which leads to strengthening of the CC bond. This was confirmed through IR studies where both [Au(PPh$_3$)L$^{1/2}$] displayed an increase in the value of ν(CC) upon co-ordination with enhancements of 190 cm^{-1} and 55 cm^{-1} respectively.

Solid state IR studies were carried out for all complexes which showed subtle changes in the ν(CC) when compared to the free ligand. The ligands display an IR stretch similar to the precursor, propargyl alcohol with a shift at 2120 cm^{-1} whereas the complexes displayed a weaker IR absorption band ranging from 2132-2252 cm^{-1} for the alkyne stretch. This slight shift to a higher wavenumber corresponds to a decrease in the difference of electronegativity between the terminal proton and the Au(I) unit and thus an increase in the strength of the alkyne bond was observed (Table 5.4). Similarly to the complexes discussed in Chapter 4, MS analysis for each of the complexes gave a peak at 721 only

5.3.3. Single crystal X-ray diffraction studies

Re-crystallisation of complexes $[Au(PPh_3)L^2]$ and $\{[Au(PPh_3)]_2L^{3/8}\}$ by vapour diffusion of diethyl ether into a concentrated THF solution yielded pale orange crystals suitable for X-ray diffraction studies. $\{[Au(PPh_3)]_2L^3\}$ has been reported previously but is included herein for comparison.

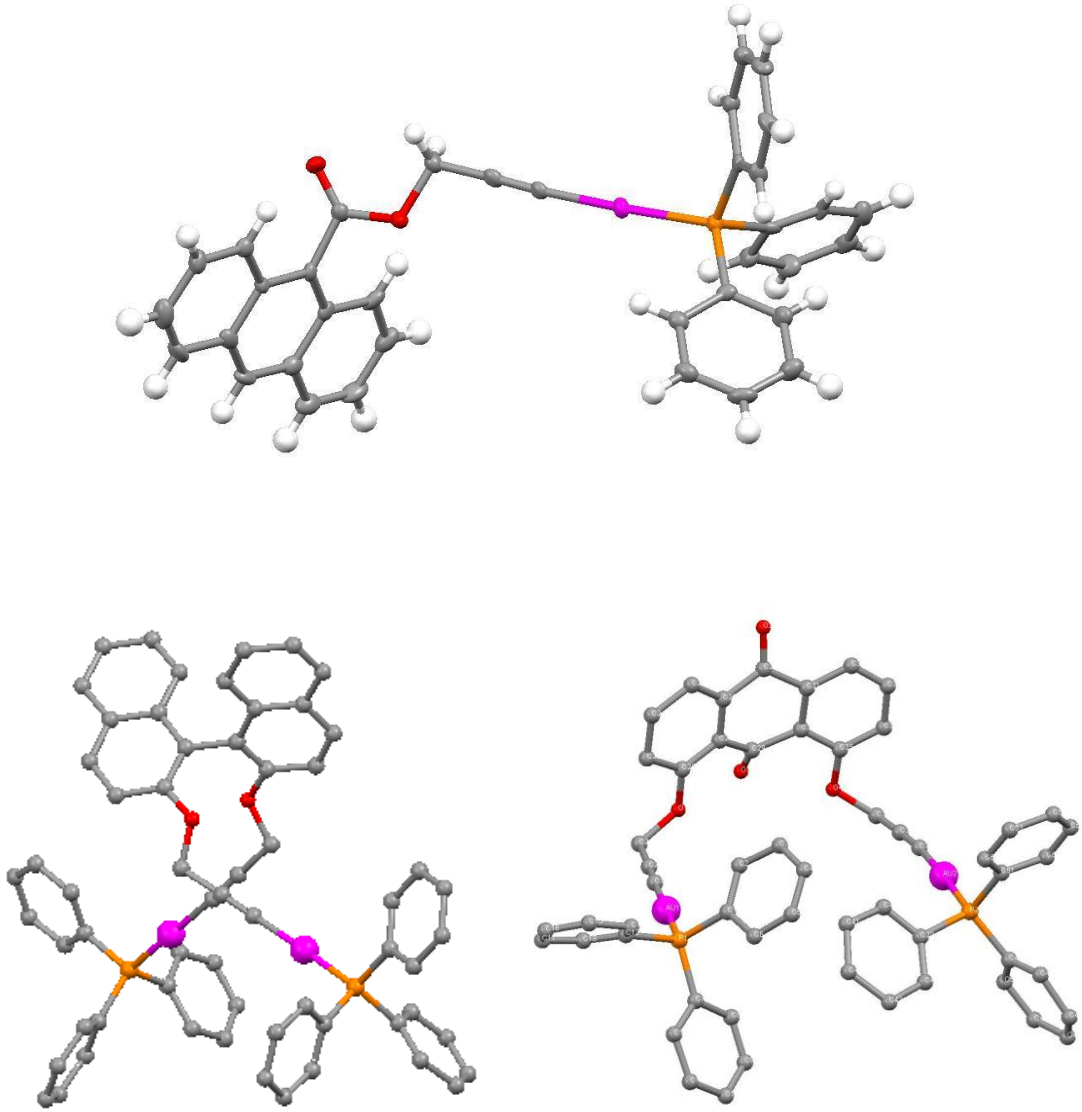

Figure 5.9 Structural representations of complexes $[Au(PPh_3)L^2]$ (top) and $\{[Au(PPh_3)]_2L^{3/8}\}$ (bottom LHS and bottom RHS respectively) (H atoms omitted for clarity).

The parameters associated with the data collections of the complexes $[Au(PPh_3)L^2]$ and $\{[Au(PPh_3)]_2L^{3/8}\}$ (Table 5.3) and the selected bond lengths and bond angles (Table 5.2) are shown below. As the $\{[Au(PPh_3)]_2L^3\}$ has been reported previously it is not discussed in greater detail herein.

For the anthracene based structure of $[Au(PPh_3)L^2]$, the C-Au-P bond angle does not show substantial deviations from linearity, 177 °. The Au-P bond length of 2.27 Å and the Au-C bond length of 2.025 Å, were both consistent with other gold(I)-acetylide complexes reported, additionally, both bond lengths were longer than those of the $[AuClPPh_3]$ starting material, consistent with the stronger *trans* influence of the acetylene group when compared to the chloride.[12-14] The C≡C bond length for complex, 1.15 Å, was again normal for complexes of this type. No evidence of intermolecular contacts between the Au(I) units was observed.[15,16]

Similarly to the $[Au(PPh_3)L^2]$ structure, the average C-Au-P bond angle does not deviate from linearity for $\{[Au(PPh_3)]_2L^8\}$ with both the Au-P and Au-C bond lengths in agreement with the literature values for gold(I)-acteylide complexes. The structure for $\{[Au(PPh_3)]_2L^8\}$ is however, slightly more interesting than that of $[Au(PPh_3)L^2]$ with the anthraquinone unit showing deviation for the planar unit expected. The structure of the non-planar anthraquinone unit shows an open-book conformation with an angle between the two terminal rings of approximately 161°. No evidence of intra- or intermolecular contacts between any Au(I) units can be seen but π-stacking was observed between the aromatic units in the packing of the asymmetric units; close contacts (closer than van der Waals radii) between adjacent molecules involving the phenyl units of the phosphine ligands and the anthraquinone rings reveal intra- and intermolecular π stacking which resulted in the unexpected conformation of the anthraquinone unit.

Table 5.2 Selected bond lengths and bond angles for the complexes: $[Au(PPh_3)L^2]$, $\{[Au(PPh_3)]_2L^3\}$ and $\{[Au(PPh_3)]_2L^8\}$.

$[Au(PPh_3)L^2]$		**$\{[Au(PPh_3)]_2L^3\}$**		**$\{[Au(PPh_3)]_2L^8\}$**	
$C_{36}H_{26}AuO_2P$				$C_{58}H_{38}Au_2Cl_6O_4P_2$	
		Bond Lengths (Å)			
Au-P	2.266 (2)	Au-P	2.227	Au-P	2.277 (4)
Au-C	2.025 (7)	Au-C	2.034	Au-C	2.01 (2)
C-C	1.15 (1)	C-C	1.16	C-C	1.13 (3)

Table 5.3 Crystal data collection and refinement details for the crystal structures of $[Au(PPh_3)L^2]$ and $\{[Au(PPh_3)]_2L^8\}$.

	$[Au(PPh_3)L^2]$	$\{[Au(PPh_3)]_2L^8\}$
Empirical formula	$C_{36}H_{26}AuO_2P$	$C_{58}H_{38}Au_2Cl_6O_4P_2$
Formula weight	718.50	1467.46
Temperature	150(2) K	293 K
Wavelength	0.71013 Å	0.71013 Å
Crystal system	Orthorhombic	Monoclinic
Space group	P b c a (61)	P2(1)/n (14)
Unit cell dimensions	a = 9.974 (2) Å	a = 18.4561 (9) Å
	α = 90.00 ˚	α = 90.00 ˚
	b = 17.5178 (3) Å	b = 11.6603 (5) Å
	β = 90.00˚	β = 98.614 (2)˚
	c = 32.8694 (8)	c = 26.6071 (7) Å
	ϒ =90.00˚	ϒ =90.00˚
Volume	5743.08 (3) $Å^3$	5661.4 $Å^3$
Z	8	4
Density (calculated)	1.662 g/cm^3	1.722 g/cm^3
F(000)	2816	2832
Crystal size	0.25 × 0.25 × 0.20	
Theta range for data collection	55.8	55.1
All reflections	12222	22508
Independent reflections	6652	12700
Observed reflections	4564	6204
Goodness-of-fit on F	1.096	1.018
R_{int}	0.0613	0.1312
Final R indices [I>2sigma(I)]	R_1 = 0.0695	R_1 = 0.0999
	wR_2 = 0.1027	wR_2 = 0.2248
R indices (all data)		

5.3.4. UV-Vis absorption spectroscopy

The UV-Vis data are summarised in Tables 5.4 and 5.5. The high energy transitions around 250 nm are attributed to ^{1}IL ($\pi \rightarrow \pi^*$) or metal perturbed ^{1}IL transitions. The low energy absorptions in the regions of 330 nm are indicative of ligand to ligand charge transfer (^{1}LLCT) transitions from the π orbital on the alkyne ligands. The anthraquinone based ligands and their complexes show an additional absorption in the region of 375-448 nm, this transition is assigned to a charge transfer transition with substantial $\pi \rightarrow \pi^*$character.

Table 5.4 Photophysical data for the ligands.

Compound	Abs	ε dm^3 mol^{-1} cm^{-1}	Em(MeCN)	Lifetimes (MeCN) ns	CC (Cm^{-1})
L^1	-	-	395	-	2062
L^2	-	-	460	-	2129
L^3	-	-	345	-	2117
L^4	276 359	3437 1050	398	-	2129
L^5	270 326 432	2448 1501 1252	409 532-560	-	2115
L^7	254 408	2432 11951	-	-	2034
L^8	254 374	29230 10428	505	-	2130

Table 5.5 Photophysical data for the complexes.

Compound	Abs	ε dm^3 mol^{-1} cm^{-1}	Em(MeCN)	Lifetimes (MeCN) ns	CC (Cm^{-1})
$[Au(PPh_3)L^1]$	220 286	10017 7154	434-494	5.65	2252
$[Au(PPh_3)L^2]$	224 251	10071 4173	452	6.7	2184
$\{[Au(PPh_3)]_2L^3\}$	228 329	17519 2860	369	< 2	2132
$\{[Au(PPh_3)]_2L^4\}$	212 273 375	15998 5542 1430	415 435	5.4	2184
$[Au(PPh_3)L^5]$	272 448	24360 10639	406 538-566	2 <	2133
$\{[Au(PPh_3)]_2L^6\}$	250 406	12700 1790	411-438 524	4.08	2246 2133
$\{[Au(PPh_3)]_2L^8\}$	257 397	19593 4700	491	2.53	2239

5.3.5. Luminescence spectroscopy

There have been a number of reports discussing the luminescent properties of hydroxy anthraquinone compounds; however, there have been no reports on the properties of alkynyl anthraquinones. Luminescence spectra were obtained in aerated acetonitrile following irradiation at λ_{ex} 340 nm and 405 nm. The luminescence data for the Au(I) complexes and their ligands are shown in Tables 5.4 and 5.5 respectively and are discussed in the following sections.

5.3.5.1.Luminescence properties of $[Au(PPh_3)L^{1/2}]$ and $\{[Au(PPh_3)]_2L^3\}$

Upon excitation at 340 nm $\{[Au(PPh_3)]_2L^3\}$ displayed a single broad emission band around 380 nm, this was a blue-shifted emission when compared to that of $[Au(PPh_3)L^{1/2}]$ and can be attributed to reduced conjugation within the ligand (Figure 5.10). Both $\{[Au(PPh_3)]_2L^{1/2}\}$ displayed emission around 480 nm in solution. $[Au(PPh_3)L^2]$ emission bands can be attributed to the chromophoric unit as these wavelengths are similar to those of their ligands, *i.e.* ^{1}IL ($\pi\rightarrow\pi^*$). $[Au(PPh_3)L^1]$ displayed a red-shifted emission when compared to the ligand (**L^1**, 395 nm, $[Au(PPh_3)L^1]$, 434-494 nm), indicating an effect of the $[AuPPh_3]^+$ unit, and is attributed to ^{1}IL/^{1}LLCT possibly with mixed character of CC ($\pi\rightarrow\pi^*$) and Au-P ($\sigma\rightarrow\pi^*$) CC.

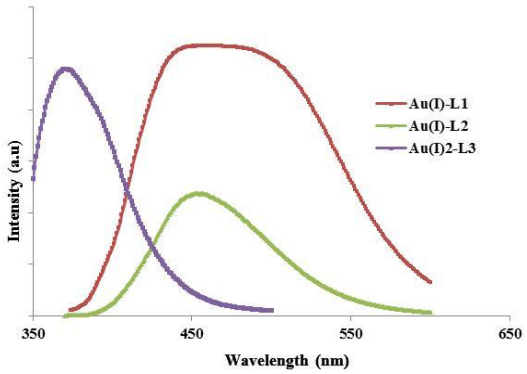

Figure 5.10 Emission spectra of $[Au(PPh_3)L^{1/2}]$ and $\{[Au(PPh_3)]_2L^3\}$ (λ_{exc} = 340 nm).

The lifetime measurements for all three complexes were recorded with an excitation of 295 nm and detection wavelengths of 380 nm for $\{[Au(PPh_3)]_2L^3\}$ and 480 nm for $[Au(PPh_3)L^{1/2}]$. A decay profile best fitting a single-exponential decay provided corresponding short-lived lifetimes for each complex in solution of < 5 ns, and thus emission was assigned as a short-lived ^{1}IL ($\pi \rightarrow \pi^*$) fluorescence.

5.3.5.2.Luminescence properties of $[Au(PPh_3)L^5]$

Following excitation at 340 nm, $[Au(PPh_3)L^5]$ displayed dual emission with a band *ca.* 430 nm and a broader band at *ca.* 550 nm. The lower energy band was attributed to AQ chromophore, whilst the higher energy band may be ^{1}IL (CC $\pi \rightarrow \pi^*$). The ligand-centred nature was confirmed through very short-lived lifetime values, < 2 ns. In order to probe the charge transfer nature of the low-energy band, different polarity solvents were used, revealing significant changes in the intensity of the band (Figure 5.11).

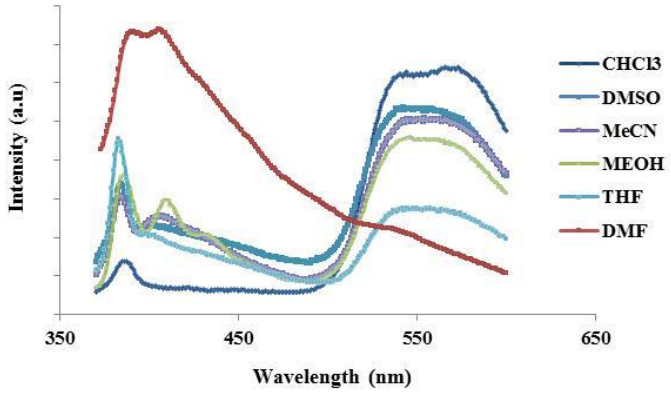

Figure 5.11 Emission spectra of $[Au(PPh_3)L^5]$ in different solvents (λ_{exc} = 340 nm)

5.3.5.3. Luminescence properties of $[Au(PPh_3)L^5]$ and $\{[Au(PPh_3)]_2L^{4/6/8}\}$

Following excitation at 340 nm for the complex $\{[Au(PPh_3)]_2L^6\}$, two emission bands were seen, at 411-438 nm, and 524 nm, but the emission profile for $\{[Au(PPh_3)]_2L^6\}$ is very different to its free ligand where only one emission band was seen with λ_{max} at 487 nm (Figure 5.12). The spectrum of $\{[Au(PPh_3)]_2L^6\}$ showed the appearance of a new band at 411-438 nm, and a red-shifted emission at 524 nm. The similarity of the di-metallic complex, $\{[Au(PPh_3)]_2L^6\}$, to the mono-metallic complex, $[Au(PPh_3)L^5]$, indicated the ligand based emission was effected by the presence of the $[AuPPh_3]^+$, the presence of the $[AuPPh_3]^+$ units in the dimer influence the electronics of the ligand in a similar fashion to the OH group on the monomer (Figure 5.12). This emission pattern is indicative of ^{1}ILCT / ^{1} LLCT possibly with mixed character of CC ($\pi \rightarrow \pi^*$) and Au-P ($\sigma \rightarrow \pi^*$) CC. The lifetime of the di-metallic Au(I) complex was larger than the monomer, however with a lifetime of < 10 ns only singlet character, ^{1}ILCT (π-π^*) / ^{1}LLCT, can be assigned with certainty.

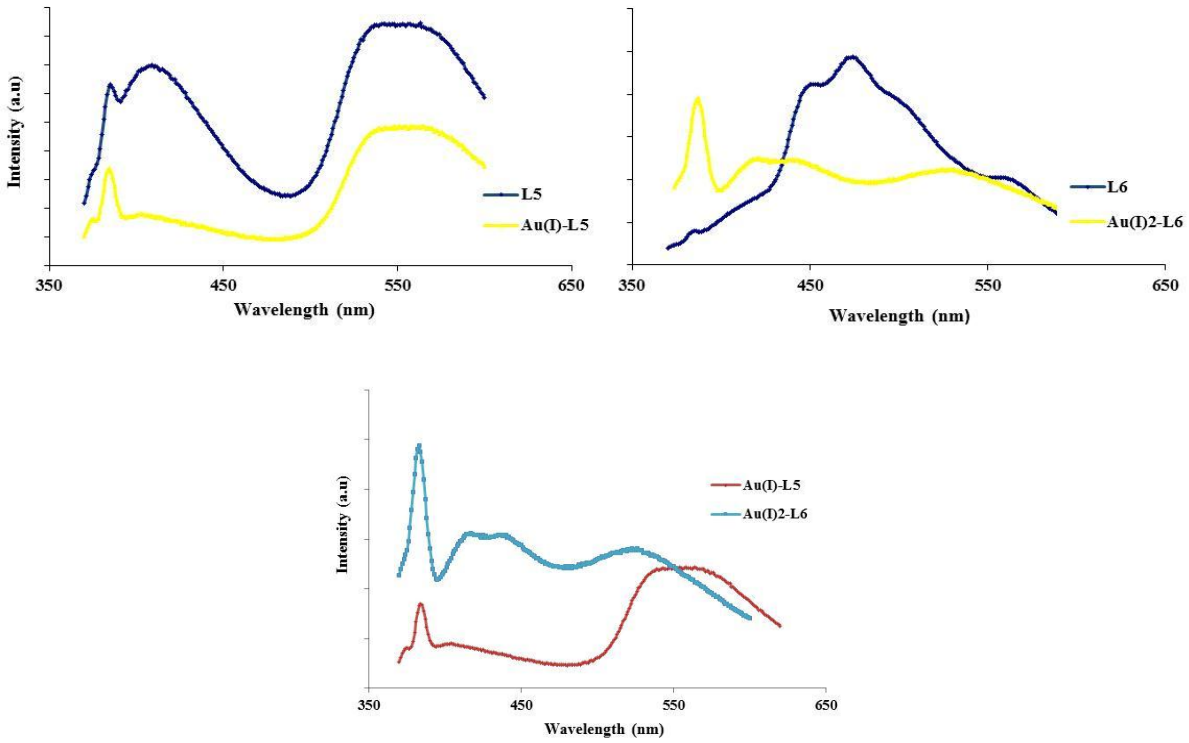

Figure 5.12 Emission spectra of L^5 with $[Au(PPh_3)L^5]$, L^6 with and $\{[Au(PPh_3)]_2L^6\}$ and $[Au(PPh_3)L^5]$ with $\{[Au(PPh_3)]_2L^6\}$. (λ_{exc} = 340 nm).

5.3.5.4. Luminescence properties of $\{[Au(PPh_3)]_2L^{4/8}\}$

For the remaining two complexes, $\{[Au(PPh_3)]_2L^{4/8}\}$, excitation at 340 nm resulted in the emission spectra displaying a single broad structure-less emission band with λ_{max} values similar to the free ligand ^{1}ILCT attributed to the chromophoric anthraquinone unit (Table 5.6). The contribution of phosphorescence (^{3}ILCT ($\pi \rightarrow \pi^*$)) has been negated due to the short-lived lifetimes, < 10 ns.

For this series of isomeric phosphinogold di-alkyne complexes, the position of the substituents on the anthraquinone has a profound effect on the positions of bands in the electronic spectra (Table 5.5). The 1,2 isomer, $\{[Au(PPh_3)]_2L^4\}$, λ_{max} of 415-435nm is blue-shifted when compared to the 1,4 and the 1,8 isomers or $\{[Au(PPh_3)]_2L^{6/8}\}$ with λ_{max} of 524nm and 491 nm respectively. A blue-shifted emission was also seen with the napthyl-ether based complex, $\{[Au(PPh_3)]_2L^3\}$, with a λ_{max} of 369 nm. The blue shift can be attributed to interaction between the two substituents (which are closer together in the naphthyl-ether and 1, 2 isomers) resulting in an increase in the HOMO→LUMO energy gap and therefore a higher energy emission was observed. The 1,4 isomer,$\{[Au(PPh_3)]_2L^6\}$, was the only one of the three dimers to exhibit a two band emission spectra, this, again, was attributed to the

position of the alkyne units however the effect was only seen when the $[AuPPh_3]^+$ unit was introduced presumably for steric reasons.

Table 5.6 The emission data for the isomeric di-alkyne ligands and their complexes, MeCN, λ_{exc} 340 (nm).

Ligand	Em(MeCN)	Compound	Em(MeCN)
4	398	$\{[Au(PPh_3)]_2L^4\}$	415-435
6	487	$\{[Au(PPh_3)]_2L^6\}$	411-438 524
8	505	$\{[Au(PPh_3)]_2L^8\}$	491

5.3.5.5. Aurophillic interactions

Both solution and solid state emission spectra were recorded for $[Au(PPh_3)L^5]$ and $\{[Au(PPh_3)]_2L^{6/8}\}$ (Figure 5.13). All three complexes show a red-shift in emission maxima in the solid state when compared to the spectra recorded in solution. This red-shift could be indicative of intramolecular aurophilic interactions occurring between the Au(I) centres. However, for $[Au(PPh_3)L^5]$, where only one Au(I) unit is present within the complex, red-shift was also observed. Given that the crystal structure of $\{[Au(PPh_3)]_2L^8\}$ (Table 5.5) showed no evidence to suggest Au(I)-Au(I) contacts, it is more likely that the red-shift is simply due to packing effects in the solid state.

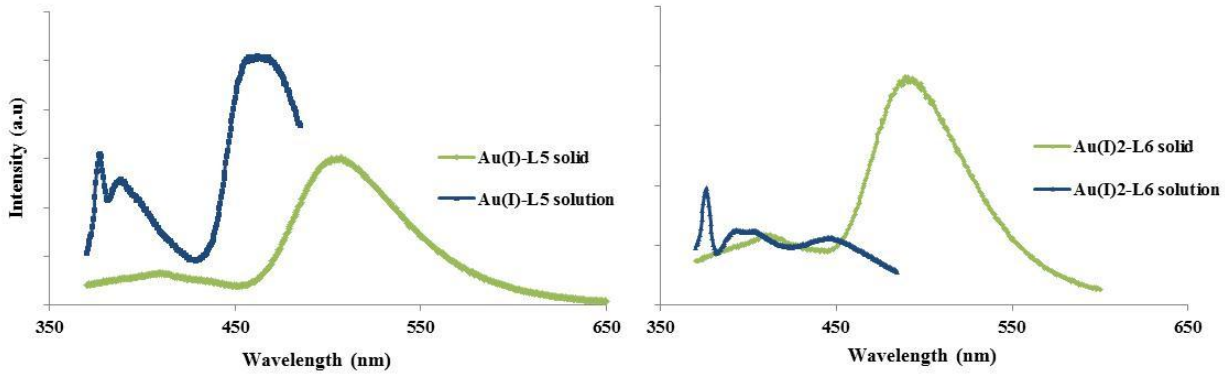

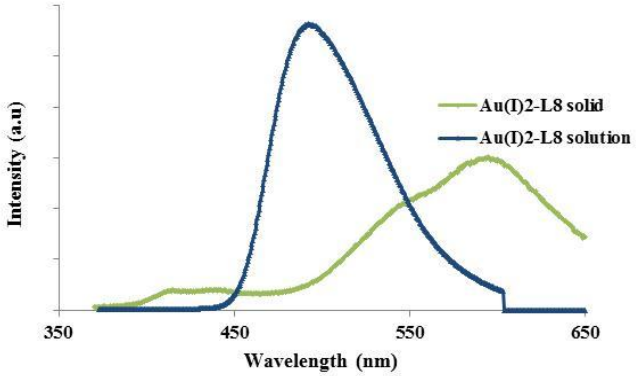

Figure 5.13 Emission spectra of $[Au(PPh_3)L^5]$ and $\{[Au(PPh_3)]_2L^{6/8}\}$ in solid and solution. (λ_{exc} = 340 nm).

5.4. Cytotoxicity investigation

A preliminary study of the cytotoxicity was undertaken for $\mathbf{L^5}$, $\mathbf{L^6}$ and $\mathbf{L^8}$ and their corresponding complexes $[Au(PPh_3)L^5]$ and $\{[Au(PPh_3)]_2L^{6/8}\}$ using the MTT assay with four different cancer cell lines: MCF-7 (breast adenocarcinoma), A549 (lung adenocarcinoma), PC3 (prostate adenocarcinoma) and LoVo (colon adenocarcinoma). For the MTT assay, the compounds were initially dissolved in DMSO, and doses of 0.1, 1, 10 and 100 μm were tested to analyse the activity of different concentrations and then compared to a control medium with no treatment. The approximate IC_{50} values for these compounds are shown in Table 5.7.

Table 5.7 Cytotoxicity data for the ligands and complexes

Ligand / Complex	IC_{50} MCF-7	IC_{50} PC3	IC_{50} A549	IC_{50} LoVo
$\mathbf{L^5}$	80	>100	>100	>100
$\mathbf{[Au(PPh_3)L^5]}$	5	50	100	100
$\mathbf{L^6}$	>100	>100	>100	70
$\mathbf{\{[Au(PPh_3)]_2L^6\}}$	5	50	>100	80
$\mathbf{L^8}$	>100	>100	>100	>100
$\mathbf{\{[Au(PPh_3)]_2L^8\}}$	5	>100	>100	>100

A comparison of the IC_{50} values in Table 5.7 shows that the Au(I) complexes are dramatically more toxic than their corresponding free ligands. The increase in the cytotoxicity of the Au(I) complexes is attributed to the presence of the Au(I) alkynyl unit.

The MCF-7 cell line is apparently a more sensitive cell line to this type of complex with all three Au(I) complexes displaying an IC_{50} value of 5 μM. The complex of the 1,4-isomer, $[Au(PPh_3)L^5]$ and $\{[Au(PPh_3)]_2L^6\}$, displayed increased cytotoxicity in the PC3 cell line with the relatively high IC_{50} values of 50 μM. $\mathbf{L^6}$ and its corresponding complex, $\{[Au(PPh_3)]_2L^6\}$, show increased toxicity towards the LoVo cell line when compared to the other compounds looked at with IC_{50} values of 70 μM and 80 μM respectively. The A549 cell line shows no sensitivity to any of the compounds in this series.

Despite the increased sensitive nature of the MCF-7 cell line to complexes of this type, when compared to the IC_{50} value of *cis*-platin (IC_{50} = 2.0 μM) these values are not sufficiently active to suggest applications solely as a therapeutic agent. However, given that the mitochondria are believed to be the key intracellular target of gold agents (Chapter 4's

discussion of TrxR), having established that these complexes display toxicity towards MCF-7s their therapeutic application and cellular distribution can be investigated *via* fluorescence microscopy.

5.5. Cellular imaging

Despite the short lived lifetimes exhibited by each of the complexes, preliminary cellular imaging experiments were carried out. For the complexes, $[Au(PPh_3)L^2]$ and $\{[Au(PPh_3)]_2L^3\}$ the cellular imaging results displayed ligand based fluorescence / auto-fluorescence only. For $[Au(PPh_3)L^1]$, apoptosis was observed immediately upon radiation which indicated that the coumarin moiety is toxic to cells.

For the anthraquinone based compounds: the di-alkyne ligand, **L^6**, and the mono and di-metallic Au(I) complexes, $[Au(PPh_3)L^5]$ and $\{[Au(PPh_3)]_2L^6\}$, were chosen for further studies as the compounds are analogous which made comparisons easy.

The ligand, **L^6**, and the mono and di-metallic gold complexes, $[Au(PPh_3)L^5]$ and $\{[Au(PPh_3)]_2L^6\}$ were each incubated with MCF-7 cells over a 30 minute period at 4 ˚C. The low temperature allows energy-dependent uptake processes, such as endocytosis, to be repressed. Following the removal of excess agent, the cells were allowed to warm to room temperature. At room temperature the cells functions normalise; energy-dependent pathways are no longer repressed allowing the accumulation and toxicity of the investigated complexes to be viewed.

The samples were imaged by confocal microscopy using an excitation of 405 nm and a detection range between 530-580 nm in accordance to the ^{3}MLCT emission reported in Table 5.5 thus eliminating autofluorescence. All three of the compounds viewed show successful uptake with > 80 % of cells showing good uptake. Initially good cell morphology was maintained for each sample, additional details are discussed in detail in the following sections

5.5.1. Cellular imaging properties of L^6

The 1,4 di-alkyne ligand showed good uptake whilst maintaining good cell morphology throughout the entire confocal session. Variable ligand based emission throughout the cytoplasm was observed. The presence of intense spots within the cytoplasm would suggest specific organelle localisation (Figure 5.14).

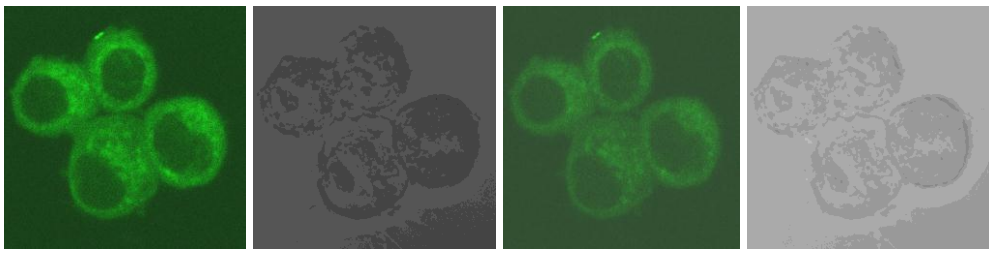

A B C D

Figure 5.14 Imaging with L^6 in MCF-7 cells showing: (A) & (C) cytoplasmic distribution; (B) & (D) transmitted light only.

5.5.2. Cellular imaging properties of $[Au(PPh_3)L^5]$

The mono-metallic Au(I) complex, $[Au(PPh_3)L^5]$, again showed good cell uptake whilst maintaining good cell morphology throughout the entire confocal session. $[Au(PPh_3)L^5]$ showed very similar cellular distribution to **L^6** but with increased luminescence intensity; increased luminescence was observed throughout the entire cytoplasm with intense spots for specific organelle distribution (Figure 5.15). The increase in intensity for $[Au(PPh_3)L^5]$ was attributed to the increased lipophilicity of the complex provided by the PPh_3 unit.

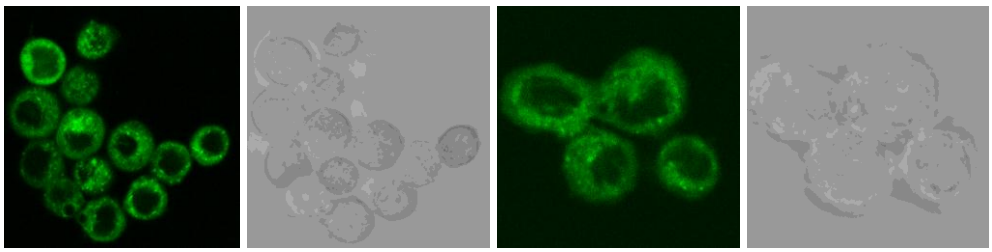

A B C D

Figure 5.15 Imaging with $[Au(PPh_3)L^5]$ in MCF-7 cells showing: (A) & (C) cytoplasmic distribution; (B) & (D) transmitted light only.

5.5.3. Cellular imaging properties of $\{[Au(PPh_3)]_2L^6\}$

The di-metallic Au(I) complex, $\{[Au(PPh_3)]_2L^6\}$, despite the additional PPh_3 unit, displayed similar luminescent intensity when compare to the mono-metallic Au(I) complex, $[Au(PPh_3)L^5]$ with both complexes displaying similar luminescence distribution to **L^6**. Unlike **L^6** and the mono-metallic complex, the di-metallic complex exhibited photobleaching with toxic effects seen upon irradiation. As the sample was irradiated, the appearance of large

vacuoles within the cells as well as a decrease in the luminescence intensity was apparent (Figure 5.16). The exact mechanism of photobleaching is unknown but with the apparent toxic effects of the di-metallic Au(I) complex there is the possibility it is linked as photobleaching which often involves the generation of toxic species (O_2 radicals).

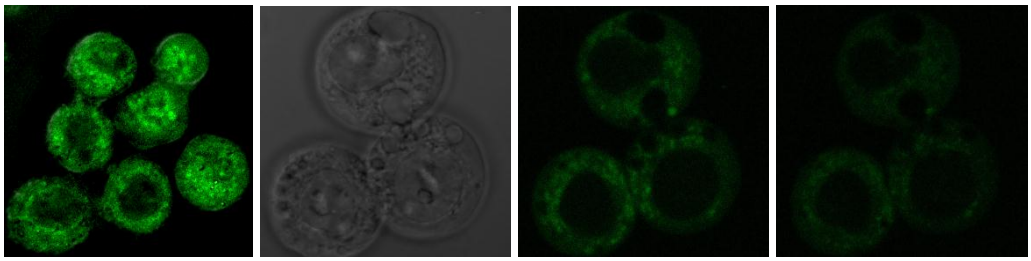

A B C D

Figure 5.16 Imaging with {[Au(PPh_3)]$_2$$L^6$} in MCF-7 cells showing: (A) cytoplasmic distribution (overlaid luminescence and transmitted light); (B) appearance of vacuoles upon irradiation (transmitted light only); (C) & (D) photobleaching (luminescence only).

5.6. Conclusion

Several mono- and di-metallic Au(I)-alkyne aromatic complexes were synthesised successfully. The ligand synthesis has shown that the choice of anthraquinone isomer has an effect on the nature and yield of the product formed. Favourable photophysical and cytotoxic properties were shown for this family of compounds, $\mathbf{L^5}$, $[Au(PPh_3)L^5]$, $\mathbf{L^6}$, $\{[Au(PPh_3)]_2L^6\}$, $\mathbf{L^8}$ and $\{[Au(PPh_3)]_2L^8\}$ suggesting suitability for applications as dual therapeutic and cellular imaging agents. The cellular imaging properties of $\mathbf{L^6}$, $[Au(PPh_3)L^5]$, $\{[Au(PPh_3)]_2L^6\}$ was investigated and all three compounds showed staining of the general cytoplasm with some intense staining of organelles. The increased lipophilicity on changing from the ligand to the mono-metallic complex resulted in increased uptake, as judged by emission intensity. However, no increase in intensity was observed from the mono-metallic to the di-metallic complex. Interestingly, upon irradiation, the di-metallic complex showed photobleaching with apparent toxic effects; the appearance of large vacuoles from within the cell was observed upon continual irradiation.

5.7. Experimental

5.7.1. Crystallography

[Au(PPh$_3$)L^2]: $C_{36}H_{26}AuO_2P$, M = 718.50, 0.25 × 0.25 × 0.20 mm^3, orthorhombic, space group *Pbca* (No. 61), a = 9.9741(2), b = 17.5178(3), c = 32.8694(6) Å, V = 5743.08(18) Å^3, Z = 8, D_c = 1.662 g/cm^3, F_{000} = 2816, MoKα radiation, λ = 0.71073 Å, T = 150(2)K, $2\theta_{max}$ = 55.8º, 12222 reflections collected, 6652 unique (R_{int} = 0.0613). Final *GooF* = 1.096, *R1* = 0.0695, *wR2* = 0.1027, *R* indices based on 4564 reflections with I >2sigma(I) (refinement on F^2), 361 parameters, 6 restraints. Lp and absorption corrections applied, μ = 5.210 mm^{-1}.

{[Au(PPh$_3$)]$_2$L^8}: $C_{58}H_{38}Au_2Cl_6O_4P_2$, M = 1467.46, monoclinic, space group $P2_1/n$ (No. 14), a = 18.4561(9), b = 11.6603(5), c = 26.6072(7) Å, β = 98.614(2)°, V = 5661.4(4) Å^3, Z = 4, D_c = 1.722 g/cm^3, F_{000} = 2832, MoKα radiation, λ = 0.71073 Å, T = 293(2)K, $2\theta_{max}$ = 55.1º, 22508 reflections collected, 12700 unique (R_{int} = 0.1312). Final *GooF* = 1.018, *R1* = 0.0999, *wR2* = 0.2248, *R* indices based on 6204 reflections with I >2sigma(I) (refinement on F^2), 686 parameters, 57 restraints. Lp and absorption corrections applied, μ = 5.561 mm^{-1}.

5.7.2. Synthesis of ligands

L^1 Coumarin acid chloride (0.5 g, 2.63 mmol) in chloroform (10 mL) and TEA (0.56 mL, 3.95 mmol) was added slowly to a solution of propargyl alcohol (0.14 mL, 2.39 mmol) in chloroform (5 mL). The solution was left to stir at 60 ˚C for 3 h. The solution was washed using sat. aq. sodium bicarbonate (3 × 10 mL) and sat. aq. ammonium chloride (2 × 10 mL). The organic layer was dried and the solvent evaporated to dryness, yielding an orange solid. The crude product was purified using column chromatography eluting with DCM. Yield: 0.387 g, 71 %. ^{1}H NMR ($CDCl_3$, 300 MHz, 298 K) δ_H: 2.54 (1H, t, (*H7*)), 4.94-4.96 (2H, m, (*H6*)), 7.29-7.33 (2H, m, (*H2*,*H3*)), 7.65-7.7 (2H, m, (*H1*,*H4*)), 7.72 (1H, s, (*H5*)) ppm.

L^2 Anthracene chloride (0.5 g, 2.25 mmol) in chloroform (10 mL) and TEA (0.49 mL, 3.48 mmol) was added slowly to a solution of propargyl alcohol (0.12 mL, 2.05 mmol) in chloroform (5 mL). The solution was left to stir at 60 ˚C for 3 h. The solution was washed using sat. aq. sodium bicarbonate (3 × 10 mL) and sat. aq. ammonium chloride (2 × 10 mL). The organic layer was dried and the solvent evaporated to dryness, yielding a pale orange solid. The crude product was purified using column chromatography eluting with DCM. Yield: 0.485 g, 86 %. ^{1}H NMR ($CDCl_3$, 400 MHz, 298 K) δ_H: 2.5 (1H, t, $^3J_{HH}$ = 2.4 Hz, (*H6*)),

5 (2H, d, $^3J_{HH}$ = 2.4 Hz, (*H5*)), 7.28-7.39 (2H, m, (*H3*)), 7.39-7.46 (2H, m, (*H4*)), 7.73 (2H, d, $^3J_{HH}$ = 8.4 Hz (*H2*)), 7.98 (2H, d, $^3J_{HH}$ = 8.8 Hz (*H5*)), 8.38 (1H, s, (*H1*)) ppm.

L^3 To an excess of potassium carbonate in acetone (40 mL) was added bis-2-naphthol (0.5 g, 1.75 mmol) and propargyl bromide (0.42 mL, 3.69 mmol). The solution was left to stir at 65 ˚C for 15 h. The solution was filtered and filtrate concentrated *in vacuo* to produce a cream solid. Yield: 0.557 g, 89 %. ^{1}H NMR ($CDCl_3$, 400 MHz, 298 K) δ_H: 2.22 (2H, t, $^3J_{HH}$ = 2.25 Hz (*H8*)), 4.51 (4H, d, (*H7*)), 7.05-7.17 (6H, m, (*H3*, *H5*, *H6*)), 7.22 (2H, t, $^3J_{HH}$ = 7.6 Hz, (*H4*)), 7.72 (2H, d, $^3J_{HH}$ = 8.2 Hz, (*H2*)), 7.83 (2H, d, $^3J_{HH}$ = 9.05 Hz, (*H1*)) ppm.

L^4 To an excess of potassium carbonate in acetone (40 mL) was added alizarin (0.5 g, 2.08 mmol) and propargyl bromide (0.32 mL, 4.37 mmol). The solution was left to stir at 65 ˚C for 15 h. The solution was filtered and filtrate concentrated *in vacuo* to produce a brown solid. Yield: 0.260 g, 40 %. ^{1}H NMR ($CDCl_3$, 400 MHz, 298 K) δ_H: 2.52-2.54 (1H, m, (*H8a*)), 2.61-2.65 (1H, m, (*H8b*)), 4.84-4.96 (4H, m, (*H7*)), 7.42 (1H, d, (*H6*)), 7.73-7.85 (2H, m, (*H2*,*H3*)), 8.18-8.30 (3H, m, (*H1*, *H4*,*H6*)) ppm. ^{13}C{^{1}H} NMR ($CDCl_3$, 101 MHz, 298 K) δ_C: 56.9, 61.0, 75.2, 77.2, 118.0, 118.4, 125.6, 126.8, 127.4, 127.9, 128.2, 132.9, 133.7, 133.8, 134.1, 135.0, 147.3, 157.1, 182.3, 182.6 ppm. MS (ES^+) *m/z*: 316.01 $[M\text{-}H]^+$, HRMS (ES^+) found *m/z* 317.0812; $[C_{20}H_{13}O_4]^+$ requires 317.0808. IR (nujol) *υ*: 1568 (CO), 1673 (CO), 2129 (CC) cm^{-1}.

L^5 To an excess of potassium carbonate in acetone (40 mL) was added 1,4 dihydroxy anthraquinone (0.5 g, 2.08 mmol) and propargyl bromide (0.499 mL, 4.37 mmol). The solution was left to stir at 65 ˚C for 15 h. The solution was filtered and filtrate concentrated *in vacuo*. The crude product was purified using column chromatography eluting with DCM. Yield: 0.085 g, 15 %. ^{1}H NMR ($CDCl_3$, 400 MHz, 298 K) δ_H: 2.49 (1H, t, (*H8*)), 4.73 (2H, d, $^3J_{HH}$ = 2.4 Hz, (*H7*)), 7.18 (1H, d, (*H1*)), 7.43 (1H, d, (*H4*)), 7.63-7.81 (2H, m, (*H2*, *H3*)), 8.13-8.24 (2H, m, (*H5*, *H6*)) ppm. ^{13}C{^{1}H} NMR ($CDCl_3$, 101 MHz, 298 K) δc: 58.4, 77.8, 115.5, 121.5, 126, 126.5, 126.5, 127.5, 128.1, 128.2, 133.6, 134.9, 135.0, 151.8, 158.7, 181.8, 188.9 ppm. MS (ES^+) *m/z*: 240 $[M\text{-}C_3H_2]^+$, 278 $[M]^+$. HRMS (ES^+) found *m/z* 278.0574; $[C_{17}H_{10}O_4]^+$ requires 278.0574. IR (nujol) *υ*: 1593 (CO), 1663 (CO), 1666 (CO), 2115 (CC) cm^{-1}. UV-vis (ε / M^{-1} cm^{-1}) (MeCN) λ_{max}: 270 (2700), 326 (552), 432 (1382) nm.

L^6 To an excess of potassium carbonate in acetone (40 mL) was added 1,4 dihydroxy anthraquinone (0.5 g, 2.08 mmol) and propargyl bromide (0.499 mL, 4.37 mmol). The solution was left to stir at 65 ˚C for 5 days. The solution was filtered and filtrate concentrated

in vacuo. The crude product was purified using column chromatography eluting with DCM. Yield 0.205 g, 31 %. ^{1}H NMR ($CDCl_3$, 400 MHz, 298 K) δ_H: 2.52 (2H, t, $^{3}J_{HH}$ = 2.4 Hz, (*H5*)), 4.79 (4H, d, $^{3}J_{HH}$ = 2.4 Hz, (*H4*)), 7.41 (2H, s, (*H3*)), 7.59-7.66 (2H, m, (*H2*)), 8.0-8.19 (2H, m, (*H1*)) ppm. $^{13}C\{^{1}H\}$ NMR ($CDCl_3$, 101 MHz, 298 K): δc: 58.3, 77.4, 123.8, 126.6, 133.6, 155.8 ppm. MS (ES^+) *m/z*: 277.05 $[M\text{-}C_3H_3]^+$, 316 $[M]^+$. HRMS (ES^+) found *m/z* 316.0746; $[C_{20}H_{12}O_4]^+$ requires 316.0730. IR (nujol) *υ*: 1582 (CO), 1671 (CO), 2119 (CC) cm^{-1}. UV-vis (ε / M^{-1} cm^{-1}) (MeCN) λ_{max}: 302 (1192), 394 (1029) nm.

L^{7} To an excess of potassium carbonate in acetone (40 mL) was added 1,8 dihydroxy anthraquinone (0.5 g, 2.08 mmol) and propargyl bromide (0.499 mL, 4.37 mmol). The solution was left to stir at 65 ˚C for 15 h. The solution was filtered and filtrate concentrated *in vacuo*. The crude product was purified using column chromatography eluting with DCM. Yield: 0.078 g, 13 %. ^{1}H NMR ($CDCl_3$, 400 MHz, 298 K) δ_H: 2.52 (1H, t, (*H8*)), 4.91 (2H, d, (*H7*)), 7.2 (1H, d, (*H3*)), 7.42 (1H, d, (*H4*)), 7.51-7.53 (1H, m, (*H2*)), 7.57-7.65 (2H, m, (*H1*, *H5*)), 7.94 (1H, d, (*H6*)) ppm. $^{13}C\{^{1}H\}$ NMR ($CDCl_3$, 101 MHz, 298 K) δ_C: 39.8, 57.2, 77.3, 118.9, 120.5, 121.2, 124.8, 135.8, 138.1, 161.0, 163.9 ppm. MS (ES^+) *m/z*: 252 $[M\text{-}C_2H_3]^+$. HRMS (ES^+) found *m/z* 279.0651; $[C_{17}H_{10}O_4]^+$ requires 279.0652. IR (nujol) *υ*: 1584 (CO), 1643 (CO), 1675 (CO), 2034 (CC) cm^{-1}. UV-vis (ε / M^{-1} cm^{-1}) (MeCN) λ_{max}: 254 (24321), 408 (11951) nm.

L^{8} To an excess of potassium carbonate in acetone (40 mL) was added 1,8 dihydroxy anthraquinone (0.5 g, 2.08 mmol) and propargyl bromide (0.499 mL, 4.37 mmol). The solution was left to stir at 65 ˚C for 5 days. The solution was filtered and filtrate concentrated *in vacuo*. The crude product was purified using column chromatography eluting with DCM. Yield: 0.354 g, 54 %. ^{1}H NMR ($CDCl_3$, 400 MHz, 298 K) δ_H: 2.52 (2H, t, $^{3}J_{HH}$ = 2.34 Hz, (*H5*)), 4.88 (4H, d, $^{3}J_{HH}$ = (*H4*)), 7.42 (2H, d, $^{3}J_{HH}$ = 8.3 Hz, (*H1*)), 7.51 (2H, t, $^{3}J_{HH}$ = 8 Hz, (*H2*)), 7.82 (2H, d, $^{3}J_{HH}$ = 7.8 Hz (*H3*)) ppm. $^{13}C\{^{1}H\}$ NMR ($CDCl_3$, 101 MHz, 298 K): δc: 57.3, 77.5, 120.4, 121.1, 133.8, 157.2 ppm. MS (ES^+) *m/z*: 277.04 $[M\text{-}C_3H_3]^+$. HRMS (ES^+) found *m/z* 316.0707; $[C_{20}H_{12}O_4]^+$ requires 316.0730. IR (nujol) *υ*: 1585 (CO), 1658 (CO), 1671 (CO), 2130 (CC) cm^{-1}. UV-vis (ε / M^{-1} cm^{-1}) (MeCN) λ_{max}: 254 (29230), 374 (10428) nm.

L^{9} To an excess of potassium carbonate in acetone (40 mL) was added 1,5 dihydroxy anthraquinone (0.5 g, 2.08 mmol) and propargyl bromide (0.499 mL, 4.37 mmol). The solution was left to stir at 65 ˚C for 15 h. The solution was filtered and filtrate concentrated *in vacuo*. The crude product was purified using column chromatography eluting with DCM.

Yield: 0.025 g, 4 %. ^{1}H NMR ($CDCl_3$, 400MHz, 298K) δ_H: 2.49 (1H, t, (*H1*)), 4.97 (2H, d, 7.23 (1H, d, (*H2*)), 7.48 (2H, d, (*H6*)), 7.65-7.73 (2H, m, (*H4*, *H5*)), 7.7-7.82 (2H, m, *(H3*, *H7*)), 7.98 (2H,d, (*H8*)) ppm. ^{13}C{^{1}H} NMR ($CDCl_3$, 101 MHz, 298K): δc: 57.3, 77.6, 119, 121.2, 121.8, 123.5, 132.9, 135.8, 138.1, 163.4 ppm. MS (ES^+) m/z: 239.21 $[M\text{-}C_3H_3]^+$. HRMS (ES^+) found *m/z* 279.0652; $[C_{17}H_{11}O_4]^+$ requires 279.0652. IR (nujol) *υ*:1583 (CO), 1634 (CO), 1664 (CO), 2112 (CC) cm^{-1}. UV-vis (ε / M^{-1} cm^{-1}) (MeCN) λ_{max}: 254 (1945), 274 (1035), 394 (568) nm.

L^{10} To an excess of potassium carbonate in acetone (40 mL) was added 1,5 dihydroxy anthraquinone (0.5 g, 2.08 mmol) and propargyl bromide (0.499 mL, 4.37 mmol). The solution was left to stir at 65 ˚C for 5 days. The solution was filtered and filtrate concentrated *in vacuo*. The crude product was purified using column chromatography eluting with DCM. Yield: 0.012 g, 3 %. ^{1}H NMR ($CDCl_3$, 400MHz, 298K) δ_H: 2.48 (1H, t, (*H1*)), 4.82 (2H, d, (*H2*)), 7.37 (2H, d, (*H5*)), 7.64 (2H, t, (*H4*)), 7.91 (2H, d, (*H3*)) ppm.

5.7.3. Synthesis of complexes

[Au(PPh$_3$)L^1]: To a round bottom flask encase in aluminium foil L^1 (0.019 g, 0.84 mmol), [$AuClPPh_3$] (0.050 g, 0.1 mmol), potassium tertiary butoxide (0.013 g, 0.1 mmol) and ethanol (2 mL) were added and stirred under nitrogen for 12 h. The solution was concentrated *in vacuo*, re-dissolved in DCM and filtered. The filtrate was concentrated *in vacuo* and the orange solid was recrystallized from THF and diethyl ether. Yield: 0.016 g, 28 %. ^{1}H NMR ($CDCl_3$, 400 MHz, 298 K) δ_H: 4.42 (2H, s, (*H4*)), 7.2-7.8 (19H, m, (*H2*, *H3*, *H5*)), 8.55 (1H, s, (*H1*)) ppm. δ ^{31}P 29.98 ppm. IR (nujol) *υ*: 1609 (CO), 1761 (CO), 2252 (CC) cm^{-1}. UV-vis (ε / M^{-1} cm^{-1}) (MeCN) λ_{max}: 220 (10017), 286 (7164), 386 (4208) nm.

[**Au(PPh$_3$)L^2]:** To a round bottom flask encase in aluminium foil L^2 (0.024 g, 0.84 mmol), [$AuClPPh_3$] (0.050 g, 0.1 mmol), potassium tertiary butoxide (0.013 g, 0.1 mmol) and ethanol (2 mL) were added and stirred under nitrogen for 12 h. The solution was concentrated *in vacuo*, re-dissolved in DCM and filtered. The filtrate was concentrated *in vacuo* and the orange solid was recrystallized from THF and diethyl ether. Yield: 0.024 g, 36 %. ^{1}H NMR ($CDCl_3$, 400 MHz, 298 K) δ_H: 5.38 (2H, s, (*H6*)), 7.21-7.67 (17H, m, (*H3*, *H7*)), 7.71-7.75 (2H, m, (*H2*)), 8 (2H, d, (*H4*)), 8.19 (2H, d, (*H1*)), 8.52 (1H, s, (*H5*)) ppm. ^{13}C{^{1}H} NMR ($CDCl_3$, 101 MHz, 298 K) δ_C: 77.4, 125.5, 127, 127.9, 129.2, 129.3, 131.9, 134.2, 134.4 ppm. δ^{31}P 29.86 ppm. MS (ES^+) *m/z*: 721.15 $[Au(PPh_3)_2]^+$. HRMS (ES^+) found *m/z* 721.1475;

$[AuC_{36}H_{26}PO_2H]^+$ requires 719.1409. IR (nujol) υ: 1720 (CO), 2184 (CC) cm^{-1}. UV-vis (ε / $M^{-1}\,cm^{-1}$) (MeCN) λ_{max}: 224 (10071), 251 (4173) nm.

{[Au(PPh$_3$)]$_2$L^3}: To a round bottom flask encase in aluminium foil L^3 (0.019 g, 0.84 mmol), [AuClPPh$_3$] (0.050 g, 0.1 mmol), potassium tertiary butoxide (0.011 g, 0.1 mmol) and ethanol (2 mL) were added and stirred under nitrogen for 12 h. Same work up as before. Yield: 0.035 g, 60 %. ^{1}H NMR ($CDCl_3$, 400 MHz, 298 K) δ_H: 4.78 (4H, s, (*H7*)), 7.05-7.21 (6H, m, (*H4*, *H5*, *H6*)), 7.22-7.42 (30H, m, (*H8*)), 7.71-7.92 (6H, m, (*H1*, *H2*, *H3*)) ppm. ^{13}C{^{1}H} NMR ($CDCl_3$, 101 MHz, 298 K) δ_C: 58. 8, 117.1, 123.4, 126.1, 127.8, 129.2, 129.3, 131.7, 134.2, 134.2, 134.4, 154.5 ppm. MS (ES^+) *m/z*: 721.29 $[Au(PPh_3)_2]^+$, 1301.48 $[M+Na]^+$. δ ^{31}P 42.6 ppm. IR (nujol) υ: 2017 (CO), 2132 (CC) cm^{-1}.UV-vis (ε / $M^{-1}\,cm^{-1}$) (MeCN) λ_{max}: 228 (17519), 326 (2860) nm.

{[Au(PPh$_3$)]$_2$L^4}: To a round bottom flask encase in aluminium foil L^4 (0.022 g, 0.073 mmol), [AuClPPh$_3$] (0.050 g, 0.1 mmol), potassium tertiary butoxide (0.011 g, 0.1 mmol) and ethanol (2 mL) were added and stirred under nitrogen for 12 h. Same work up as before. Yield: 0.043 g, 48 %. ^{1}H NMR ($CDCl_3$, 400 MHz, 298 K) δ_H: 4.99-5.07 (4H, m, (H7)), 7.31-7.58 (32H, m, (*H2*, *H5*, *H8*)), 7.61-7.66 (1H, m, (*H4*)), 8.1-8.3 (3H, m, (*H1*, *H3*, *H6*)) ppm. ^{13}C{^{1}H} NMR ($CDCl_3$, 101 MHz, 298 K) δ_C 77.2, 128.9, 129.1, 131.5, 134.3, 134.6 ppm. δ^{31}P 42.46 ppm. MS (ES^+) *m/z*: 721.15 $[Au(PPh_3)_2]^+$. IR (nujol) υ:1720 (CO), 2184 (CC) cm^{-1}. UV-vis (ε / $M^{-1}\,cm^{-1}$) (MeCN) λ_{max}: 212 (15998), 273 (5542), 375 (1430) nm.

[Au(PPh$_3$)L^5]: To a round bottom flask encase in aluminium foil L^5 (0.020 g, 0.0735 mmol), [AuClPPh$_3$] (0.040 g, 0.08 mmol) and potassium tertiary butoxide (0.009 g, 0.80 mmol) and ethanol (2 mL) were added and stirred under nitrogen for 12 h. Same work up as before. Yield: 0.015 g, 28 %. ^{1}H NMR ($CDCl_3$, 400 MHz, 298 K) δ_H: 5.01 (2H, s, (*H7*)), 7.16-7.23 (2H, m, (*H2, H3*)), 7.3-7.42 (15H, m, (*H8*)), 7.62-7.79 (2H, m, (*H1,H4*)) 8.12-8.19 (2H, m, (*H5, H6*)) ppm. ^{13}C{^{1}H} NMR ($CDCl_3$, 101 MHz, 298 K) δ_C 76.2, 129.1, 129.3, 131.6, 134.2, 134.4, 134.5, 154.2 ppm. MS (ES^+) *m/z*: 721.15 $[Au(PPh_3)_2]^+$. δ^{31}P 42.4 ppm. IR (nujol) υ: 1593 (CO), 1664 (CO), 1665 (CO), 2133 (CC) cm^{-1}. UV-vis (ε / $M^{-1}\,cm^{-1}$) (MeCN) λ_{max}: 272 (24360), 448 (10639) nm.

{[**Au(PPh$_3$)]$_2$L^6}:** To a round bottom flask encase in aluminium foil L^6 (0.016 g, 0.05 mmol), [AuClPPh$_3$] (0.060 g, 0.12 mmol), potassium tertiary butoxide (0.011 g, 0.1 mmol) and ethanol (2 mL) were added and stirred under nitrogen for 12 h. Same work up as before. Yield: 0.022 g, 36 %. ^{1}H NMR ($CDCl_3$, 400 MHz, 298 K) δ_H: 5.01 (4H, s, (*H4*)), 7.23-7.45

(15H, m, (*H5*)), 7.52-7.55 (2H, m, (*H2*)), 7.68 (2H, s, (*H1*)), 8.1-8.15 (2H, m, (*H3*)) ppm. $^{13}C\{^{1}H\}$ NMR ($CDCl_3$, 101 MHz, 298 K) δ_C 58.2, 123.2, 123.5, 125.3, 129.2, 129.3, 131.7, 133.5, 134.3, 134.4 ppm. $\delta^{31}P$ 42.46 ppm. MS (ES^+) *m/z*: 721.15 $[Au(PPh_3)_2]^+$.IR (nujol) υ: 1666 (CO), 1898 (CO), 2021 (CC) cm^{-1}. UV-vis (ε / M^{-1} cm^{-1}) (MeCN) λ_{max}: 250 (12700), 406 (1790) nm.

{$[Au(PPh_3)]_2L^8$}: To a round bottom flask encased in aluminium foil L^8 (0.010 g, 0.03 mmol), $[AuClPPh_3]$ (0.035 g, 0.07 mmol), potassium tertiary butoxide (0.023 g, 0.2 mmol) and ethanol (2 mL) were added and stirred under nitrogen for 12 h. Work up as before to yield an orange solid. Yield: 0.018 g, 50 %. ^{1}H NMR ($CDCl_3$, 300 MHz, 298 K) δ_H: 5.08 (4H, s, (*H4*)), 7.33-7.52 (15H, m, (*H5*)), 7.63 (2H, t, (*H1*)), 7.79-7.81 (2H, m, (*H2*)), 7.83 (2H, m, (*H3*)) ppm. $^{13}C\{^{1}H\}$ NMR ($CDCl_3$, 101 MHz, 298 K) δ_C 77.3, 129.2, 129.3, 131.6, 134.3, 134.5 ppm. MS (ES^+) *m/z*: 721.29 $[Au(PPh_3)_2]^+$. $\delta^{31}P$ 42.48 ppm. IR (nujol) υ: 1584 (CO), 1667 (CO), 2129 (CC), 2239 (CC) cm^{-1}. UV-vis (ε / M^{-1} cm^{-1}) (MeCN) λ_{max}: 257 (19593), 397 (4700) nm.

5.8. References:

1. K.W. Bair, C. W. Andrews, R. L. Tuttle, V. C. Knick, M. Cory and D. D. McKee, *J. Med. Chem*., 1991, **34**, 1983.
2. B. K. Banik and F. F. Becker, *Bio. Med. Chem*., 2001, **9**, 593.
3. Y**.**L. F. Lui, T. C. Row and L. Yang, *J. Biol. Chem*., 1984, **259**, 9182.
4. J. R. Choi, S. C. Jeoung and D. W. Cho, *Chem. Phys. Lett*., 2004, **385**, 384.
5. G. Z. Jin, G. Y. Song, X. G. Zheng, Y. Kim, D. E. Sok and B.Z Ahn, *Pharma. Res*., 1998, **21**, 198.
6. G. -Z. Jin, J. H. Chung, Y. Kim, D. E. Sok and B.Z Ahn, *Pharma. Med. Chem*., 1998, **331**, 380.
7. G. -Z. Jin, Y. –J. You, Y. Kim, N.-H. Nam and B.Z Ahn, *Eur. J. Med. Chem*., 2001, **36**, 366.
8. S. J. Formosinho and L. G. Arnaut, *J. Photochem. Photobiol. A: Chem.,* 1993, **75**, 21.
9. C. Millani, A. Romani and G. Favaro, *J. Phys. Org. Chem*., 2000, **13**, 141.
10. H. Scheffler, Y. You and I. Ott, *Polyhedron*., 2010, **29**, 66; (b) C. P. Bagowski, Y. You, H. Scheffler, D. H. V, Lecken, G. J. Schmitz and I. Ott, *Dalton. Trans*., 2009, 10799.
11. P. J.Barnard, L. E. Wedlock, M. V. Baker, B. S. J. Price, D. A. Joyce, B. W. Skelton, and J. H. Steer, *Angew. Chem. Int. Ed.*, **2006**, *45*, 5966; (b) M. C. Lagunas, *Annu. Rep. Prog. Chem.,* 2007, **103**, 234.
12. F. Caruso, M.Rossi, J. Tanski, C. Pettinari,and F. Marchetti *J. Med. Chem*., 2003, **46**, 1737.
13. R. C. Bott, G. A. Bowmaker, R. W. Bucklery, P. C. Healy and M. C. S. Perera, *Aust. J. Chem*., 1999, **52**, 271.
14. P. Pyykkö, J. Li, and N. Runeberg, *Chem. Phys. Lett*., 1994, **218**, 133.
15. W. J. Hunks, M. A. MacDonald, M. C. Jennings and R. J. Puddephatt, *Organometallics.,* 2000, **19**, 24.
16. R. J. Puddephatt,.*Chem.Commun*., 1998, 105.
17. L. A. Mullice, F. L. Thorp-Greenwood, R. H. Laye, M. P. Coogan. B. M. Kariuki and S. J. A. Pope, *Dalton. Trans*., 2009, 6836.

Chapter 6. Luminescent Multi-Metallic Complexes Incorporating an Au(I) Alkyne Unit Towards Dual-Functional In Therapeutic And Cellular Imaging Applications.

6.1. Introduction

The synthesis and applications of emissive hetero-metallic complexes is an area of growing research interest. In many of the hetero-metallic systems inclusive of d^6 and/or d^{10} TM ions, reported to date, either alkynyls and or polydentates have been applied in the development of the ligand systems.[1-3]As an extension of the previous work on Re(I) diimines (Chapters 2 and 3) and Au(I) alkynyl complexes (Chapters 4 and 5) attempts have been made to synthesize novel hetero-metallic complexes based around both d^6 and d^{10} TM ions combining the use of both alkyne and diimine units.

6.1.1. Requirements for the co-ordination of low spin d^6 metals

Heavy transition metals with a d^6 configuration, such as Re(I), Ru(II) and Ir(III), when bonded to one or more aromatic bidentate ligands show the ideal photophysical and redox properties required to be useful luminophores. The reducibility of the bidentate ligand make them fitting candidates for allowing the $d\pi \rightarrow \pi^*$ ^{3}MLCT to occur. Therefore, when synthesising a ligand suitable for co-ordinating metal ions such as Re(I), Ru(II) and Ir(III), in order to display the desirable luminescence properties, it is usually necessary to include a bidentate unit.

6.1.2. Requirements for the co-ordination of Au(I)

In recent years the interest in Au(I) complexes has increased owing to the intriguing photophysical properties which are dependent on: the nature of the ligand, geometry of the gold and more interestingly, the presence of Au(I)-Au(I) aurophilic interactions. Since the first report on the rich luminescent properties of Au(I) alkynes in 1993[4], Au(I) alkynyls have been used to synthesise a range of mono and hetero-metallic complexes inclusive of a Au(I) alkyne unit.[1] The versatile nature of the TM alkynyl has led to several different studies on the reactivity of alkynes toward TM ions.[1,5-8]

Various attempts to synthesise luminescent gold complexes were discussed in the earlier chapters; the latter half of Chapter 4 and then Chapter 5 reported the successful co-ordination of a $[AuPPh_3]^+$ unit to a series of varying alkyne units. Therefore when considering the design of a ligand system suitable for the synthesis of a hetero-metallic complex inclusive of an Au(I) unit, it was decided to include an alkyne unit.

6.1.3. The addition of an alkyne unit to an aromatic ring

Alkynes are one of the most important structural building blocks in organic chemistry, and can be found in a variety of applications including pharmaceuticals and in molecular material applications in nanomaterials.[9,10] The versatile palladium catalyzed cross coupling reaction between a terminal alkyne and an organic halide for the synthesis of a new sp^2-C and sp-C carbon-carbon bond was first reported in 1975 by Heck,[11] Cassar[12] and Sonogashira.[13] The former two reactions are based on an extension of the well-known Heck reaction of alkenes.

6.1.4. Palladium catalyzed coupling

Several variations of palladium catalyzed cross and homo coupling reactions exist for the formation of new carbon-carbon bonds in organometallic chemistry, including: Heck:- alkene and aryl halide coupling, Suzuki:- aryl halide and boronic acid coupling, Sonogashira:- aryl halide and alkyne coupling and Negishi:- organo-halide and organo-zinc coupling. Palladium is a key component in these reactions with a zero valent palladium generally being the active catalyst; Pd(II) is more stable than Pd(0) over long periods of time and so some coupling reactions use Pd(II) as the catalyst precursor as it is known to reduce in the presence of amines/phosphines to Pd(0) under the reaction conditions.[14,15]

Palladium catalysts commonly used in these coupling reactions include, $Pd(PPh_3)_4$, [tetrakis(triphenylphosphine)palladium(0)] and $Pd_2(dba)_3$, tris-[(dibenzylideneacetone)dipalladium(0)]. The inclusion of strong σ donor ligands on the palladium increases the electron density on the palladium and thus increases the rate of the oxidative insertion (often the rate determining step), whilst the presence of bulky groups on the palladium relates to the Tolman angle (sterics), dictating the strength of the bonds and the orientation of the ligands around the palladium centre (PdL_2 is favoured over PdL/PdL_3).[16]

6.1.4.1. Sonogashira coupling of alkynes

Sonogashira demonstrated the use of a palladium-copper co-catalyst for the successful coupling of an alkyne unit and a halide under more favorable and milder conditions than the previously used Castro-Stephens coupling; a Castro-Stephens coupling is carried out at high temperatures in the absence of a catalyst.[17] 'Sonogashira' coupling reactions have been reported in the absence of copper (discussed in detail below), the absence of palladium, in nickel-copper co-catalysed 'Sonogashira' couplings,[18] and in the absence of both copper and palladium in a gold catalyzed 'Sonogashira' coupling using Au/CeO_2.[19,20]

6.1.4.1.1. Copper-free Sonogashira couplings

The presence of the copper co-catalyst in a Sonogashira coupling reaction increases the reactivity of the alkyne unit allowing the coupling reaction to be carried out under milder conditions. Sonogashira couplings can be carried out in the absence of a copper co-catalyst but the exact mechanism for coupling is still under debate. The absence of a copper co-catalyst does eliminate the potential of any homo-coupling side-reactions of the alkyne, this coupling is referred to as Glaser coupling and involves the coupling of two alkyne units in the presence of a copper(I) halide salt and oxygen forming an alkyne dimer.[21-23] However, carrying out a Sonogashira coupling in the presence of a copper-co catalyst and in an inert atmosphere can negate Glaser homo-coupling reactions.

Alkynyl silanes are well documented in Sonogashira reactions; the presence of a TMS group on the alkyne allows more control over reactivity by minimizing side reactions. Additionally, both the starting materials and products of TMS-based reactions are generally non-toxic.[24]

6.1.4.1.2. Catalytic Cycle

The formation of the new C-C bond proceeds *via* the activation of the organo-halides by Pd(0). Pd(0) activates the organo-halide by oxidative addition into the carbon halogen bond forming Pd(II). The copper halide reacts with the terminal alkyne to produce copper(I) acetylide which acts as an activated species for the coupling reaction. Transmetallation then occurs followed by reductive elimination to give the coupling product (Figure 6.1).

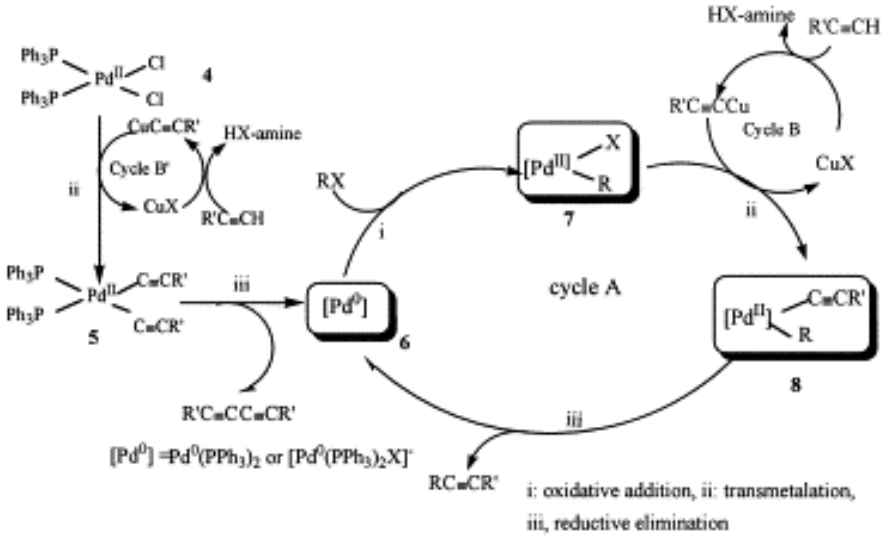

Figure 6.1 Outline of the reaction scheme for Pd–Cu catalyzed cross-coupling of sp^2-C halides with terminal acetylenes. Reproduced from ref. 25.

6.1.5. Hetero-metallic complexes including Au(I) alkynyls

The photophysical properties of a series of novel mono- and di-metallic alkynyl Au(I) complexes were discussed in detail in chapters 4 and 5. A discussion of varying hetero-metallic complexes inclusive of an Au(I)-alkyne unit takes place in the following section.

6.1.5.1. Au(I)-M (M=Cu(I)/Ag(I)) alkynyl complexes

Koshevoy *et al.*[26,27] reported a series of novel hetero-metallic alkynyl coinage cluster complexes inclusive of an Au(I) unit. Unique photophysical properties were observed for complexes of this type and the potential to form hetero-metallic supramolecular complexes due to of the mixed M-M interactions between the closed-shell d^{10} ions was recognised. Self-assembled cluster complexes of this type arranged with the Au(I) phosphine alkynyl in a 'belt' formation; the Au(I) σ-bonded to the alkynyl groups 'wraps' the Cu(I)/Ag(I) units which interact with the centred Au(I) units (Figure 6.2). Both solid and solution state luminescence measurements for the Au/Ag complex resulted in roughly the same emission maxima for both complexes being observed with the maxima within the range of 526-641 nm. A bathochromic shift and a decrease in emission intensity was seen when Cu(I) was exchanged for Ag(I) within the cluster core.[27]

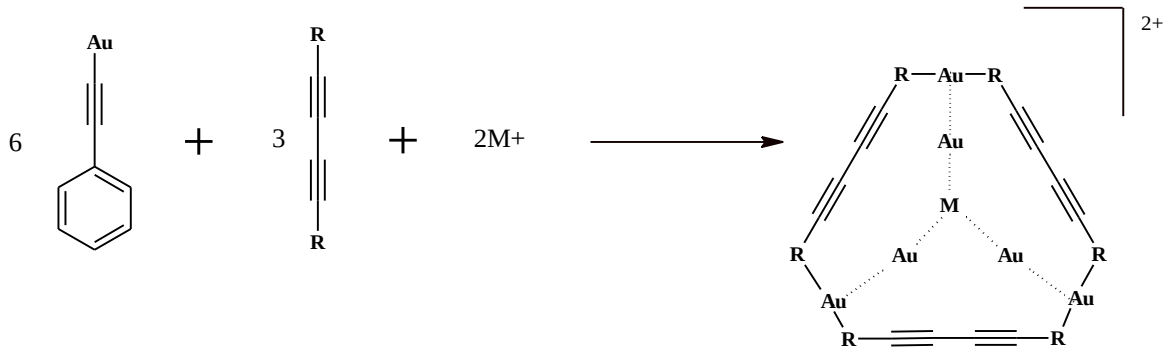

Figure 6.2 Au = Ph-C_2-Au-C_2-Ph. R = PPh_2, M = M_2 = Cu(I) / Ag(I).[27]

A second report by Koshevoy e*t al.*[26] discussed the properties of a tetra-nuclear Au(I)-Cu(I) tppm-based cluster complex, (tppm = tri(diphenylphosphine)methane). Unlike the previous examples by this group, these novel complexes displayed π-bonding of the Cu(I) unit to the alkyne. Complexes of this type gave emission in the range of 550-680 nm and lifetimes in the μs range which were attributed to the phosphorescent nature of the emission.[26]

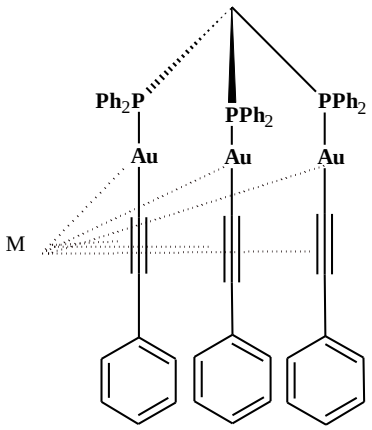

Figure 6.3 Complex structure omitting Au(I)-Au(I) interaction.[26]

Yam *et al.*[28] also reported Au(I) alkynyl-Cu(I)/Ag(I) type complexes where the Au(I) was, σ-bonded and the Cu(I)/Ag(I) units were π- bonded to the alkynyl group. In the absence of Cu(I) and Ag(I), the luminescence of the Au(I) complex was centred on 454 nm. On addition of the Cu(I) metal centre, the π^* C≡C orbital (alkyne) was lowered giving rise to a red shifted emission between 606-664 nm.[28]

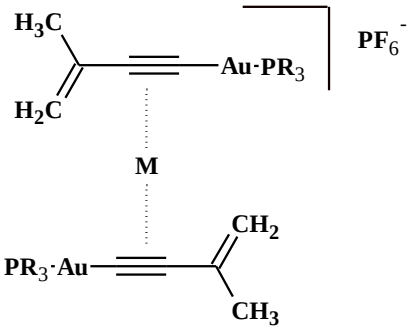

Figure 6.4 R = Ph / *p*-Tol, M = Cu(I) / Ag(I).[28]

6.1.5.2. Au(I)-Re(I) alkynyl complexes

There are only a few examples of Au(I)-Re(I) hetero-metallic complexes reported to date. The first Au(I)-Re(I) hetero-metallic complex was reported by Yamamoto *et al.*[29] in 2004 where the effect of the two luminescent centres on the photophysical properties of was reported for the following complexes (Figure 6.5).[29]

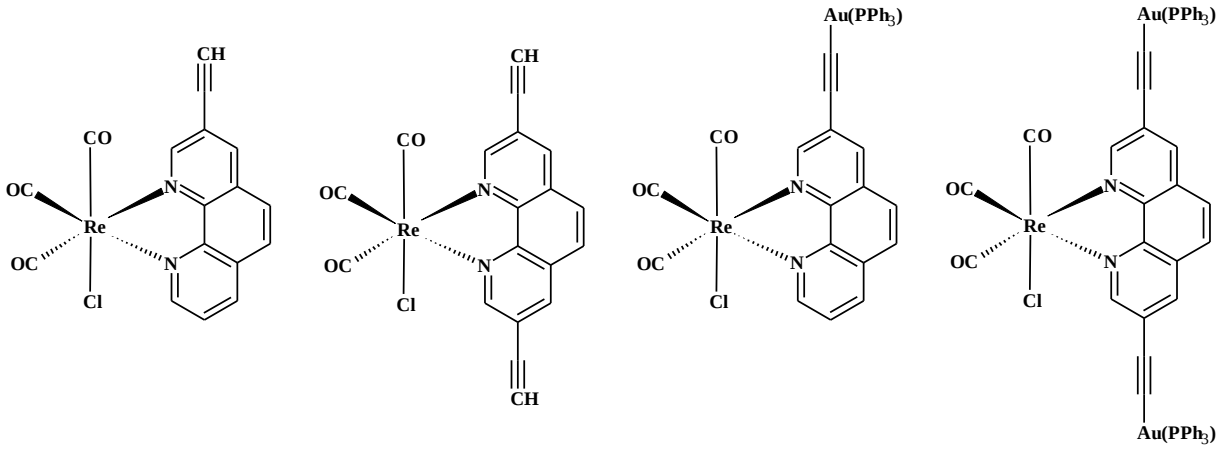

Figure 6.5 Re(I) and Au(I)-Re(I) complexes.[29]

The mono- and di-metallic Au(I) precursor complexes (not shown in Figure 6.5) displayed intense phosphorescence at room temperature with an excitation wavelength of 450 nm. The emission profiles of the hetero-metallic complexes (RHS Figure 6.5) were similar to those of the mono-metallic Re(I) complexes (LHS Figure 6.5) with a broad structure-less emission around 650 nm being observed only (absence of the Au(I) ligand based emission seen in pre-cursor). A higher quantum yield was observed for the hetero-metallic complexes when compared to the mono-metallic Re(I) complexes and this increase was attributed to intra-molecular energy transfer from the Au(I) to the Re(I) unit.[29]

Zuo *et al.*[30] reported the synthesis of a second tri-hetero-metallic complex, $Au(I)_2$-Re(I), with 1,2-dithiolene units included as the Au(I)-binding moieties. Little change was

observed between solid and solution state emission for all three complexes (Figure 6.6). When compared to the mono-metallic Re(I) complex, the ^{3}MLCT emission of the tri-metallic complex was significantly red-shifted; Re(I) 530 nm, $Au(I)_2$-Re(I) 597 nm. The red-shift in emission maxima was attributed to the presence of increased conjugation *via* the Au(I) units which reduced the HOMO-LUMO separation. A peak at 468 nm in both the di-metallic $Au(I)_2$ complex and the $Au(I)_2$-Re(I) tri-hetero-metallic complex is indicative of perturbed Au(I)- ligand based emission of the dithiolene.[30] No quantum yield measurements were reported for these complexes.

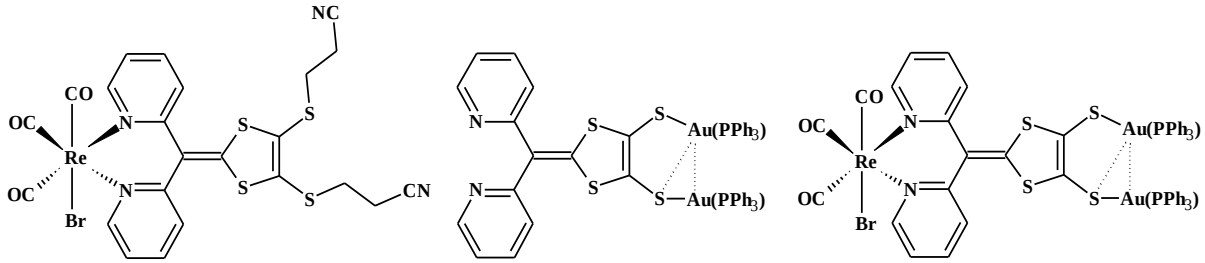

Figure 6.6 Re(I) mono-metallic (LHS), $Au(I)_2$ di-metallic (centre) and Re(I)-$Au(I)_2$ tri-metallic (RHS) complexes.[30]

Yam *et al.*[31] reported the synthesis of a novel series of Au(I)-Re(I) hetero-metallic complexes based on $[Re(CO)_3(bipy)]^+$ fragments substituted with the 4-ethynylpyridine Au(I) binding unit (Figure 6.7). With an excitation wavelength of >350 nm, emission ranging from 510-580 nm for each of the complexes was observed with little change in the maxima between solid and solution state emission.[31] Similarly to the emission profile of the hetero-metallic complex reported by Yamamoto *et al.* (but unlike the hetero-metallic complex reported by Zuo *et al.*) there was an absence of the alkyl based Au(I) emission, present in the precursor, indicating efficient intramolecular energy transfer from the Au(I) to the Re(I) unit. No quantum yield measurements were recorded for this series of complexes.

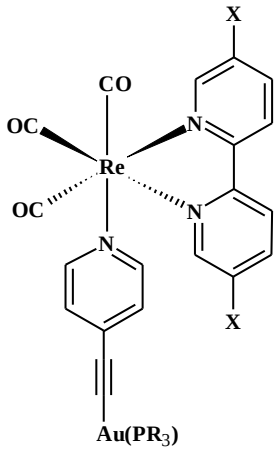

Figure 6.7 X = H / ^{t}Bu, R = PPh_3 / P(*p*-Tol)$_3$.[31]

Following on from the previously discussed Au(I)-Re(I) hetero-metallic complex by Yam *et al.*[31], Ferrer *et al.*[32] attempted to synthesise a Au(I)-Re(I)$_2$ tri-metallic type complex based on the same structure (Figure 6.8), using a similar procedure. However, a di-metallic Re(I) cation was produced from this reaction which indicated a transmetallation process had occurred; the ethynylpyridine group was transferred from the Au(I) to the Re(I).[32]This was the only report to highlight the importance in the order of metal addition in the synthesis of a hetero-metallic complex.

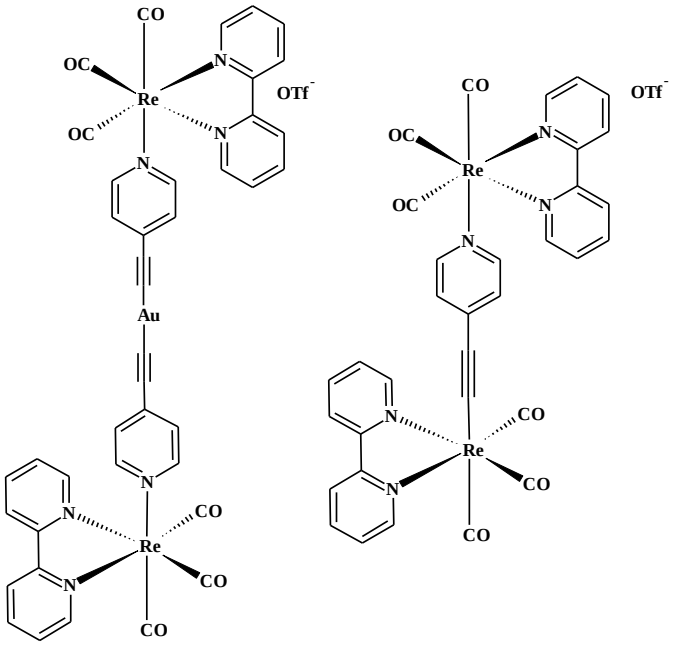

Figure 6.8 Target compound (LHS), actual compound (RHS).[32]

With only a few reports to date, little research has been devoted to hetero-metallic complexes inclusive of both Re(I) and Au(I) units. From the complexes that have been reported, no general predictions can be made in terms of the synthesis or photophysical properties and so in any attempt to synthesise complexes of this type it is necessary to start with simple ligand systems.

6.2. Overview

This chapter reports the synthesis of novel hetero-metallic complexes based around an Au(I)-alkyne unit. The hetero-metallic complexes investigated include: Au(I)-Re(I), Au(I)-Ru(II) and Au(I)-Ir(III). The first half of this chapter is devoted to investigating the synthesis and luminescent properties of a hetero-tri-metallic complex consisting of both Au(I) and Re(I) ions. Additionally, reported herein is the first application of a complex of this type in cellular imaging and a discussion of its potential use as a therapeutic agent is also included. The latter half of this chapter reports the synthesis of an analogous pair of novel ligands (varying in linking groups) and a discussion of both the successes and failures encountered during the attempts to synthesise the hetero-metallic species based on Au(I)-Re(I), Au(I)-Ru(II) and Au(I)-Ir(III) complexes which followed.

6.3. Results and discussion (part 1)

6.3.1. Synthesis of a bi-functional ligand

The simplest synthetic route to a ligand which will allow the incorporation of the two different metal ions (discussed above) is *via* a diimine central unit, however, commercially available diimines with additional functionality are costly. Various synthetic routes were therefore explored in an attempt to synthesise a functionalised diimine from low costing starting materials and these routes are discussed in detail below.

2,6-dibromopyridine is a commercially available, cheap organo-halide starting material with the functionality to undergo a coupling reaction. A homo-coupling reaction of the aryl halide would provide a cheap, synthetic route to the commercially available functionalised diimine ligand, 6,6'-dibromo-2,2'-bipyridine, a ligand equipped with halides permitting further reactivity (Figure 6.9). There are numerous reports on the synthesis of the target compound with yields varying from 10% to 79%,[33] however, when following literature precedent much smaller yields were obtained.

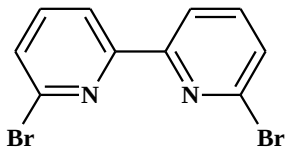

Figure 6.9 Target compound, 6,6'-dibromo-2,2'-bipyridine.

There are several coupling reagents andcoupling catalysts known which could assist in the formation of the target compound (Figure 6.9), including Gilman reagent, a 'turbo' Grignard reagent and Negishi coupling. All three methods of coupling were explored.

6.3.1.1 Synthesis of L^1

Gilman reagent coupling proceeds *via* the formation of an organocuprate, R_2CuI, where R is an organic radical. They are typically prepared at low temperatures as organocuprates are thermally labile. Organocuprates react well with organo-halides to form a new carbon-carbon bond.[16] This methodology was followed and 6,6'-dibromo-2,2'-bipyridine, $\mathbf{L^1}$,was formed with an 18 % yield.

An alternative reagent in a coupling reaction is the turbo Grignard reagent. An aryl Grignard compound couples with an aryl-halide to form the new carbon-carbon bond. However, when this methodology was followed there was no evidence of product formation.

The inclusion of a catalyst, for example nickel or zinc chloride can enhance the reactivity and selectivity in Grignard coupling reactions.[5]

Negishi coupling is a Pd catalysed cross-coupling reaction between an organo-halide and an organo-zinc compound to form a new carbon-carbon bond. This was the more favourable coupling route out of the three discussed with **L^1** being formed in the highest yield of 42 % (Figure 6.10).

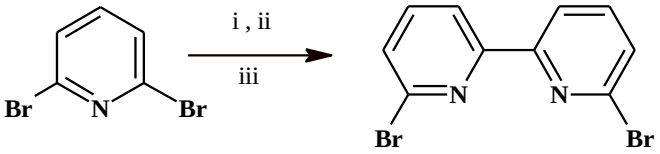

Figure 6.10 Synthesis of L^1. Reagents: (i) BuLi; (ii) $ZnCl_2$; (iii) $Pd(PPh_3)_4$, 2,6 dibromopyridine.

Negishi coupling was carried out *via* the lithiation of 2,6 dibromopyridine (0.5 eq.) using BuLi (1.6 M) at -78 ˚C. $ZnCl_2$ was then added to the reaction mixture to form the more reactive organo-zinc precursor required for coupling. The addition of both the $Pd(PPh_3)_4$ catalyst and the second 0.5 eq. of 2,6 dibromopyridine (organo-halide) followed after 20 minutes. Product formation was confirmed using ^{1}H NMR spectroscopy; **L^1** was formed in a moderate yield of 42 %. Co-ordination of **L^1** to Re(I) was now achievable, but further adaptation was required to allow successful co-ordination of a Au(I) moiety.

6.3.1.2. Synthesis of L^2 and L ^{3}

Despite **L^2** and **L^3** being reported previously[5] they are included herein as they provide a synthetically pleasing route for the synthesis of a novel, hetero-metallic complex. Following literature precedent for a Sonogashira cross-coupling reaction, two equivalents of trimethylsilyethylene were coupled to **L^1**, forming **L^2** (Figure 6.12). The removal of the TMS groups was achieved using potassium fluoride or potassium carbonate under mild conditions to produce **L^3** in low and moderate yields; 19 % and 78 % respectively.

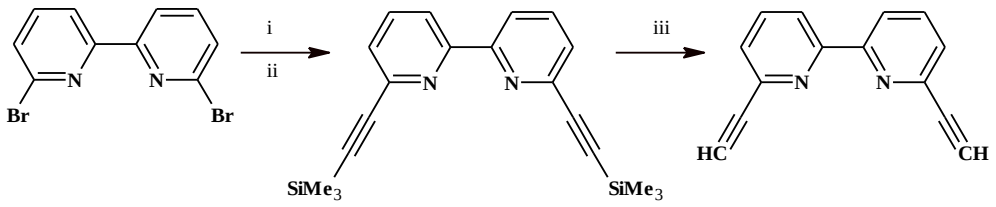

Figure 6.11 L^1 (LHS), L^2 (centre) and L^3 (RHS). Reagents: (i) CuI, $Pd(OAc)_2$, PPh_3; (ii) TMS ethylene; (iii) KF.

6.3.1.3. Attempts to further functionalise the ligands

The small number of hetero-metallic complexes inclusive of Re(I) and Au(I) units to date are generally based around a single diimine and an alkyne unit. In an attempt to expand the functionality within the complexes in question, a series of coupling reactions were carried out using $\mathbf{L^1}$ and $\mathbf{L^3}$, as well as a mono-alkyne bipyridine (Figure 6.12) to extend the number of diimine units within the ligand systems.

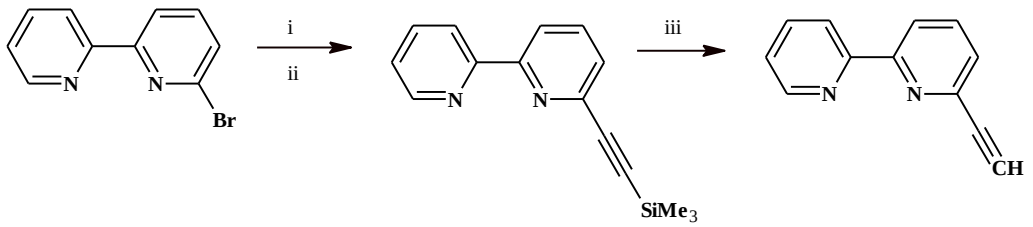

Figure 6.12 Synthesis of 2-ethynylbipyridine from commercially available 6-bromo-2,2'-bipyridine. Reagents: (i) CuI, $Pd(OAc)_2$, PPh_3; (ii) TMS ethylene; (iii) KF.

Sonogashira coupling reactions were carried out between $\mathbf{L^1}$ with $\mathbf{L^3}$ and $\mathbf{L^1}$ with the newly formed 2-ethynylbipyridine (Figure 6.13). The reactions were carried out following the same procedure as above, but in both cases there was little evidence of the product forming. Both the ratio of catalyst used and the nature of the catalyst ($Pd(OAc)_2$ and $Pd(PPh_3)_4$ were varied for both reactions with little visible effect. With little change expected in the ^1H NMR spectra for the complexes MS were carried out for initial characterisation; MS data for $\mathbf{L^1}$ with $\mathbf{L^3}$ showed evidence of product formation but no pure products were obtained despite attempts at purification by chromatography and crystallisation.

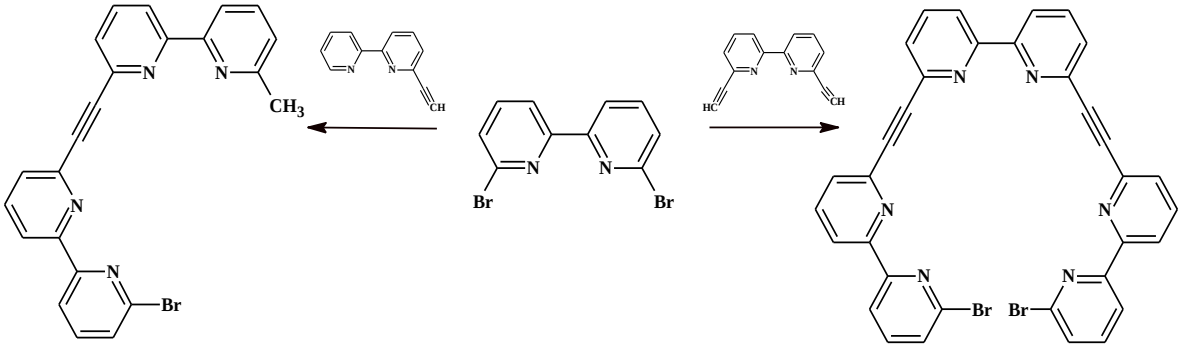

Figure 6.13 Predicted possible outcomes from the coupling reactions of L^1 with L^3 and 2-ethynylbipyridine.

A Sonogashira coupling of $\mathbf{L^1}$ with 4-bromopyridine was also attempted using $Pd(OAc)_2$ following the same coupling procedure as above but an unexpected compound was recovered [$C_{12}H_8BrPdCl_2$] (Figure 6.14). The nature of the complex formed indicated, with the presence of C-Br bond, that the catalytic cycle did not work and so an alternative synthetic approach was taken to functionalise the aromatics.

Figure 6.14 Unexpected product.

6.3.1.4. Synthesis and reactivity of L^4 and L^5

$\mathbf{L^4}$ and $\mathbf{L^5}$ were synthesised by heating hydrazine with 6-bromo-2-2'-bipyridine and $\mathbf{L^1}$ respectively (Figure 6.15). Although the syntheses of ligands of this type are known,[34] the nature of the products formed seemed to be dependent on the scale of the reaction. In large scale reactions the reduction of both 6-bromo-2,2'-bipyridine and 6,6-dibromo-2,2'-bipyridine to bipyridine and/or 6-hydroxy-2,2'-bipyridine was evident in the ^{1}H NMR spectra with the absence of the expected peak at +6.5 ppm for the predicted product and the presence of only four peaks in the aromatic region. This result was confirmed using IR spectroscopy and MS spectrometry. Small scale reactions provided $\mathbf{L^4}$ and $\mathbf{L^5}$ in moderate yields.

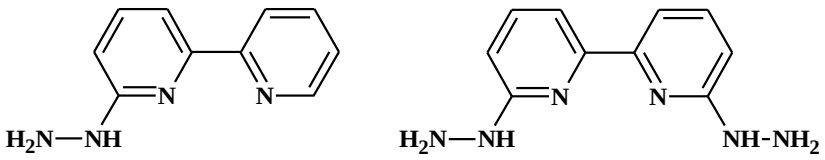

Figure 6.15 L^4 (LHS) and L^5 (RHS)

Mimicking the conditions required for the formation of $\mathbf{L^4}$ and $\mathbf{L^5}$ (high temperatures and small scale), $\mathbf{L^4}$ was reacted with $\mathbf{L^1}$, but again, 2,2'-bipyridine was recovered. It was suspected that the reduction of $\mathbf{L^1}$ results from the presence of palladium, left over from the Sonogashira coupling, since the presence of palladium and hydrazine will act as a reducing agent rather than a nucleophile. $\mathbf{L^1}$ was subsequently washed with EDTA and the reaction was repeated. Although a number of attempts were made to further functionalise the diimine unit whilst still maintaining the ability to add an alkyne unit, no successful route was found.

6.3.2. Synthesis and characterisation of the complexes

The synthesis, together with the photophysical properties of the di-metallic gold complex, {[Au(PPh$_3$)]$_2$L^3}, has been reported previously[5] but is discussed herein for easy referral when discussing the novel tri-hetero-metallic complex {Re(CO)$_3${[Au(PPh$_3$)]$_2$(L^3)Br}. The synthesis of the following mono-, di- and tri-metallic complexes of **L$^{1-3}$** was achieved following literature precedent. The pure complexes were isolated in moderate yields ranging from 30 % for [Re(CO)$_3$(L^2)Br] to 76 % for {[Au(PPh$_3$)]$_2$L^3}.

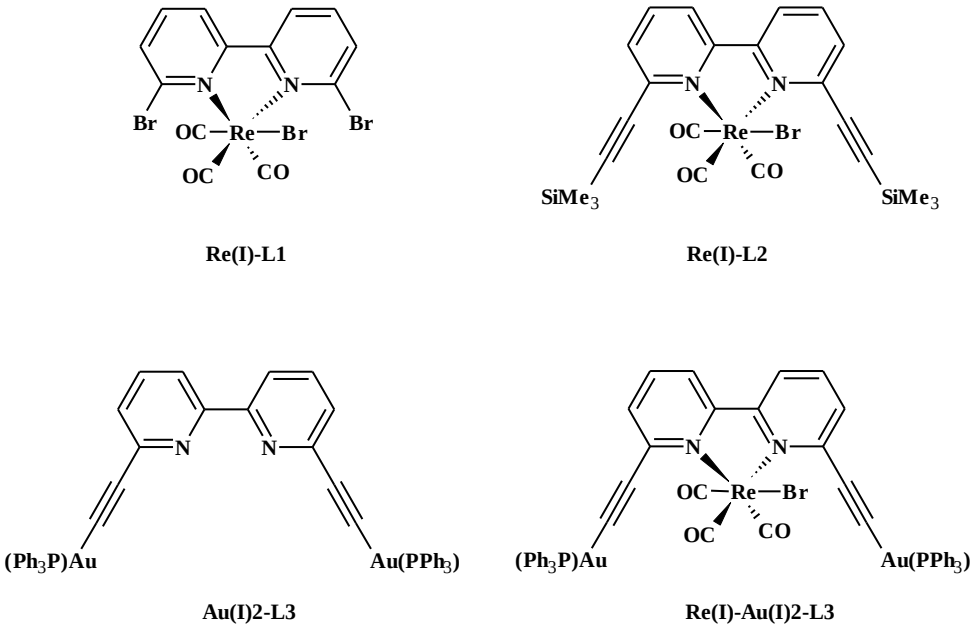

Figure 6.16 The complexes discussed herein.

Characterisation of the complexes was achieved using a variety of spectroscopic and spectrometric techniques the analysis of which is discussed in more detail in this section. ^{1}H NMR spectra were obtained for each complex in $CDCl_3$ or CD_3CN, comparison to the free ligand confirmed the successful co-ordination of the ligands to the Re(I) and or Au(I) units.

6.3.2.1. The synthesis and characterisation of [Re(CO)$_3$(L$^{1-3}$)Br]

In the ^{1}H NMR spectrum of [Re(CO)$_3$(L^1)Br] a shift of the four aromatic protons in positions 4,4'- and 3,3'-, to higher frequency (+7.42 ppm and +7.61 ppm to +7.88 ppm respectively) was observed; for [Re(CO)$_3$(L^2)Br], a shift of the aromatic proton, in positions 5,5'-, to lower frequency, (+8.43 ppm to +7.68 ppm), was observed. The contrasting nature of this NMR data is attributed to the co-ordination of the [Re(CO)$_3$Br] unit; the difference in the

electron density at the 5,5- position is enhanced for $\mathbf{L^2}$ > $\mathbf{L^1}$ upon co-ordination of the $[Re(CO)_3Br]$.

An attempt was made to synthesise the analogous mono-metallic complex of $[Re(CO)_3(L^{1/2})Br]$ using $\mathbf{L^3}$ but an insoluble, non-fluorescent compound resulted. The presence of un-protected alkynes within $\mathbf{L^3}$ adds additional co-ordination sites suitable for co-ordination of the Re(I) units, this can lead to the formation of a coordination polymer (Figure 6.17). The formation of a polymer, either through coordination chemistry or through metal-induced polymerisation of the alkynes could account for the limited solubility and the non-fluorescent nature of the compound.

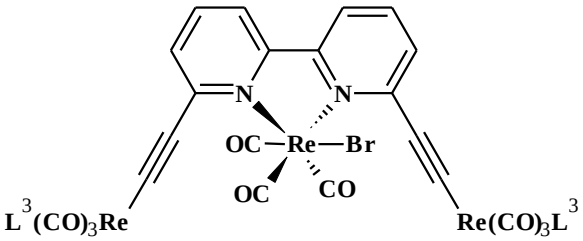

Figure 6.17 Potential polymer type compound.

An alternative synthetic route to form $[Re(CO)_3(L^3)Br]$ was carried out using $[Re(CO)_3(L^2)Br]$ and KF following the same procedure for the synthesis of $\mathbf{L^3}$ but again an insoluble product resulted.

6.3.2.2. Synthesis of rhenium alkynes

The reactivity of alkynes toward TM ions has been subject of many studies, however, little research has been devoted to Re(I) alkyne bonding. Insight regarding the nature of the polymer formed in the reaction between $\mathbf{L^3}$ and $[Re(CO)_5Br]$ requires an understanding of the requirements necessary to form Re(I) alkyne bonds, and the tolerance of the reactions to various functional groups. To further probe these conditions, a series of reactions were carried out between $[Re(CO)_3(bipy)MeCN]^+$ and the following commercially available alkynes: phenyl acetylene, propargyl alcohol and ethyl propiolate (Figure 6.18).

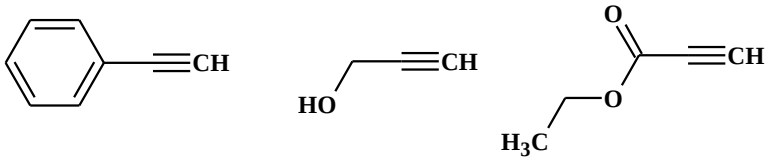

Figure 6.18 phenylacetylene (LHS), propargyl alcohol (centre) and ethylpropiolate (RHS).

The first reaction was carried out following literature precedent[35] using thallium hexafluorophosphate for the formation of a Re(I) acetylene compound (Figure 6.19).

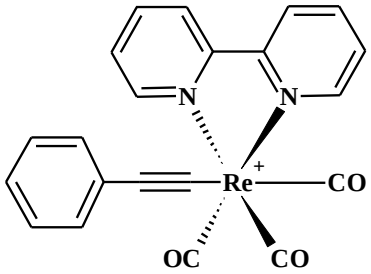

Figure 6.19 $[Re(CO)_3(bipy)phenylacetylene]^+$

The Re(I) acetylene compound was successfully formed, however, following the same method, using propargyl alcohol and ethylpropiolate, there was no evidence of a reaction occurring; starting material was recovered only. With no further understanding on the conditions required to form the Re(I)-alkyne units, the synthesis of $[Re(CO)_3(L^3)Br]$ using $\mathbf{L^3}$ was unlikely.

6.3.2.3. Synthesis of the hetero-metallic complex

The order of metal ion addition has proven important in the synthesis of hetero-metallic complexes of this nature and so both the protected and the unprotected alkyne ligands, $\mathbf{L^2}$ and $\mathbf{L^3}$, were used to synthesis the di-metallic complex $\{[Au(PPh_3)]_2L^3\}$. Similarly to the reported synthesis of $\{[Au(PPh_3)]_2L^3\}$, little change in the ^1H NMR spectra of the ligand was seen upon co-ordination of the gold to the terminal alkynes (except the loss of the terminal proton). The $^{31}P\{^1H\}$ NMR spectra of the complexes gave a signal in agreement to the literature, with a single peak at +42.66 observed.

The successful co-ordination of $[Re(CO)_3Br]$ was achieved following literature precedent forming a novel tri-hetero-metallic complex, $\{Re(CO)_3\{[Au(PPh_3)]_2L^3\}Br\}$, in a 62 % yield (no transmetallation was seen). In the ^1H NMR spectrum of the complex, one broad peak in the aromatic region, equating to all thirty six protons, was observed. The $^{31}P\{^1H\}$ NMR spectrum consisted of a single peak with a chemical shift which had moved to a lower frequency, from +42.66 to +35.6 ppm. The difference in ^{31}P NMR shifts between the di-metallic and tri-hetero-metallic complex can be explained in terms of the donating ability; the presence of Re(I) lowers the electron density on the diimine which in-turn lowers the electron density at the Au(I)-P unit. This was also confirmed through IR studies; $\{[Au(PPh_3)]_2L^3\}$,

C≡C 2116 cm^{-1} and {[$Re(CO)_3${$Au(PPh_3)$}$]_2L^3$}Br}, C≡C 2151 cm^{-1}; the introduction of the Re(I) unit induces a 'pull'of electron density from the diimine unit, and this results in the strengthening of the C≡C unit (observed through an increase in the *v*(CC) of 35 cm^{-1}) and a decrease in the electron density at the Au(I)-P unit. MS analysis for the complexes gave a peak at 721 only, and this peak has been reported by Schmidbaur *et al.*[36] and attributed to the breakdown of complex within the mass spectrometer and then recombination to form $[Au(PPh_3)_2]^+$.

6.3.2.4. Single crystal X-ray diffraction studies

Re-crystallisation of complexes $[Re(CO)_3(L^1)Br]$ and $[Re(CO)_3(L^2)Br]$ yielded pale orange crystals suitable for X-ray diffraction studies. The crystals were obtained *via* vapour diffusion of diethyl ether into a concentrated dichloromethane solution.

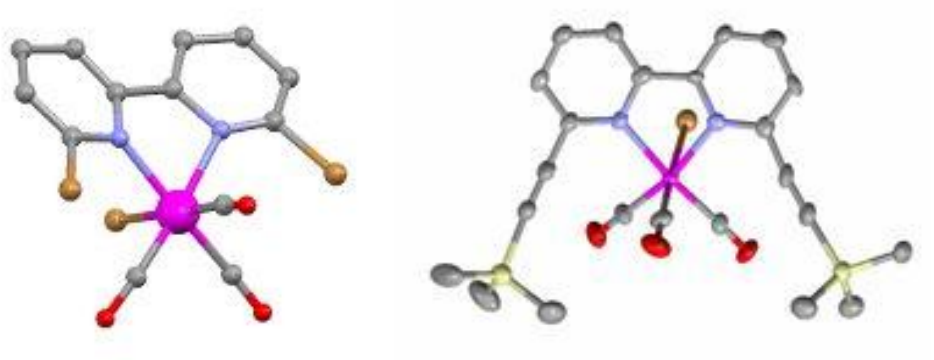

Figure 6.20 Structural representations of complexes $[Re(CO)_3(L^1)Br]$ and $[Re(CO)_3(L^2)Br]$ (H atoms omitted for clarity).

The parameters associated with the data collections of the novel complexes, $[Re(CO)_3(L^1)Br]$ and $[Re(CO)_3(L^2)Br]$ (Table 6.2), and the selected bond lengths and bond angles (Table 6.1) are shown below.

Table 6.1 Selected bond lengths and bond angles for the complexes: $Re(CO)_3(L^1)Br]$ and $[Re(CO)_3(L^2)Br]$.

$[Re(CO)_3(L^1)Br]$	**$[Re(CO)_3(L^2)Br]$**
$C_{13}H_6Br_3N_2O_3Re$	$C_{23}H_{24}BrN_2O_3ReSi_2$
Bond Lengths (Å)	
Re-Br 2.619 (2)	Re-Br 2.614 (1)
Re-N 2.204 (6)	Re-N 2.19 (9)
C-Br 1.879 (8)	C-Si 1.87 (1)
	C-C 1.19 (2)

Table 6.2 Crystal data refinement details for the crystal structures of $[Re(CO)_3(L^1)Br]$ and $[Re(CO)_3(L^2)Br]$.

	$[Re(CO)_3(L^1)Br]$	$[Re(CO)_3(L^2)Br]$
Empirical formula	$C_{13}H_6Br_3N_2O_3Re$	$C_{23}H_{24}BrN_2O_3ReSi_2$
Formula weight	664.13	698.73
Temperature	150(2)K	150(2)K
Wavelength	0.71013Å	0.71013Å
Crystal system	Monoclinic	Monoclinic
Space group	P2(1)/*m*	P2(1)/a
Unit cell dimensions	a = 6.4833 (4) Å	a = 13.5076 (4) Å
	α = 90.00 ˚	α = 90.00 ˚
	b = 14.3775 (10) Å	b = 13.9248 (4) Å
	β = 105.961(4) ˚	β = 107.145(2) ˚
	c = 9.0151 (5) Å	c = 14.3606 (3)
	ϒ =90.00˚	ϒ =90.00˚
Volume	807.93 $Å^3$	2581.06 $Å^3$
Z	2	4
Density (calculated)	2.730 g/cm^3	1.798 g/cm^3
F(000)	604	1352
Crystal size	0.20 × 0.20 × 0.20	0.20 × 0.20 × 0.20
Theta range for data collection	55.1 ˚	56.6
All reflections	3204	22858
Independent reflections	1915	6356
Observed reflections	1701	4903
Goodness-of-fit on F	1.050	1.204
R_{int}	0.0415	0.1201
Final R indices [I>2sigma(I)] R indices (all data)	R_1 = 0.0456 wR_2 = 0.1117	R_1 = 0.0959 wR_2 = 0.1500

6.3.3. UV-Vis absorption spectroscopy

The UV-Vis data are summarised in Table 6.3. The high energy transitions around 250 nm are attributed to ^{1}IL ($\pi \rightarrow \pi^*$) or metal perturbed ^{1}IL transitions. The moderately low energy absorptions in the regions of 330 nm are indicative of ligand to ligand charge transfer (^{1}LLCT) transitions from the π orbital on the alkyne ligands. The transitions in the region of 340-400 nm are assigned to the spin allowed transfer (^{1}MLCT) (d $\pi \rightarrow \pi^*$).

Table 6.3 Photophysical data for the complexes (part 1). λexc = 340 nm.

Compound	Abs (nm)	ε (dm^3 mol^{-1} cm^{-1})	Em(MeCN) (nm)	Lifetimes (MeCN) (ns)
$Re(CO)_3(L^1)Br]$	258	8248		
	324	7757	625	< 2
	397	1380		
$Re(CO)_3(L^2)Br]$	253	1450	480	
	280	914	619	29.4
	335	709		
$\{[Au(PPh_3)]_2L^3\}$	228	17519	477	< 2
	329	2860		
$\{Re(CO)_3\{[Au(PPh_3)]_2L_3\}Br\}$	268	11149	475	
	309	6351	588	1.59
	375	3038		

6.3.4. Luminescent spectroscopy

Luminescence spectra were obtained in aerated acetonitrile and dichloromethane following irradiation at λ_{ex}: 340 nm, 370 nm and 405 nm. DCM was included for ease of comparison to the literature values recorded. The data and spectra recorded in acetonitrile at 405 nm are shown in Table 6.3 and Figure 6.21.

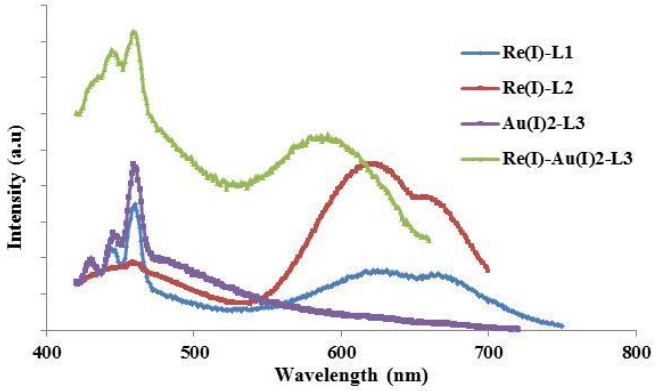

Figure 6.21 Steady state emission spectra recorded in acetonitrile (λ_{exc} 405 nm).

Neutral complexes, $[Re(CO)_3(L^1)Br]$ and $Re(CO)_3(L^2)Br]$, differ only in the functional group appended to the aromatic chromophore, bromide and trimethylsilylethylene respectively. Both display an emission band around 620 nm which is attributed to a ^{3}MLCT transition. The only appreciable difference between the spectra (λ_{exc} 405 nm) was the presence of an additional emission band centred on 480 nm for $[Re(CO)_3(L^2)Br]$, this broad emission band was present in both $\{[Au(PPh_3)]_2L^3\}$ and $\{Re(CO)_3\{[Au(PPh_3)]_2L^3\}Br\}$. The absence of the gold units in $[Re(CO)_3(L^2)Br]$ indicated the emission present at 480 nm in all three complexes, $[Re(CO)_3(L^2)Br]$, $\{[Au(PPh_3)]_2L^3\}$ and $\{Re(CO)_3\{[Au(PPh_3)]_2L^3\}Br\}$, was likely to be perturbed, ^{1}IL fluoresecence, CC ($\pi \rightarrow \pi^*$).

Neutral Re(I) diimine complexes generally show lifetimes in the order of hundreds of ns but the luminescence lifetime of $[Re(CO)_3(L^1)Br]$ was too short to be reliably measured (Figure 6.22), for $[Re(CO)_3(L^2)Br]$ a lifetime of 29.4 ns was observed. The unexpectedly short lifetimes for these complexes can be attributed to non-radiative quenching.

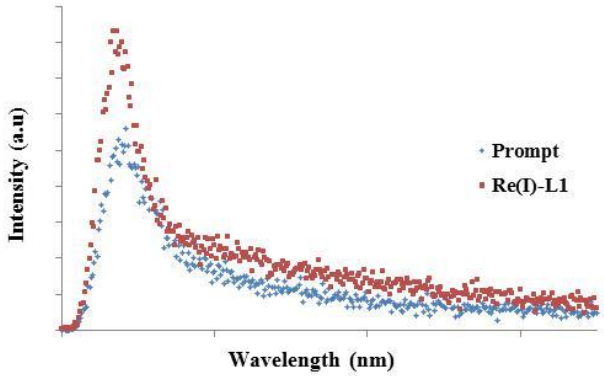

Figure 6.22 Lifetime spectrum of $[Re(CO)_3(L^1)Br]$. (λ_{exc} = 295 nm).

6.3.4.1. Luminescent properties of $\{Re(CO)_3\{[Au(PPh_3)]_2L^3\}Br\}$

$\{Re(CO)_3\{[Au(PPh_3)]_2L^3\}Br\}$ is a dual emissive complex with ligand-based emission observed at 475 nm and ^{3}MLCT based emission at 588 nm. Similarly to its precursor complex, $\{[Au(PPh_3)]_2L^3\}$, $\{Re(CO)_3\{[Au(PPh_3)]_2L^3\}Br\}$ showed no evidence of Au(I)-based phosphorescence in solution (Figure 6.23). The ^{3}MLCT based emission for the hetero-metallic complex was blue-shifted by *ca*. 30 nm when compared to the analogous complexes $[Re(CO)_3(L^1)Br]$ and $[Re(CO)_3(L^2)Br]$. Both the presence of the ligand-based emission peaks in the luminescent spectra and the short luminescence lifetime of the tri-metallic-complex suggest that there was no intramolecular transfer of energy from the ligand based states to the MLCT levels, but the very low lifetime of the neutral complex (Table 6.3) does indicate quenching of the luminescent lifetime and so the possibility of RET cannot be completely ruled out.

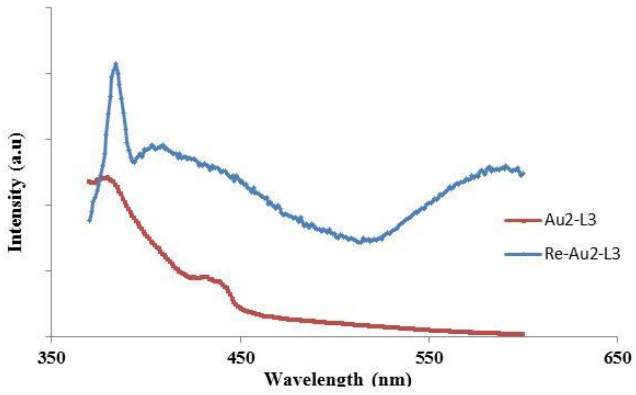

Figure 6.23 Steady state emission spectra recorded in acetonitrile for $\{[Au(PPh_3)]_2L^3\}$ and $\{Re(CO)_3\{[Au(PPh_3)]_2L^3\}Br\}$ (λ_{exc} 345 nm).

6.4. Cytotoxicity investigation

A preliminary study of the cytotoxicity of the tri-hetero-metallic complex was undertaken using the MTT assay with four different cancer cell lines: MCF7 (breast adenocarcinoma), A549 (lung adenocarcinoma), PC3 (prostate adenocarcinoma) and LoVo (colon adenocarcinoma). For the MTT assay, the compound was initially dissolved in DMSO, and doses of 0.1, 1, 10 and 100 μm were tested to analyse the activity of different concentrations and then compared to a control medium with no treatment. The approximate IC_{50} values for the compound is shown in in Table 6.4.

Table 6.4 Cytotoxicity results for $\{Re(CO)_3\{[Au(PPh_3)]_2L^3\}Br\}$

Complex	**IC_{50} MCF7**	**IC_{50} PC3**	**IC_{50} A549**	**IC_{50} Lovo**
$\{Re(CO)_3\{[Au(PPh_3)]_2L^3\}Br\}$	5	70	5	5

A comparison of the IC_{50} values in Table 6.4, shows that the tri-hetero-metallic complex, $\{Re(CO)_3\{[Au(PPh_3)]_2L^3\}Br\}$, is apparently more toxic than the di-homo-metallic, type complexes $\{[Au(PPh_3)]_2L\}$ reported in Chapter 4. The tri-hetero-metallic complex shows considerably less cytotoxicity to PC3 (prostate) than the other three cell lines tested with an IC_{50} value 14 times higher. The cytotoxicity values in MCF-7, A549 and LoVo were considerably higher than that of cisplatin (IC_{50} = 2.0 μM)[37] and so applications solely as a therapeutic agent is unlikely. Similarly to the complexes discussed in Chapter 4, the MCF-7 cell line showed sensitivity to the tri-hetero-metallic complex and so its therapeutic application and cellular distribution were investigated *via* confocal fluorescence microscopy.

6.5. Cell imaging of $\{Re(CO)_3\{[Au(PPh_3)]_2L^3\}Br\}$

With the ^{3}MLCT based emission preferable to an excitation wavelength of 405 nm, the novel tri-hetero-metallic complex, $\{Re(CO)_3\{[Au(PPh_3)]_2L^3\}Br\}$, was investigated for its suitability as a cellular imaging agent or sensor. $\{Re(CO)_3\{[Au(PPh_3)]_2L^3\}Br\}$ was incubated with MCF-7 cells over a 30 minute period at 4 ˚C. The low temperature allows energy-dependent uptake processes, such as endocytosis, to be omitted. Following the removal of excess agent, the cells were allowed to warm to room temperature. At room temperature the cells functions normalise and energy-dependent pathways are no longer omitted allowing the accumulation and toxicity of the investigated complexes to be viewed.

The sample was imaged by confocal microscopy using an excitation wavelength of 405 nm and a detection range between 560-610 nm, in accordance with the ^{3}MLCT emission reported in Table 6.3 (thus eliminating autofluorescence). The complex showed successful uptake with > 90 % of cells showing rhenium based emission whilst maintaining good cell morphology.

The hetero-metallic complex, $\{Re(CO)_3\{[Au(PPh_3)]_2L^3\}Br\}$, showed variable levels of intensity of rhenium based emission throughout the entire cell. The cytoplasm and nucleus exhibit background emission with the presence of intense spots indicative of specific-localisation; the presence of intense spots/regions (hot spots) within the cytoplasm indicates accumulation of the complex within certain organelles. The intense spots in the centre of the nucleus are similar to the di-rhenium ester complex discussed in Chapter 3 which was indicative of nucleolar staining. Further studies are required for this complex with incubation at lower temperature and a co-localisation experiment.

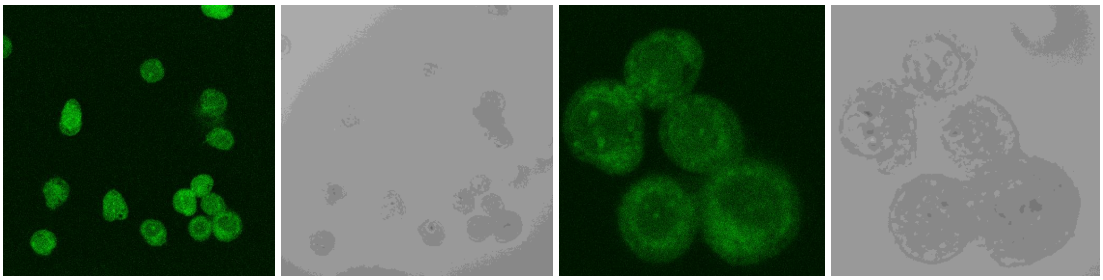

A B C D

Figure 6.24 Imaging with $\{Re(CO)_3\{[Au(PPh_3)]_2L^3\}Br\}$ in MCF-7 cells showing: (A) & (C) cytoplasmic & necleolar distribution; (B) & (D) transmitted light only.

6.6. Conclusion

The first half of this chapter highlighted the investigation into the synthesis of a novel tri-hetero-metallic complex, $\{Re(CO)_3\{[Au(PPh_3)]_2L^3\}Br\}$, and the additional attempts to add further functionality to ligands of this nature through a variety of coupling reactions. The cytotoxicity studies on the tri-hetero-metallic complex demonstrated its cytotoxic profile for four different tumour cell lines; MCF-7, PC3, A459 and LoVo. The IC_{50} values for MCF-7, A549 and LoVo were identical with an IC_{50} value of 5 μM. For PC3 an IC_{50} value fourteen times higher was observed. The cellular uptake and localisation potential of the hetero-metallic complex in MCF-7 cells was also investigated. The complex shows good cellular uptake with both specific and non-specific localisation throughout the entire cell. Both the cytotoxic and photophysical properties confirm the complex suitability as both an imaging and or a therapeutic agent. Additional investigations into the selectivity towards cancer cells over healthy cells for this complex could be performed as well as the additional confocal microscopy experiments discussed previously.

6.7. Di-hetero-metallic complexes

The first half of this chapter was based around a tri-hetero-metallic complex inclusive of one rhenium unit and two gold units and promotes its suitability as both a therapeutic and cellular imaging agent. The latter half of this chapter is dedicated to the synthesis of di-hetero-metallic complexes inclusive of different d^6 TM and a Au(I) moiety and discusses their potential future applications.

6.8. Results and discussion (part 2)

6.8.1. Synthesis of pre-cursor ligands for the formation of di-hetero-metallic complexes

The simplest synthetic route to a ligand suitable for the synthesis of a di-hetero-metallic complex is *via* a diimine unit with one additional functional moiety only. Omitting the commercially available 6-bromo-2,2'-bipyridine (due to expense) two synthetic procedures for a ligand of this type were carried out. 2-(2-4-methyl pyrimidine) pyridine (Figure 6.25) and 5-methyl-2,2'-bipyridine (Figure 6.26) were produced *via* two-step synthesis following literature precedent in yields of 74 % and 58 % respectively.[38]

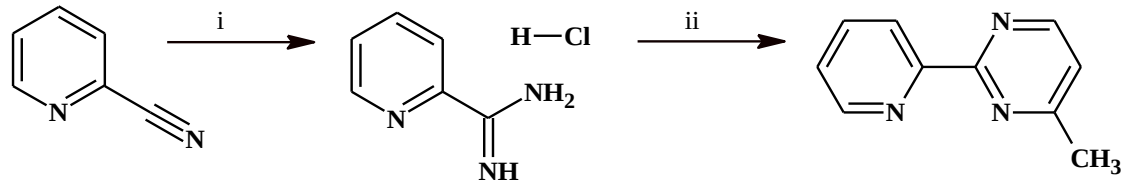

Figure 6.25 Synthesis of 2-(2-4-methyl pyrimidine) pyridine Reagents; (i) K^{t}BuO, MeOH, 4,4 dimethoxy-2-butanone; (ii) K^{t}BuO, 4,4 dimethyl oxybutan-2-one Δ.

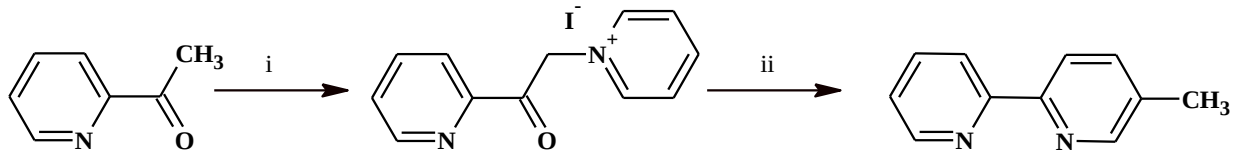

Figure 6.26 Synthesis of 5-methyl-2,2'bipyridine. Reagents; (i) iodine, pyridine, N_2(g), Δ; (ii) methacrolein, ammonium acetate, formamide, Δ.

2-(2-4-methyl pyrimidine) pyridine and 5-methyl-2,2'-bipyridine differ in the position of the methyl group (6 and 5 respectively) which can affect their reactivity. To form a hetero-metallic complex, both precursors require the addition of an alkyne unit for the successful co-ordination to a gold moiety. The alkyne unit can be added in one of two ways; the first is *via* the formation of an alkyl bromide and then the addition of an alkyne unit (*via* a Sonogashira coupling reaction); the second is *via* the formation of an acid group (oxidation of the methyl) followed by the addition of the alkyne unit *via* a condensation reaction. Both routes were carried out on 2-(2-4-methyl pyrimidine) pyridine and 5-methyl-2,2-bipyridine.

6.8.2. Reactivity of 2-(2-4-methyl pyrimidine) pyridine

6.8.2.1.Bromination of 2-(2-4-methyl pyrimidine) pyridine

Azobisisobutyronitrile (AIBN) is a radical initiator commonly used as a photo initiator in the production of vinyl-based polymers such as PVC. It can be used as a catalyst in radical bromination when using N-bromosuccinimide (NBS). The formation of 2-(2-4-bromo methyl pyrimidine) pyridine was attempted following literature precedent using AIBN[38] however, only starting material remained.

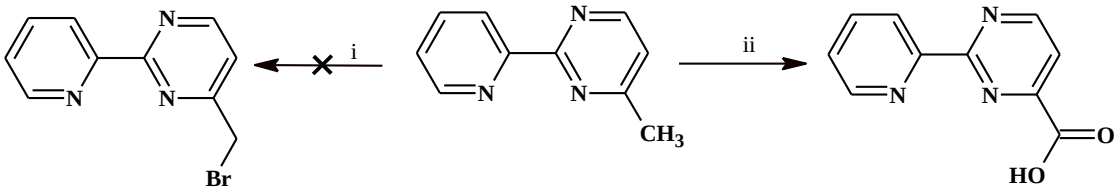

Figure 6.27 Reagents; (i) *N*-bromosuccinimide, benzoyl peroxide, CCl_4; (ii) Na_2CO_3, $KMNO_4$, Δ.

6.8.2.2. Oxidation of 2-(2-4-methyl pyrimidine) pyridine

Organic oxidations of aromatic methyl groups using selenium oxide have also been reported, but when attempted there was no evidence of any reaction having occurred.[39]An alternative oxidation reaction using an excess of potassium permanganate in the presence of sodium carbonate was carried out which produced the desired product, albeit in a low yield.[40]

6.8.3. Reactivity of 5-methyl-2,2'-bipyridine

6.8.3.1.Bromination of 5-methyl-2,2'-bipyridine

The formation of 5-bromomethyl-2,2'-bipyridine was attempted following literature precedent using AIBN[37] however, only starting material remained. With both 2-(2-4-methyl pyrimidine) pyridine and 5- methyl-2,2'-bipyridine having resulted in no reaction, the quality of the AIBN initiator was suspected to be poor and so benzoyl peroxide was used as an alternative radical initiator. 5-bromomethyl-2,2'-bipyridine was subsequently formed in a 24 % yield. Despite the successful formation of 5-bromomethyl-2,2'-bipyridine, no further reactions were carried out with this ligand precursor as low levels of stability were observed when the compound was left over short periods of time at room temperature. The decreased stability of the complex is believed to result from the occurrence of intermolecular reactions between the bipyridine nitrogen and the alkyl bromide.

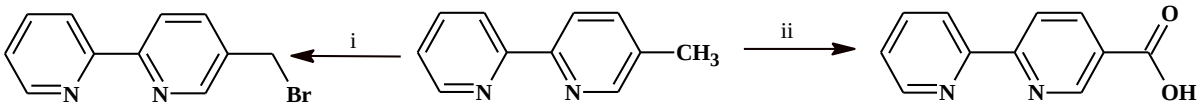

Figure 6.28 Reagents; (i) *N*-bromosuccinimide, benzoyl peroxide, CCl_4; (ii) Na_2CO_3, $KMNO_4$, Δ.

6.8.3.2. Oxidation of 5-methyl-2,2'-bipyridine

Organic oxidation using an excess of potassium permanganate in the presence of sodium carbonate was carried out on 5-methyl-2,2'-bipyridine which produced 5-carboxylic acid-2,2'-bipyridine in a 54 % yield.[40] Having produced a suitably functionalised bipyridine in a moderate yield, further work with this ligand precursor was carried out. The addition of an alkyne unit to 5-carboxylic acid,-2,2'-bipyridine *via* a condensation reaction was then carried out using two different functionalised alkynes.

6.8.4. N-methyl propargyl amine

N-propargyl amines are heavily used as MAO-inhibitors. MAO is an acronym for monoamine oxidase; it is an enzyme found on the outer membrane of the mitochondria in most cells in the body and catalyses the deamination of monoamines.[41-43]MAO inhibitors can act as an anti-depressant and can also be used in the treatment of Alzheimers and Parkinsons disease. Too much or too little MAO activity can lead to psychiatric and neurological disorders.[43,44] There have been numerous studies on the structure-activity relationship of N-propargyl amines inclusive of N-methyl propargyl amine which have concluded that the structure of the propargyl amine is essential in their inhibitor function.[45-48] The presence of N-methyl propargyl amine within a complex adequate for cellular imaging promotes an innovative method for investigating its inhibiting function.

Propargyl alcohol and N-methyl propargyl amine were used to produce novel ligands, **L^6** and **L^7** in excellent yields of 83 % and 84 % respectively. The position of the alkyne protons, CH_2 and CH, in the ^1H NMR spectra were used to distinguish the products from starting material.

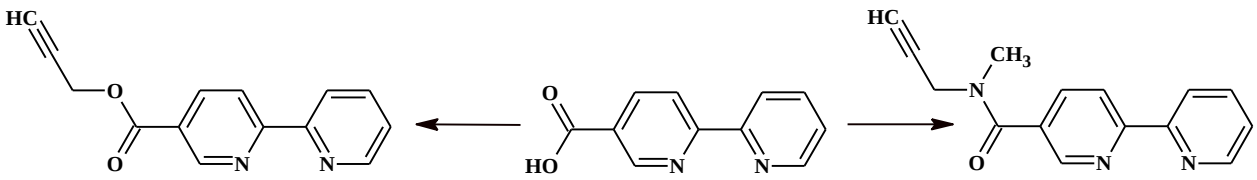

Figure 6.29 L^6 (RHS) & L^7 (LHS)

6.8.4.1. Characterisation of L^7

The ^{1}H NMR spectra of $\mathbf{L^6}$ was very similar to its pre-cursor, 5-carboxylic acid-2,2'-bipyridine differing only in the appearance of a doublet and triplet of the alkyne unit in the aliphatic region of the spectrum. The ^{1}H NMR spectra of $\mathbf{L^7}$ suggested the product consists of interconverting rotational isomers, resulting from the diastereotopic nature of the CH_2 unit within the molecule. The integration of peaks within the aliphatic region of the spectrum indicated the presence of the isomers in a 50:50 ratio, 2.32-2.37 and 2.48-2.57 ppm, 3.02-3.23 ppm, 3.91-3.98 and 4.22 and 4.42 ppm are assigned to C*H* alkyne, CH_3 and CH_2 alkynes of the two rotamers respectively. The presence of two isomers was less obvious in the aromatic region of the spectrum with only the two aromatic protons closest to the aliphatic chain (*ortho*. and *meta*. to the nitrogen) displaying less structured, broad peaks at 7.82-7.98 and 8.61-8.74 ppm.

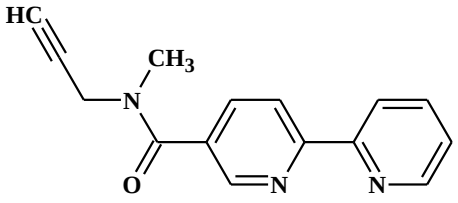

Figure 6.30 L^7

6.8.5. Synthesis and characterisation of the complexes

6.8.5.1. Synthesis and characterisation of $[Re(CO)_3(L^6)Br]$ and $[Re(CO)_3(L^7)Br]$

The successful co-ordination of a $[Re(CO)_3Br]$ unit to $\mathbf{L^6}$and $\mathbf{L^7}$ was achieved following literature precedent forming a novel mono-metallic complexes in low yields of 25 % and 20 % respectively. The ^1H NMR spectra for both complexes were recorded in $CDCl_3$ and displayed changes in the aromatic region of the spectrum only. The comparison to the free ligand confirmed the successful co-ordination of the ligands to Re(I). A shift in the aromatic protons to higher frequency was evident with the number of signals and their intensities fitting well for the target compounds. For $[Re(CO)_3(L^7)Br]$ the presence of rotational isomerism was also evident.

Solid state IR studies were carried out for the complexes which show little change in the ν(CC) when compared to the ligands; the ligands display an IR stretch similar to their precursors, propargyl alcohol with a shift at 2120 cm^{-1}, the complexes display a weaker IR absorption band ranging from 2105-2152 cm^{-1} for the alkyl stretch. Three strong CO bonds ranging from 1665-2032 cm^{-1} were also displayed. MS analysis for each of the complexes gave a parent peak suitable for the loss of the $[C_3H_2]^+$ alkyne only.

6.8.5.2. Synthesis and characterisation of $[Ir(PPy)_2(L^6)]^+$ and $[Ir(PPy)_2(L^7)]^+$

The complex, $[Ir(PPy)_2(L^6)]^+$, was synthesised following literature methodology[50] with a yield of 23 %.[49] $\mathbf{L^6}$ was heated with $\{[Ir(PPy)_2Cl]_2\}$ in methoxyethanol at 110 ˚C for 3.5 hours. Sodium tetrafluoroborate was then added to the solution and after stirring for 5 minutes the product was extracted into DCM. The ^1H NMR spectra were recorded in $CDCl_3$ and again displayed changes in the aromatic region only. The comparison to the free ligand confirmed the successful co-ordination of the $[Ir(PPy)_2]$ unit with both a shift in the aromatic protons of the ligand to higher frequency and the presence of additional aromatics whose number and signal integrations fit well. Solid state IR studies were carried out for the complexes which show little change in the ν(CC) when compared to the ligand with a shift at 2124 cm^{-1}. MS analysis for the complex gave a parent peak at 739.17 with an isotope pattern consistent with the predicted product.

The same reaction conditions were carried out for $\mathbf{L^7}$, however, despite the absence of starting material in the crude ^1H NMR spectra, no product was successfully isolated. The difference in the reactivity of the two ligands can only be attributed to the nature of the linker units (the ester/amide linking units). The presence of an amide on the bipyridine presumably

leads to increased reactivity when compared to the ester; $\mathbf{L^7}$ is presumably more 'activated' upon co-ordination of the Ir(III) unit and this activation could suggest decomposition.

6.8.5.3. The attempted synthesis of $[Ru(bipy)_2(L^6)]^{2+}$ and $[Ru(bipy)_2(L^7)]^{2+}$

$\mathbf{L^{6/7}}$ were reacted with $\{[Cl_2Ru(bipy)_2](H_2O)_2\}$ following the same method used for the synthesis of the iridium complexes. The reactions were monitored by TLC and after heating for 48 hours work-up was conducted. The products were purified using column chromatography where both $\mathbf{L^6}$ and $\mathbf{L^7}$ were recovered along with a product consisting of aromatic protons only. Further characterisation of the unpredicted product by XRD presented a structure for a ruthenium biproduct (Figure 6.31). The reaction with $\mathbf{L^{6/7}}$ was repeated using the more reactive $[(H_2O)_2Ru(bipy)_2]^{2+}$ complex as a precursor, however, in both cases the ruthenium biproduct and ligand starting material was recovered.

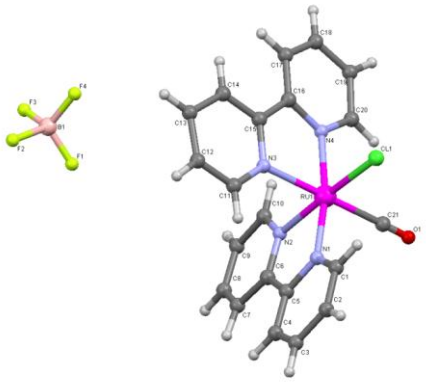

Figure 6.31 Structural representations of the ruthenium biproduct (H atoms omitted for clarity).

6.8.6. UV-Vis absorption spectroscopy

The UV-Vis data for the compounds are summarised in Table 6.5. A high energy band (below 330nm) typically assigned to spin-allowed intra ligand (IL) ($\pi \rightarrow \pi^*$) transitions was noted for all complexes. The transitions in the region of 340-400nm are assigned to the spin allowed ^{1}MLCT (d $\pi \rightarrow \pi^*$).

Table 6.5 Photophysical and IR data for the ligands and the complexes (part 2). λ_{exc} = 340/360 nm, IR recorded in solid state.

Compound	Abs	ε dm^3 mol^{-1} cm^{-1}	Em(MeCN)	Lifetimes (MeCN) ns	CC (Cm^{-1})
L6	251 293	553 992	365	-	2112
L7	252 305	2678 698	356	-	2116
$[Re(CO)_3(L^6)Br]$	252 298	18382 14645	401 525	27.8	2152
$[Re(CO)_3(L^7)Br]$	297 379	13527 23034	463	30	2105
$[Ir(PPy)_2(L^6)]^+$	259 281 316 376	21015 18382 9349 2706	445 602	15 60	2124

6.8.7. Luminescence spectroscopy

Luminescence spectra were obtained in aerated acetonitrile following irradiation at λ_{ex} 350-430 nm. The luminescence data for these complexes are shown in Table 6.5 and are discussed in detail in the following sections.

6.8.7.1. Luminescent properties of $[Re(CO)_3(L^6)Br]$ and $[Re(CO)_3(L^7)Br]$

The emission of L^6 appears to be one major transition centred around 365 nm. L^7 has a two peaks centred emission at 356 nm which can be attributed to rotational isomers and/or presumably $\pi \rightarrow \pi^*$ for mixed alkyne and bipyridine (Figure 6.33). Both the emission and excitation spectra obtained for $[Re(CO)_3(L^6)Br]$ and $[Re(CO)_3(L^7)Br]$ can be viewed in Figure 6.32. In the emission spectra of the complexes, the major transition is now ^{3}MLCT at 525 nm for the ester, $[Re(CO)_3(L^6)Br]$, and at 463 nm for the amide, $[Re(CO)_3(L^7)Br]$. The defined structure of $[Re(CO)_3(L^6)Br]$ can be attributed to the alkyne-based emission presumed to be obscured by ^{3}MLCT. For $[Re(CO)_3(L^7)Br]$, despite the observation of rotational isomers in the ^{1}H NMR, only one peak is visible in the emission spectra indicating similarity of the ^{3}MLCT energy of the two isomers. The emission peak in $[Re(CO)_3(L^7)Br]$ is red-shifted when compared to $\mathbf{L^7}$, 356 nm and 463 nm respectively, and attributed to the presence of rhenium. The lifetimes of the two neutral rhenium based complexes are within the expected timescale.

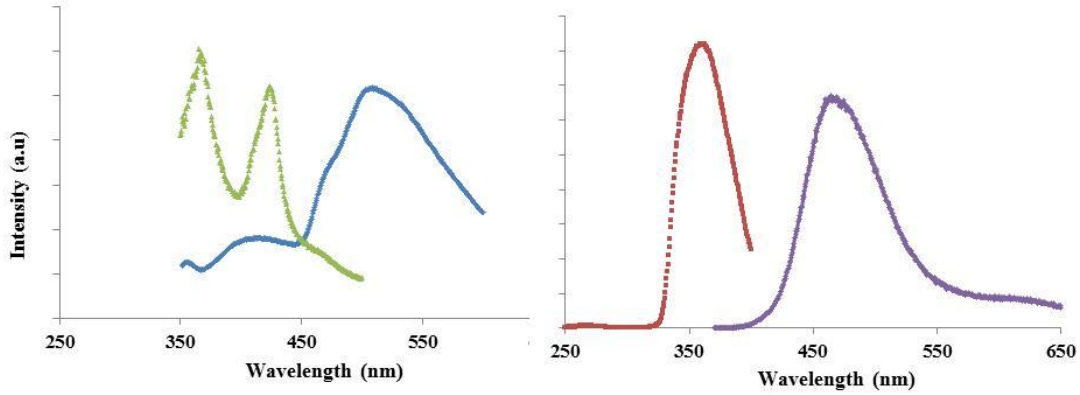

Figure 6.32 Steady state excitation and emission spectra of $[Re(CO)_3(L^6)Br]$ (LHS) and $[Re(CO)_3(L^7)Br]$ (RHS). (λ_{exc} = 350 nm)

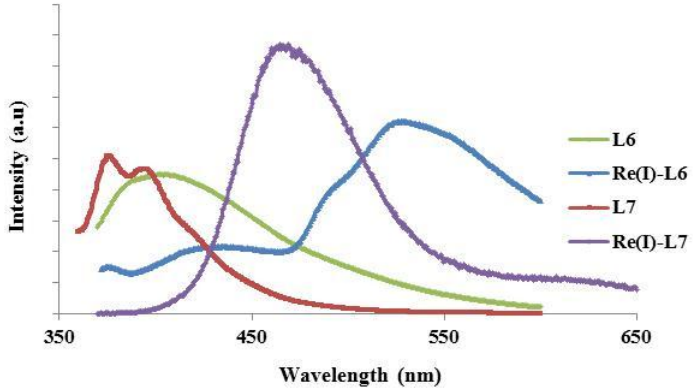

Figure 6.33 Steady state emission spectra of L^6, $[Re(CO)_3(L^6)Br]$, L^7 and $[Re(CO)_3(L^7)Br]$ (λ_{exc} = 350 nm)

6.8.7.2. Luminescent properties of $[Ir(PPy)_2(L^6)]^+$

The Ir(III) complex, $[Ir(PPy)_2(L^6)]^+$, displayed broad emission with peaks centred at 445 nm and 602 nm tentatively assigned to red-shifted ligand based emission (upon co-ordination) and ^{3}MLCT to the bipyridine, however, contribution from the phenylpyridine transitions cannot be excluded.[50] The lifetime of this complex was lower than predicted for complexes of this type suggesting quenching of the excited state may be occurring.

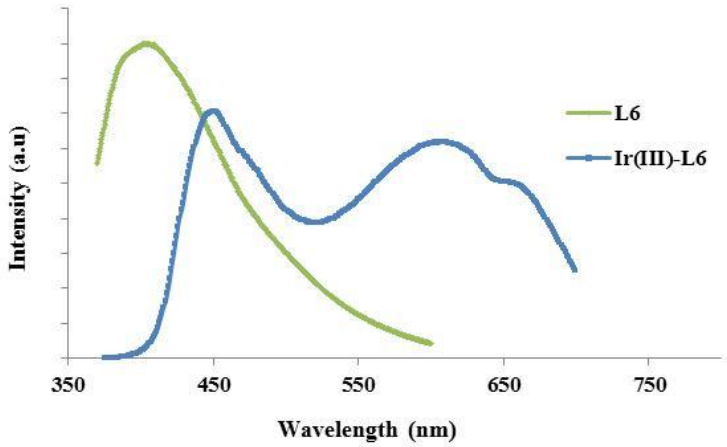

Figure 6.34. Steady state excitation and emission spectra of $[Ir(PPy)_2(L^6)]^+$. (λ_{exc} = 360 nm)

The synthesis of the novel complexes: $[Re(CO)_3(L^6)Br]$, $[Re(CO)_3(L^7)Br]$ and $[Ir(PPy)_2(L^6)]^+$ is a suggested route to the synthesis of novel, hetero-metallic systems with potential to act as both cellular imaging and therapeutic agents. However, due to the time restriction of the PhD, the hetero-metallic complexes inclusive of these starting materials have yet to be synthesised.

6.9. Conclusion

The aim of the second half of this chapter was to synthesise a series of di-hetero-metallic complexes inclusive of a d^6 TM ion and a Au(I) moiety to determine their potential applications. The successful synthesis of two ligands, $\mathbf{L^6}$ and $\mathbf{L^7}$, was achieved with excellent yields of 83 % and 84 % respectively. The successful synthesis of three novel mono-metallic complexes; $[Re(CO)_3(L^6)Br]$, $[Re(CO)_3(L^7)Br]$ and $[Ir(PPy)_2(L^6)]^+$ in low-moderate yields was also achieved.

The photophysical properties of both $[Re(CO)_3(L^6)Br]$ and $[Ir(PPy)_2(L^6)]^+$, promote their potential suitability as imaging agents. With small changes within a complex having already proved to have major effects in both the photophysical properties and cellular localisation observed, a confocal microscopy experiment could be performed. Additionally, all three complexes could be used as starting material for the synthesis of a variety of di-hetero-metallic complexes. Following on from the first half of this chapter, where-by a tri-hetero-metallic complex inclusive of $Au(I)_2$-Re(I) displayed suitability as both an imaging and/or therapeutic agent, all three mono-metallic complexes show promising potential.

6.10. Experimental

6.10.1. Crystallography

[Re(CO)$_3$(L^1)Br] $C_{13}H_6Br_3N_2O_3Re$, M = 664.13, 0.2 × 0.2 × 0.2 mm^3, monoclinic, space group $P2_1/m$ (No. 11), a = 6.4833(4), b = 14.3775(10), c = 9.0151(5) Å,□□ = 105.961(4)°, V = 807.93(9) Å^3, Z = 2, D_c = 2.730 g/cm^3, F_{000} = 604, MoK□ radiation,□□ = 0.71073 Å, T = 150(2)K, 2□$_{max}$ = 55.1º, 3204 reflections collected, 1915 unique (R_{int} = 0.0415). Final *GooF* = 1.050, *R1* = 0.0456, *wR2* = 0.1117, *R* indices based on 1701 reflections with I >2(I) (refinement on F^2), 107 parameters, 0 restraints. Lp and absorption corrections applied,□□ = 14.949 mm^{-1}.

[Re(CO)$_3$(L^2)Br] $C_{23}H_{24}BrN_2O_3ReSi_2$, M = 698.73, 0.2 × 0.2 × 0.2 mm^3, monoclinic, space group $P2_1/a$ (No. 14), a = 13.5076(4), b = 13.9248(4), c = 14.3606(3) Å, b = 107.145(2)°, V = 2581.06(12) Å^3, Z = 4, D_c = 1.798 g/cm^3, F_{000} = 1352, MoKa radiation, l = 0.71073 Å, T = 150(2)K, 2q_{max} = 56.6º, 22858 reflections collected, 6356 unique (R_{int} = 0.1201). Final *GooF* = 1.204, *R1* = 0.0959, *wR2* = 0.1500, *R* indices based on 4903 reflections with I >2sigma(I) (refinement on F^2), 295 parameters, 0 restraints. Lp and absorption corrections applied, m = 6.375 mm^{-1}.

6.10.2. Synthesis of the ligands

L^1 To a solution of 2,6 dibromopyridine (2 g, 8.44 mmol) in anhydrous ether (45 mL) at -78 ˚C was added BuLi (5.28 mL, 8.44 mmol) and the solution left to stir for 2 h. Zinc chloride (9.3 mL, 9.3 mmol) was then added followed by the addition of dry 2,6 dibromo pyridine (2 g, 8.44 mmol) and the palladium tetrakis catalyst (0.94 g, 10 %) 20 minutes later. The solution was allowed to reach room temperature and left for an additional 15 h. H_2O (50 mL) was added to the solution and product extracted into DCM. The organic layer was dried and the solvent evaporated to dryness, yielding a white solid. Yield: 2.22 g, 42 %. ^{1}H NMR ($CDCl_3$, 400 MHz, 298 K) δ_H: 7.42 (2H, d, $^3J_{HH}$ =7.7 Hz, (*H1*)), 7.61 (2H, t, $^3J_{HH}$ =7.8 Hz (*H2*)), 8.32 (2H, d, $^3J_{HH}$ =7.6 Hz (*H3*)) ppm.

L^2 To a solution of L^1 (0.6 g, 1.92 mmol) in diisopropylamine and THF (10 mL) under N_2(g) was added CuI (10 mg), $Pd(OAc)_2$ (10 mg) and PPh_3 (30 mg) and stirred at 50 ˚C for 20 minutes. To the resulting solution was added trimethylsilylethylene (0.824 g, 8.4 mmol) and the reaction left at 25 ˚C for 20 h. The solution was cooled, filtered and filtrate evaporated to

dryness, yielding a white solid. Yield: 126 mg, 19 %. ^{1}H NMR ($CDCl_3$, 400 MHz, 298 K) δ_H: 0.28 (18H, s, (*H4*)), 7.42 (2H, d, (*H3*)), 7.82 (2H, t, (*H2*)), 8.43 (2H, d, (*H1*)) ppm.

L^{3} L^{2} (110 mg, 0.316 mmol) and KF (40 mg, 0.695 mmol) in MeOH (20 mL) were stirred at RT for 2 h. The resulting solution was filtered through a plug of silica and filtrate evaporated to dryness, yielding a cream solid. Yield: 62 mg, 58 %. ^{1}H NMR ($CDCl_3$, 400 MHz, 298 K) δ_H: 3.22 (2H, s, (*H4*)), 7.57 (2H, d, (*H3*)), 7.88 (2H, t, (*H2*)), 7.53 (2H, d, (*H1*)) ppm.

L^{6} 5-COOH-2,2 bipyridine chloride (200 mg, 1 mmol) was added to a solution of TEA (0.281 mL, 2 mmol) and propargyl alcohol (62 mg, 1.1 mmol) in chloroform (30 mL) and stirred for 3 hours 60 ˚C. Aqueous work up followed by the organic solvent being evaporated to dryness, yielding a cream solid. Yield: 162 mg, 83 %. ^{1}H NMR ($CDCl_3$, 400 MHz, 298 K) δ_H: 2.53 (1H, t, $^{3}J_{HH}$ = 2.4 Hz, (*H9*)), 4.91 (2H, d, $^{3}J_{HH}$ = 2.4 Hz (*H8*)), 7.25-7.44 (1H, m, (*H3*)), 7.72-7.86 (1H, m, (*H5*)), 8.33-8.51 (3H, m, (*H2, H4, H6*)), 8.61 (1H, d, $^{3}J_{HH}$ = 4.7 Hz, (*H1*)), 9.21 (1H, s, (*H7*)) ppm.^{13}C{^{1}H} NMR ($CDCl_3$, 101 MHz, 298 K) δ_C: 52.8, 76.7, 120.6, 122, 124.7, 125, 137.2, 138.3, 149.5, 150.8, 155, 160 ppm. MS (ES^+) *m/z*: 238.07 $[M]^+$. IR (nujol) 1727 (CO), 2122 (CO) cm^{-1}.UV-vis (ε / M^{-1} cm^{-1}) (MeCN) λ_{max}: 251 (555), 293 (992) nm.

L^{7} 5-COOH-2,2 bipyridine chloride (200 mg, 1 mmol) was added to a solution of TEA (0.281 mL, 2 mmol) and N-methyl propargyl amine (76 mg, 1.1 mmol) in chloroform (30 mL) and stirred for 3 hours 60 ˚C. Aqueous work up followed by the organic solvent being evaporated to dryness, yielding a cream solid. Yield: 210 mg, 84 %. ^{1}H NMR ($CDCl_3$, 400 MHz, 298 K) δ_H: 2.22-2.31 (1H, m, (*H10a*)), 2.32-2.42 (1H, m, (*H10b*)), 3.02-3.23 (6H, m, (*H8a, H8b*)), 3.91-4.04 (2H, m, (*H9a*)), 4.33-4.42 (2H, m, (*H9b*)), 7.42-7.34 (2H, m, (*H3a, H3b*)), 7.72-7.80 (2H, m, (*H5a, H5*)), 7.82-7.98, 2H, m, (*H6a, H6b*)), 8.32-8.43 (4H, m, (*H2a, H2b, H4a. H4b*)), 8.61-8.64 (2H, m, (*H1a,H1b*)), 8.67-8.78 (2H, m, (*H7a, H7b*)) ppm. ^{13}C{^{1}H} NMR ($CDCl_3$, 101 MHz, 298 K) δ_C: 29.7, 336.8, 77.7, 120.7, 121.5, 124.4, 131, 136.2, 137.1, 147.8, 149.4, 155.2,157.4, 168.9 ppm. MS (ES^+) *m/z*: 251.1 $[M]^+$. IR (nujol) 1588.57 (CO), 1633.89 (CO), 2117.94 (CC) cm^{-1}. UV-vis (ε / M^{-1} cm^{-1}) (MeCN) λ_{max}: 213 (1840), 253 (2678), 305 (698) nm.

6.10.3. Synthesis of the complexes

***fac*-[Re(CO)$_3$(L^1)Br]** $Re(CO)_5Br$ (48 mg, 0.12 mmol) and L^1 (41 mg, 0.132 mmol) were heated at 70 ˚C in toluene (5 mL) for 12 h. The resultant precipitate was filtered, washed with toluene and dried *in vacuo* to yield an orange solid. The crude product was purified using column chromatography eluting with DCM. Yield: 58 mg, 73 %. ^{1}H NMR ($CDCl_3$, 400 MHz, 298 K) δ_H: 7.88-7.99 (2H, m, (*H2, H3*)), 8.29 (1H, d, (*H1*)) ppm. $^{13}C\{^1H\}$ NMR ($CDCl_3$, 101 MHz, 298 K) δ_C: 123.2, 131.1, 140.9, 146.4, 158.8, 161.6 ppm. MS (ES^+) *m/z*: 666.76 $[M]^+$, HRMS (ES) found m/z 686.6081 $[M+H]^+$; $[^{185}ReNaC_{13}H_6O_3N_2Br_3]^+$ requires 686.7341. IR (nujol) υ: 1892 (CO), 1995 (CO), 2022 (CO) cm^{-1}. UV-vis (ε / M^{-1} cm^{-1}) (MeCN) λ_{max}: 258 (8248), 324 (7757), 397 (1380) nm.

***fac*-[Re(CO)$_3$(L^2)Br]** $Re(CO)_5Br$ (160 mg, 0.4 mmol) and L^2 (150 mg, 0.43 mml) were heated at 70 ˚C in toluene (5 mL) for 12 h. The resultant precipitate was filtered, washed with toluene and dried *in vacuo* to yield an orange solid. The crude product was purified using column chromatography eluting with DCM. Yield: 75 mg, 30 %. ^{1}H NMR ($CDCl_3$, 400 MHz, 298 K) δ_H: 1.19 (18H, s, (*H4*)), 7.51 (2H, d, (*H3*)), 7.72 (2H, t, (*H2*)), 7.93 (2H, d, (*H1*)) ppm. ^{13}C NMR (($CDCl_3$) 300 MHz, 298K) δ_c: 30.13, 122.5, 130, 130.4, 138.5, 159.2 ppm. MS (ES^+) (%) *m/z*: 734.99 $[M+Cl^-]^+$. HRMS (ES) found m/z 619.0886 $[M-Br]^+$; $[ReC_{23}H_{24}O_3N_2Si_1]^+$ requires 619.0876. IR (nujol) υ: 1923 (CO), 2022 (CO) cm^{-1}. UV-vis (ε / M^{-1} cm^{-1}) (MeCN) λ_{max}: 253 (1450), 280 (914), 335 (709) nm.

***fac*-{Re(CO)$_3${[Au(PPh$_3$)]$_2$L^3}Br}** $Re(CO)_5Br$ (11 mg, 0.026 mmol) and $[[AuPPh_3]_2L^3]$ (30 mg, 0.0267 mmol) were heated at 70 ˚C in toluene (5 mL) for 12 h. The resultant precipitate was filtered, washed with toluene and dried *in vacuo* to yield a dark orange solid. Yield: 24 mg, 62 %. ^{1}H NMR ($CDCl_3$, 400 MHz, 298 K) δ_H: 7.29-7.68 (36H, m, (*H1-H4*)) ppm. $^{13}C\{^1H\}$ NMR ($CDCl_3$, 101 MHz, 298 K) δ_C: 77.2, 129.2, 129.4, 132, 134.1, 134.9 ppm. δ^{31}P 35.9 ppm. MS (ES^+) *m/z*: 721.15 $[Au(PPh_3)_2]^+$. IR (nujol) υ: 1908 (CO), 1995 (CO), 2034 (CO), 2151 (CC) cm^{-1}. UV-vis (ε / M^{-1} cm^{-1}) (MeCN) λ_{max}: 268 (11149), 309 (6351), 375 (3038) nm.

***fac*-[Re(CO)$_3$(L^6)Br]:** $Re(CO)_5Br$ (75 mg, 0.185 mmol) L^4 (48 mg, 0.203 mmol) were heated at 70 ˚C in toluene (5 mL) for 12 h. The resultant precipitate was filtered, washed with toluene and dried *in vacuo* to yield a dark orange solid. Yield: 27 mg, 25 %. ^{1}H NMR ($CDCl_3$, 400 MHz, 298 K) δ_H: 2.59 (1H, t, $^3J_{HH}$ = 2.4 Hz, (*H9*)), 4.91 (2H, d, $^3J_{HH}$ = 2.4 Hz (*H8*)), 7.49-7.58 (1H, m, (*H3*)), 7.96-8.04 (1H, m, (*H5*)), 8.20-8.32 (2H, m, (*H4*, *H6*)), 8.49-

8.54 (1H, m, (*H2*)), 8.99 (1H, d, $^{3}J_{HH}$ = 4.5 Hz, (*H1*)), 9.51 (1H, s, (H7)) ppm. $^{13}C\{^{1}H\}$ NMR (CDCl3, 101 MHz, 298 K) δ_C: 53.9, 76.4, 122.5, 124.6, 128.1, 128.2, 139.3, 140, 153.7, 154.4, 159, 177.6 ppm. MS (ES^+) *m/z*: 550 $[M\text{-}C_3H_2]^+$, 587.93 $[M]^+$. IR (nujol) υ: 1735 (CO), 1900 (CO), 2022 (CO), 2152 (CC) cm^{-1}. UV-vis (ε / M^{-1} cm^{-1}) (MeCN) λ_{max}: 218 (42428), 252.5 (18382.3), 298 (14645)) nm.

***fac*-[Re(CO)$_3$(L^7)Br]:** $Re(CO)_5Br$ (80 mg, 0.197 mmol) L^5 (54 mg, 0.217 mmol) were heated at 70 ˚C in toluene (5 mL) for 12 h. The resultant precipitate was filtered, washed with toluene and dried in *vacuo* to yield a dark orange solid. Yield: 24 mg, 20 %. ^{1}H NMR ($CDCl_3$, 400 MHz, 298 K) δ_H: 2.31 (1H, d, (*H10a*)), 2.42 (1H, d, (*H10b*)), 3.08-3.23 (6H, m, (*H8a,Hb*)), 3.88-3.94 (2H, m, (*H9a*)), 4.2-4.44 (2H, m, (*H9b)),* 7.48-7.51 (2H, m, (*H4a*, *H4b*)), 7.96-7.81 (2H, m, (*H5a*, *H5b*)), 8.11-8.22 (6H, m, (*H3a,H3b*, *H5a,H5b*, *H7a*, *H7b*)), 8.98-9.02 (3H, m, (*H2a*, *H2b*, *H1a*), 9.12 (1H, m, (*H1a*)) ppm. $^{13}C\{^{1}H\}$ NMR (MeOD, 101 MHz, 298 K) δ_C: 27.8, 31.8, 35.1, 76.2, 114.5, 121.2, 122, 125.7, 136.1, 137.3, 149.7,151.4, 151.6, 153, 154.7, 163.7, 186.4, 194.7 ppm. MS (ES^+) *m/z*: 564.08 $[M\text{-}C_3H_2]^+$. IR (nujol) *υ*: 1664.5 (CO), 1902.43 (CO), 2023.44 (CO), 2105.4 (CC) cm^{-1}. UV-vis (ε / M^{-1} cm^{-1}) (MeCN) λ_{max}: 297 (13527), 379.5 (23034) nm.

[Ir(PPy)$_2$(L^6)]: $[Ir(PPy)_2Cl]_2$ (50 mg, 0.063 mmol) and L^4 (30 mg,0.12 mmol) were heated at 110 ˚C in methoxy ethanol (5 mL). The resultant solution was dried *in* vacuo, re-dissolved in acetonitrile (10 mL) and a spatula of $NaPF_6$ added. The resultant precipitate was filtered and filtrate dried *in vacuo* to yield an orange solid. Yield 21 mg, 23 %. ^{1}H NMR ($CDCl_3$, 400 MHz, 298 K) δ_H: 2.49 (1H, t, $^{3}J_{HH}$ = 2.4 Hz, (*H9*)), 4.71 (2H, d, $^{3}J_{HH}$ = 2.4 Hz (*H8*)), 6.18-6.28 (2H, m, (*H15*)), 6.81-7.02 (6H, m, (*H3*, *H4*, *H12*, *H16*)), 7.32-7.43 (3H, m, (*H6*, *H14*)), 7.56-7.75 (4H, m, (*H13*, *H17*)), 7.8-7.88 (3H, m, (*H2*, H11)), 8.18-8.27 (1H, m, (H6)), 8.49 (1H, s, (*H1*)), 8.62-8.74 (1H, m, (*H7*)), 9.61-9.82 (2H, m, (*H10*)) ppm. MS (ES^+) *m/z*: 739.17 $[M]^+$, IR (nujol) υ: 1734 (CO), 2124 (CC) cm^{-1}. UV-vis (ε / M^{-1} cm^{-1}) (MeCN) λ_{max}: 258.5 (21015), 280.5 (18382.3), 316 (9349), 375.5 (2706) nm.

6.11. References:

1. K.-L. Cheung, S.-K. Yip and V. W.-W. Yam, *J. Organomet. Chem*., 2004, **689**, 4451.
2. Himmelspach, M. Finze, and S. Raub, *Angew. Chem. Int. Ed*., 2011, **50**, 2628.
3. O. M. Abu-Salah and A. R. Al-Ohaly, *J. Organomet. Chem*., 1983, **255**, 39.
4. D. Li, X. Hong, C. M. Che, W. C. Lo and S. M. Peng, *J. Chem. Soc*., 1993, 2929.
5. P. Li, B. Ahrens, A. D. Bond, J. E. Davies, O. F. Koentjoro, P. R. Raithby and S. J. Teat, *Dalton. Trans*., 2008, 1635.
6. M. Ferrer, L. Rodríguez, O. Rossell, J. C. Lima, P. Gómez-Sal and A. Martin, *J. Organomet. Chem*., 2004, **23**, 5096.
7. Z. N. Chen, N. Zhao, Y. Fan and J. Ni, *Coord. Chem. Rev*., 2009, **253**, 1.
8. S. S. Y. Chui, M. F. Y. Ng, C.-M. Che, *Chem. Eur. J*., 2005, **11**, 1739.
9. S. Patai, *The Chemistry of the Carbon Carbon Triple Bond*, 1978.
10. P. F. Schwab, M. D. Levin and J. Michl, *J. Chem. Rev*., 1999, **99**, 1863.
11. H. A. Dieck and F. R. Heck, *J. Organomet. Chem*., 1975, **93**, 259.
12. L. Cassat, *J. Organomet. Chem*., 1975, **93**, 253.
13. K. Sonogashira, Y. Tohda and N. Hagihara, *Tet. Lett*., 1975, **16**, 4467.
14. L. Kohnen and R. L. Danheiser, *Organic. Synth*., 200, **84**, 77.
15. D. Mery, K. Heuze, and D. Astruc, *Chem. Commun*., 2003, **15**, 1934.
16. C. Barnard, *Platinum Metals Rev*., 2008, **52**, 38.
17. R. D. Stephens and C. E. Castro, *J. Organomet. Chem*., 1963, **28**, 3313.
18. O. Vechorkin, D. Barmaz, V. Proust, and X. Hu, *J. Am. Chem. Soc.*, 2009, **131**, 12078.
19. C. Gonzalez-Arallano, A. Abad, A. Corma, H. Garcia, M. Iglesias and F. Sanchez, *Angew. Chem. Int. Ed.*, 2007, **46**, 1536.
20. Corma, R. Juarez, M. Boronat, F. Sanchez, M. Iglesias and H. Garcia, *Chem. Commun*., 2011, **47**, 1446.
21. J. Seechurn, M. O. Kitching, T. Colacot, and V. Snieckus, *Angew. Chem. Int. Ed*., 2012, **51**, 5062.
22. W. P. V. Bohm and W. A. Herrmann, *Eur. J. Org. Chem.*,2000, **200**, 3679.
23. D. Mery, K. Heuze, and D. Astruc, *Chem. Commun*., 2003, **15**, 1934.
24. M. Lee and S. Chang, *J. Am. Chem. Soc*., 2000, **122**, 12011.
25. K. Sonogashira, *J. Organomet. Chem*., 2002, **653**, 46.
26. J. R. Shakirova, E. V. Grachova, V. V. Gurzhiy, I. O. Koshevoy, A. S. Melnikov, O. V. Sizova, S. P. Tunik and A. Laguana, *Dalton. Trans*., 2012, **41**, 2941.
27. I. O. Koshevoy, P. V. Ostrova, A. J. Karttunen, A. S. Melnikov, M. A. Khodorkovskiy, M. Jaukka, J. Jänis, S. P. Tunik and T. A. Pakkanen, *J. Chem. Soc*., 2010, **39**, 9022.
28. V. W.-W. Yam, K.-L. Cheung, E. C. C. Cheng, N. Zhu and K. K. Cheung, *J. Chem. Soc*., 2003, 1830.
29. Y. Yamamoto, M. Shiotsuka and S. Onaka, *J. Organomet. Chem*., 2004, **689**, 205.
30. W. Liu, R. Wang, X.-H. Zhou and Z.-Z.Yoou, *Organometallics*., 2008, **27**, 126. K. L.
31. K. L. Cheung, S. K. Yip, V. W. W. Yam, *J. Organomet. Chem*., 2004, **689**, 4451. .
32. M. Ferrer, L. Rodríguez, O. Rossell, J. C. Lima, P. Gómez-Sal and A. Martin, *J. Organomet. Chem*., 2004, **23**, 5096.
33. X. Li, C. L. D. Gibb, M. E. Kuebel and B. C. Gibb. *Tetrahedron.*, 2001, **57**, 1175.
34. D. B. Moron, G. O. Morton and D. J. Allbright, *J. Heterocyclic. Chem*., 1986, **23**, 1071.
35. B. J. Liddle, S. V. Lindeman, D. L. Reger and J. R. Gardinier, *Inorganic Chemistry*., 2007, **46**, 8484.

36. S. E. Thwaite, A. Schier and H. Schmidbaur, *Inorganica Chimica Acta*., 2004, **357**, 1549.
37. Ott, X. Qian, Y.Xu, D. H. W. Vlecken, I. J. Marques, D. Kubutat, J. Will, W. S.
38. Sheldrick, P. Jesse, A. Prokop and C. P. Bagowski, *J. Med. Chem*., 2009, **52**, 763.
39. R. Ballardini, V. Balzani, M. Clemente-Leon, A. Credi, M. T. Gandolfi, E. Ishow, J. Perkins, J. F. Stoddart, H.-R. Tseng and S. Wenger, *J. Am. Che. Soc*., 2002, **124**, 12786.
40. E. L. Trump and M. X. Zhou, *Trans. Kansas. Ac. Sci*., 1993, **96**, 167.
41. S. Dash, S. Patel and B. K. Mishra, *Tetrahedrom*., 2009, **65**, 707.
42. F. Tipton, S. Boyce, J. O'Sullivan, G. P. Davey and J. Healey, *Curr. Med. Chem*., 1965.
43. H. Meyer, N. Ginovart, A. Boovariwala, S. Sagrat, D. Hussey, A. Garcia, T. Young, N. P-Rieder, A. A. Wilson, S. Houle, *Arch. Gen. Psychiatry*., 2006, **63**, 1206.
44. E. F. Domino and S. S. Khanna, *Am. J. Psychiatry*., 1976, **133**, 323.
45. J. Schildkraut, J. M. Herzog, P.J. Orsulak, S.E. Edelman, H. M. Shein and S. H. Frazier, *Am. J. Psychiatry*., 1976, **133**, 438.
46. P. Riederer, L. Lachenmayer and G. Laux, G, *Curr. Med. Chem*., 2004, **11**, 2033.
47. P. H. Yu, B. A**.** Davis, D. A. Durden, A. Barber, I. Terleckyj, W. G. Nicklas and A. A. Boulton, *J. Neurochem*.,1994, **62**, 697.
48. H. Yi , W. Maruyama, Y. Akao , T. Takahashi, K. Iwasa, M. B. Youdim and M. Naoi, *J. Neural. Transm*., 2006, **113**, 21.
49. O. B-Am, T. Amit, O. Weinreb, M. B. Youdim and S. Mandel S, *J. Alzheimers. Dis.* 2010, **21**, 361.
50. M. S. Lowry, W. R. Hudson and R. A. Pascal, Jr and S. Bernhard, *J. Am. Chem. Soc*., 2004, **126**, 14129.